Final
Project Technical Report
of ISTC 1867p

Development of Methods for Diagnostics
of Discharges in Supersonic Flows
(From 1 August 2000 to 1 August 2001 for 12 months)

Alexey Petrovich Ershov
(Project Manager)
Faculty of Physics of Moscow State University

September 2001

REPORT DOCUMENTATION PAGE

Form Approved OMB No. 0704-0188

Public reporting burder for this collection of information is estibated to average 1 hour per response, including the time for reviewing instructions, searching existing data sources, gathering and maintaining the data needed, and completing and reviewing this collection of information. Send comments regarding this burden estimate or any other aspect of this collection of information, including suggestions for reducing this burder to Department of Defense, Washington Headquarters Services, Directorate for Information Operations and Reports (0704-0188), 1215 Jefferson Davis Highway, Suite 1204, Arlington, VA 22202-4302. Respondents should be aware that notwithstanding any other provision of law, no person shall be subject to any penalty for failing to comply with a collection of information if it does not display a currently valid OMB control number. PLEASE DO NOT RETURN YOUR FORM TO THE ABOVE ADDRESS.

1. REPORT DATE (DD-MM-YYYY) 30-08-2001	2. REPORT TYPE Final	3. DATES COVERED (FROM - TO) 01-08-2000 to 01-08-2001

4. TITLE AND SUBTITLE
Development of Methods for Diagnostics of Discharges in supersonic Flows
Unclassified

5a. CONTRACT NUMBER

5b. GRANT NUMBER

5c. PROGRAM ELEMENT NUMBER

6. AUTHOR(S)
Ershov, Alexei ;

5d. PROJECT NUMBER

5e. TASK NUMBER

5f. WORK UNIT NUMBER

7. PERFORMING ORGANIZATION NAME AND ADDRESS
M.V. Lomonosov Moscow State University (MSU)
Faculty of Physics
Moscow 119899, Russiaxxxxx

8. PERFORMING ORGANIZATION REPORT NUMBER

9. SPONSORING/MONITORING AGENCY NAME AND ADDRESS
EOARD
PSC 802 Box 14
FPO, 09499-0200

10. SPONSOR/MONITOR'S ACRONYM(S)

11. SPONSOR/MONITOR'S REPORT NUMBER(S)

12. DISTRIBUTION/AVAILABILITY STATEMENT
APUBLIC RELEASE
,

13. SUPPLEMENTARY NOTES

14. ABSTRACT

The application of three independent methods of plasma diagnostics ? probe, spectroscopic and microwave - for diagnostics of discharges in supersonic gas flows has been investigated.

15. SUBJECT TERMS
EOARD; Propulsion; engines and Fuels; combustion & Ignition

16. SECURITY CLASSIFICATION OF:			17. LIMITATION OF ABSTRACT Public Release	18. NUMBER OF PAGES 223	19. NAME OF RESPONSIBLE PERSON Fenster, Lynn lfenster@dtic.mil
a. REPORT Unclassified	b. ABSTRACT Unclassified	c. THIS PAGE Unclassified			19b. TELEPHONE NUMBER International Area Code Area Code Telephone Number 703767-9007 DSN 427-9007

Standard Form 298 (Rev. 8-98)
Prescribed by ANSI Std Z39.18

ABSTRACT

The application of three independent methods of plasma diagnostics – probe, spectroscopic and microwave - for diagnostics of discharges in supersonic gas flows has been investigated.

The methods of measurements of charged particle densities, gas and vibrational temperatures, intensity of electrical fields in plasma, have been developed under the conditions characteristic for electric discharge plasmas in supersonic gas flows .

A PC-controlled probe measurement circuit with an opto-galvanic isolation was developed and performed. It is based upon the transformation of measured analogue signal to digital sequence, the transmission of the said sequence via optic fiber line for the required distance and the inverse transformation of the digit code to the analogue signal.

New methods of plasma diagnostics are developed. A class of regimes is analyzed, in which the voltage-current characteristic is determined by the "inviscid flow region". New analytical formulae for these regimes in high, moderate and low discharge electric fields are deduced. They correspond with numerical simulation data and experiments, and can be recommended for diagnostics for most cases of the plasma aerodynamic experiments.

For conditions when the voltage-current characteristic is determined by both the "inviscid flow region" and the diffusion layer, two-dimensional non-stationary mathematical model was developed, and detailed numerical simulation has been carried out. Two new effects on the voltage-current characteristics have been found out: the synergetic interaction of the gas density profile formation in the high-speed flow with 1) the ambipolar diffusion, and 2) with plasma chemical reactions. They want further studies.

Spectral methods of measurement of electron density, rotation and vibration temperatures were analyzed and adapted to the conditions of the discharge in the supersonic airflow. The non-stationary kinetic model for substantiation of spectroscopic methods of diagnostics of chemically active non-equilibrium non-stationary plasma was developed.

It was shown experimentally, that the transversal discharges in supersonic flows are realized in the mode of periodic re-breakdowns between the anode and cathode jets of the discharge, that results in pulses of a discharge current, voltage and input electrical power.

The experimental investigation of spatial and temporary evolution of plasma parameters of the transversal direct and pulse-periodic discharges in supersonic airflow was carried out with Mach number M=2 in a pressure range 40 –200 Torr. Under these conditions a change in discharge currents from 0.1 up to 25 A results in a change in the values of an electron density from 10^{12} cm^{-3} up to 10^{14} cm^{-3}, the gas temperature from 1000 K up to 4000 K, the vibrational temperature from 8000 K to 3500 K, an electrical field from 300 V/cm to 20 V/cm.

A numerical simulation of a supersonic flow over pulse-periodic discharge is carried out and the classification of flows depending on the pulse frequency is proposed.

The regime of long single pulses is characterized by formation of a long high temperature region with size depending on the ambient flow velocity and the pulse duration. It was shown that the time characteristics of energy source, chosen for experiments, allow to simulate the results of an action of the steady energy source on a supersonic flow.
At increasing the pulse repetition frequency the regime of a pulsing temperature trace with a pulsing heading shock wave is realized. The further frequency increasing leads to the quasi-steady regime, when the resulting flow does not depend on the pulse form and duration and is identical to the steady solution.

The experimental investigation of spatial and temporary evolution of plasma parameters of the plasmadynamic discharge in supersonic airflow was carried out with Mach number M=2 in a pressure range 100 –500 Torr. Influence of the addition of propane to air on plasma parameters of discharge was investigated.

CONTENTS

CHAPTER I REVIEW

ELECTRIC PROBE DIAGNOSTICS FOR HIGH PRESSURE FLOWING PLASMA

The review includes the works on the subjects of the project published in the Russian Academy of Sciences journals during last five years (1996-2000).

The list of the reviewed journals is the following:

1. Doklady Physics
2. Technical Physics
3. Journal of Experimental and Theoretical Physics
4. Technical Physics Letters
5. Journal of Experimental and Theoretical Physics Letters
6. Instruments and Experimental Technique
7. Journal of Communications Technology and Electronics
8. High Temperature
9. Plasma Physics Reports
10. Journal of Applied Mechanics and Technical Physics
11. Mechanics of a Liquid and Gas
12. Engineering- Physical Journal

The works published earlier, in the previous five years, if they are connected to the works of the considered period are also studied in the review.

Nomenclature

e – Magnitude of electron charge

k - Boltzmann's constant

l - mean free path

R , d – probe radius and diameter

$Kn = l/R$ – Knudsen number

l_d – Debye length

$a = l_d/R$ - Debye length to probe radius ratio

N_∞ - unperturbed value of charged particle density

n_+, n_- - density of ions and electrons to unperturbed value of charged particle density accordingly

T_+ , T_- - Temperatures of ions and electrons accordingly,

$t = T_+/T_-$,

j - Electrical potential with respect to a plasma potential

$y = e j /k T_-$ - Non-dimensional electrical potential,

D_+, D_- - Diffusion coefficient of ions and electrons accordingly,

$b = D_+/D_-$ - Ion diffusion coefficient to electron diffusion coefficient ratio

U_∞ - Undisturbed flow velocity

ν - Viscosity

Re$= 2 U_\infty R/\nu$ – gas-dynamic Reynolds number, based on a diameter

$Sc_+ = \nu/D_+$ - Ion Schmidt number

Sc – ambipolar Schmidt number

Re$_e$ = Re Sc –electric (diffusion) Reynolds number

Pr – Prandtl number

Pe = Re Pr - Peclet number]

Nu_d - local Nusselt number, based on a diameter

I – probe current

J, j - dimension and dimensionless current density accordingly

$r_s = (D_+ / N_\infty a_e)^{1/2}$ - recombination length

a_T, l_T - heat-transfer coefficient and heat conductivity coefficient accordingly

8

Introduction

The results of the development of electric probe diagnostics for high pressure flowing plasma achieved by the end of the seventies were summarized by P. Chung, L. Talbot and K. Touryan in the book [I.1]. The progress in probe diagnostics attained by the end of the 80th, was outlined in the review of M.Benilov [I.2] and monography of B.V.Alekseev and V.A.Kotelnikov [I.3].

The theoretical aspects of the problem for all cases were emphasized. Modes are considered analytically, each being determined by a set of strong inequalities of the kind

$$P_i >> 1, P_J << 1,$$

where P_i are dimensionless criteria parameters.

The most important dimensionless criteria parameters for probe diagnostics are Knudsen number $Kn = l/R$ (λ is mean free length of particles, R is probe radius), ratio of Debye length l_d to probe radius $a = l_d/R$, Reynolds number, Mach number etc.

The change of a sign even in one of the inequalities modifies the physics of plasma interaction with a probe essentially and leads to the transition to other mode.

There are formulas to connect I – V probe characteristic and parameters of plasma for some modes, but these formulas are unknown for other modes.

The boundary areas of parameters, where $P_i » 1$, are not generally described analytically, the diagnostics for these cases being complicated. As a rule, the modes, characteristic for plasma devices such as the glow discharge, plasma electronics device have been investigated well in recent years.

Only the new scientific research [I.4] for the case of intermediate – average pressure has been summarized since the time the papers [I.2, I.3] were published.

The papers concerning the main theme of the project-diagnostics of the gas discharges in supersonic air flows and flame plasma – are the only ones, which are considered below.

§ 1. Flowing high pressure plasma

Many important regimes of a probe in flowing high pressure plasma have been thoroughly investigated by the present time [I.1 - I.3]. However each case of diagnostics of various plasma objects by electrical probes has its own peculiarities.

There have appeared works devoted to the analysis of the phenomena the influence of which has been studied less in comparison with the main processes characterizing probe current. However these phenomena are of importance for probe diagnostics of gas discharges in supersonic air flows. Such gas discharges are characterized by nonsteady state of the parameters and great difference in gas and electron temperatures even at high pressure [I.5]. Moreover the significant gas heating at high electric power in the discharge leads either to the necessity of cooling a probe or restricting its exposition time in the studied discharge. In both cases probe surface temperature differs appreciably from gas temperature.

Besides the magnitude of the probe current can be influenced by the processes of ionization - recombination, including the processes with negative ions, as plasma of air and its mixture with hydrocarbon is of interest.

The results of theoretical research obtained during the considered period are studied below. We should take into account the following factors of probe interaction with plasma:

- nonsteady state of a probe – plasma system
- plasma non-equilibrium (difference between electron and gas temperature)
- probe surface temperature
- kinetics of ionization - recombination

1.1 Nonsteady state of a probe characteristic

Stationary operational modes of a probe were studied in most cases for high pressure plasmas.

Less attention was given to the study of the problem of non-stationary I–V probe characteristic. There are two reasons for non stationarity of probe characteristic to appear in the experiment: in the case of the transition of a probe from one state to another when a probe potential is modified due to an external source or when a space potential is modified in the location of a probe.

The limit on the maximum range rate ? ? ? and the limit on a spectrum of oscillations of discharge potential up to which it is possible to use the quasi-stationary theory are determined from what is mentioned above.

The similar problem was considered earlier analytically and numerically in [I.6] for a spherical probe in a limiting case ($\alpha \to 0$) of thin space charge layer. The most detailed numerical calculations have been made in [I.3] for a spherical probe in stationary plasma for the wide range of criteria parameters. The effect of probe current surge (non-monotone evolution of probe current in time) has been detected as a result of this theoretical research.

In the surveyed work [II.1] the solution of a non-stationary problem for a spherical probe with a thick space charge layer has been considered analytically for small potential. The plasma is assumed to be stationary and two-temperature, but the temperature ratio of ions and electrons $\boldsymbol{t} = T_+/T_-$ is constant throughout the space, as well as the temperatures. The chemical reactions are frozen.

The system of probe equations in a non-stationary mode in a dimensionless form has the following form:

$$\boldsymbol{b}^{-1}\, \P\, n_+/\P\, t - \tilde{N}(\tilde{N}n_+ + \boldsymbol{t}^{-1}\, n_+\tilde{N}\boldsymbol{y}) = 0 \tag{1}$$

$$\P\, n_-/\P\, t - \tilde{N}(\tilde{N}n_- - n_-\tilde{N}\boldsymbol{y}) = 0 \tag{2}$$

$$\boldsymbol{a}^2\, \boldsymbol{D}\boldsymbol{y} = n_- - n_+ \tag{3}$$

Here n_+ and n_- - ion and electron densities referred to the value of charged particles density at infinity, $\boldsymbol{y}$- the dimensionless electrical potential connected with dimensional (is counted from a potential of plasma) ratio $\boldsymbol{y} = e\,\boldsymbol{j}\,/k\,T_-$, e - charge of an electron, k- a

Boltzmann's constant, $b = D_+/D_-$ - ion diffusion coefficient to electron diffusion coefficient ratio. A time scale is R^2/D_-, a distance scale - probe radius R.

When $\alpha \to \infty$ Poisson equation (3) is transformed to Laplace equation $\boldsymbol{D}y = 0$ and equation (1), (2) become independent of each other.

If we take $\boldsymbol{y} = - ?\boldsymbol{j}\ /?T_+$ to connect dimensionless and dimensional potentials and accept R^2/D_+, as a time scale the equation (1) becomes (2). Thus it will suffice to consider the equation (2) together with Laplace equation. The analytical solution for time evolution of an electron (ion) current is expressed in terms of an integrated exponential function.

For convenience the obtained dependence $I\ (t)$ at two values of an initial potential of a probe surface $\boldsymbol{y}\ (t \pounds 0) = \boldsymbol{c}$ are presented graphically in Fig.1. The current modification pattern at small t is shown in the Figure as a separate fragment. One can see that at the
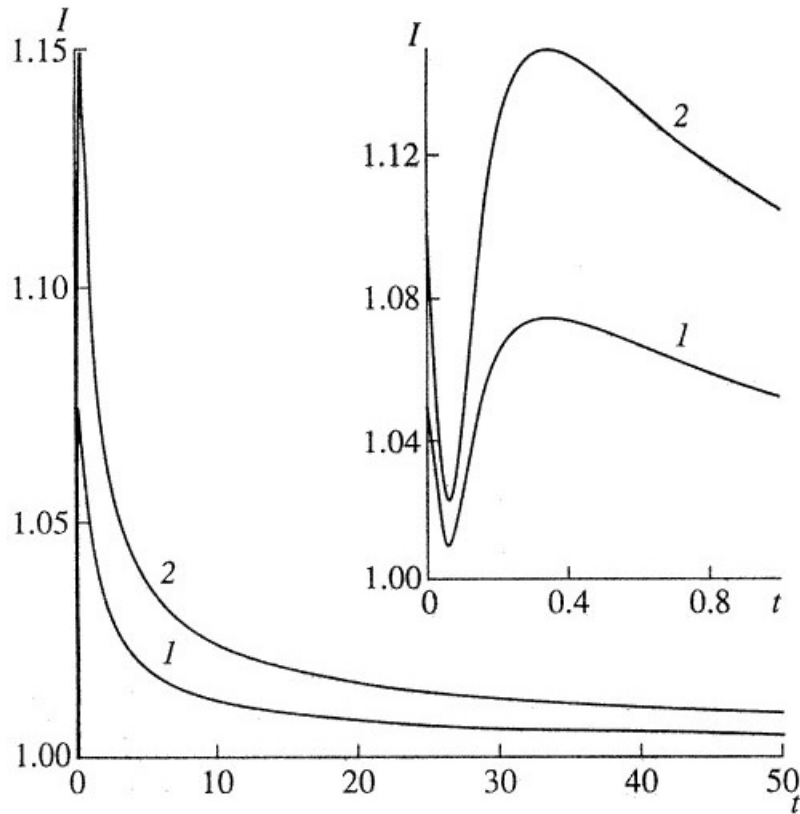
Fig.1.1. Evolution of an electron (ion) current for various initial probe potentials:

$1 - \boldsymbol{y} = 0.1, 2 - 0.2.$

first moment when a probe potential falls the current decreases sharply, then begins to increase, achieving a maximum, which magnitude exceeds the initial value $I\,(0)$. Then the current returns to the unit according to the law $\sim 1/t^{1/2}$.

Thus the found analytical solution can be used to test the numerical calculations under the complicated conditions.

1.2 Thermal analogy in the theory of electrostatic probe

The ion current of a probe in continuum plasma achieves saturation (i.e. does not depend on a probe potential) in the case of a thin space charge ($\alpha \rightarrow 0$) and enough high probe potentials. This case is convenient for diagnostics not only from the point of view of experiment, but to a larger extent for the theoretical description. It is enough to solve only one partial equation [I.7] instead of a set of nonlinear elliptical ones. It is the convective mass transfer equation for weakly ionized incompressible isothermal plasma and frozen chemical responses.

The paper [II.2] shows the mathematical equivalence of the determination of a probe saturation current and Nusselt number for the heat irradiation from the physical body having the same form.

In fact the convective mass transfer equation (the equation, which describes distribution of density n) in the dimensionless form is

$$0{,}5 \; Re \; Sc \; (u \; \tilde{N}n) - Dn = 0 \qquad (4)$$

where $Sc = v/D_+$ is ion Schmidt number. The factor 0,5 for isothermal plasma is due to the diffusion of charged particles on a probe being ambipolar.

The boundary conditions of the equation (4) for a cylindrical probe oriented across an incident flow (and a spherical probe) are

$$n\big|_{r=1} = 0 \,, \qquad\qquad n\big|_{r \to \infty} = 1 \,,$$

The dimensionless current density of saturation j is expressed by [I.10]

$$j = 2 \frac{\partial n}{\partial r}\bigg|_{r=1} \qquad (5)$$

13

Local Nusselt number, based on a diameter d cylindrical or spherical probe

$$Nu_D = \frac{\boldsymbol{a}_T d}{\boldsymbol{l}_T} = 2 \frac{\partial T}{\partial r}\Big|_{r=1} \quad , \tag{6}$$

where $\boldsymbol{a}_T$, $\boldsymbol{l}_T$ - heat-transfer and heat conductivity coefficients in a problem of convective heat exchange for an incompressible viscous liquid with permanent physical characteristics is found from a solution of the equation

$$Re\ Pr\ (u\tilde{N}T) - \boldsymbol{D}T = 0 , \tag{7}$$

where T - dimensionless temperature with boundary conditions

$$T\big|_{r=1} = 0 , \qquad T\big|_{r\to\infty} = 1 ,$$

As may be seen the two problems have become completely identical under the following simple condition

$$Sc = 2\ Pr . \tag{8}$$

Then an electrical Reynold's number $Re_e = Re\ Sc$ and Peclet number $Pe = Re\ Pr$ are correlated:

$$Re_e = 2\ Pe. \tag{9}$$

The considered thermal analogy was known previously. It seems to have been first mentioned in [I.8], but it hasn't been properly studied. Thus only the limiting cases of convection: weak influence - Re << 1 and strong influence - Re >> 1 were considered in the book [I.1]. The intermediate case was investigated in [I.9]. However heat exchange of the cylinder in a viscous liquid at the same Reynold's numbers was investigated numerically much earlier [I.10, I.11]. The calculations [I.9] would be unnecessary if the thermal analogy were well known.

The paper [II.2] has compared the results [I.9 - I.11] related to the various physical phenomena but obtained when one and the same mathematical problem is solved. The results of this comparison are shown in Fig.2.

The results of calculations of a dimensionless integrated saturation current i are presented in Fig.2 for a cylindrical probe as dependence on number Re_e, determined from a radius. Here the current i is average gradient of charged particle density on a surface of a probe

14

on the contour of the cylinder. The comparison should be made at an average Nusselt number Nu, determined from a radius.

It can be seen from Fig.1.2, the results of calculations for $Sc = 1,5$ are very close to the results [I.10] for $Pr = 0,73$.
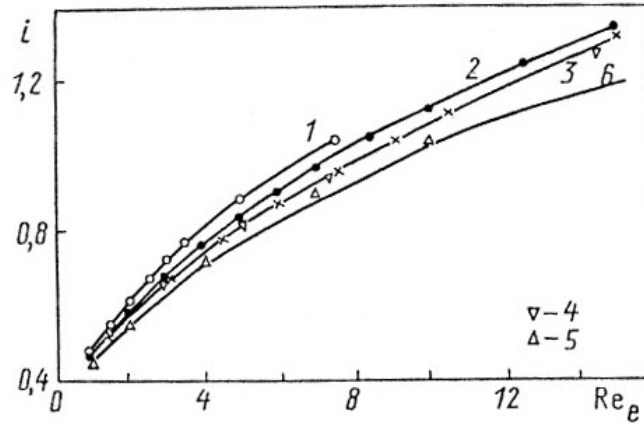
Fig.1.2. Dependence of a dimensionless saturation current on a cylindrical probe on an electrical Reynold's number.

Curves 1- 3 – the results of [I.9] 1- Sc = 0,5; 2 – 1; 3- 1,5; 4 ? 5 – re-counted results of [I.10]: 4- Pr = 0,73; 5 – 1; 6 - re-counted result of [I.12].

The formula, approximating the results of calculations at $Sc = 1$ is suggested in [I.9]:

$$i = 0,43 \, Re_e^{\,0,42} \tag{10}$$

The transition to a dimensional current I is carried out by the relation:

$$I = 4 \, p \, e \, N_\yen \, D_i \, L \, i \tag{11}$$

The formula (10) is applied only when Re_e £ 15. Complicated non-stationary and stallable phenomena occur when Re has larger values at a back surface of the cylinder. Thus it seems reasonable to use experimental data on heat exchange of the cylinder for diagnostics of plasma when $Re > 15$.

The uniform equation defining heat irradiation from the circular cylinder circulated by a transversal airflow in a range of Reynold's numbers from $5 \cdot 10^{-3}$ up to $1 \cdot 10^{5}$ is presented in work [I.12] (Re is determined from a radius). This equation is an approximation of experimental data. It can be written for saturation current as

$$i = 0,092 + 0,190 \, Re_e^{\,0,5} + 0,146 \, (Re_e/0,73)^{z} \qquad (12)$$

where $\zeta = 0,247 + 0,0476 \, Re_e^{\,0,168}$.

This equation is obtained for Pr = 0,73, that corresponds to Sc = 1,46. This dependence also is presented in Fig.1.2.

Thus, the ion density for laminar incompressible plasma is determined from saturation current in a ratio (11), for large $Re > 15$ the formula (12) should be used, and for Re_e £ 15 - formula (10).

The similar formulas of an ion saturation current for a spherical probe are:

$$I = 8 \, \boldsymbol{p} \, e \, N_{\yen} \, D_i \, R \, i \qquad (13)$$

where

$$i = 1 + 0,2 \, Re_e^{\,0,62} \qquad (14)$$

The work [II.3] devoted to the determination of a saturation current in a critical point of a probe is close to [II.2]. The probes of a more complicated construction are used along with usual cylindrical probes for diagnostics of flowing plasma. The working (conducting) surface of such probes is only a small part of a surface in a neighbourhood of a frontal critical point of the cylinder. The calculations for this case were conducted earlier by authors [I.13 - I.15] supposing that the flow along the cylinder occurs in a mode of a boundary layer, i.e. in an approximation $Re \gg 1$. It is supposed that the equations of a boundary layer at $Re \sim 1$ are incorrect. The saturation current density in [II.4] in contrast to [I.13 - I.15] was determined by a numerical solution of the full equations of plasma movement and mass transfer of charged particles in the range Re from 1 up to 70. These calculations were supplemented by the calculations [II.5]. The results of all investigations were summarized in [II.3] and the final comparison of the

16

results is shown in Fig.1.3. The comparison shows that the dependence of densities of an ion current in the critical point of a cylindrical probe obtained in an approximation $Re \gg 1$ is true for $Re \sim 1$.
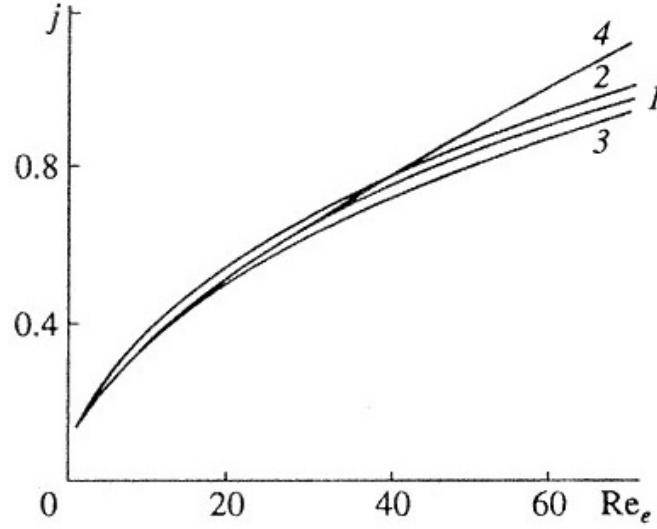
Fig.1.3. A dimensionless saturation current density in a critical point of a cylindrical probe versus an electrical Reynold's number for $Sc_+ = 1$: 1 - [I.13], 2 - [I.15], 3 - [I.14], 4 - [II.4].

The simplest analytical expression of the results for the cylindrical probe is:

$$j = 1{,}22 \; Sc_i^{\;-0.1} \; Re_e^{\;0{,}5} \tag{15}$$

where the dimensionless saturation current density j is connected with dimensional J by a relation:

$$J = e \, N_¥ D_+ \, j \, / R \tag{16}$$

The similar relation for a spherical probe obtained in [II.3] with the help of thermal analogy is:

$$j = 1{,}42 \; Sc_i^{\;-0.1} \; Re_e^{\;0{,}5} \tag{17}$$

17

1.3. The difference in electron and gas temperature

The most detailed model of an ion saturation current in collision of weakly ionized flowing plasma with the frozen chemical responses [I.7] is limited by isothermic state of plasma. However the analysis of the results for less common case made in the work [I.16] (limited by large numbers Re, but taking into account the separation of electron and gas temperatures) shows that it can lead to errors.

The temperature difference for the case of incompressible weakly ionized plasma with the frozen chemical responses is taken into account in the work [II.6].

In the frameworks of a simple model [I.16] analogous to [I.7] one can show that the dimensionless densities of electron j_- and ion saturation currents j_+ on a cylindrical and spherical probe are equal:

$$j_\pm = (1 + t^{\mp}) \frac{\partial n}{\partial r}\Big|_{r=1} \qquad .$$

Here r - dimensionless radial coordinate in terms of probe radius R, $t = T_+/T_-$. The constancy of temperatures through the field of flow is assumed by the model.

The approximating formula for a dimensionless ion saturation current is obtained in [II.6] in an approximation of cold ions, i.e. for the $t \circledR 0$:

$$i = 0.74\,(1 + t^{-1})\,Pe^{\,0.49}, \quad 1 \pounds Pe \pounds 18 \tag{18}$$

It has been obtained due to the earlier works [I.17] and [II.7] where the problem of heat exchange was considered. The numerical calculations are conducted in [II.6] for not too small t. The final relation for i is convenient to present as the dependence on an electrical Reynold number :

$$i = 0.58\,(1 + t^{-1})^{0.6}\,Re^{\,0.4}, \tag{19}$$

The dimensional current on a full surface of a cylinder is equal

$$I = 2\,\pi\,e\,N_¥\,D_+\,L\,i \tag{20}$$

The similar formulas for a spherical probe look like in an approximation of "cold" ions

$$i = (1 + t^{-1})(1 + 0.43\,Pe^{\,0.69}, \qquad Pe{\sim}1 \tag{21}$$

18

for $t ³ 1/7$

$$i = 1 + t^{-1} + 0.28 \, (1 + t^{-1})^{0.34} \qquad Re^{0.66} \qquad (22)$$

The dimensional current on a full surface of a sphere is

$$I = 4 \, \pi \, e \, N_¥ \, D_+ \, R \, i \qquad (23)$$

To get these formulas we assume the ion and electron temperatures to be constant but the assumption is not fulfilled in practice.

The temperature of electrons is changed under the influence of an electron thermal conductivity, electrical field and energy exchange between electrons and heavy particles. Thus the energy balance equation of electrons should be considered. Temperature of ions decreases in the vicinity of a colder probe surface. However numerous data (see below) show the weak influence of probe surface temperature on a saturation current for thermal equilibrium plasma. This enables us to hope to get an acceptable error when determining charged particle density in two-temperature plasma using the formulas mentioned in this paper.

1.4. Probe surface temperature influence

Theoretical description of probe operation mode in a flowing continuum plasma often supposes the probe temperature to be equal to the temperature of a flow, which is a constant in a flow field. However in experiments with plasma of high pressure the situation is different - the probe surface temperature is always considerably lower than the flow temperature. It is bounded from above by the temperature of a beginning of thermal electron emission which can noticeably destort the values of an ion probe current. Rather low temperature of a probe surface is achieved either by its forced cooling or by probe short location in plasma. As a result the diffusion coefficients of ions and electrons as well as neutral gas density are essentially changed in the flow field for a cooled probe.

The influence of these factors on the characteristics of a spherical probe in stationary plasma was studied earlier in [I.18]. And their influence on a saturation current of spherical and cylindrical probes in flowing plasma for large Re was studied in [I.13]. The effect of probe temperature on a saturation current of a spherical probe in slowly flowing

19

plasma (Re << 1) is investigated in [I.19]. So these studies have showed the weak dependence of a probe saturation current on the probe surface temperature.

The case of a cylindrical probe located in slow flowing plasma when a space charge layer is thin was considered in [II.8 - II.9]. The probe was both at moderate potentials and at large negative potentials when its current was determined by a total flow of positive and negative particles. However the probe had the temperature of a mainstream in all cases. In works [II.10 - II.11] the case when the temperature of a probe is lower than temperature of a mainstream is considered. And it is maintained constant for moderate [II.10] and large [II.11] values of potential. The ion temperature is equal to the temperature of neutral particles. Two cases similar to [I.18] are considered for the temperature of electrons: local thermal equilibrium with enclosing gas and frozen temperature of electrons. The temperature dependence of ion and electron diffusion coefficients for the case of an equilibrium is square-law: $D_+ = D_- \sim T^2$, for the case of frozen temperature $D_- \sim T$.

The calculated probe characteristics for the case of equilibrium electron temperature are presented in Fig.1.4.
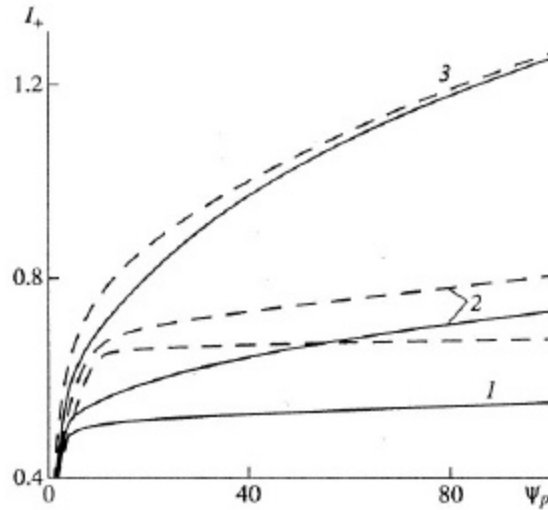
Fig.1.4. I – V characteristic of a cylindrical Lanmuir probe for $Re = 0.2$ and $T_p =$ 0.25 for the equilibrium electron temperature: 1 a = 0.001, 2 - 0.01, 3 - 0.1. Dashed lines - uncooled probe $T_p = 1$.

As it is evident the I - V characteristic for large potentials differs little from the I - V characteristic of an non-cooled probe. The more the ratio of Debye radius to the probe radius and probe potential is the less this difference is.

I - V characteristics for frozen electron temperature are shown in Fig.1.5. Their difference from I - V characteristics of an uncooled probe, just as for equilibrium temperature, is insignificant.
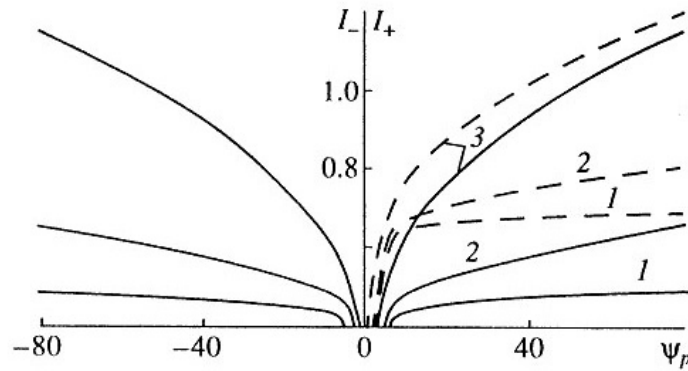
Fig.1.5. I – V characteristic of a cylindrical Lanmuir probe for $Re = 0.2$ and $T_p =$ 0.25 for the frozen electron temperature: 1 a = 0.001, 2 - 0.01, 3 - 0.1. Dashed lines - uncooled probe $T_p = 1$.

The calculated values of a probe current versus probe temperature are presented in Fig.1.6 for various potentials of a probe and relations α. It can be seen the probe current for a fixed potential depends weakly on the probe temperature though the temperature dependence is more explicit for frozen temperature of electrons.

Thus, the cylindrical probe indications in slow flowing plasma for large potentials depend weakly on probe surface temperature.
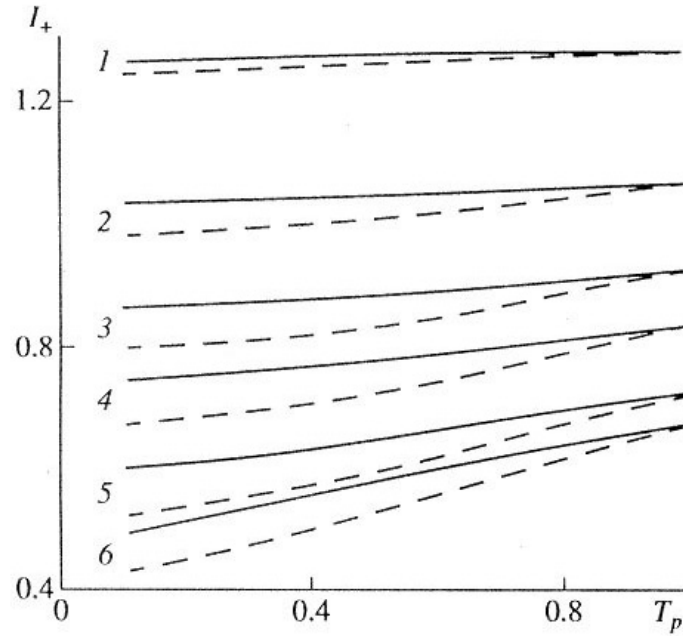
Fig.1.6. Calculated values of a probe current versus probe temperature for various probe potentials and relations a for f Re = 0.2.

Equilibrium electron temperature: 1 - $\alpha = 0.1$, $y = 100$; 2 - $y = 50$; 3 - $y = 25$;
4 - $\alpha = 0.01$, $y = 100$; 5 - $y = 25$; 6 - $\alpha = 0.001$, $y = 25$. Dashed lines - frozen
temperature of electrons.

1.5 Influence of kinetic processes

The problem of a spherical probe located in dense weakly ionized plasma, containing negative ions is considered in [II.12]. The paper examines the conditions under which the main process of primary charged particles formation is the process of volume ionization, the negative ions being formed then as the result of dissociative attachment of electrons. The reverse reactions are the processes of dissociative ion - ion and ion - electron recombination. The task parameters are the square of the relation of a Debye radius to a probe radius a^2, the square of the relation of recombination length $r_s = (D_+ / N_\infty a_e)^{1/2}$ to a probe radius $w = (r_s/R)^2$, dimensionless potential y, and also the factor which determines the amount of electrons in plasma and can be changed from zero (for completely electronegative plasma) up to unit (electropositive plasma). Both diffusion

22

and mobility coefficients, as well as the relation of ion temperature to electron are supposed to be constant.

If a^2 and w are small parameters it is convenient to use a method of sewing together asymptotic expansions. This method can be applied to a broad class of peculiar problems, the problem of an electrical probe in a mode of a continuous medium being one of them. When the problem was solved it has been shown that probe perturbed plasma is divided naturally into space charge layer, quasineutral inhomogeneous plasma and quasineutral homogeneous plasma. The width of the last area is about a probe radius, the width of quasineutral inhomogeneous plasma is about recombinational length of ions. The calculated distribution of a potential and charge particle density in the indicated areas are presented in Fig.1.7-1.8.
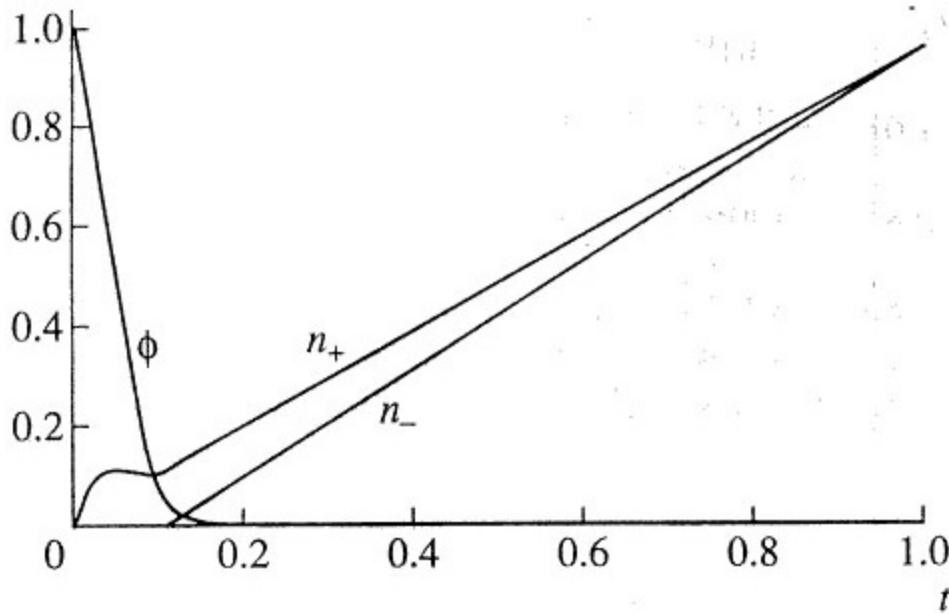
Fig.7. Distribution of charge particle density and potential in perturbed area of plasma.
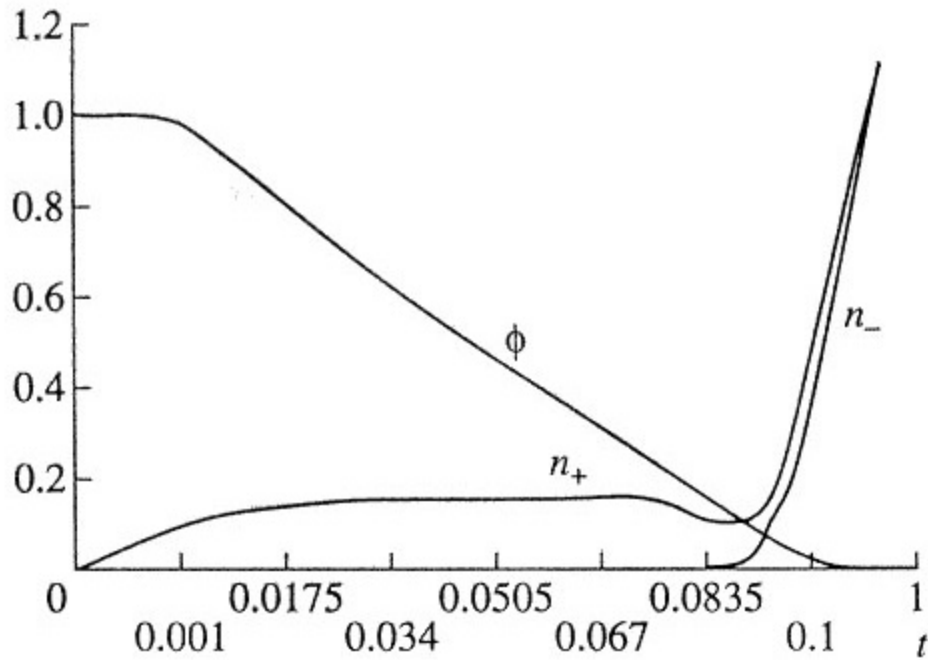
Fig.8 Distribution of charge particle density and potential in space charge layer

§ 2 Plasma of flames

For the case of a flame the spectral methods of temperature measurements of a flame and concentration of admixture atoms are usually used. The equilibrium density of electron are subsequently calculated from the Saha equation. As flame has a complex structure it is necessary to apply the probe method for diagnostics of flame plasma.

By the present time a certain progress has been made in the development of the probe theory in a mode of continuous environment. It enables to study thinner effects influencing on a probe current, such as processes of ionization and recombination of the charged particles. Thus there is an opportunity of studying physicochemical processes in flames.

The preliminary results of the theory development for diagnostics of a flame plasma with weakly ionised admixtures are considered in the paper [II.13]. The analysis is conducted with respect to the influence of various factors on the indications of a probe entered into a

flame. The influence of a convective motion of plasma on the indications of a probe is one of the factors.

The development of the theory describing a probe operation in the collision plasma with $Re_e \sim 1$ for plasma of flames was first given in [1.17]. The analytical expressions for probe saturation current for two model distributions of velocity of gas around of a cylindrical probe were obtained in it. The probe and the spectral measurements made for a flame of acetylene-air mixture with an addition agent of natrium have shown that the concentration of the charged particles found from the given formulas is 2 or 3 times as much as that calculated from the Saha equation.

Experimental works carried out previously in flame plasma with admixtures also marked the increase of the charged particles concentration and that was 100 times increase. So we can speak about abnormal currents on a probe in a flame [I.20]. As it was shown in the paper [I.20] the cause of these abnormal currents was the fact that plasma motion was not taken into account in the theory applied when interpreting probe measurements.

The research of the authors [1.17] continued in [1.9] where the saturation current on a cylindrical probe was calculated numerically for a field of velocities from Navier - Stokes equation. However the application of the improved formula has not resulted in the rapprochement of concentration found from probe and spectral measurements, on the contrary the difference has grown. Later the calculations carried out in [1.9] were confirmed when the thermal analogy (see §1, unit 1.2) from the theory of a probe was compared with experimental data on a convective heat exchange of the cylinder.

Thus the consideration of movements only appears to be insufficient to explain current increase on probe in a flame plasma.

To eliminate this discrepancy the theoretical model was extended in [I.21], the negative ions and chemical reactions between components of plasma were taken into account. The main attention was paid to the influence of negative ions on the indications of a probe. As it was carried out in [I.21] the calculations of equilibrium structure of combustion products of hydrocarbonaceous fuel have shown, that at temperature of a flame

T=2200 K (it being registrated in the experiments [I.21]) the concentration of negative ions in an incident undisturbed flow is close to that of the ions, and negative ions were the ions HCO_3^- which were not considered previously within chemical kinetics.

The presence of a plenty of negative ions in a free propane-air flame was then experimentally confirmed by methods different from the probe one [I.22-1.23].

The introduction of negative ions in the theoretical model has resulted in a good agreement between the calculated currents of saturation with experimental data [I.21]. However in the experiments [I.23] it was revealed that the agreement was violated at low concentration of the charged particles in flame when an agent of sodium was added. The formation of negative ions also doesn't explain the excess of concentration of the charged particles above equilibrium in measurements [I.9] carried out in hotter acetylene-air flame.

There are two reasons to cause the influence of negative ions directly on the indications of a probe [I.21]. The first one is connected to their additional formation because of gas cooling at the surface of a probe. It leads to the fall of an electron concentration and increase of positive ions concentration and ionic saturation current. The second one is connected to the reduction of an ambipolar diffusion coefficient, i.e. the increase of Re_e number that also increases the ionic saturation current. Nevertheless all these don't explain a divergence received in [I.9], at least, in flame with an addition agent of sodium.

The papers [II.14 - II.15] continued to consider the problems touched upon in [I.9]. An ionic saturation current is influenced by the reaction rates of ionisation of admixture atoms and recombination of the charged particles and this was considered in the papers [II.14-II.15]. If we take into account that reactions rates are finite it will result in the increase of an ionic saturation current compared with the frozen chemical reactions. The result depends on the surface the phenomena which can be shown mathematically in different types of boundary conditions on the surface of a probe. The reactions of ionisation – recombination can be to a great extent responsible for the distinction in the concentration of the charged particles in an acetylene-air flame with alkaline admixtures.

26

It is indirectly confirmed by the data [II.16] obtained for plasma of flame with addition of barium.

It is interesting to note that the calculations made in [II.14] have shown that the increase of a probe current due to chemical reactions is caused largely by a back surface of a probe than by a front one. However it is impossible to explain this discrepancy only by influence of chemical reactions. The analysis [II.13] has shown that the absence of ionisation equilibrium in a zone of measurements can be another cause for the difference of equilibrium values in ion concentration of sodium and lithium obtained from probe measurements.

§ 3. Experimental technique of probe measurements

The probe techniques usually used in the experiments have a number of disadvantages limiting their application for diagnostics of dense plasma with a great difference in electronic and ionic temperatures. They are:
$\Rightarrow$ difficulties in the use for diagnostics of the pulsed discharges,
$\Rightarrow$ a probe overheating at large plasma densities,
$\Rightarrow$ difficulties in installing a zero voltage, etc.

The strict requirements are imposed on the source of electrical probe displacement and scheme measurements by diagnostics of dense plasma and the large flows on probe particles and energy.

The paper [II.17] has offered the scheme of measuring pulsed probe diagnostics of parameter of dense gas discharge plasma. It includes a single probe, scanning generator and measuring complex. The construction of a probe is traditional: the anode of the discharge chamber is chosen as a support electrode. The scanning generator consists of two connected contours (1 - ? $_L$, R_p, VS_1, C_p and 2 - C_p, VS_2, R), controlled by keys VS_2 and VS_2 having bilateral conductivity (Fig.1.9). The short circuit of the contour 2 occurs through a probe and studied plasma. The start and maintenance of semisters in a conducting condition is carried out by a terister key forming a step of a voltage with

duration exceeding the duration of a discharge pulse. The switching on the starting terister and measuring circuits is made by the generator of the detained pulses GZI-6 with the fixed delays relative to the pulsed discharge.

The scanning generator works in the following way: in the initial state the memory capacity $?_L$ is charged up to negative potential $\varphi_?$, but the common capacity of both contours C_p is charged up to positive potential $\varphi_?$ relative to the anode. As both VS_1 and VS_2 keys are in a non-conducting state a probe-anode capacity is charged up to potential φ depending on the isolated probe potential. At the moment of keys short circuit (opening of teristers) the probe voltage $\varphi_?^*$ is determined by the signs of these three potentials.
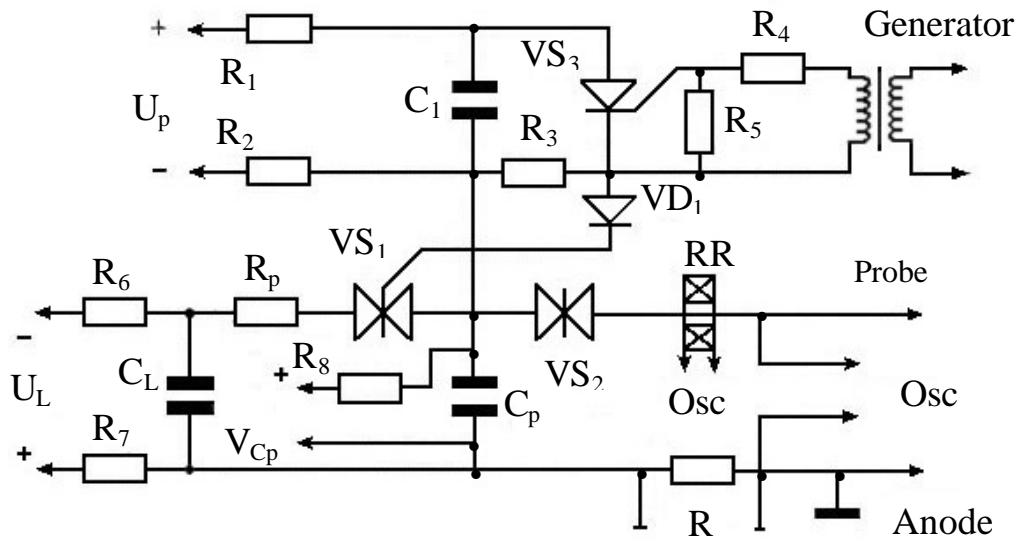
Fig.9 The probe sweep generator

Further the capacity C_p specifying voltage on a probe starts to be charged negatively both at the expense of a current of the memory capacity and at the expense of a current on a probe. The parameters of elements of the generator circuit were selected depending on the expected electronic and ionic flows on a probe determined by the concentration of ions N_i and the temperatures of electrons and ions T_+, T_-.

For example, for the pulsed high current discharge with $N_i \sim 10^{14}$ cm^{-3} and $T_- \sim 5$-20 eV the chosen parameters are: $?_L = 6$ µF, $C_p = 1,75$ µF, $R_p = 10$? m, $R = 0$, $\varphi_? = -(50-70)$ V, $\varphi_? = -(40-60)$ V. The scanning generator duration in this case runs to 20 µs. The oscillogram of a voltage pulse formed by the scanning generator is shown in Fig.1.10.
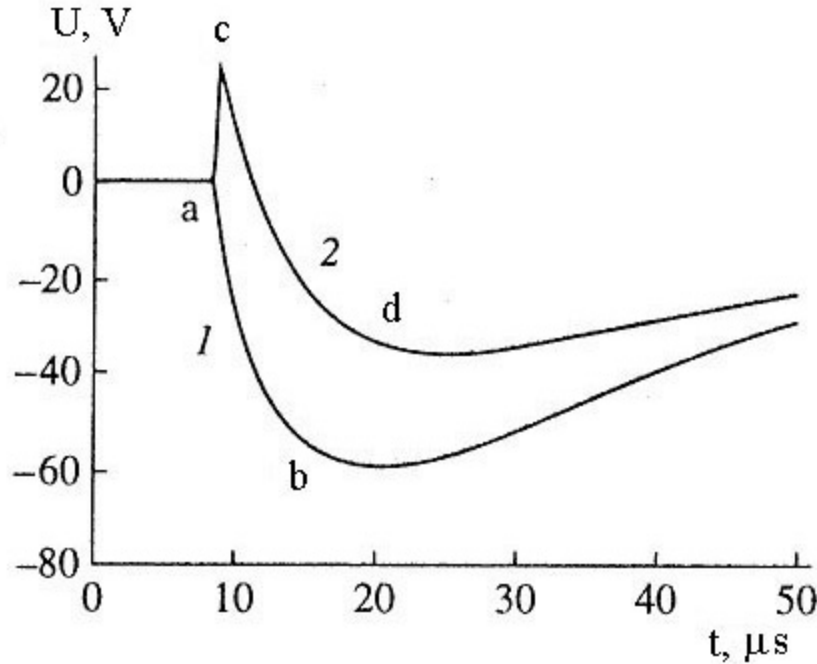
Fig.10 Oscillogram of sweep voltage for two operational modes of the circuit:
1 - the potential of plasma is lower the anode potential, 2 - the potential of plasma above the anode one (a - b), (c - d) - allotted works, where the measurements are made.

When the values of an energy flux density are high the high-speed probes have successfully been used during the recent years. The design and the scheme of controlling of such probes allow to place them into a studied area quickly (in a fractions of a second) and to remove them from it when the measurements come to an end. The research by high-speed probes with a pneumatic drive unit are being carried out on installations PISCES (USA) [I.24] and NAGDIS (Japan) [I.25], the probes with an electromagnetic drive unit are used in Germany.

29

The paper [II.18] has described the high-speed probe for measuring parameters of plasma in installation ″Lenta″ (Kurchatov institute, Russia) with the high radial resolution (30 points per 1 cm) at the energy flux density up to 100 MW/m^2 . In installation ″Lenta″ the plasma has been formed when an electron beam is passing through crossed electrical and magnetic fields.

The mobile probe is moving by gearing transfer. Alongside with a quick-response high accuracy of position can be achieved in contrast with pneumatic or magnetic drive units. The device for fast positioning of a probe consists of the moving mechanism, placed in the chamber, step-servo motor, rotation input and electrical input. The scheme of the probe moving mechanism is shown in Fig.1.11. It contains a driving shaft 3 with a gear wheel 4, mobile carriage 8 with gear 5, roller bearing 7 and directing support 6. The device provides the following parameters: complete time of a probe movement ≤0,5 s, length of a one side working course ≥80 mm. The Langmuir probe 10 made from tungsten wire is installed on the mobile carriage. The length of the probe is 5 mm, probe diameter is 0,5 mm. The ceramic insertion from alund served as electrical isolation of a probe.

The reciprocal movement of the device is performed by the step-servo motor. The shaft of the motor is connected by the coupler with the rotation input 2. The shaft rotary movement is transformed to a reciprocal movement of the carriage with a probe by the gearing transfer consisting of a gear wheel, rigidly fixed on the shaft, and gear, located on the carriage.

As the construction of the gearing cohesion is simple enough due to its own reduction it enables to choose the relation of a rod motion and the diameter of a wheel corresponding to the quick-response drive.

The smooth carriage course is provided by four roller bearings located on the directing supports. The mobile carriage and the directing supports are made of a stainless steel. Mass of the carriage is equal 700.
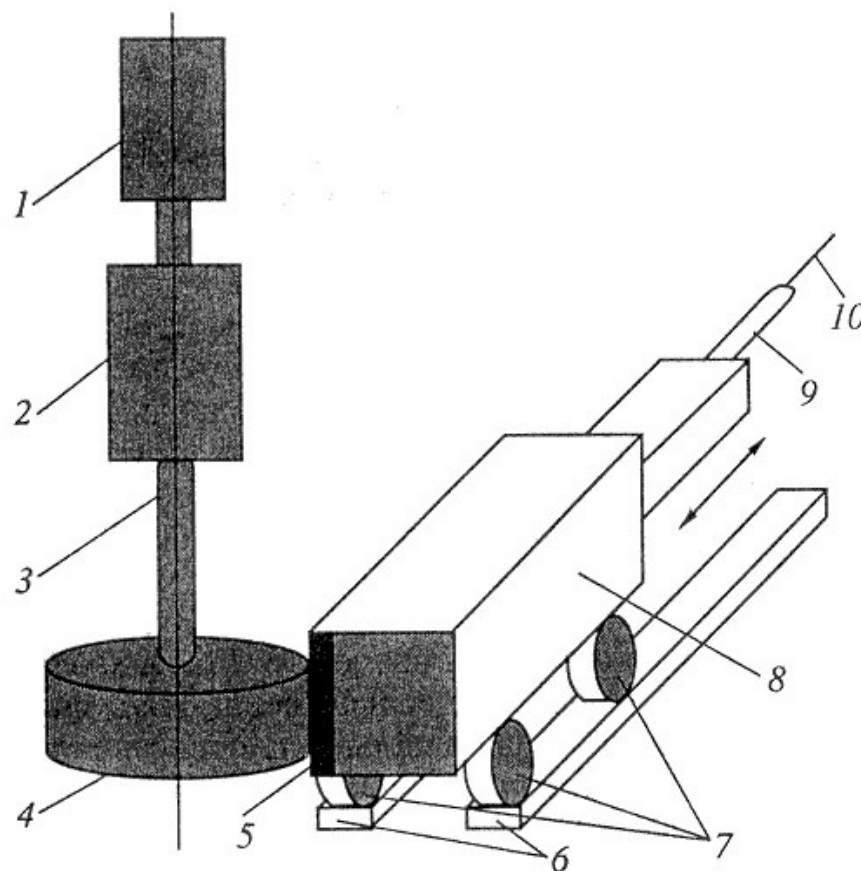
Fig.1.11 Scheme of the mechanism of probe transition.

1 - motor, 2 – silphon input of rotation, 3 - shaft, 4 - cog-wheel, 5 - rack, 6 - guide lines, 7 – frictionless bearing, 8 - movable carriage, 9 - ceramic isolation of a probe, 10 - probe.

To determine a probe location in the displacement mechanism a reohord is used. The traveller of reohord is rigidly connected to the carriage. The silvered wide sliding contacts, fixed to avoid the displacement by a brass coupler and a restricted screw are placed on the traveller.

To control a probe we use the hardware-software complex PROSCAN consisting of the computer with a plate PAC-ADC, controlling block of the probe engine, monitoring system of the device location and software. The complex enables to change and to check a direction of a probe motion, and to stop the device in the fixed place.

When the discharges formed by the field of allocated sources (antennas) are studied there is a problem of correct measurement of local plasma parameters. There are some difficulties when the Langmuir probe connected with the recording equipment by radiofrequency cables is used for this purpose. In fact the conductors placed in strong variable fields are passive electrical vibrators.

Firstly it can result in the appearance of the secondary discharges around them and that would change distribution of currents and charges on the studied antenna. By experience the influence of well conducting cables could be so strong that the structure of the antenna-discharge system and accordingly the characteristics of an emitter can be changed.

Secondly, as we detect the large variable electromotive force between plasma and the ground, the appreciable additional current deforming the true current-voltage characteristic of a probe occurs on non-linear probe layer.

The perturbations of studied system and distortion of the probe characteristics can be reduced considerably when we exclude the radio-frequency cables from construction and supply the optical control for a probe feeding and transfer of the information on a probe current and voltage into the recording equipment.

In the paper [II.19] the construction of a probe with the information transfer on a light guide and induction feeding is described. This construction in contrast with a feeding from accumulators enables to establish a voltage on a probe when the size of the data unit as a whole is small enough. Such probe was used to measure parameters of the high-frequency discharge created on the thin metal antenna at low air pressure. The antenna is a metal rod of 70 cm in length and 1 mm in diameter made in a raylon shell of 2 mm in diameter. The antenna was placed in the glass chamber of 1 m in length and 20 cm in diameter. The air pressure in the chamber is varied from 0.1 up to 1 Torr. The antenna was excited by the HF generator. with frequencies equal to 1-6 MHz.

The probe device is shown in Fig.1.12. The probe is mounted in the dielectrical ring case with external and internal diameters of 6 cm and 5 cm accordingly and height 0,5 cm.

The frame multi-coil antenna is stacked in the case and the radio-circuit is built-in. The antenna excitation is performed by a alternative magnetic field created by Helmholtz solenoids which are outside of the discharge. The detected voltage from the antenna moves on the electrodes of a probe and supplies the amplifier of a probe current. The signal from the amplifier output operates a light-emitting diode. The signal from a light-emitting diode is transferred to the photo-detector by light guide. The voltage on the electrodes of a probe is varied by the change of a magnetic field of Helmholtz solenoids.
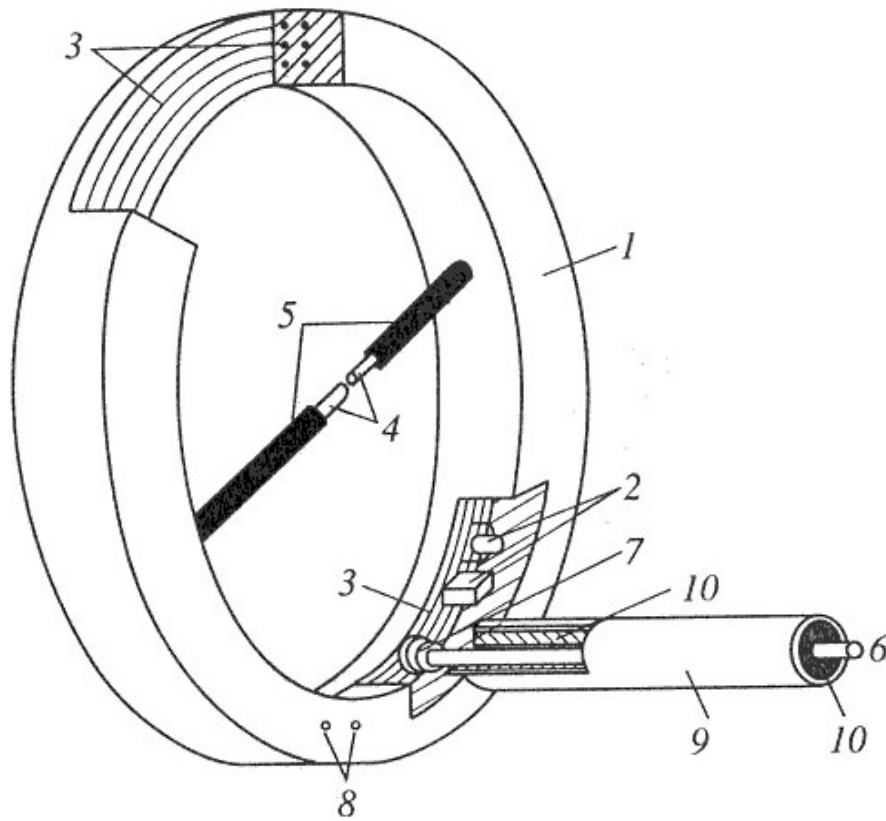

Fig.12 Probe construction.

1 - probe body, 2 - radiocircuit elements, 3 - frame antenna, 4 - probe electrodes,
5 - insulators, 6 - light-guide, 7 - light-emitting diode, 8 contacts of an external probe feed used for graduation, 9 - glass tube, 10 - light intercepting dielectric tube.

The measuring circuit was calibrated before making measurements. To registrate the calibration curves the known ohmic resistance and a microammeter were first connected to the probe electrodes. In doing so the feeding of the probe electronic circuit was performed from an external source of constant voltage that enables to establish the correlation between a probe current and the voltage on an output of the photo-detector. Then a microammeter and external feeding were disconnected, and the probe with the connected resistor was located in a field of Helmholtz solenoids. It allowed to find the correlation between a voltage of a probe feeding and a voltage on an output of the photo-detector. Two calibration curves were made based on the obtained dependencies. The first curve reflected the correlation between a voltage of the feeding generator and voltage on a probe, the second one reflected the correlation between a voltage on an output of the photo-detector and a probe current.

The high-frequency field near the antenna was directed basically on a radius. The perpendicular arrangement of electrodes to a radial component of a field has enabled to minimize a high-frequency potential difference between them.

The authors of the article [II.19] have noted that the investigated structure is very sensitive to the presence of diagnostic devices in the area of the discharge. Their presence could result in the change of number and shape of standing wave loops and lead to low-frequency modulation of the discharge, etc. These effects are easily observed even visually. The perturbations of the discharge were very strong when probes with radio engineering cables were used whereas the application of the described probe as a rule did not lead to any essential distortions in the discharge structure.

The density and temperature of plasma were measured in [II.19] by the described probe. The typical probe curve (Fig.1.13) was obtained for the following experimental conditions: pressure in the chamber is equal to 0,5 Torr, frequency of a signal stimulating the antenna f=5 MHz, amplitude of a voltage on an input of antenna is equal to 300 V, area of a probe surface S=0,5 cm^2. The values of concentration and temperature of electrons obtained accordingly to the standard procedure are equal to $N_{\text{¥}} \approx 5 \cdot 10^8$??$^{-3}$, $T_e \approx 3$ eV.
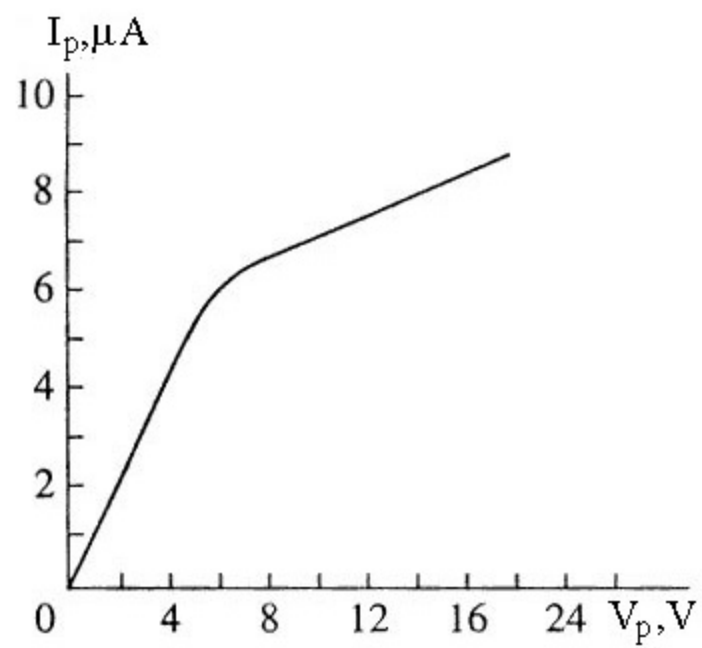
Fig.1.13 Experimental probe curve.

REFERENCES to CHAPTER I

I. Quoted references

1. Chung P., Talbot L., Touryan K. Electric probes in stationary and flowing plasmas: Theory and application. New York.springer-Verlag. 1975.

2. Benilov M.S. Theory of Electrical Probes in Flows of High Pressure Weakly Ionized Plasma (a review). High Temperature. Vol. 26, No. 5, 1988, pp. 780-793 / Teplofizika vysokih temperatur. 1988, V.26, ? 5, PP. 993-1004 (in Russian).

3. Alekseev B.V., Kotelnikov V.A. Probe method for plasma diagnostics. Moscow. Energoatomizdat. 1988. 240 p. (in Russian)

4. Tichy M., Kudrna P., Behnke J.F., Csambal C. and Klagge S. Langmuir probe diagnostics for medium pressure and magnetized low-temperature plasma. J.Phys. IV France 7, 1997. (Colloque C4, Supplement au Journal de Physique III d'octobre 1997).

5. Ershov A.P., Zorina I.G., Timofeev B.I., Chuvashev S.N. Kinetics and scaling in plasma aerodynamics. Applied physics / Pricladnay fizika. 1999. ? 5. PP.112- 122 (in Russian).

6. Cohen I.M. Transient current overshoot to electrostatic probes in continuum, slightly ionized plasmas. Phys. Fluids. 1973. V.16. N 5. P.700.

7. Benilov M.S., Tirsky G.A. On saturation currents on a probe in dense plasma. Journal of Applied Mechanics and Technical Physics /Prikladnay mehanika i tehnicheskay fizika. 1979. ? 6. PP.16 - 24. (in Russian).

8. Smy P.R. The use of Langmuir probes in the study of high pressure plasmas. Advances in Physics. 1976. V.25. N 5. PP. 517 – 553.

9. Egorova Z.M., Kashevarov A.V., Tzchai N.S. Ion saturation current on electrical probes in plasma flows at small Reynold's numbers. Journal of Applied Mechanics and Technical Physics/ Prikladnay mehanika i tehnicheskay fizika. 1990. ? 1. PP.159-163 (in Russian).

10. Dennis S.C.R., Hudson J.D., Smith N. Phys. Fluids. 1968. V.11. N 5. P.933-940.

11. Apelt C.J., Ledwich M.A. J. Fluid Mech. 1979. V.95. N 4. P.761-777.

12. Fund R.M., Kesvani K.K. Int. J. Heat Mass Transfer. 1972. V.15. N3. P.559-562.

13. Benilov M.S., Rogov B.V., Tirsky G.A. Theoretical determination of an ion saturation current on electrical probes in subsonic flows of plasma. High Temperature/ Teplofizika vysokih temperatur. 1981. V.19. ? 5. PP.1031 - 1039 (in Russian).

14. Chen Xi. Ion saturation current density and specific heat flux on a cylindrical probe immersed in a dense plasma flow. J. Phys. D: Appl. Phys. 1982.V.15. N 9. PP.1695 - 1708.

15. Roter V., Bergman F. Measurement of an ion saturation current by cylindrical probes in high-current argon arc at atmospheric pressure. ? ??. Physics and technique /engineering/ of low temperature plasma. Minsk. Proc. ITM A.V.Likova.1977.P.62 (in Russian).

16. Lam S.H. A general theory for the flow of weakly ionized gases. AIAA J. 1964. V.2 N2. P.256.

17. Egorova Z.M., A.V. Kashevarov, Fomina E.M., Tzchai N.S. On a measurement of charged particle density by a cylindrical Langmuir probe in a flame plasma. High Temperature / Teplofizika vysokih temperatur. 1988. V. 26. ? 3. PP. 577- 581 (in Russian).

18. Chapkis R.L., Baum E. Theory of a cooled spherical electrostatic probe in a continuum gas. AIAA J.1971.V.9. N10. P.1963.

19. Benilov M.S., Rogov B.V., Tirsky G.A. On an ion saturation current on an electrical probe in slowly flowing plasma. Journal of Applied Mechanics and Technical Physics / Prikladnay mehanika i tehnicheskay fizika. 1982. ? 3. P.5 (in Russian).

20. Clements R.M., Smy P.R. Anomalous currents to a spherical electrostatic probe in a flame plasma. J. Phys. D. 1969. V.2. N11. P.1731.

21. Benilov M.S., Kosov V.F., Rogov B.V., Sinelshikov V.A. Saturation currents on electrical probes in flows of chemical reacting plasma with different kinds of ions.

High Temperature/ Teplofizika vysokih temperatur. 1987. V.25. ? 3. P.573 (in Russian).

22. Benilov M.S., Grine V.M., Lash A.A. Reduction of electron density in plasma of products of combustion in consequence of formation of negative ions. High Temperature / Teplofizika vysokih temperatur.1991.V.28. ? 3. P.620 (in Russian).

23. Kosov V.F., Molotkov V.I., Nefedov A.P. Measurements of charge particle density in plasma of products of combustion by electrical probe methods. High Temperature / Teplofizika vysokih temperatur. 1991. V.29. N4. P.633 (in Russian).

24. LaBombard B., Conn R.W. Preprint UCLA-PPG-1228, 1989.

25. Ezumi N., Ohno N., Vesugi Y. et al. Proc. Of 24th European Conference on Controlled Fusion and Plasma Physics. Berchtesgaden. Germany. 1977.v.21A.Part III.p.1225.

II. Review references

1. Kashevarov A.V. A Problem of Nonstationary Theory of Electric Probe in Collision Plasma: Analytical Solution High Temperature / Teplofizika vysokih temperatur. 2000. V.38. ? 1. PP.147-164 (in Russian).

2. Kashevarov A.V. Thermal analogy in theory of Langmuir probe. Engineering-Physical Journal / Ingenerno – fizicheskiy zurnal. 1995. V.68. ? 4. PP.629-632 (in Russian).

3. Kashevarov A.V. On a saturation current density in a critical point of an electrical probe. High Temperature/ Teplofizika vysokih temperatur. 1995. V.33. ? 1. PP. 140 – 144 (in Russian).

4. Kashevarov A.V. On probe measurements in a flame plasma. High Temperature / Teplofizika vysokih temperatur.1992. V.30. ? 6. P. 1220. (in Russian).

5. Kashevarov A.V. Mechanics of a Liquid and Gas //Mehanika jidkosty i gaza.1994. ? 1. P.43. (in Russian).

6. Kashevarov A.V. Electric-Probe Diagnostics of Two-Temperature Collision Plasma High Temperature / Teplofizika vysokih temperatur. 1999.V.37. ? 1. PP.150-163. (in Russian).

7. Kashevarov A.V. Exact solution of a problem of convective heat exchange for an elliptical cylinder and plate in a liquid with small Prandtl number. Mechanics of a Liquid and Gas /Mehanika jidkosty i gaza. 1996. ? 3. P.26 (in Russian).

8. Egorova Z.M., Kashevarov A.V. On volt-ampere characteristic of a cylindrical Langmuir probe in a slowly flowing plasma. Journal of Applied Mechanics and Technical Physics / Prikladnay mehanika i tehnicheskay fizika. 1993. ? 2. PP.3-10 (in Russian).

9. Kashevarov A.V. Volt-ampere characteristic of a cylindrical Langmuir probe in a slowly flowing plasma at large probe potentials. High Temperature / Teplofizika vysokih temperatur. 1994. V.32. ? 2. PP.173-176. (in Russian).

10. Egorova Z.M., Kashevarov A.V. Cooled cylindrical Langmuir probe in a slowly flowing plasma. Journal of Applied Mechanics and Technical Physics / Prikladnay mehanika i tehnicheskay fizika. 1994. V.35. ? 4. PP.3-12. (in Russian).

11. Kashevarov A.V. Characteristic of a cooled cylindrical probe in a slowly flowing plasma at large potentials. High Temperature / Teplofizika vysokih temperatur.1996. V.34. ? 4. PP.519-524. (in Russian).

12. Bektursunova R.M., Kunakov S.K. Asymptotic theory of an electrostatic probe in a weakly ionized plasma with negative ions. Plasma Physics Reports /Fizika plasmi. 1999. V.25. ? 11. PP.993-997. (in Russian).

13. Kashevarov A.V. The Use of Electric Probes for Diagnostics of Seeded Flame Plasma. High Temperature/ Teplofizika vysokih temperatur. 1998. V.36. ? 5. PP.700-705. (in Russian).

14. Egorova Z.M., A.V. Kashevarov , Chai N.S. On an ion saturation current on electrical probes in a flame plasma with an alkaline dope /additive/. High Temperature / Teplofizika vysokih temperatur.1992.V.30. ? 3. P.448. (in Russian).

15. Kashevarov A.V. On the influence of recombination kinetics to a saturation current of Langmuir probe in a flame plasma with a dope. High Temperature / Teplofizika vysokih temperatur. 1994. V.32. ? 1. PP.12-15. (in Russian).

16. Egorova Z.M., Kashevarov A.V., Chai N.S. Determination of charged particle density in a flame plasma with a dope of barium. High Temperature/ Teplofizika vysokih temperatur. 1993. V.31. ? 2. P.190. (in Russian).

17. Mozgrin D.V., Fetisov I.K., Hodachenko G.V. Impulse probe technique for determination of plasma parameters of high current diffuse low pressure discharge. Plasma Physics Reports /Fizika plazmy. 1999. V.25. ? 3. P.283-288. (in Russian).

18. Kurnaev V.A., Litnovsky A.M., Petrov V.B., Staina T.A., Hripunov B.I., Chernyatev Yu. V., Schapkin V.V. High-speed probe for a measurement of parameters of plasma with high power flux density. Instruments and Experimental Technique / Pribory i Technika Experimenta. 1999. ? 5. P.153-156. (in Russian).

19. Bazanov V.S., Smirnov V.A., Umnov A.L. Langmuir probe for undisturbed diagnostics of parameters of plasma HF discharge in a near field of antennas. Instruments and Experimental Technique / Pribory i Technika Experimenta. 1999. ? 3. P.112-115. (in Russian).

CHAPTER II   EXPERIMENTAL SETUP

§ 1. Draft scheme of the experimental setup

Draft scheme of the experimental setup for development and testing of diagnostic methods is shown in Fig.2.1. The experimental setup is built around a stainless steel cylindrical gas/vacuum chamber. The chamber is three meters long and one meter in diameter. It consists of two sections that can form a vacuum-tight junction with help of a lever-operated gate.   At the installation and adjustment of diagnostic and experimental equipment inside the chamber its section can be easily separeted. Twenty-six windows with different diameters (10-50 cm) are located on its lateral surface, that allows to visualize discharge processes and to provide the vacuum-tight transport of electric current and electric signals.

The supersonic channel was mounted along chamber's vertical diameter. The outside end of the channel was connected with the compressor through the electric valve. A vacuum pumps allow to achieve a pressure into chamber up to 1 Torr. Supersonic flow was formed in the test channel (or in the chamber) by opening an electric valve and filling with the air or air-propane mixture through a converging-diverging nozzle with Mach number M = 2. A cylindrical dielectric nozzle had diameter of its critical cross section 15.4 mm and an outlet diameter 26 mm.

The pressure in the gas/vacuum chamber was varied in a range p = 10 - 500 Torr. The pressure in the receiver of the compressor was varied in a range p_0 = 1-10 atm. The flow duration was about 1 - 2 seconds.

The experiments were carried out for the direct current (DC), pulse-periodic (PP) discharges and pulse plasma jets.

The DC discharge was fed by a controlled electric power source with voltage up to 5 kV and current up to 10 A.

The pulsed periodic discharges was fed by a power supply unit with voltage up to 24 kV, current up to 40 A, pulse duration 1 - 500 μs, repetition rate 1 - 1000 Hz, maximal pulsed power up to 1 MW and average power consumption about 1 kW.

The plasmadynamic discharge was created with use of a magnetoplasma compressor type electrode unit. The pulse energy was stored in a100 µF capacitor which was charged by the power supply unit up to the voltage of 5 kV. The pulsed discharge switch joined the capacitor and magnetoplasma compressor type electrode unit.

The valve and power supplies (and also recording equipment) was controlled the system of a synchronization (see §3, on the block scheme is not shown).

The complex of diagnostic methods was used for a measurement of microscopic parameters of the discharges:

- schlieren method
- high-speed photography
- probe method
- spectroscopic methods
- microwave method

A schlieren setup was used for the supersonic airflow visualization.

High-speed photography was used for the investigation of dynamics of pulse-periodic discharge.

The electrical probes were used for a measurement of a plasma density, floating potential and electric field in plasma. The special scheme of a PC-controlled double probe with an optocouple galvanic isolation on base of a fiber optical waveguide was performed in frame of project. Measured signals were registered by the digital oscilloscope based on module of analog input / output and two-channel broadband submodule of analog input ADM212 50 M with personal computer IBM Pentium III, and also digital storage oscilloscope Tektronix TDS-210.

In the second type of the circuit the optical output is formed with an optocoupler, and the exchange of signals with the computer is carried out through standard computer cable. The voltage between the probes at the measurement of the probe characteristics was changed stepwise by the computer.

A PC-controlled analyzer of optical spectra based on a spectrograph was used for registration of plasma radiation spectra. The sensor of plasma radiation based on CCD

image sensor Toshiba TCD 1300D forms a video signal directly proportional to the radiation intensity in the spectral band 300 – 900 nm. The measured spectra were used for determination of gas temperature and electron density.
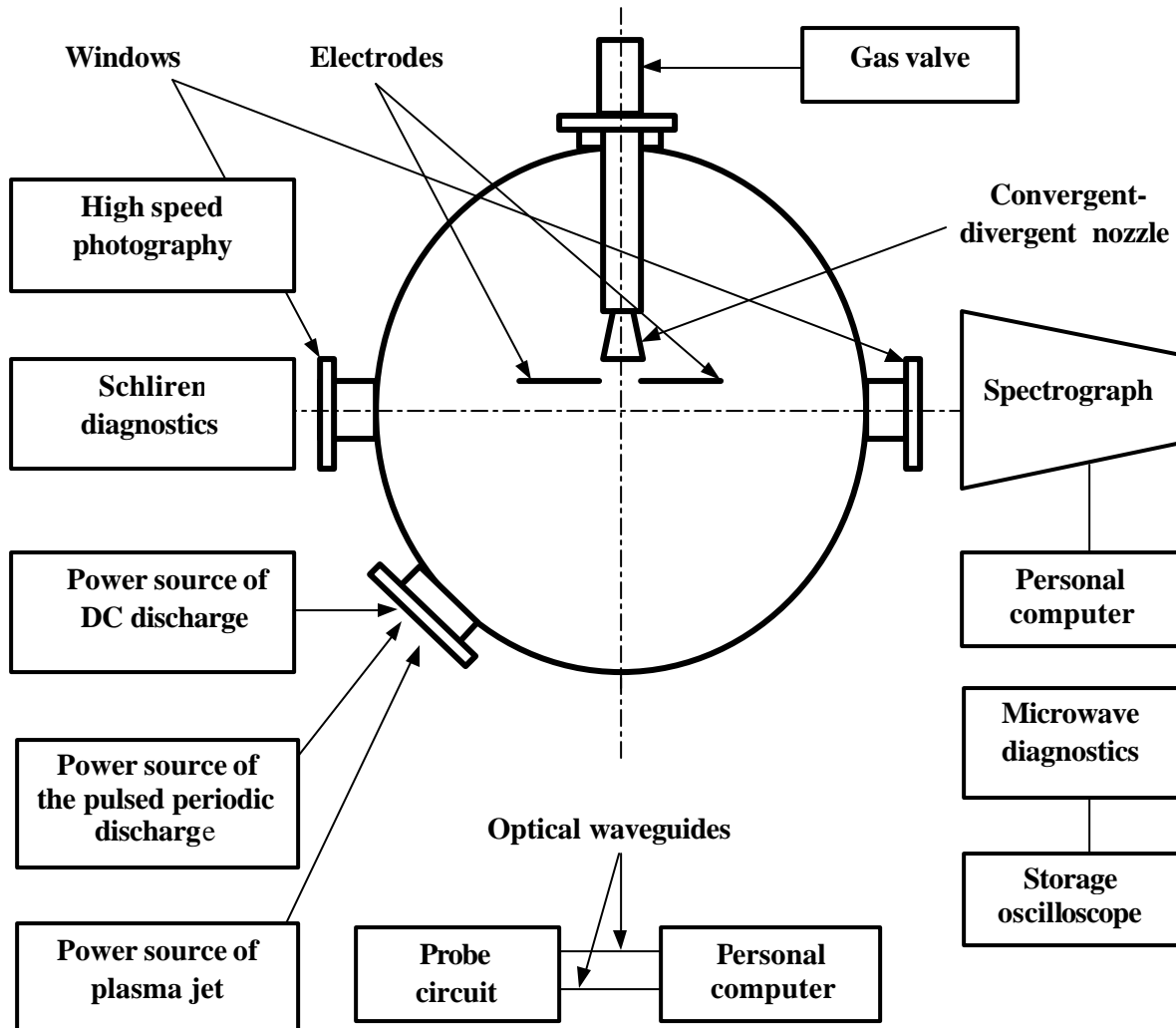
Fig.2.1. Draft scheme of the experimental setup.

For independent measurements of plasma electron density, a microwave (λ = 8 mm) interferometer was used. Double-beam pulsed storage oscilloscopes C8-17 with a pass band 10 MHz and sensitivity 1 mV/cm were used for registration of wave-form of the microwave interferometer signals.

§ 2. Air duct

2.1 The test channel

Study of plasma formation under electrical discharge is conducted in round cross section duct (Fig.2.2.), which is varied along the length and consists of:

- section where mixing of air and fuel is provided;
- supersonic contoured nozzle of nominal M= 2.0;
- insulator section of constant 23 mm diameter (constant cross section F_{ins}) and 150 mm maximal length;
- combustor section of constant cross area $2F_{ins}$.

The test channel was mounted in vacuum chamber and fixed to flanges of chamber windows, but the position of channel along the vertical axis could be changed, providing possibility visual observation of flow field and discharge in channel and measurements of gasgynamic flow parameters. To provide starting of duct and on-design flow regime the initial pressure in vacuum chamber was decreased down to $\sim 5 \times 10^{-3}$ bar and it was increased during the run affecting on flow in isolator section. In so doing time of the run is defined by the time of filling the vacuum chamber of 3 m^3 volume.

Gaseous fuel is supplied into the mixer in channel receiver installed and is mixed with air mainly before the nozzle critical cross section. In accordance with the preliminary researches mixing completeness of considered mixer is approximately 95-98 % as mixing process is realized by four-staged consecutive mixing of supplied fuel with swirl air flow, injected with the velocity on the level one up to 100 m/s. Receiver diameter was accepted equal to 64 mm according to conditions of placement and effective operation of mixer. The angle of nozzle subsonic part is equal to 45 degrees. Nozzle exit diameter was chosen equal to 23 mm and based on condition that inner diameter of quarts combustor tube is 34 mm and insulator cross section area is one half of combustor area. Diameter of nozzle critical cross section inserts is chosen equal to 17.0 mm with taking into account of boundary layer thickness. Fuel/air mixture is accelerated in supersonic nozzle and further comes along the insulator section of 150 mm maximum length. Radiuses of subsonic and supersonic parts of nozzle insert were accepted equal to 14 mm and 4 mm correspondingly. Nozzle
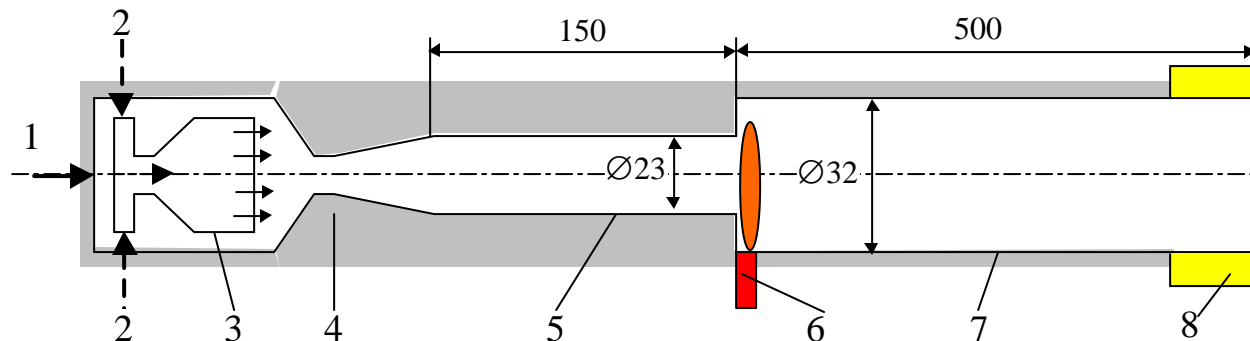
Fig.2.2 Schematic of test channel

1 – fuel supply, 2 – air supply, 3 – mixer, 4 – supersonic nozzle, 5 – section ? 1 («insulator»), 6 – plasma generator, 7 – combustor (section ? 2), 8 – measurement section
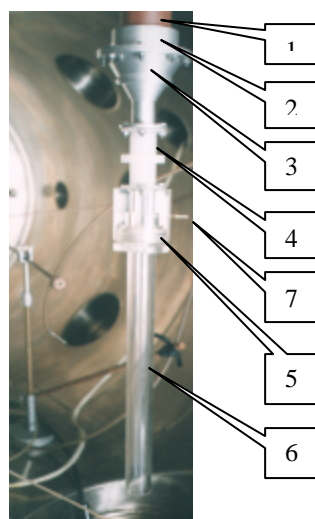
Fig.2.3. Photo of the test channel in installed vacuum chamber

1 – subsonic part of the channel, 2 – mixer, 3 – receiver, 4 – insulator channel, 5 – connecting unit (discharge chamber), 6 – combustor, 7 – electrodes of plasma generator

inserts were manufactured from aluminum alloy. Insulator involves the section from insulated and radio-transparent (plexiglas) material manufactured. This section is used for connection of insulator channel and quartz combustor tube and for installation of plasma generators. The centering and fixation of quartz tube is provided by ribbon sealings.

The constant area section (#2), that is combustor, following the insulator section was manufactured from quartz tube of 32 mm inner diameter and ~ 4 mm wall thickness for visualization of flow field and electric discharge. The area of #2 section is increased two times in comparison with insulator section to avoid heat choking in case of air/fuel mixture combustion.
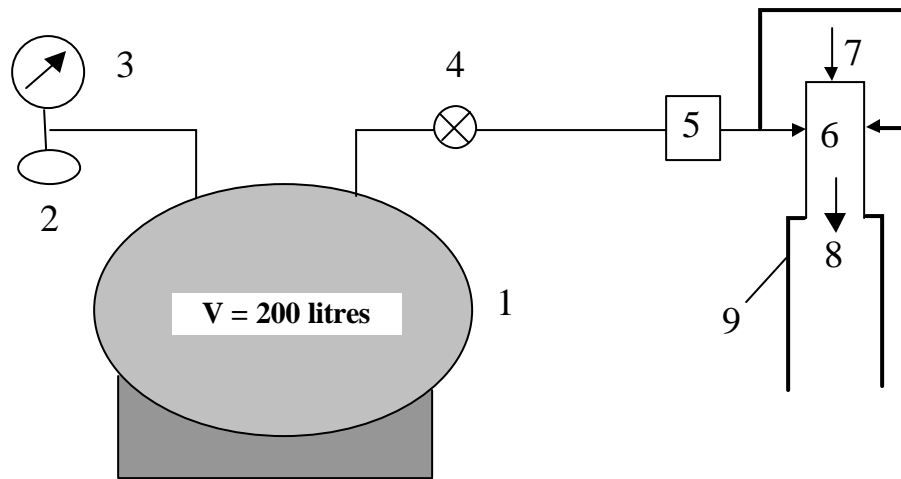
2.2 Air storage and supply system.

This system involves (Fig.2.3):

- vessel of 200 litres volume with compressor device on it installed, which increases the air pressure up to 12 bar;

- reducer, manometer and pressure gauge;

- electric valve of time operation $\tau \sim 1$ms.

Air system provides quasi-stable flow regime during 1-3 seconds at ambient total temperature and total pressure Ptr=2-6 bar. For the regime when Ptr=1 bar the air supply system provides the air into the test channel during 1-3 seconds through electric valve on vacuum chamber installed. In case of regime when air pressure more than atmospheric one the electric valve is connected to the air high-pressure system.
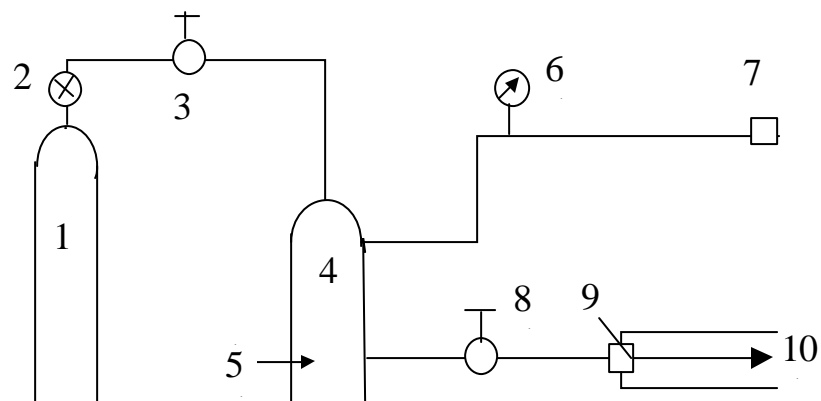
2.3 Fuel storage and supply system

The propane supply system consists of a standard propane tank, the gasification vessel, valves, injector and mixing chamber (Fig. 2.4.). The gasification vessel is needed for providing definite initial gas pressure and for determination of propane flow rate. The necessary level of the flow rate is changed mainly by means of throttling orifice diameter at the injector entrance. The orifice diameter is diminished when combustor fuel/air equivalence ratio β of mixture is large (d$\approx$2 mm at $\beta$$\approx$0.5). In this case pressure in gasification chamber is sufficiently large (4-8 bar) for nearly constant fuel flow rate during the test run (2-3 sec) and the exact pressure drop measuring is possible.

Fig. 2.4. Schematic of air high pressure system
1 – compressor and high pressure air tank ($P_t \leq 12atm$), 2 – pressure gauge, 3 – manometer, 4 – locking tap, 5 – electric valve, 6 – air to channel, 7 – fuel, 8 – to mixer, 9 – test channel

Fig. 2.5. Schematic of fuel storage and supply system
1 – fuel balloon (V=50 liters), 2 – locking tap, 3 – reducer (control valve), 4 – fuel receiver (V=10 liters), 5 – Ch-? thermocouple, 6 – manometer, 7 – pressure gauge, 8 – electric valve (Di=6mm), 9 – fuel throttling nozzle, 10 – fuel into the mixer

Fuel injector and mixing chamber have some swirlers to provide homogeneous mixture resulted at rather large air pressure drop ($\Delta p_c/p_c \approx 10\%$). Connector manifolds – flexible or steel - are used between the fuel tank, valves and injector. Inner diameter of fuel pipe is 6 mm, excepting local contractions in valves and in throttling unit.

Fuel supply system operates by the next steps: 1 – to suck off the air from the gasification vessel, 2 – to fill this vessel by the gaseous fuel through the reducing valve till working pressure, 3 – to wait some time till the gas takes room temperature in closed volume, 4 – to open the electric valve during the run time.

Tests of fuel system were conducted and it was concluded this system is ready for researches with required fuel/air mixtures.

2.4. The schlieren setup

The schlieren setup was used for determination of a flow structure and Mach numbers. The optical schematic of setup is given in a Fig.2.6 . Xenon or incandescent lamps (1) were used as sources of light. The pulse duration of light is equal 1 μs, if xenon lamp was used. The lamp radiation with the help of lens optics was focused on entrance aperture of setup (2). The area of a round aperture was equal 1 mm^2. Aperture was placed in focal plane of a long-focus objective (F = 1500 mm) (3), forming light beam by diameter 15 cm. Illumination of beam on the sectional area was uniform. The axis of symmetry of light beam was superposed with centers of windows of pressure chamber (4).

After pressure chamber the light beam was focused on exit aperture (5) by the long-focus lens (F = 1500 mm) (3a). The sectional area of exit aperture was equaled 1 mm^2 too. A schlieren picture was registered by the camera (6).

The synchronization of xenon lamp was realized from camera. The special metal wedge was located along axis of flow in area of light beam for visualization and definition of Mach corner.
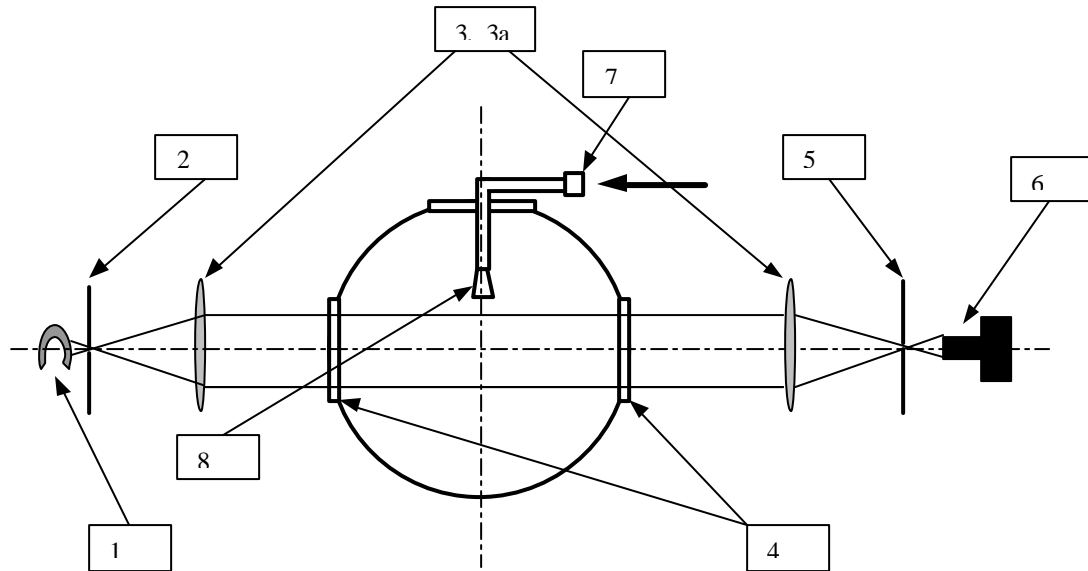
Fig.2.6. The optical schematic of schlieren setup:

1 - xenon or incandescent lamps; 2 - entrance aperture; 3 - long-focus objective; 3a - long-focus lens; 4 - windows; 5 - exit aperture; 6 - camera;　　air from receiver of compressor; 7 - pneumovalve; 8 - Laval nozzle.

The various modes of the outflow and structure of stream were investigated. The various modes of setup operations are shown in Fig.2.7 as an example. One can see that influence of electrodes, which were placed near to outflow face of Laval nozzle, on structure of stream is rather essential.

The Fig.2.7.a and 2.7.d correspond to modes of nozzle operations with overexpansion, when the pressure in outflow face of nozzle is less than pressure of air in pressure chamber. The oblique shocks departing from electrodes and units of their fastening are well visible in Fig.2.7a especially. The Fig.2.7.c correspond to mode of nozzle operations with underexpansion and Fig.2.7.b correspond to rated conditions of nozzle operations. The influence of electrodes and units of their fastening inside of nozzle on structure of flow is expressed rather strongly in all cases.

c   d
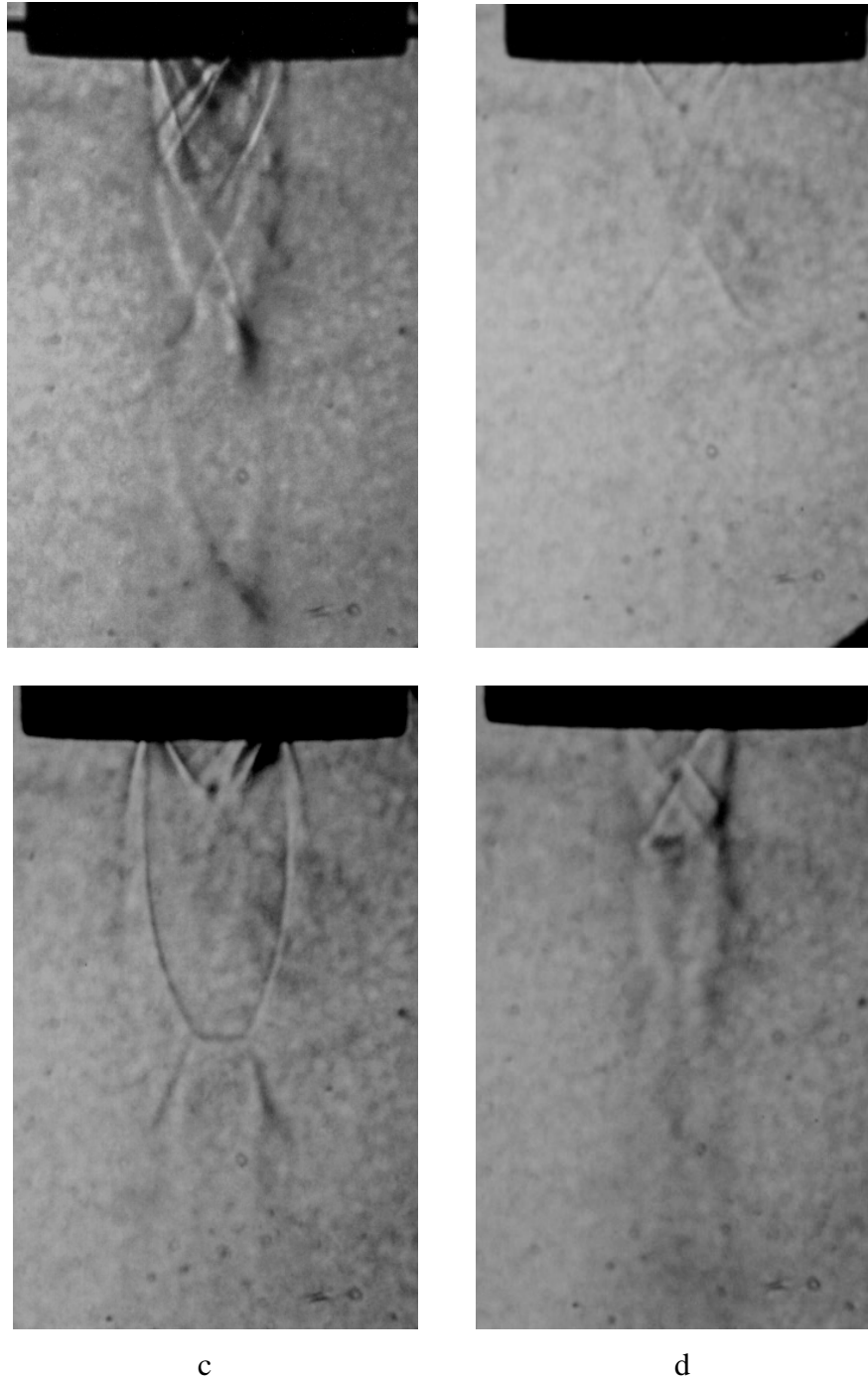
Fig.2.7 Schlieren picture of flow

a – The pressure of air in pressure chamber.P = 200 Torr (with electrodes), the
pressure in receiver of compressor $P_0 = 4$ atm.;

b - P = 100 Torr (without electrodes), $P_0 = 1$ atm.;

c - P = 100 Torr (without electrodes), $P_0 = 4$ atm.;

d - P = 500 Torr (without electrodes), $P_0 = 4$ atm.

§3. Synchronization and Power Supply Systems

The total system of synchronization, which has been applied in the current installation, made it possible to carry out experimental measurements in three independent work regimes: a pulsed periodical regime for the electrode plasma discharge power supply, a single pulse regime for plasma generation by the pulsed plasmatron, and a regime of the DC plasma discharge.

3.1 The electronic circuit of switching on of the airflow valve

The electronic circuit of switching on of the airflow valve was the main control element at all the three regimes of the system of synchronization. Draft temporary dependencies for parameters in this electronic circuit are presented in Fig. 2.8.
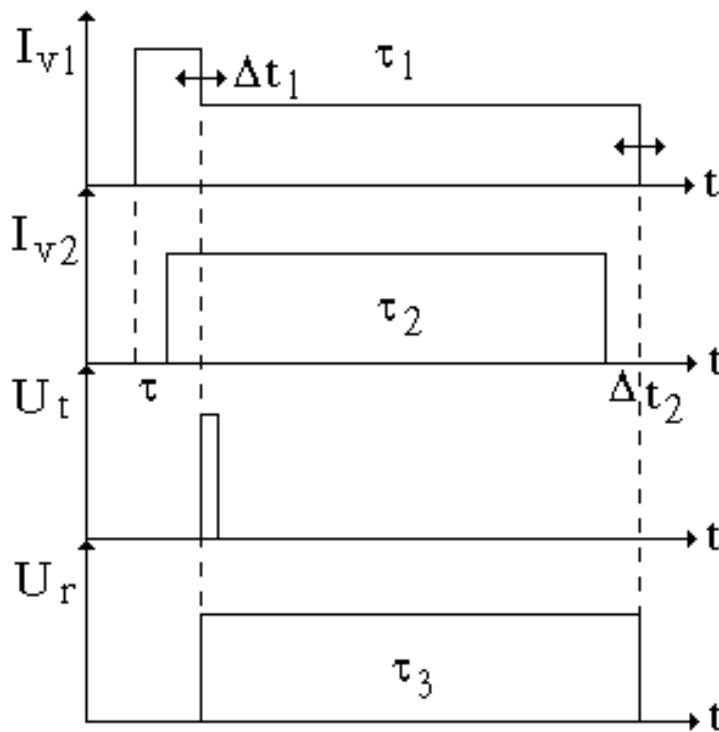
Fig.2.8.

As the trigger button was on, the electron relay reacted, a current I_{v1} appeared in the winding of the air valve magnet, and the valve was set open. Some $\tau \sim 0,2$ s later, another electron relay supplied the valve of the gas flow, current I_{v2} appeared in its winding, and the gas valve was also set open. As the magnet starting current exceeded the magnet normal current, one more relay switched on an additional resistance sequentially with the magnet winding with a delay Δt_1. This very relay produced

either a τ_3-long pulse, which switched on the high-speed photo camera, or a 100-μs pulse, which switched on the synchronization scheme (U_t) (in case of measurements without photographic registration). The delay between the moments of opening the valves and the pulse of switching on the synchronization scheme was $\Delta t_1 = 0,1 \div 1$ s. It was chosen to meet the condition of achievement of the steady flow of air or the gas-air mixture. The time period when the air valve was open, and that of the gas valve, could be varied in a range of $\tau_1 = 1 \div 5$ s. The gas valve always was opened a little later and closed $\Delta t_2 = 0,2$ s earlier than the air valve, and a condition $\tau_1 > \tau_2$ was always met. The working period τ_3 of the high-speed photo camera was practically equal to the time period when the air valve was open.

3.2 Scheme of synchronization for the pulsed periodical discharge

A schematic diagram of synchronization for the pulsed periodical discharge regime is presented in Fig.2.9. Consider at first the option of measurements without photographic registration.

The starting pulse was generated by the electronic circuit of opening the valves (1), it entered the input of the multi-channel delay generator (2), which made it possible to control continuously (with a discretion of about 2 ms) the delay of an output pulse relatively an input pulse. The delayed output signal ($\tau \sim 0,2\mu$s long) entered the input of the system of control of the synchronization circuit, which contained two units: the control circuit itself (4), and a pulse generator with a stable repetition rate (3). Synchronization pulses were generated in two independent outputs of the control circuit, they entered the starting inputs of intermediate generators ? - 5 - 54 (5) ? ? - 5 - 27? (12).

The signals from the first generator (5), on the one hand, switched on the control oscilloscope (11), on the other hand, switched on (with a certain delay in a range of 40 $\div$ 80 μs) the input stage of the generator of high voltage pulses. The amplified signal from the input stage entered the cathode follower (7), then the modulator driver (8), the signal of which switched on the output modulator (9). The modulator generated 5 $\div$ 25-kV pulses, which were transported to the electrode unit (10) through a coaxial cable. The pulse duration was controlled by the generator ? -5 -54 (5), it could be varied in a range of 1μs...1 ms.
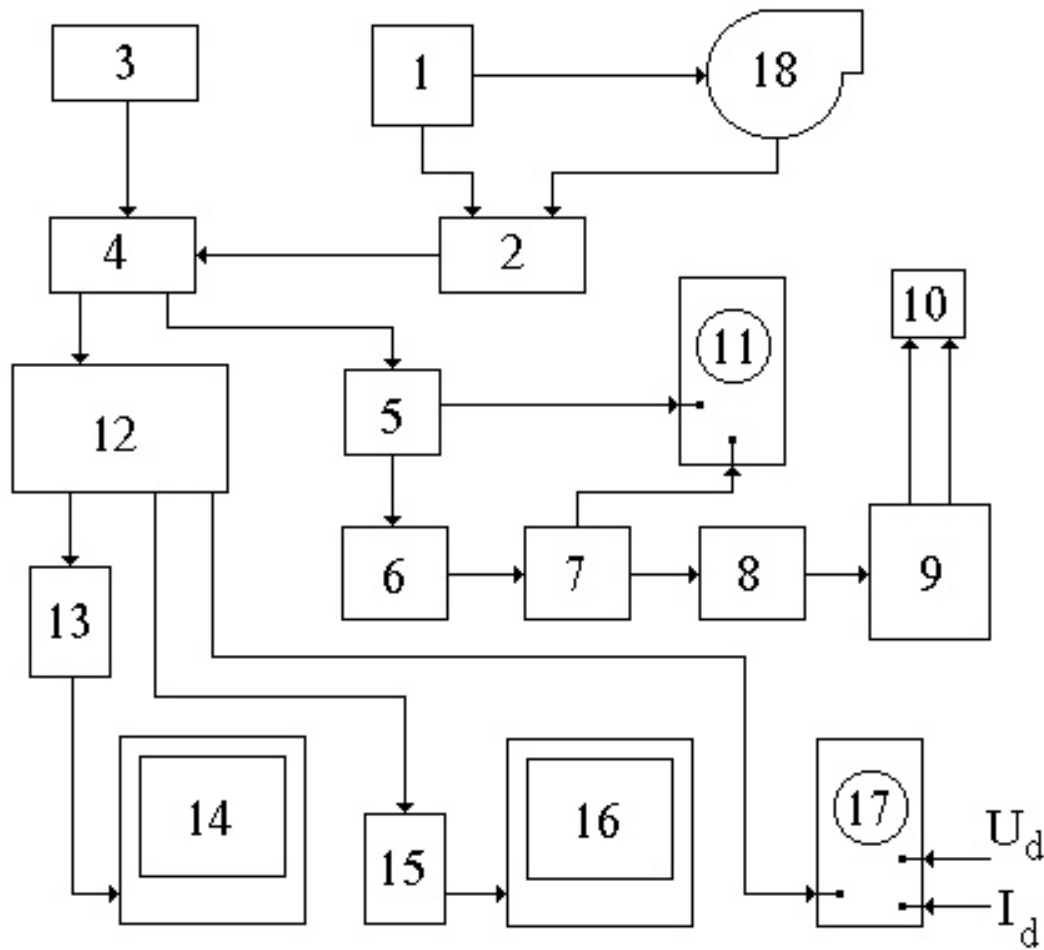
Fig.2.9.

The cathode follower output signal also entered the input of the oscilloscope (11) for supervision of the modulator pulse shape.

The second intermediate multi-channel generator ?-5-27? (12) switched on the registering oscilloscopes in a pre-determined moment of time. It was started by a pulse of a separate output channel of the synchronization control circuit. The output signal from the synchronized pulse channel of this generator switched on the pulsed storage oscilloscope ?-8-17 (17) practically with no delay. This oscilloscope registered the discharge current and voltage (I_d and U_d). Two more output channels of this generator provided delayed synchronized pulses, which switched on oscilloscopes (13) and (15) used for measuring various probe characteristics. The delay time relatively the discharge starting moment could be varied from 10 µs to 2 ms. This delay was determined primarily by the time of drift of the discharge plasma in the gas flow from the electrodes to a place where probes were fixed, or radiation spectra were

measured. In order to minimize the electromagnetic noise, and to stabilize the synchronization, an optron-based optical isolation was applied for transport of starting signals of the oscilloscopes (13) and (15).

In case of operation of the set up with photo registration of the phenomena under investigation, the initial stage of synchronization process was somewhat different. In this case, the electronic unit of control of the air valve generated a starting pulse (U_r), which entered the input of the unit (18) of control of the high-speed photo. In a certain moment this unit produced a synchronization pulse corresponding to the starting moment of registration of the plasma phenomenon on a photo film. This very pulse was applied for starting the generator (2). After that, the synchronization system operated in the same way as in the previous case.

Consider operation of the system of control of the synchronization circuit in more details. Fig.2.10 shows the corresponding temporary dependencies of pulses that switch on different parts of the circuit.

The synchronization pulse generator (3, Fig.2.9) formed a continuous sequence of pulses (U_g) with a fixed frequency, which could be chosen in a range from 1 to 10^6 Hz. Each of the pulses was 1 μs long, its rising time was 10÷40 ns. Such a low rising time, together with high stability of the repetition rate, provided a high time base accuracy of the signals that switch on different parts of the circuit.

The sequence of pulses was guided to the input of the control system (4), which was initially closed. As the signal (U_{t1}) of starting of the control system was formed by the generator (2), the trigger (which had been keeping closed the system input) was set open, and the control system started to work with a packet of a certain number of pulses (U_s), beginning from the first one after the moment of opening. The number of pulses in a packet could be varied in a range of 1...10^4 with a step from 1 to 100, respectively (in the Fig.2.10, this number is equal to five). The last pulse closed the trigger,
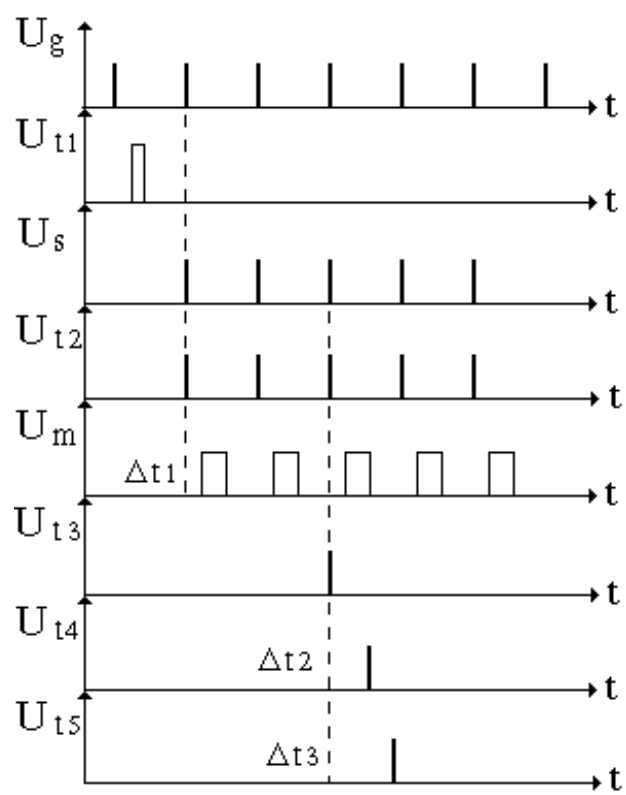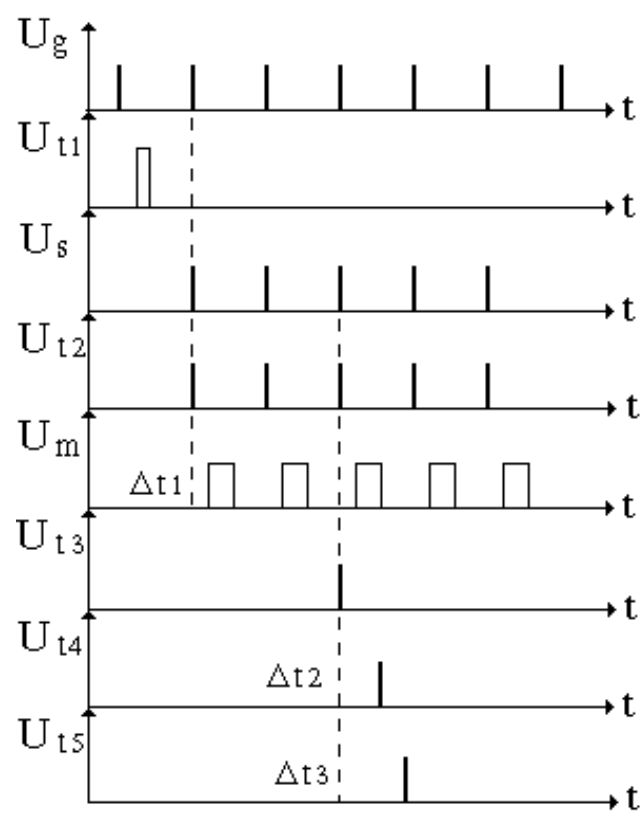
???. 2.10.

and the system returned into the initial, closed state. Under conditions of the current experiments, the frequency of pulses of the synchronization pulse generator was 10 Hz, and the number of pulses in a packet was varied in a range of 20...30, which was determined by the time of open state of the air valve (2...3 s).

The packet of pulses (U_{t2}) entered the input of the generator (5). Signals with no delay from one of the outputs of the generator switched on the oscilloscope (11), which was used for supervision of shape of the high-voltage signal of the modulator. Signals with $\Delta t_1 = 40 \div 80\ \mu s$ delay from another output of the generator switched on the generator of high-voltage pulses − the modulator (U_m). Thus, the repetition rate of the high-voltage pulses, which energized the discharge, was controlled by the synchronization pulse generator, their number in the packet was controlled by the synchronization control system, and their length was controlled by the generator (5), it could vary from 5 μs to 1 ms.

In order to start the oscilloscopes, which operate in a pulsed (single time) regime (13, 15 and 17, Fig.2.9), one of the packet pulses was applied. For so doing, one of electronic units of the synchronization control system selected one pre-determined pulse (1-st, or 2-nd, ..., or last). The choice of the of starting pulse number depended on the discharge type and the position of registering probes.

The selected signal from a separate output channel of the synchronization control circuit was applied to start the many-channel generator ? - 5 - 27? (12). The pulse from the synchronization output of this generator with practically no additional delay started the oscilloscope 17, see Fig. 2.9, which registered the discharge current and voltage (U_{t3}). The other two output channels of the generator (12) formed starting pulses (U_{t4}) and (U_{t5}), which were transported with the optical isolation to the oscilloscopes (13 and 15, Fig.2.9), which registered various probe characteristics. For these channels it was possible to choose independent delay of the output relatively the input in ranges $\Delta t_2 = 10 \div 2000\ \mu s$ and $\Delta t_3 = 10 \div 1000\ \mu s$. The actual delay time depended on the plasma time of flight in the airflow from the electrodes to a position of the probe or to a position of plasma radiation registration at spectral measurements.

3.3 Power supply of the pulsed-periodical discharge

The pulsed-periodical discharge was formed with use of the source of high-voltage pulses (modulator) on base of partial discharges of a capacitor. Its output stage schematic diagram is presented in Fig.2.11. It works in the following way. In the initial state, a negative bias(E_{c1}) is applied to the control electrode of the modulator's lamp (L), and the latter is closed, its current is equal to zero. Then the capacitor $?_1 = 1,6\ \mu F$ is being charged through a resistor $R_1 = 25\ k\Omega$ and a diode D, the final voltage is that of the power supply source $U_o = 5 \div 25\ kV$. In a certain synchronized moment of time, a positive pulse is applied to the control electrode through a capacitor $?_2$, this pulse opens the the modulator's lamp. The capacitor starts to discharge through the open lamp and a matched load resistance $R_6 = 3,5\ k\Omega$. Then a high-voltage pulse of negative polarity is formed on this resistor. The discharge circuit containing the electrodes and the discharge gap is connected by a coaxial cable (a - b) in parallel to the load resistor. Thus, if the modulator's lamp is open, the high voltage is applied to the electrodes, and breakdown and sequent gas discharge take place.
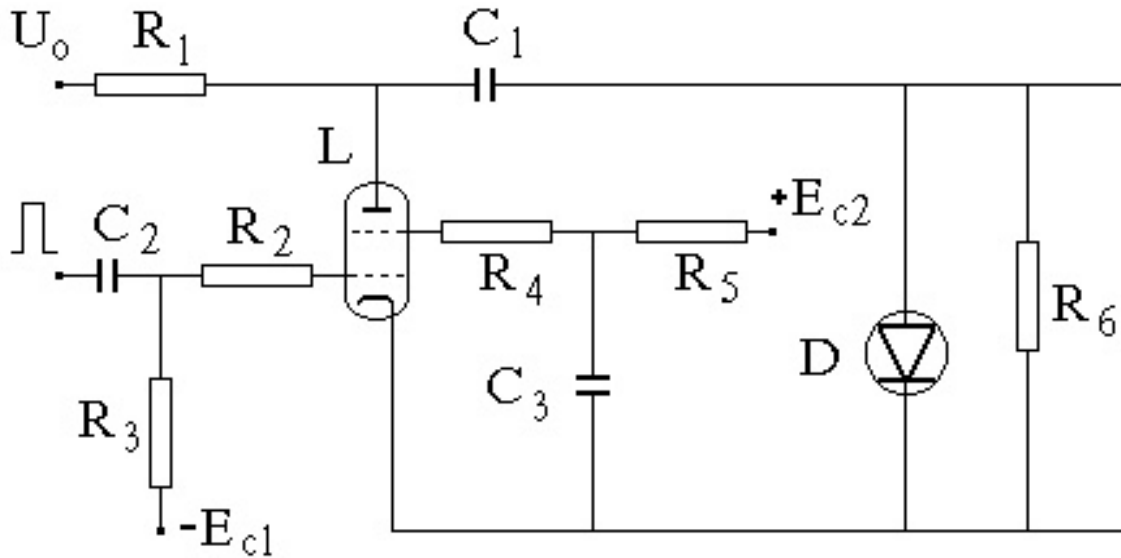

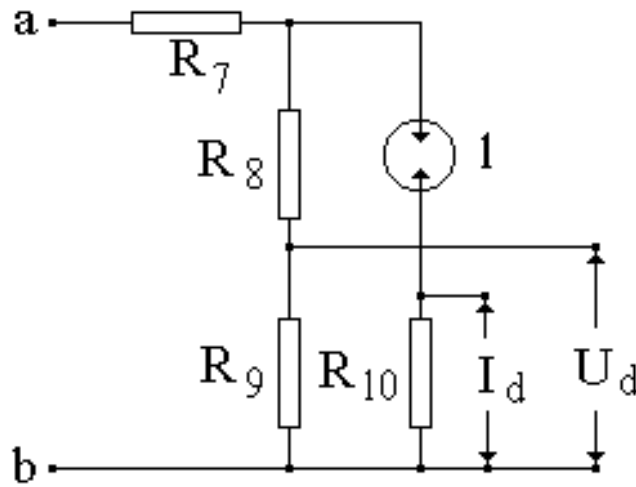**Fig.2.11**

The time of charging of the capacitor $?_1$ depends on the time constant $\tau = 40$ ms of the circuit $R_1\ ?_1$, and the time of discharge depends on the time constant of the circuit $R_6\ ?_1$ and the time of opening of the modulator's lamp. Thus, the discharge duration is determined entirely by the duration of the synchronizing pulse ($\tau_?$), which enters the

input of the output stage, if $\tau_? \gg 1/R_6C_1$. Under this condition, the voltage of the capacitor $?_1$ holds practically equal to U_o during all the discharge. If the magnitude of $\tau_?$ is comparable with the time constant of the $R_6?_1$ circuit, then the capacitor voltage decays during the discharge period. To provide the normal regime of work of the modulator's lamp, a constant positive bias is applied to its screening electrode. To provide it, a constant voltage power source E_{c2} and a circuit containing resistors R_4, R_5 and a capacitor C_3 are applied.


Fig. 2.12.

3.4 Electrical scheme of the pulsed discharge connection

Fig. 2.12 presents the electrical schematic of the pulsed discharge connection. The discharge current in the inter-electrode gap (1) could be varied by a choice of a ballast resistor $R_7 = 0 \div 500\ \Omega$. The discharge voltage was measured with use of a potential divider on base of low-inductance resistors R_8, R_9 with the ratio coefficient $k = 800$. The signal registered on the resistor R_9 was transported to one of the channels of the two-ray pulsed memory oscilloscope $?$-8-17. To measure the discharge current, a shunting resistor $R_{10} = 0,16\ \Omega$ was connected in parallel with the electrodes. R_{10} is much less than the plasma column resistance. The signal from the resistor R_{10} was transported to the second channel of the oscilloscope $?$-8-17.

3.5 Synchronization scheme of plasmadynamic discharge

Fig. 2.13 shows the electrical schematic of synchronization of work of different parts of the installation at studying of interaction with supersonic airflow of the plasma generated by the pulsed plasmatron (the plasmadynamic generator of plasma).
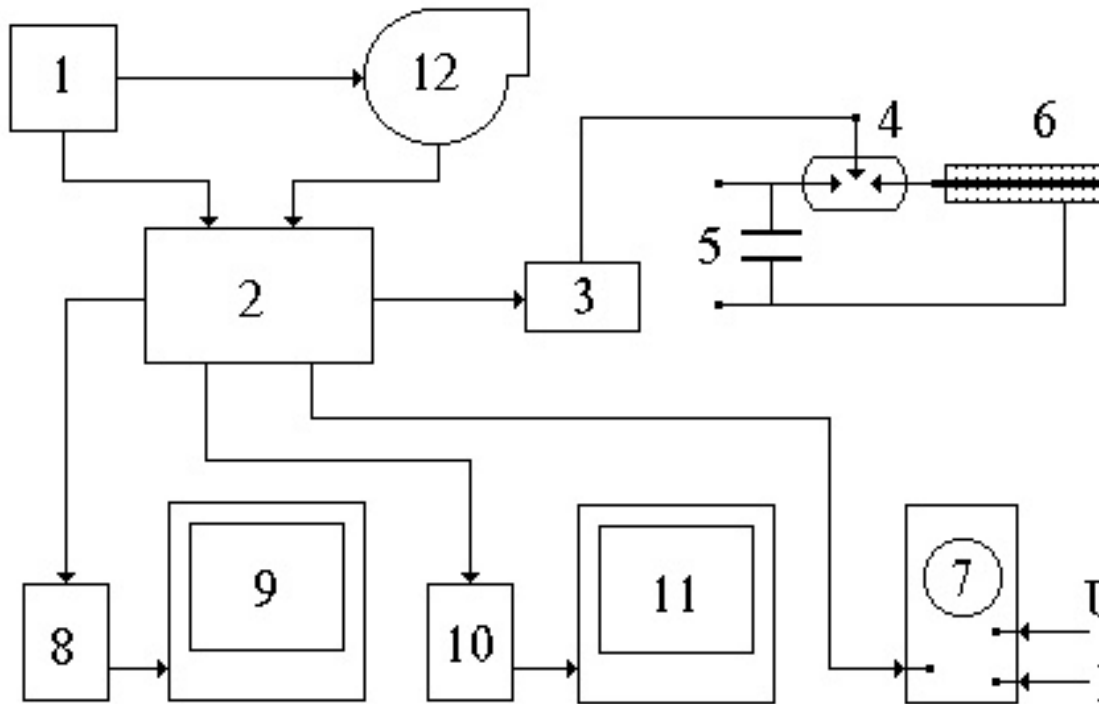
Fig. 13

Analogously to the case of the pulsed-periodical discharge, the synchronization system provided measurements in two regimes − with and without photo registration of the plasma processes. In both cases the main control element of the synchronization circuit is the control electronic circuit of the air valve (1), which is used for organization of the airflow. In the case of experiments with no photo registration, the valve control circuit forms a starting pulse, which is delayed relatively the valve opening moment for about 0.5 s (as well as in the case of pulsed-periodical discharge). This pulse starts the many-channel generator of delayed pulses, which in this case is the main regulating unit of the synchronization system. It provides starting of other units of the synchronization circuit with pre-determined time delays. First of all, a signal formed in the output of the generator of delayed pulses (with a 50-μs delay relatively the input pulse) is applied to start the high-voltage pulse generator (3)

for igniting of the discharge switch of the plasmatron. As the switch (4) is on, the energy stored in the capacitor (5) is consumed for supplying the plasmadynamic plasma generator (6), and a high-speed plasma jet was formed. A starting signal for the oscilloscope (7) was formed in the second channel of the generator of delayed pulses. This oscilloscope registered the discharge voltage and electric current. The time delay between the moments of starting the oscilloscope and the igniting pulse is also 50 μs (the oscilloscope is on before the discharge). At probe measurements other channels of the generator of delayed pulses provide signals for starting registering oscilloscopes (8) and (10), signals of which are processed by personal computers (9) and (11).

In the case of experiments with photo registration (analogously to the case of the pulsed-periodical discharge) the generator of delayed pulses was started by a signal from the high speed camera control unit. The work of the high speed camera was determined by the electronic control unit of the air valve. All the other units of the synchronization system worked in accord with the above considered principle.

### 3.6 The electrical scheme of switching on the pulsed plasma generator

Fig. 2.14 presents the electrical schematic of switching on the pulsed plasma generator. The generator had an outer electrode in a form of a 10 cm$\times\varnothing$11mm (internal) thin cylindrical tube (3). The internal high-voltage electrode (2) was a 4-mm tungsten rod positioned coaxially inside the outer electrode. An insulator made of a transparent acrylic plastic was positioned in the inter-electrode space. The plasmatron worked in the following way. The capacitor ?$_?$ was charged by a power supply unit to high voltage U_o , which varied in a range of $3 \div 5$ kV. The resistor R_1 restricted the charging current. As the igniting pulse was applied to the discharger (1), the high voltage was applied to the plasmatron's electrodes. After that, an electric discharge was formed along the end surface of the dielectric element, and the plasma jet was generated.

The discharge voltage was defined by a potential divider made with low-inductance resistors R_2, R_3 with the ratio coefficient $k = 2000$.
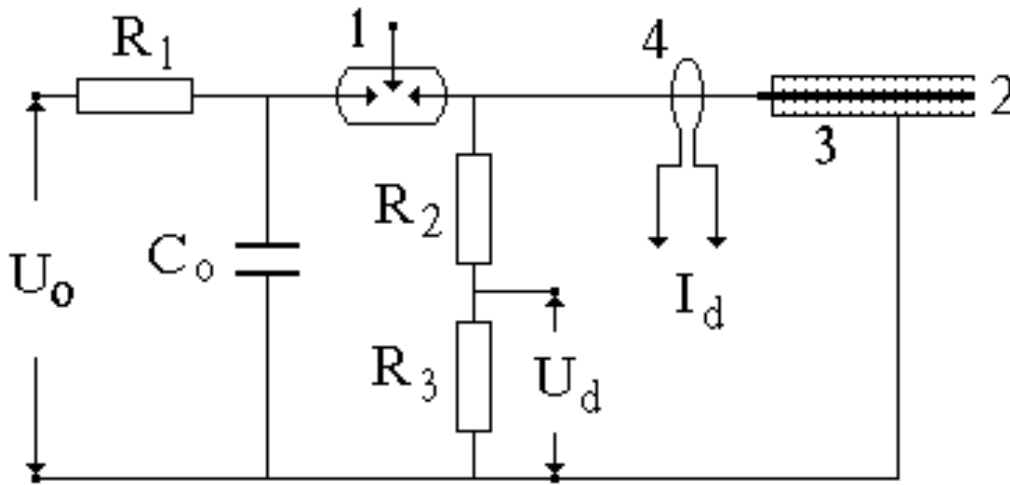
???. 2.14

The signal measured on the resistor R_3 was applied to one of the input channels of the two-channel pulsed memory oscilloscope ?-8-17. The discharge current was registered with the Rogvski coil (4), which overlapped the electrical pathway of the internal electrode of the plasma generator. The Rogvski coil worked in the regime of a current transformer, for so doing it was connected with a 15-Ω output resistor. To minimize the electric noise, the resistor was positioned just near the input of the second channel of the same pulsed memory oscilloscope ?-8-17. Fig.2.15 shows typical oscilloscope pictures of the discharge current and voltage.
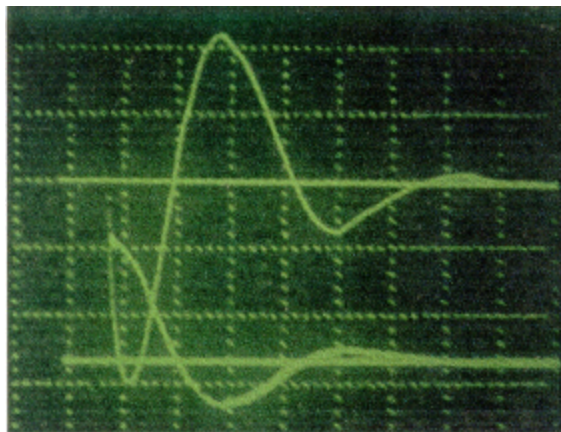
**Fig.2.15 Typical form of discharge current and voltage of plasma jet.**
Temporary scale factor is 20 µs/div.
Upper beam – discharge current, scale factor is 2 V/div ($I_{max} \approx 20$ kA),
lower beam – discharge voltage, scale factor is 1 V/div

3.7 The synchronization scheme of DC discharge

The schematic diagram of synchronization of units of the installation at studies of interaction of the supersonic airflow with the plasma formed by a DC generator is presented in Fig. 2.16.
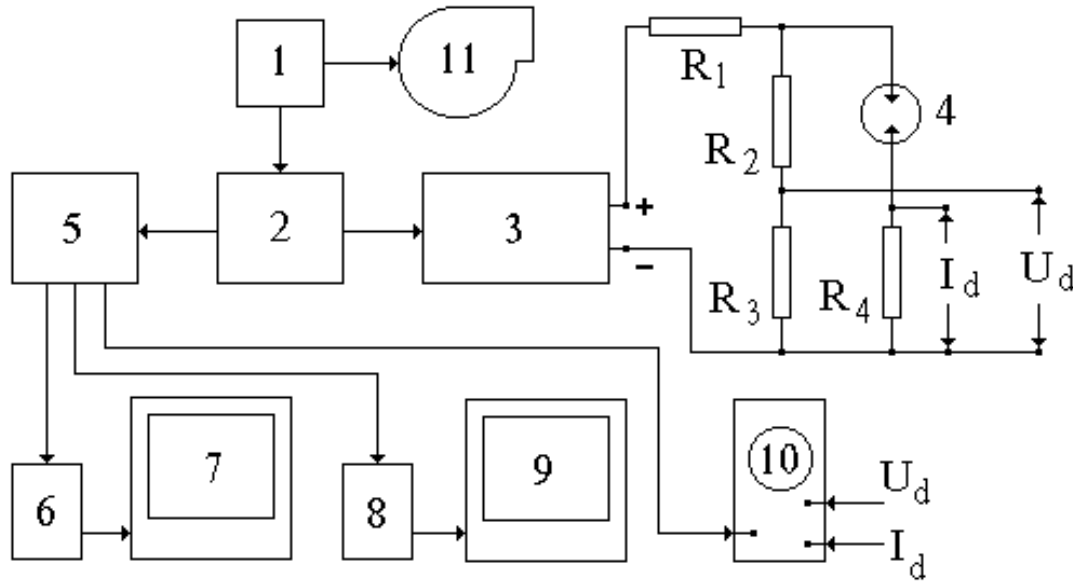
Fig. 2.16

Analogously to the two previous cases, the main control unit of the synchronization system was the electronic circuit of control of the air valve (1), which was applied for formation of the supersonic airflow. The valve control circuit forms the signal, which is delayed for about 0.5 s relatively the moment of opening the valve (analogously to the case of the pulsed-periodical discharge). This pulse starts the generator ? - 5 - 46- ? (2), which in this case is the main regulating unit of the synchronization system, and it makes it possible to start other units of the system with pre-determined delays. First of all, this generator forms the pulse, which controls the time of start and the duration of work of the DC power supply unit (3). The generator (2) provides variation of the delay time of starting of the DC power supply unit in the range from 0 to 1 s, and the duration of work in the range from 0.1 to 1 s. The switching on of the DC power supply unit applied the primary circuit of the high-voltage transformer. The output parameters of this unit were the following: maximal output voltage $U_o = 4$ kV, maximal discharge current $I_o = 4$ A. The output high voltage of the power supply unit was applied to the discharge gap (4) through the ballast resistor R_1. The discharge current could be controlled by variation of the magnitude of resistance of R_1. Note

that the control of discharge current could be also carried out by variation of the output voltage of the DC power supply unit.

The discharge voltage was measured with use of the potential divider based on resistors R_2, R_3 with the ratio coefficient $k = 1000$. In general, one could apply standard ordinary DC voltmeters and ammeters for measurement of the discharge voltage and current. However, the vibrations of parameters at the DC discharge were studied with use of the pulsed two-ray memory oscilloscope ? - 8 - 17 (10). At so doing, measurement of the discharge voltage was carried out with transport of the signal on the resistor R_3 to the input of one of the channels of this oscilloscope. To register the discharge current, the shunt resistor R_4 was connected in series with the inter-electrode gap (4), and the signal on this resistor was applied to the input of the second channel of the same oscilloscope.

For synchronization of the oscilloscopes, the additional generator ? - 5 - 46-? (5) was applied, it was analogous to the generator (2). The pulse from the synchronization channel of the generator (2) started the generator (5) with practically no delay. In its turn, the generator (5) formed pulses (which were delayed on pre-determined periods of time) for starting the registering oscilloscopes, including the oscilloscope (10). The delay time could be varied in the range of 10 μs ÷ 1 s. Thus, the application of the additional generator with such delays made it possible to register necessary signals with sufficiently short scanning time (e.g., 0.1÷ 1 ms) by oscilloscopes in any moment of the DC discharge (the discharge time was up to 1 s).

At carrying out different probe measurements, the other output channel of this generator formed pulses for starting the registering oscilloscopes (6) and (8), the signals from them were processed by the personal computers (7) and (9). The delay time in this case could be varied from 10 μs to 1 s.

In case of photo registration, the high-speed camera (11) worked separately. Its starting was carried out by a pulse from the electronic circuit of control of the air valve, and the duration of recording and the necessary delay were determined by the regime of work of the control unit of the high-speed camera itself. This made it possible to register different moments of the DC discharge with different duration of recording.

CHAPTER III THEORETICAL BACKGROUND
OF THE PROBE DIAGNOSTICS

Introduction

Values of basic parameters characteristic for the plasma aerodynamic experiments are the following:, external (discharge) electric field $E_0 = 0...1.5 \cdot 10^3$ V/cm, gas temperature $T_{z0} = 100...2000$ K, airflow speed ≈ 500 m/s, Mach number $M_0 = 0.1...3$, plasma concentration $n_{i0} = 10^{13}...10^{15}$ cm^{-3}, gas pressure $p_{g0} = 10...1000$ Torr, electron temperature $T_{e0} = 1...3$ eV, local plasma potential oscillations up to 2 kV [1]. Under such conditions, the probe diagnostics is possible, the light-guide fiber technique and the double cylindrical probes (with probe radius $R = 0.1...1$ mm and probe length $L >> R$) should be used [2].

The known methods of probe diagnostics [3-7] cannot be applied directly at such a complex of parameters. E.g., in [3,4] the external electric field is not accounted for, in [6] the airflow is slow, there are no chemical reactions, and the electron branch of the voltage –current characteristic is considered, which is absent in the double probe case. The current work considers a non-emitting double probe in intense external and probe electric fields, in subsonic and supersonic gas flows, with respect to plasma chemical reactions and other issues important under the conditions mentioned above.

§1. Background of a Detailed Description of Probe-Plasma Interaction

An interpretation of probe voltage-current characteristics in terms of plasma parameters is based on consideration of transport of charged particles in the vicinity of the sounding probe surface, see, e.g., References [3-7]. The consideration in our case should be based on the following equations [8].

The Navier-Stokes equations for neutral components dynamics:

$$\partial \rho_g / \partial t + \text{div}(\rho_g \mathbf{v}_g) = 0, \quad \rho_g \, d\mathbf{v}_g / dt = -\mathbf{grad} p_g + q + \mathbf{F}, \qquad (1.1)$$

$$n_g dE_g / dt = -p_g \text{div} \, \mathbf{v}_g + Q + W,$$

(here n_g, ρ_g, p_g, $\mathbf{v}_g$, E_g are the gas concentration, density, pressure, velocity and internal energy of translations and rotations, q and Q are the viscous terms, the terms $\mathbf{F}$ and W account for forces and energy flows from the plasma, $\rho_g = m_{mol} n_g$, m_{mol} is a molecule mass, k_B is the Boltzmann constant. In our case the force $\mathbf{F}$ is negligible [1], as well as the effect of W for the characteristic size of the probe vicinity (0.1...1 mm). That's why the effect of plasma components on the neutral gas was neglected. In our case the Reynolds number is not very high (Re = 1...300), i.e. a laminar gas flow takes place.

For plasma regions, quasi neutral approximation was applied instead of the Poisson equation:

$$n_e = n_i - n_- \tag{1.2}$$

(n_e, n_i, n_- are concentrations of electrons, positive and negative ions). The applicability of this approximation is considered below.

For the electromagnetic field in the plasma region, quasi steady ($\partial/\partial t \approx 0$) Maxwell equations (except the Poisson equation) at low values of the magnetic Reynolds number $Re_m \ll 1$ were applied:

$$\mathbf{rot}\ \mathbf{E} = 0, \quad \mathbf{j} = \sigma\ \mathbf{E}, \quad \mathbf{rot}\ \mathbf{B} = \mu_0 \mathbf{j}, \quad \mathrm{div}\ \mathbf{B} = 0 \tag{1.3}$$

in a case ($\partial/\partial t \approx 0$), ($\sigma = e\ n_e\ \mu_e$ is the conductivity, $\mu_e = e/(m_e \nu_e)$ is the electron mobility in the electric field $\mathbf{E}$, $\mathbf{B}$ is the magnetic field induction, $\mathbf{j}$ is the density of current, $\mu_0 = 4\pi 10^{-7}$ H/m, e and m_e are the electron charge and mass, ν_e is the frequency of electron collisions). The last three equations (1.3) with account to the expression of $\mathbf{E}$ via the gradient of the electric potential j and to the identity div $\mathbf{rot}$ $\mathbf{?}$ $\equiv 0$ valid for any vector $\mathbf{?}$, yield

$$\mathrm{div}(n_e\ \mu_e\ \mathbf{grad}\ j) = 0. \tag{1.4}$$

This equation can be used for calculation of $\mathbf{E}$ and j in a quasi-neutral plasma.

Balance of negative ions

$$\partial n_- / \partial t + \mathrm{div}(n_- \mathbf{v}_-) = K_a - K_{ii} - K_d, \tag{1.5}$$

here K_a, K_{ii}, K_d are rates of electron attachment, ion-ion recombination and dissociative detachment, respectively, $\mathbf{v}_-$ is the negative ions velocity. As the characteristic temperature and positive ions concentration are relatively high, the effect of negative ions on the probe voltage-current characteristics is comparatively weak; in the current studies it was neglected.

Balance of positive ions:

$$\partial n_i/\partial t + \mathrm{div}(n_i\mathbf{v}_i) = K_I - K_R. \tag{1.6}$$

here $\mathbf{v}_i$ is the positive ions velocity, K_I, K_R are the rates of ionization and (dissociative) recombination (see, e.g., [9]),

$$K_I = \boldsymbol{F}\, n_i\, n_g\, A(T_e), \tag{1.7}$$

$$\boldsymbol{F} = ((1 + 4\, C_F)^{1/2} - 1)/((1 + 4\, C_F)^{1/2} + 1)/\, C_F,$$

$$C_F = T_e\, \nu'_{ei}\, /(2\nu'_{ee}\, I_i\,), \quad \nu'_{ee} = n_e\, (2e(I_i + T_e)/m_e)^{1/2}\, \Sigma_{ee}\,,$$

$$\nu'_{ei} = n_g(2e(I_i + T_e)/m_e)^{1/2}\, \Sigma_{ei}\,,$$

$$\Sigma_{ee} = a_0^2\, 16\pi(2/((I_i + T_e)/27.2))^2 \ln\Lambda,$$

$$\ln\Lambda = 23 + 1.5\, \log_{10}(T_e) - 0.5\, \log_{10}(10^{-6}n_e);$$

here the factor $\boldsymbol{F}$ takes into account the deviation of the distribution function from the Maxwell one due to ionization, see, e.g., Reference [8]; I_i is the ionization energy for the molecules, a_0 is the Bohr radius (here and lower T_e is in eV, the rest values are in the basic SI units).

Consider determination of the speeds of electrons and ions. Strictly speaking, the movement of plasma charged particles in case of weak ionization $n_e/n_g \leq 10^{-4}\ ...10^{-5}$, is described by the kinetic equations. If one represents the electron distribution function $f = f(v)$ (here v is the velocity absolute value of an electron) in the two-term approximation, $f(v) = f_0(v) + \mathbf{v}/v\, \boldsymbol{f}_1(v)$, the kinetic equation for the isotropic part f_0 yields the following expression for the mean electron velocity [10]

$$\boldsymbol{v}_e = \boldsymbol{v}_g - [(n_e n_g)^{-1}\tilde{\mathbf{N}}(n_g D_e n_e) + \boldsymbol{m}_t\, \mathbf{E_r} \tag{1.8}$$

$$- \kappa_1\, D_e \mathbf{e}\, (\mathbf{e}\cdot\tilde{\mathbf{N}}\ln n_e) - \kappa_2\, \mathbf{e}\, (n_g/E_r)\tilde{\mathbf{N}}\cdot(\mathbf{E_r}\,/n_g) - \kappa_3\, \mathbf{e}\, (\mathbf{e}\cdot\tilde{\mathbf{N}}\ln(E_r/n_g)) - ...],$$

$$D_e = 4\pi/(3n_g)_0\int^\infty v^3 f_0/\sigma_m \, dv, \quad \pmb{m}_t = 4\pi e/(3n_g m_e) \,\, _0\int^\infty v^2/\sigma_m \, \partial f_0/\partial v \, dv,$$

here σ_m is the electron scattering transport cross section, $\mathbf{e} = \mathbf{E_r}/E_r$, κ_j are the kinetic coefficients, $\mathbf{E_r}$ is the microscopic electric field (meaned over the plasma fluctuations, see below). κ_j depend on the sort of gas, the shape of the electron distribution function $f = f(v)$, and on the parameter E_r/n_g. Their absolute values have the same order of magnitude as the electron diffusion coefficient D_e, they can be positive or negative; for the N_2 plasma they are plotted, e.g., in [10]. The terms containing the kinetic coefficients result in considerable (about 0.5...1.5 times) changes in electrons movement: e.g., they define the anisotropy of electron diffusion along and across the electric field, non-linear changes in the drift velocity in case of gradients of plasma parameters, etc. However, if one understands that the problem deals with plasma diagnostics, and takes into account the real accuracy of cross sections, plasma characteristics, and the model in the whole, one can conclude that in the first approximation it is possible to neglect these complicated issues by assuming $\kappa_j \approx 0$, i.e. by modeling the electron movement on base of the "classical" approximate equation:

$$\pmb{v}_e \approx \pmb{v}_g - [(n_e n_g)^{-1}\tilde{\mathbf{N}}(n_g n_e D_e) + \pmb{m}_t \, \mathbf{E_r} \,]. \tag{1.9}$$

The expressions for ions corresponding to (1.8) are still more complicated, for the two-term approximation is not so accurate for ions as it is for electrons. However, the ion diffusion itself is slow comparatively the ambipolar diffusion. It can be neglected at all, or (with the same accuracy) one can apply the "classical" expression [11]:

$$\mathbf{v}_i = \mathbf{v}_g + \mu_i \mathbf{E} - D_i\nabla\ln n_i - D_i T_e n_e/(T_i n_i)\nabla\ln n_e - D_i\nabla\ln T_g - D_i T_e/T_g \nabla\ln T_e, \tag{1.10}$$

$$\mu_i = e/(m_{mol}\nu_{im}), \, D_i = k_B T_g /(\nu_{im} \, m_{mol}),$$

here μ_i is the ion mobility, ν_{im} is the cross section of elastic ion-molecule collisions; if $n_i = n_e$, (1.10) looks like

$$\mathbf{v}_i = \mathbf{v}_g - 1/n_i D_a\nabla n_i + \mu_i \mathbf{E} - D_i\nabla\ln T_g - D_i T_e/T_g \nabla\ln T_e, \, D_a = D_i(1+ T_e/T_g) \tag{1.11}$$

(D_a is the ambipolar diffusion coefficient). This expression accounts for the ion-gas friction, the drift in the external electric field, the ambipolar diffusion and (approximately) the thermal diffusion.

Note that the application of the term "ambipolar diffusion" corresponds to exclusion from the explicit consideration of the so-called ambipolar electric field $\mathbf{E}_a$, which is bound with charge partition in regions with high gradients of plasma parameters, i.e. the electric field in the computations $\mathbf{E}$ differs from the microscopic electric field $\mathbf{E}_r$:

$$\mathbf{E}_r = \mathbf{E} + \mathbf{E}_a, \ \mathbf{E}_a \approx -1/n_e \mathbf{grad}\,(k_B\,T_e n_e/e). \quad (1.12)$$

Then the simplest form of the Ohm law, $\mathbf{j} = \sigma\mathbf{E}$, can be applied. If one wishes to consider $\mathbf{E}_r$ instead of $\mathbf{E}$, then the expression for the ion velocity looks like

$$\mathbf{v}_i = \mathbf{v}_g + \mu_i\mathbf{E}_r - (D_i/n_i)\mathbf{grad}\,n_i - D_i\,\mathbf{grad}\,\ln T_g, \quad (1.13)$$

and the Ohm law is

$$\mathbf{j} = \sigma[\mathbf{E}_r + 1/n_e \mathbf{grad}\,(k_B\,T_e n_e/e)], \quad (1.14)$$

i.e. the electron diffusion must be taken into account explicitly, that is bound with additional computational difficulties.

Actually, if one neglects the electron thermal diffusion for simplicity, then the equation for electrons movement in the internal field $\mathbf{E}_r$ looks like

$$\mathbf{v}_e = -\mu_e/n_e \nabla(k_B T_e n_e/e) - \mu_e\,\mathbf{E}_r. \quad (1.15)$$

Reduce it to the traditional Ohm law $\mathbf{j} = \sigma\mathbf{E}$ for the effective external field $\mathbf{E}$:

$$\mathbf{j} = -e\,n_e\,\mathbf{v}_e = e\,n_e\,\mu_e[1/n_e \nabla(k_B T_e n_e/e) + \mathbf{E}_r] = \sigma[1/n_e \nabla(k_B T_e n_e/e) + \mathbf{E}_r],$$

then the equation for ions movement (the ion thermal diffusion is also neglected for simplicity) in the internal field $\mathbf{E}_r$

$$\mathbf{v}_i = \mathbf{v}_g - \mu_i/n_i \nabla(k_B T_i n_i/e) + \mu_i\,\mathbf{E}_r \quad (1.16)$$

in terms of $\mathbf{E}$ looks like

$$\mathbf{v}_i = \mathbf{v}_g - \mu_i/n_i \nabla(k_B T_i n_i/e) + \mu_i\,[\mathbf{E} - (1/n_e)\nabla(k_B T_e n_e/e)],$$

that coincides with (1.11). But if one takes the equation for ions movement with the ion diffusion coefficient D_i instead of the ambipolar diffusion coefficient D_a, and considers the external field $\mathbf{E}$ instead of $\mathbf{E}_r$, it is equivalent to neglecting of the electron diffusion in the electron movement equation. The corresponding error in the

account of diffusion is as high as the factor of $(1+ T_e/T_g) \approx 10$ times. Thus, the ambipolar field is strong, it cannot be neglected, it can be stronger than the external electric field **?**.

The electric field **?** in our case can be defined by the mentioned above steady $(\partial/\partial t = 0)$ Maxwell equations. Really, **?** defines correctly the movement of electrons and ions, i.e. the electric current density and the magnetic fields are also correct. Some deviations arise at computation of the electric potential $\varphi_?$, as it is defined by integrating of **?**$_?$, while our computations deal with **?**. Estimate with use of (1.12) the difference $\Delta\varphi = \varphi_? - \varphi$, which corresponds to integrating along a direction **?**:

$$\Delta\varphi = \varphi_? - \varphi = {}_{?1}\!\int^{?2} (\text{?}_? - \text{?})\,dx = {}_{?1}\!\int^{?2} [-(1/n_e)\partial(k_B T_e n_e/e)\partial\,?]dx \qquad (1.17)$$

$$= (T_{e1} - T_{e2})\,k_B/e - {}_{?1}\!\int^{?2}[k_B T_e/e\,\partial\,(\ln n_e)/\partial\,?]dx,$$

One can see that the difference $\Delta\varphi$ is about $k_B T_e/e \approx 1$ V. It takes into account, e.g., the well known charging of a wall in a contact with a plasma. The characteristic voltage in the probe diagnostics is as a rule much higher than 1 V, i.e. $\Delta\varphi$ can be neglected. It means that consideration of **?** instead of **?**$_?$ is correct.

Temperature of electrons in our case is defined by an equation

$$n_e dE_e/dt + p_e \text{div } \mathbf{v_e} = - \text{div } \lambda_e \text{ grad } T_e + S_F - S_e, \qquad (1.18)$$

$$\lambda_e = 5/2\, e^2\, T_e\, n_e\, /(m_e v_e\,),\ S_E = \sigma E^2,$$

here $E_e = 3/2 k_B T_e$ is the kinetic energy of electrons, $p_e = n_e k_B T_e$ is the electron gas pressure, λ_e is the electron gas heat conductivity, S_e is the total power of electron energy exchange at inelastic collisions, in molecular gases it is primarily bound with vibration (index i) and electron (e) state excitations (+) and inverse processes of de-excitation (−): $S_e = S_{ej+} - S_{ej-} + S_{ev+} - S_{ev-}$. In the air, air-fuel mixtures and in products of air-fuel combustion one can use the following approximation [9]:

$$S_{ev+} = h\mathbf{n}_V\, n_g\, n_e (2k_B T_e/m_e)^{1/2}\, \sigma_{01} \exp(-h\mathbf{n}_V/\, k_B T_e)/[1 - \exp(-h\mathbf{n}_V/\, k_B T_e))]^2,\ (1.19)$$

$$S_{ev-} = h\mathbf{n}_V\, n_g\, n_e (2k_B T_e/m_e)^{1/2}\, \sigma_{01} \exp(-h\mathbf{n}_V/k_B T_v)/[1 - \exp(-h\mathbf{n}_V/\, k_B T_v))]^2,$$

here $\sigma_{01} \approx 10^{-16}$ cm^2 is the mean cross section of excitation of the first vibration quantum of nitrogen N_2, $h\mathbf{n}_V \approx 0.29$ eV is the vibration quantum, T_v is the vibration

temperature. For the diagnostic problem the deviation of T_e from the ambient flow value $T_{e¥}$ is of the most interest. When a part of plasma liquid passes through regions with a comparatively high field intensity, then $T_e > T_{e¥}$; heat transfer into the probe can result in local values $T_e < T_{e¥}$. The latter has a comparatively weak effect on the probe voltage-current characteristics, because in our case the heat transfer into the probe is negligible (see below). In a weakly ionized plasma in a comparatively strong electric field and in an intensive energy exchange with neutral particles one can neglect the "hydrodynamic" terms in the left hand part of (1.18). Then (1.18) defines an implicit dependence of T_e on E/n_g at given T_v. This dependence has been calculated beforehand at $T_v = 0$ as a function $T_e = F_0(E/n_g)$, electron excitations of nitrogen and oxygen have been accounted for at calculation of S_{ej+} and S_{ej-}, the cross sections have been taken from [8]. This function can be applied in case of $T_v > 0$ with a different argument, which depends on T_v:

$$T_e = F_0[(E^2/n_g^2 + S_{ev-}/\sigma n_g^2)^{1/2}]. \tag{1.20}$$

For plasmas of air, air-fuel or exhaust gases one can use approximations based on experimental data [9]

$$K_R = n_e n_i \beta' /T_e^{1/2}, \beta' = 3.3\ 10^{-14}; \tag{1.21}$$

$$\log_{10} A = -13.6\ (\log_{10}(T_e))^2 + 15.7\ \log_{10}(T_e) - 21.4,$$

$$\Sigma_{ei} \approx 10^{-21}\ T_e, \nu_e = n_g \Sigma_e (2eT_e/m_e)^{1/2},$$

$$\Sigma_e = 0.8\ 10^{-20}\ T_e^2 + 0.43\ 10^{-19}\ T_e + 0.8\ 10^{-19},$$

$$\nu_{im} = \Sigma_{im}\ n_g(2\ k_B T_g /m_{mol})^{1/2},$$

$$\Sigma_{im} \approx 2.2\ 10^{-18} + 2\pi a_0^2\ (3.70.10^6/T_g)^{1/2}.$$

The final probe signal − current − is formed as an integral over all the sounding electrode surface,

$$I = -\int e n_e \mathbf{m_e}\ E_n\ dA^- + \int e n_i \mathbf{m_i} E_n dA^+, \tag{1.22}$$

here E_n is the electric field near the surface, dA^- and dA^+ are fractions of surface that attract negative and positive charges, respectively (because of the corresponding field direction).

§2. Formulae for Probe Voltage-Current Characteristics

2.1. An Analysis of Profiles of Plasma Parameters Near a Probe

The potential fall near the probe, which defines the voltage-current characteristic, is a sum of falls: φ_D in the Debye sheath, φ_a in the diffusion layer (or the "viscous boundary layer", where $|\mathbf{grad}\,(D_a\,n_i)| > |\mu_i \mathbf{E_0}|$), and φ_E in the drift area (or the "non-viscous flow region", where $|\mu_i \mathbf{E_0}| >> |\mathbf{grad}\,(D_a\,n_i)|$).

The current study considers processes in the diffusion layer and in the drift area. If φ_D is negligible, these processes define the probe voltage-current characteristic. Such a situation is characteristic for the major part of the plasma parameters, especially for the cases of sufficiently high characteristic gas density, which are characteristic for realistic full-scale systems of plasma aerodynamics. This results from an analysis of comparative yields of φ_D, φ_a and φ_E. In [4] these yields are estimated on base of an asymptotic analysis of solutions of the equations that describe a weakly ionized gas in a vicinity of a probe in a subsonic plasma flow. It had been assumed that Re $>>1$, $\boldsymbol{e}$ $<<1$, here Re$=v_g R/D_i$ is the Reynolds number, $\boldsymbol{e} = k_B T_g e_0/(n_e e^2 R^2)$, $\boldsymbol{e_0}$ is the dielectric constant. If $\boldsymbol{e}\,Re^2 >>1$, then $\varphi_D << \varphi_E$, i.e. the Debye sheath potential fall φ_D is negligible. The corresponding voltage-current characteristic grows monotonously and has no saturation. In the opposite case, $\boldsymbol{e}\,Re^2 <<1$, the voltage-current characteristic stops to grow at high voltages due to a growth of φ_D at high probe potential. For the plasma of air $\boldsymbol{e}Re^2 \approx 0.13*10^{-33}*v_g{}^2*n_g{}^2/n_e$ (basic SI units are applied here). For the values characteristic for plasma aerodynamic experiments $v_g = 600$ m/s, $n_e\,/n_g =10^{-6}...10^{-4}$, $n_g =(1...3)10^{24}$ m^{-3} the parameter $\boldsymbol{e}Re^2$ varies from 2 to 2000, and for the values characteristic for realistic full-scale systems of plasma aerodynamics $v_g= 2$ km/s, $n_e/n_g =10^{-6}...10^{-4}$, $n_g =(1...3)10^{24}$ m^{-3}, the parameter $\boldsymbol{e}Re^2$ varies from 10 to 10,000. It means that one can neglect the effect of φ_D on the probe voltage-current characteristics for the most cases of interest.

Analogous conclusion about a possibility of neglecting of processes in the Debye layer results from an analysis of chemical reactions (see below). Thus, the consideration of only quasi-neutral plasma regions is correct.

The potential fall in the diffusion layer φ_a is also negligible, if the layer's thickness r_a is much less than the probe's radius R. Actually, assume a linear radial plasma density

profile across the cylindrical diffusion layer and a constant plasma density in the drift area,

$$n_i\ (R<r<R+r_a)= n_{i0} +(n_{i\yen} - n_{i0})(r-R)/r_a,\ \ n_i(R+r_a<r<r_\yen) = n_{i\yen},$$

and consider electric current conservation along a current tube for $R<r<R+r_a$, $r = R$ and $R+r_a <r<r_\yen$ with account to the fact that the ambipolar diffusion can be interpreted as a drift of ions in the ambipolar electric field (see above):

$$\Delta I = 2\pi r h e n_i \mathbf{m} E(R<r<R+r_a) = 2\pi R h e n_{i0} v_{i0} = 2\pi r h e n_{i\yen}\mathbf{m}E(R+r_a <r<r_\yen).$$

The resulting ratio of the potential falls is

$$\varphi_a/\varphi_E = {}_R\!\int^{R+ra} E(r)\mathrm{d}r/{}_{R+ra}\!\int^{r\yen}E(r)\mathrm{d}r =$$

$$1/[R/r_a - n_0/n_\yen(R+r_a)/r_a]\ \ln\{Rn_\yen/[(R+r_a)n_0]\}/\ln[r_\yen/(R+r_a)].$$

The boundary plasma density is small ($n_0/n_\yen\!<\!\!<\!1$) but limited [3], (in accord with the boundary conditions, see below), i.e. the logarithmic factors do not change the order of magnitude. If $r_a/R\rightarrow0$, then $\varphi_a/\varphi_E \rightarrow0$.

The diffusion characteristic length r_a for a temporary evolution of an initially stepwise profile of concentration is

$$r_a = (tD_a)^{1/2},$$

here the time coordinate t can be expressed via the length l of a path of an element of plasma along the probe surface as

$$t = \int (1/v_g)\ \mathrm{d}l \approx l/v_g,\ l \approx R\mathbf{y},$$

here $\mathbf{y}$ is the azimuth coordinate. Estimates have shown that $r_a << R$ for a major part of the characteristic plasma parameters, especially for those characteristic for realistic full-scale systems of plasma aerodynamics. In most cases of interest the probe voltage-current characteristic depends primarily on ion transport processes in the drift area, however for some cases of plasma aerodynamic experiments the diffusion layer is also important. The latter case in the scope of the current work has been considered numerically. In a contrast, the current analytical effort considers the other case, when the drift area is of interest. Then all the ions, which enter the interface of the drift area

and the diffusion layer, will get to the probe surface, because the Debye sheath and the diffusion layer are both narrow and transparent.

Consider the equations (1.6) and (1.11). With account to (1.3), (1.4), the equations $\mathbf{j} = \sigma\mathbf{E}$, $\sigma = en_e m_e$, $\text{rot } \mathbf{B} = \mu_0\mathbf{j}$, and the mathematical identity $\text{div}(\text{rot } \mathbf{A}) \equiv 0$ valid for any vector $\mathbf{A}$, and in case that $n_i\mu_i/(\mu_e n_e) \ll 1$, one can represent the drift term in the equation of ion concentration in the following form:

$$\text{div}(n_i\,\mu_i\mathbf{E}) = \text{div}(n_i\,\mathbf{E}\,\mu_e(\mu_i\,/\mu_e)) = \text{div }[\mu_i\,n_i\,/(en_e\mu_e)\,(e\,n_e\,\mathbf{E}\,\mu_e)] \approx \text{div }[\mu_i\,/(e\mu_e)\,\mathbf{j}] =$$
$$(\mathbf{j}/e)\mathbf{grad}(\mu_i/\mu_e) + \mu_i\,/(e\mu_e)\,\text{div }(\text{rot } \mathbf{B}/\mu_0) = \;(\mathbf{j}/e)\mathbf{grad}(\mu_i/\mu_e).$$

One can see that this term vanishes if the assumption that $(\mu_i\,/\mu_e) = \text{const}$ is correct (this is approximately true for For plasmas of air, air-fuel or exhaust gases). Thus, the drift term $\text{div}(n_i\mu_i\mathbf{E})$ gives a little input in the equation of plasma concentration. If the ambipolar diffusion and the reactions of ionization and recombination are also negligible, the plasma is expanding and compressing together with the neutral gas. It means, that then the value $x=n_i/n_g$ is constant, and on the interface of the drift and diffusion regions this value is equal to the unperturbed one in the ambient flow $?_¥$, that is essential for the diagnostic application. This equality is approximate: (μ_i/μ_e) is still varying, and in the next approximation one has to take it into account. Together with diffusion, it can result in a transport of plasma density along electric field lines, the value of $?$ can deviate from $?_¥$, especially in regions where the gas is locally rarefied. However, the numerical simulation has shown that even in the worst cases $?$ still changes much weaker than other plasma and gas parameters. Moreover, the effect of these deviations on the probe current is not strong. It makes it possible to assume that $x= ?_¥$.

Consider field distribution along the probe surface. The probe charge produces electric field around its surface, that provides the probe current. The external (discharge) electric field must be also taken into account, as it can be much higher than the probe field, especially due to the well-known effect of field concentration by conductors. The summary (probe and external) field (with no account to plasma effect) for a sufficiently long ($L/R \gg 1$) cylindrical probe with its axis normal to the ambient discharge field $\mathbf{E_0}$ in a medium with even conductance distribution can be approximated as [6]

73

$$\mathbf{E} = \mathbf{E_0} (1 - R^2/r^2) + \mathbf{r^0} 2(R^2/r^2) (\mathbf{E_0} \mathbf{r^0}) + \mathbf{r^0} V_p/(r\ln(L/R)), \tag{2.1}$$

here $\mathbf{r^0}$ is the unit radial vector, V_p is the probe voltage. The field component normal to the surface $E_n = (\mathbf{E_0} \mathbf{r^0})$ is

$$E_n = E_0 \cos\psi (1 + R^2/(R+r_a)^2) + V_p/((R+r_a)\ln(L/R)), \tag{2.2}$$

here ψ is the azimuth angular coordinate. If one neglects r_a in comparison with R, then

$$E_n \approx 2 E_0 \cos\psi + V_p/(R \ln(L/R)). \tag{2.3}$$

For a double probe (two cylinders with axes in a direction $\mathbf{z}$, situated in a plane normal to $\mathbf{E_0}$, $\mathbf{z} \perp \mathbf{E_0} \perp \mathbf{v_g}$), the sum of the values of current to the probes equals to zero. One of the probes absorbs only ions, while the other one absorbs both ions and electrons. Then, a consideration of (1.22) with respect to $m_i/m_e \ll 1$ yields that the probe is necessarily charged so that the relative area A^-/A^+ of the surface where electrons are absorbed would be as small as $m_i/m_e \ll 1$. (2.3) yields that the region with $E_n > 0$ appears at the probe potential

$$V_p^0 = 2 E_0 (R \ln(L/R)). \tag{2.4}$$

A probe potential can be expressed as $V_p = V_p^0 + \Delta V_p$. The normal field near the probe surface (or better to say on the interface with the diffusion layer, see above) in accord with (2.3), (2.4) is

$$E_n \approx 2 E_0 \cos y + 2 E_0 + \Delta V_p/(R \ln(L/R)), \tag{2.5}$$

i.e. the field near the probe is defined by the external field, if $E_0 \gg E_{0*} = \Delta V_p/(2R\ln(L/R))$, and by the difference of potentials between the two probes, if $E_0 \ll E_{0*}$.

2.2. Probe Voltage Current Characteristics

Consider a cylindrical probe (axis $\mathbf{z}$) in a plasma flow $\mathbf{v_g}$ and ambient field $\mathbf{E_0}$ ($\mathbf{z} \perp \mathbf{E_0} \perp \mathbf{v_g}$). The field is enhanced far before the probe: e.g., at $y = \pi/2$, the characteristic size of the region of doubled field is about R. However, at supersonic and even at transonic flow the gas density is also enhanced before the probe, and the resulting characteristic parameter E/n_g that defines electron temperature and ionization

is low at $y = \pi/2$. That is why one can consider there $x = x_¥$. The plasma flow separates in the critical point of the cross section of the probe cylinder, where $y = \pi/2$, $E_n \approx - 2E_0 + V_p/(R \ln(L/R))E_0$, and rejoins in the opposite side, where $y = 3\pi/2$, and again $E_n \approx - 2 E_0 + V_p/(R \ln(L/R))E_0$. One half of plasma flows through the region near the probe with an enhanced field, which has a maximum

$$E_{max} = 4 E_0 + \Delta V_p/(R \ln(L/R)) \tag{2.6}$$

at $y = \pi$. The corresponding yield to the total ion current

$$I_{i1} = LR \, _{\pi/2}\int^{3\pi/2} en_{i1}(y)\textbf{m}E_n \mathrm{d}y = \tag{2.7}$$
$$= LR \, _{\pi/2}\int^{3\pi/2} e^2 x(y) \, [2 E_0 (1 - \cos y) + \Delta V_p/(R \ln(L/R))]/[\Sigma_{im}(2 k_B T_g m_{mol})^{1/2}]\mathrm{d}y =$$
$$= \Xi_1 x_¥ LR \, _{\pi/2}\int^{3\pi/2} e^2[2 E_0 (1 - \cos y) + \Delta V_p/(R \ln(L/R))]/[\Sigma_{im}(2 k_B T_g m_{mol})^{1/2}]\mathrm{d}y.$$

Here the factor $\Xi_1 \geq 1$ takes into account deviation of the ionization degree distribution from a uniform one (primarily due to the plasma chemical reactions of ionization); if ionization is negligible, then $x \gg x_¥$, $\Xi_1 \approx 1$. If the variation of $T_g^{1/2}$ is negligible, then

$$I_{i1} = RL[2(\pi+2)E_0 + \pi\Delta V_p/(R \ln(L/R))]x_\infty\Xi_1 e^2/ [\Sigma_{im}(2 k_B T_g m_{mol})^{1/2}]. \tag{2.8}$$

The other half of plasma flows in a relatively attenuated field, with a minimal point near $y = 0$. The total current on this side of the probe contains ion and possibly electron current terms, $I_2 = I_e + I_{i2}$. The ion current term
$$I_{i2} = RL \, _{-\pi/2}\int^{\pi/2} en_{i2}\textbf{m}E_n \mathrm{d}y =$$
$$RL [E_0 2(\pi-2) + \pi\Delta V_p/(R \ln(L/R))]x_\infty\Xi_2 e^2/[\Sigma_{im}(2 k_B T_g m_{mol})^{1/2}]. \tag{2.9}$$

Here the factor Ξ_2 accounts for deviations of x from $x_¥$, that primarily results from the plasma chemical reactions; if they are negligible, then $\Xi_2 = 1$. Additional ionization here (i.e. $\Xi_2 > 1$) is possible if $E_0 \ll E_{0*}$, then $\Xi_1 = \Xi_2$. If $E_0 \gg E_{0*}$, an additional recombination (i.e. $\Xi_2 < 1$) is possible; this comparatively slow process does not seem to alter the ion concentration considerably. Note that then I_{i2} is $(4...5) (\Xi_1 /\Xi_2) \gg 1$ times less than the ion current on the opposite side: the first factor results from the enhanced ion drift speed, the last one − from the reactions. It altogether shows that it

is possible to use an approximate formula valid for both cases $E_0 \gg E_{0*}$ and $E_0 \ll E_{0*}$,

$$I_{i2} = RL[E_0 \, 2(\pi-2) + \Xi_1 \pi \Delta V_p/(R \, \ln(L/R))] x_\infty \, e^2/[\Sigma_{im}(2 \, k_B T_g \, m_{mol})^{1/2}]. \qquad (2.10)$$

The electron term

$$I_e \equiv \int e n_{e2} \mathbf{m}_e \, E_n \, dA^- \; = \; RL_{\psi+} \int^{\psi-} e n_{e2} \mathbf{m}_e \, E_n \, d\psi$$

exists only if A^- is not a zero, i.e. the normal field E_n changes its direction; it is possible only if $\Delta V_p > 0$. The zero field points correspond to

$$\mathbf{y}_\pm = \pm \, (\Delta V_p/(2 \, E_0 \, R \, \ln(L/R)))^{1/2} \; .$$

$|\mathbf{y}_\pm| \ll 1$ at considerable values of the ambient field, $E_0 \gg E_{0*} \; = \; \Delta V_p/(2R \, \ln(L/R))$. Then the field between $\mathbf{y}_-$ and $\mathbf{y}_+$ is

$$E_n \, (\mathbf{y}) \approx 2 \, E_0 \, \mathbf{y}^2 + \Delta V_p/(R \, \ln(L/R)),$$

it defines the electron current; integration yields as a by-product a result

$$I_e = RL \, n_{e2} \, e \mathbf{m}_e \, (2^{3/2}/3)[\Delta V_p/(R \, \ln(L/R))]^{3/2}/E_0^{1/2}, \qquad (2.11)$$

which coincides with [6]. The probe voltage $V_{p0} = V_p + \Delta V_{p0}$ providing zero total probe current can be obtained from the equality of ion and electron currents, $I_e = I_{i1} + I_{i2}$; at $E_0 \gg 2/(\pi+2)E_{0*}$, and $\Xi_1 - 1 \ll 1$, the equations (2.8),(2.10),(2.11) yield

$$\Delta V_{p0} = R \, \ln(L/R)[3\pi \, 2^{1/2} \, (\mathbf{m}_i/\mathbf{m}_e)(\, n_{i\infty}/n_{e2})]^{2/3} E_0. \qquad (2.12)$$

E.g., for $n_{e2} = n_{i2}$, $E_0 = 1$ kV/cm, $R = 0.5$ mm, $L = 5$ mm, $T_e = 2$ eV, $T_g = 300$ K the extra voltage ΔV_{p0} amounts to ≈ 6 V. For comparison, the corresponding probe voltage level $V_{p0} \gg - 180$ V. Note that ΔV_{p0} is proportional to E_0, and is rather small in comparison with RE_0.

The total voltage-current characteristic of the double probe (see Fig.3.1) can be deduced on base of the fact that for a given current I the total voltage is a sum of the voltages U_+ and U_- of the positively-biased and negatively-biased probes. At voltage

76

growth the electron current grows quicker than the ion current, which yields $U_- \gg U_+$, i.e. the total voltage-current characteristic depends on the probe that collects primarily ions.

Thus, if $E_0 \gg E_{0*}$ and $\Xi_1 = 1$, then the probe voltage-current characteristic $I = I(U)$ (here $U = \Delta V_p - \Delta V_{p0}$ is the difference of potentials of the two probes) is the following: at $U \leq -\Delta V_{p0}$, the probe current $I = -I_{is}$, here $I_{is} \equiv (I_{i1} + I_{i2})$ is the ion saturation current, in this region I is practically independent of voltage U :

$$I_{is} = RL\, E_0\{[2(\pi+2)\, \Xi_1 + 2(\pi-2)]\, x_\infty e^2/ [\Sigma_{im}(2\, k_B T_g\, m_{mol})^{1/2}].} \qquad (2.13)$$

At $-\Delta V_{p0} < U < 0$, the positive electron current $I_e \sim \Delta V_p^{2/3}$ (2.11) is added to the ion voltage-independent term. The total current passes the $I = 0$ point at $U = 0$. As the difference of potentials $|U|$ grows, E_{0*} grows too, the condition $E_0 \gg E_{0*}$ becomes false, ΔV_p cannot be neglected in the formulae for $I_{i1} + I_{i2}$, and one has to take into account the term depending on U:

$$|I| = RL[E_S\, \Xi_1 + 2(\pi-2)E_0]\, x_\infty e^2/[\Sigma_{im}(2\, k_B T_g\, m_{mol})^{1/2}], \qquad (2.14)$$
$$E_S = [2(\pi+2)E_0 + 2\pi\, (|U+\Delta V_{p0}|)/(R\ln(L/R))].$$

The value of ΔV_{p0} can be estimated from (2.12). If $E_0 \approx E_{0*}$, or $E_0 \ll E_{0*}$, then $|U| \gg |\Delta V_{p0}|$, and ΔV_{p0} can be neglected in (2.14). If $E_0 \ll E_{0*}$, then (2.14) looks like

$$I = 2\pi UL/\ln(L/R)\, \Xi_1\, x_\infty e^2/[\Sigma_{im}(2\, k_B T_g\, m_{mol})^{1/2}]. \qquad (2.15)$$

The probe current here is proportional to the probe voltage, if $\Xi_1 - 1 \ll 1$. Note that at $L/R \gg 1$, the probe current is practically independent of the probe radius R.

If the voltage bias U changes its polarity, then the two probes interchange their roles and voltage-current characteristics, that results in a symmetry of the total voltage-current characteristic of the double probe: $I(U) = -I(-U)$.

The formulae (2.13),(2.15),(2.14) can be used for plasma diagnostics in cases of dominating ion drift in the external (discharge) electric field, in the probe's electric field, and in the general, intermediate case, respectively. In the case $E_0 \gg E_{0*}$, the saturation current is measured; in the opposite case $E_0 \ll E_{0*}$, the slope I/U is informative; both of them at $U = \text{const}$ give current signals proportional to the plasma

value to be measured, that makes it possible to provide a very high temporary resolution. In all the cases, the unperturbed value of $x_{\Psi} = n_{i\Psi}/n_{g\Psi}$ is obtained. The dependence of the resulting x_{Ψ} on T_g is rather weak (even weaker than $\sim T_g^{1/2}$, if the temperature dependence of Σ_{im} is accounted for). If $E_0 \gg E_{0*}$, then E_0 must be also measured, that can be carried out with use of the same probe technique. All of it is valid if the reaction factor Ξ_1 is known.
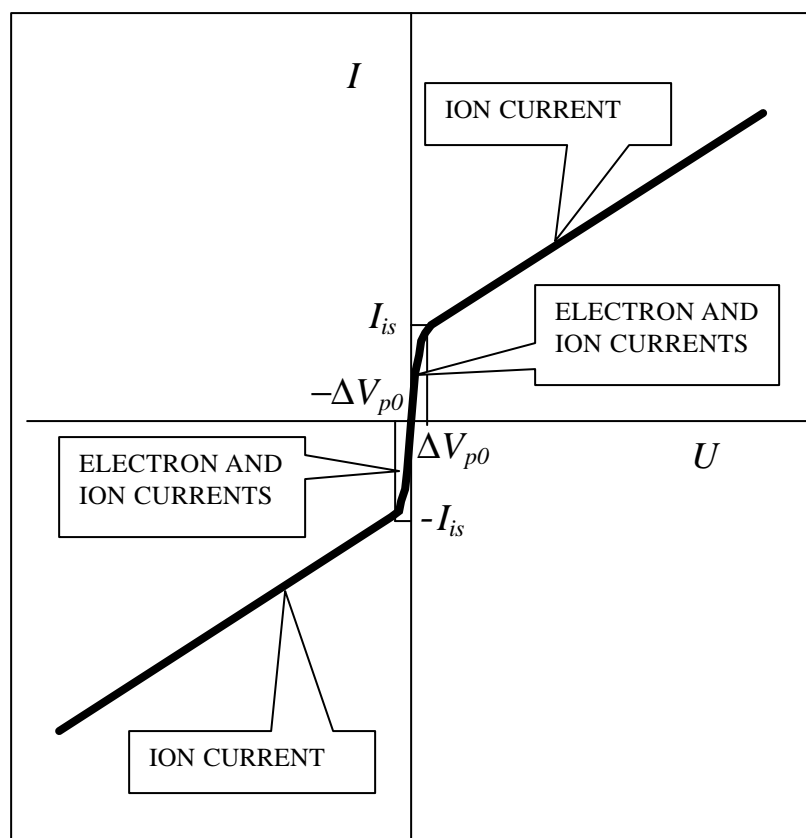
Fig.3.1. Theoretical total voltage-current characteristic of a double probe

§ 3. Plasma Chemical Reactions Near a Probe

To make the probe diagnostics possible, it is necessary to define the factor Ξ_1. Regions of parameters where it is unavailable limit the applicability of the probe diagnostics. Numerical simulation [2] has shown that Ξ_1 can be about 5...10 at moderate parameters ($R = 0.5$ mm, $E_0 = 200$ V/cm, $T_{g\ast} = 700$ K, $n_{i\ast} = 10^{14}$ cm^{-3}, $v_{g\ast} = 600$ m/s, $n_{g\ast} = 0.6 \ 10^{18}$ cm^{-3}, $T_{e\ast} = 1.7$ eV), and it depends on the gas density profile around the probe, i.e. on the Mach number M_∞. Mass calculations of Ξ_1 in a many-dimensional space of essential parameters on base of this model are too complicated. Our analysis of the numerical data has resulted in the following simplified model, which computation time was about $10^3 \ldots 10^4$ times as less, with a comparative reliability of results.

The model is based on the fact that ionization depends only on processes in the plasma flow tube near the half of the probe surface where the field is enhanced. The model is based on: 1) − the previously computed profiles of gas density $\rho_g = \rho_g \ (l)$ and speed $v_g = v_g \ (l)$ along the tube, $l = R\mathbf{y}$; 2) − the dependence (1.20) of T_e on E (for $T_v = 0$); 3) − the formula (2.5) for the electric field $E = E(\mathbf{y})$; 4) − formulae (1.7), (1.21) for $K_I(\mathbf{y})$ and $K_R \ (\mathbf{y})$; 5) − the equation for relative ion concentration x

$$[n_g(\mathbf{y}) \, v_g \ (\mathbf{y})/R] \partial x \ /\partial \mathbf{y} = K_I(\mathbf{y}) - K_R \ (\mathbf{y}), \tag{3.1}$$

which is derived from (1.6), (1.10) for the drift region (diffusion neglected) with respect to no effect of drift on x (see above), the dependence of T_e on E in accord with (2.7), and the formulae (2.5), (2.8) for $K_I(\mathbf{y})$ and $K_R \ (\mathbf{y})$. The factor Ξ_1 results from integration of probe current (1.22) with and without account for the reactions.

A similarity analysis has shown that Ξ_1 depends on parameters $RA \, (T_{e\infty}) n_{g\ast}/v_{g\ast}$, $E_{max}/n_{g\ast}$, Re_∞, M_∞, $x_\ast$, and $4E_0 \ /[\Delta V_p/(R \ln(L/R))]$. The first of them defines a relative time of presence of an elementary mass in the region of ionization. $E_{max}/n_{g\ast}$ is the traditional discharge parameter that defines electron energy. The influence of M_∞ is bound with a profile of density that creates a zone with enhanced local E/n_g . The influence of $x_\ast$ is bound with changes in the distribution function of electrons. The

effect of the last parameter is bound with a difference in field distributions over the probe surface for the cases of negligible and considerable values of external electric field. Actually, at low values of the external field this distribution is even, and in the opposite case it has a maximum on the one side of the probe, and a minimum on the other side.

Some results of calculations of Ξ_1 are shown in Fig.3.2. An analysis of the model and the numerical data show that Ξ_1 becomes higher with growth of the flow Mach number M_∞, plasma concentration $n_{i\infty}$, maximal electric field E_{max}, decrease of the gas flow speed $v_{g\infty}$ and density $n_{g\infty}$; the thicker is the probe, the higher is ionization. The parameters $RA(T_{e\infty})n_{g\infty}/v_{g\infty}$ and $E_{max}/n_{g\infty}$, are the most important. The dependence on M_∞ growth is in a way analogous to the effect of some growth of $E_{max}/n_{g\infty}$. Some weak dependence on x_∞ appears at low x_∞. The effect of the parameter $4E_0$ /[$\Delta V_p/(R$ ln(L/R))] is weak at $M_\infty \geq 1$, because then ionization is defined by narrow rarefied regions of flow, where the electric field is close to E_{max} for both cases of low and high values of E_0. For a subsonic flow the effect of fall of values of this parameter is analogous to some growth of values of $RA(T_{e\infty})n_{g\infty}/v_{g\infty}$.

There is a region of parameters where $\Xi_1 = 1...3$, in which Ξ_1 can be calculated reliably. These data on Ξ_1 can be used to adjust the diagnostic formulae (2.13)...(2.15). It is also a region with $\Xi_1 \gg 1$ and a very strong dependence of Ξ_1 on plasma and field parameters. No reliable probe diagnostics is possible there, for the initial plasma parameters become unavailable due to the additional ionization. The boundary between the two regions is rather distinct.

In some cases chemical reactions can affect the relative value of φ_D. Analytical studies [12] have shown that in a plasma with non-equilibrium chemical reactions the value of φ_D is negligible if

$$\varepsilon/\chi^2 \gg 1. \tag{3.2}$$

Here ε and χ are dimensionless parameters, which depend on plasma parameters in the ambient flow (indices ∞),

$$\varepsilon = h_\infty^2/R^2, \; h_\infty = [\varepsilon_0 k_B T_{e\infty}/(e^2 n_{e\infty})]^{1/2}, \tag{3.3}$$
$$\chi = d_\infty^2/(2R^2), \; d_\infty = [4n_i D_{i\infty}/(K_{R\infty}(1 + D_{i\infty}/D_{e\infty}))]^{1/2}.$$

For the characteristic parameters listed above, the condition $\varepsilon/\chi^2 \ll 1$ is met with a considerable reserve. Note that density and size dependencies are the following: $D_{i¥} \sim 1/n_{g¥}$, $K_{R¥} \sim n_{e¥}$, i.e. $\varepsilon \sim 1/(R^2 n_{e¥})$, $\chi \sim 1/(R^2 n_{g¥} n_{e¥})$, $\varepsilon/\chi^2 \sim R^2 n_{g¥}^2 n_{e¥}$. It means that under conditions of full-scale experiments with engines (higher R and $n_{g¥}$), the value of ε/χ^2 will be still higher.
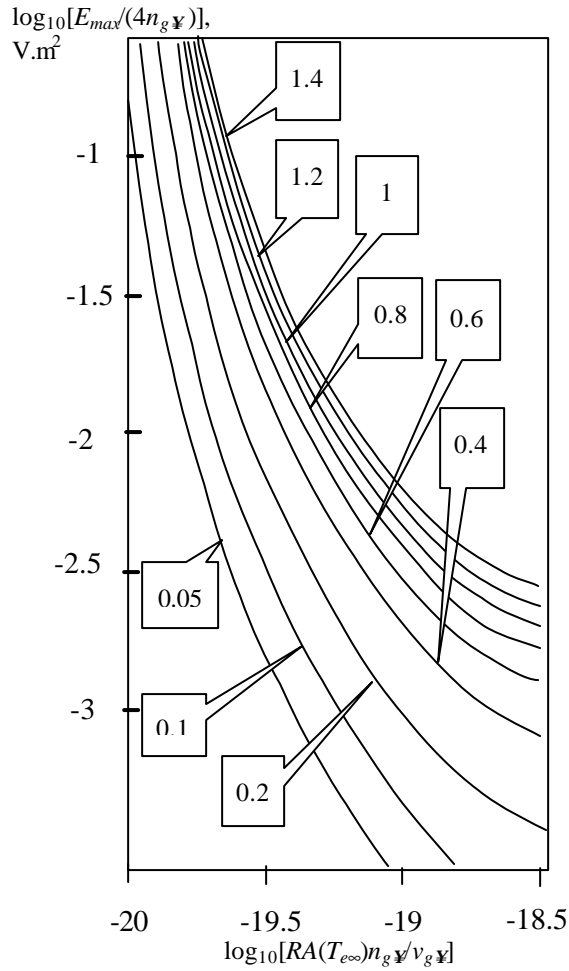
Fig. 3.2. Value of $\log_{10}(\mathbf{X}_1)$ at $M_¥ = 1.1$,
$A(T_{e¥}) = 0.3\ 10^{-18}\text{m}^3\text{/s}$ and $n_{i¥} = 10^{20}\,\text{m}^{-3}$

§4. Mathematical Modeling. Posing the problem

A direct computer simulation with account for processes in thin boundary layers is complicated. However, if one applies a strongly irregular mesh, and the boundary layer is not very thin, the direct computer simulation becomes realistic. E.g., at the probe radial size $R \cong 10^{-4}$ m, the Reynolds number Re $\approx (0.3\text{-}0.5)*10^3$, it was sufficient to apply a triangular mesh with characteristic cell size that quickly decreases at approaching the probe surface; the mesh had about 200 cells along the probe surface, and about 20,000 cells total. A series of simulation problems has been solved numerically with use of a PC with the Pentium III processor.

The neutral gas dynamics was simulated on base of (1.1) in the 2D planar approximation with the apparent boundary conditions, which are traditional for computations of flow over a body: zero velocity on the probe surface, ambient plasma flow parameters on the input boundary, and a free exit on the opposite side. This system of equations is separate from the rest, plasma equations, for the plasma effects on the neutral gas are neglected. The problem (1.1) was solved beforehand. The simulation of plasma processes was based on a system of 3 equations relatively the functions n_i, T_e, $\boldsymbol{j}$. The plasma concentration is defined by (1.6) with use of the formulae (1.7), (1.21), the electric potential is defined by (1.4), the electron temperature is defined by (1.18). Consider boundary conditions for these equations.

4.1. Boundary Conditions for Plasma Concentration

On the outer boundaries of the computational region the plasma concentration is equal to that of the ambient flow.

On the boundary near the probe surface the plasma concentration n_e is traditionally taken to be a zero [3, 4]. This condition is approximate, and it is invalid in our case. It introduces a singularity into the mathematical problem: the equation (1.4) becomes degenerate on the boundary, that results in computational difficulties. In other words, the plasma conductance (which is in a direct proportion to n_e) tends to zero on the boundary, and no electric current can leak through this "insulating layer". A correct definition of the boundary condition necessitated a special analysis of the ion kinetics in this region.

In the plasma volume the ion distribution function is close to the Maxwell function, which is shifted in the velocity space for the ion drift velocity v_i. The temperature in the Maxwell function $?_i$ is in our case close to the local gas temperature. The ion distribution function near the boundary has no particles that move from the metal surface (ions are neutralized there, i.e. they vanish as ions and appear as neutral particles). The rest ion distribution function here can be also considered to be close to the Maxwell function, which is shifted for the ion drift velocity:

$$f_i\,(v_{in},v_{it})= C\,\exp\{-\,m_i\,[(v_n\text{-}v_{in}\,)^2+v_t^2]/\,(2k_BT_i)\} \qquad (4.1)$$

here v_n is the component of the velocity of chaotic ion movement, which is normal relatively the boundary surface, v_t is the tangent component of this chaotic velocity. The mean normal component of the total ion velocity on the boundary v_b is defined by integrating of this distribution function:

$$v_b = {}_0\!\int^\infty_0\!\int^\infty v_n f_i(v_n, v_t)\,2\pi\,v_t\,\mathrm{d}v_n\,\mathrm{d}v_t\,/_0\!\int^\infty_0\!\int^\infty f_i(v_n, v_t)\,2\pi\,v_t\mathrm{d}v_n\,\mathrm{d}v_t.$$

The resulting function

$$v_b = \{v_{in}+\,2^{-1/2}\pi^{-1/2}T_i^{1/2}\,\exp[-m_iv_{in}^2/(2k_BT_i)]+v_{in}\mathrm{erf}[v_{in}(2k_BT_i/m_i)^{-1/2}]\}/ \quad (4.2)$$
$$\{1 + \mathrm{erf}[v_{in}(2k_BT_i/m_i)^{-1/2}]\}$$

can be approximated with a good accuracy ($\approx 1...5\%$) by a formula

$$v_b = v_{in} + v_{iT}/2\,\exp(-2\,[v_{in}\,/\,v_{iT}]^2). \qquad (4.3)$$

Here v_{iT} is the arithmetic mean thermal ion velocity, $v_{iT} = [8k_BT_i/(\pi m_i)]^{1/2}$. Thus, at $v_{in} \gg v_{iT}$ the boundary mean ion velocity is equal to the drift velocity v_{in}, and at $v_{in} \ll v_{iT}$ it approaches the value $v_{iT}/2$, which is characteristic for a boundary condition of the diffusion equation near an absorbing wall (see, e.g., [13]).

This normal ion velocity v_b is the necessary boundary condition for the equation of ions movement.

4.2. Boundary Conditions for Electron Temperature

On the outer boundaries of the computational region the plasma temperature is equal to that of the ambient flow.

On the boundary with a metal probe, the following boundary condition is applied for the plasma temperature [14, 15]:

$$(j_e \ r^0) \ (H_e/e - j) = 1_e \ (\tilde{N} T_e \ r^0), \quad H_e = 2.5 \ k_B T_e, \quad j_e = e n_e \ v_e, \tag{4.3}$$

here r^0 is the unit vector normal to the boundary surface. In our case, the electron current is absent along all (or practically all) the surface, because all the electrons are repelled back to the plasma volume by the electric field. With respect to this condition, $j_e = 0$, the expression (4.3) reduces to

$$1_e(T_e) \tilde{N} T_e = 0,$$

and as $1_e(T_e) > 0$, one can get $\tilde{N} T_e = 0$. That's why the current computations applied the boundary condition

$$\partial T_e / \partial r = \text{const.} \tag{4.4}$$

4.3. Boundary Conditions for Electric Potential

The value of probe potential $j = j_0$ defines the boundary condition on the probe surface.

On the infinitely far outer boundaries of the computational region the plasma potential must tend to zero. However, the realistic computational mesh cannot be made infinitely large, and the potential must be defined for the boundary size $r \approx R_b < \infty$. The difference of the boundary plasma potential from the ideal zero, that results from finitute of R_b, must be accounted for at interpretation of numerical results. Actually, a couple of endless equipotential coaxial cylinders with radii R and R_b is modeled. Such a system defines a potential in a medium with an even distribution of conductance (that for our case is true for $r >> R$, and approximately true for $r \approx R$)

$$j_m(r) = j_0 \ \ln(R_b/r)/\ln(R_b/R), \tag{4.5}$$

and the corresponding electric field

$$E_m(r) = j_0 \ /[r\ln(R_b/R)]. \tag{4.6}$$

One can see that $E_m(r)$ depends explicitly on R_b/R. This dependence is rather strong even at $R_b \approx 10R$. It is apparent that it is impossible to enhance R_b/R considerably due to computational difficulties. Note that at $R_b/R \rightarrow \infty$ the electric field vanishes in all the volume. These difficulties are bound with the cylinders are infinitely long in the 2D approximation. The probe should be better considered as a long ($L>>R$), but finite cylinder with a potential V_p; it defines an electric field in a medium with an even distribution of conductance

$$E = V_p/(r\ln(L/R)) \qquad (4.7)$$

and the corresponding potential

$$\boldsymbol{j}_p = V_p\ln(L/r)/\ln(L/R). \qquad (4.8)$$

In order to fit the model of infinitely long cylinders to this, more adequate approach, these potentials must define the same electric fields, i.e.

$$\boldsymbol{j}_0 /[r\ln(R_b/R)] = V_p/(r\ln(L/R)),$$

that gives the fitting factor $?_b$ for the potential, which is bound with the peculiarities of the 2D model and the finitute of R_b/R in realistic computations:

$$V_p = ?_b\boldsymbol{j}_0 , ?_b= \ln(L/R) / \ln(R_b/R). \qquad (4.9)$$

At characteristic values of $R_b = 5...10R$ and $L \approx 50...100$ R the value of $?_b$ is 1.4...2.8, i.e. it obligatorily must be accounted for at the analysis of computed probe voltage-current characteristics. The application of this factor makes it possible to get sufficiently correct boundary conditions at moderate values of $R_b = 5...10R$.

The computer simulation of the gas dynamics of flow over the probe was carried out with use of the implicit free-LaGrange method [16], which belongs to the class of methods considered in [17, 18]. It applies an irregular triangular mesh that moves with the gas, the mesh is much denser near the probe and is rather rarefied near the outer boundaries. It made it possible to resolve the probe boundary layers, and to provide a sufficient distance from the outer boundaries. The plasma part of the problem was solved with use of a fixed mesh, which had resulted from the solution of

the gas dynamical part of the problem, and with the corresponding distributions of gas temperature, density and velocity.

4.4. Computation Results

Characteristic results of computer simulation are presented in Fig. 3.3–3.27.

The following values of input parameters (for boundary conditions) were used: $R = 0.05$ mm, $v_{g¥} = 600$ m/s, $T_{e¥} = 1.5$ eV, $n_{e¥} = 10^{19}$ m^{-3}, $n_{g¥} = 10^{24}$? $^{-3}$, $T_g = 300$? and $T_g = 1000$?, $\boldsymbol{j}_p = 1 - 50$ V.

Fig.3.3–3.12 correspond to a supersonic gas flow (M = 1.5, the initial gas temperature is 1000 K), and Fig. 3.15–3.24 correspond to a subsonic gas flow (M = 0.88, the initial gas temperature is 300 K, all the other boundary conditions coincide with the subsonic case). For a comparison, some results of computations of the plasma parameters with a constant electron temperature $T_e = 1.5$ eV, i.e. with no account for the plasma chemical reactions, are shown in Fig. 3.13–3.14 for the supersonic and in Fig. 3.25–3.26 for the subsonic cases. Fig. 3.27 shows the resulting voltage-current characteristics.
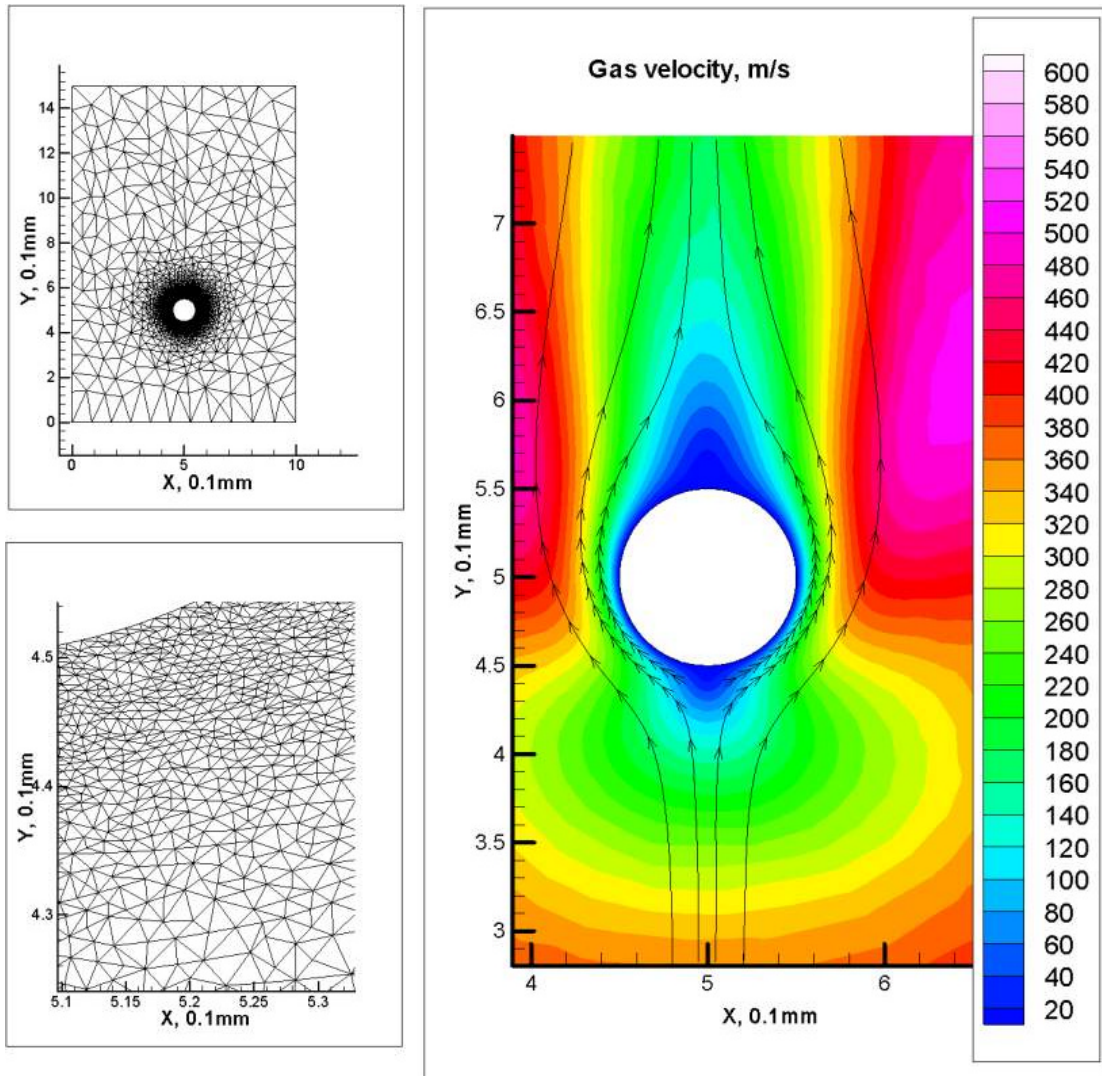
Fig. 3.3. The computational mesh and the plasma velocity distribution at M = 1.5
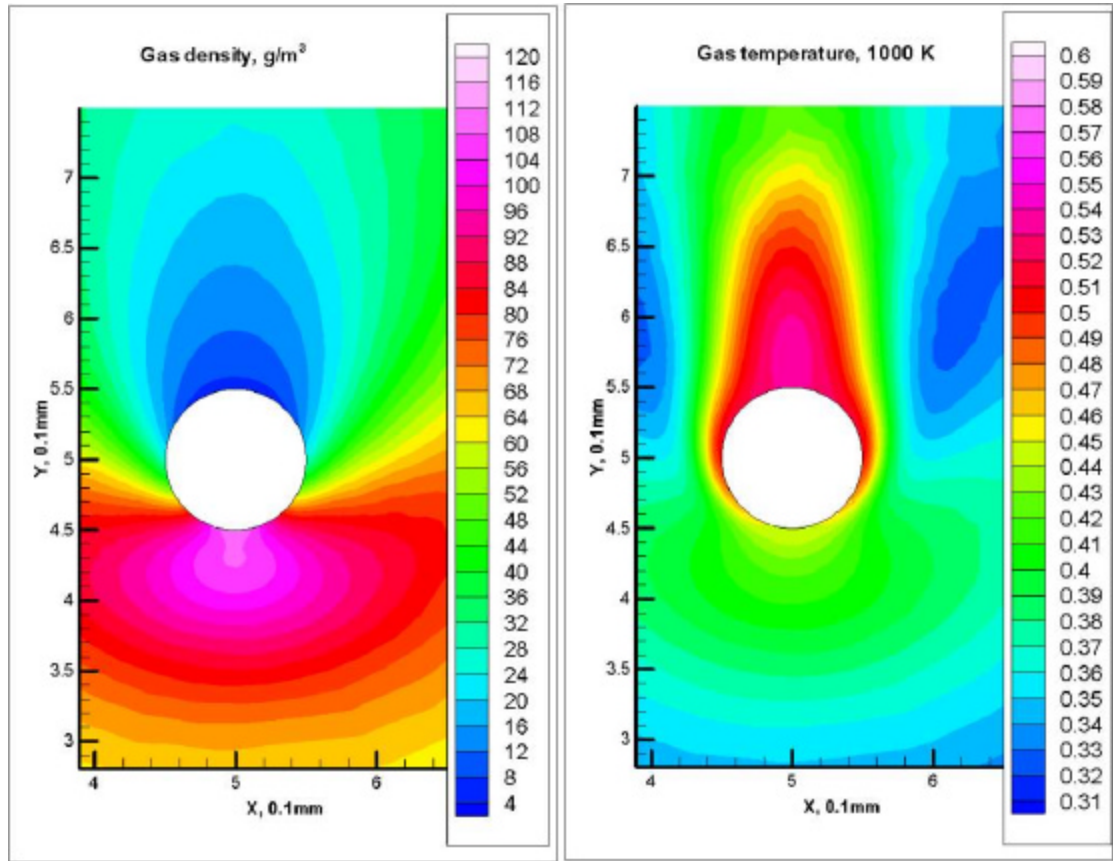
Fig. 3.4. Distributions of gas density and temperature at M = 1.5
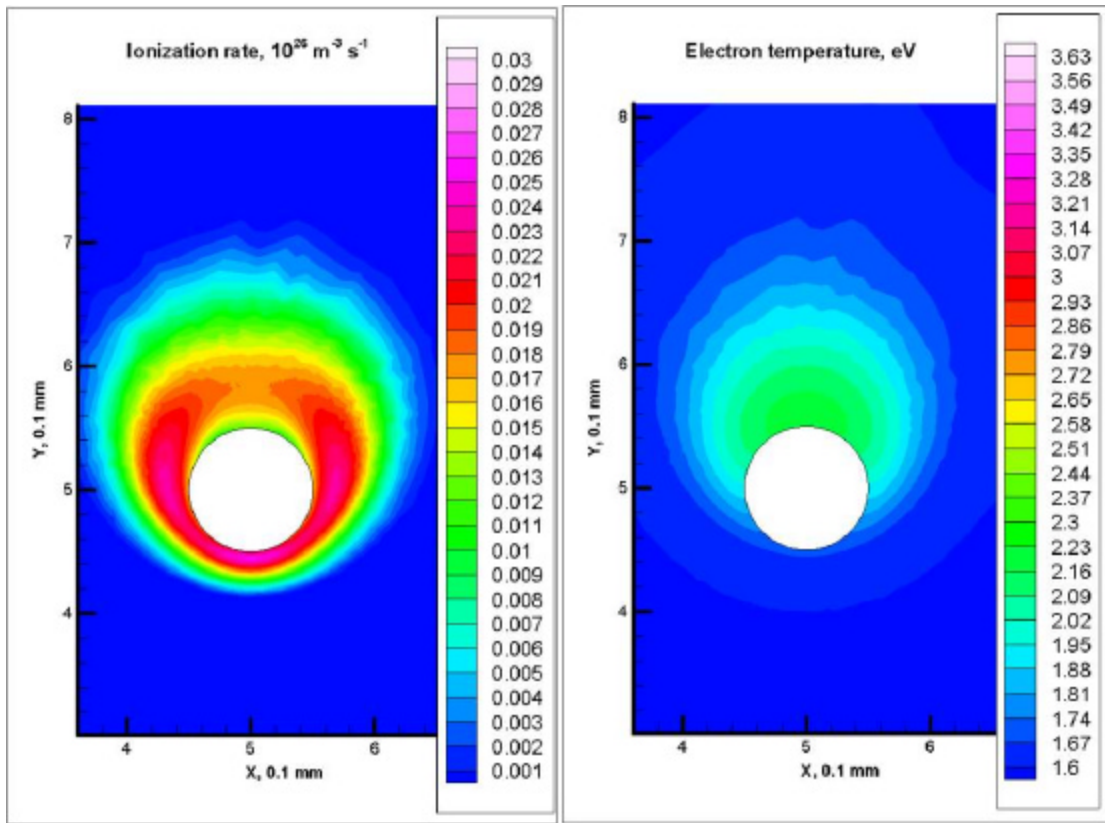
Fig. 3.5. Distributions of plasma ionization rate and electron temperature at M = 1.5 and the probe potential of 16 V
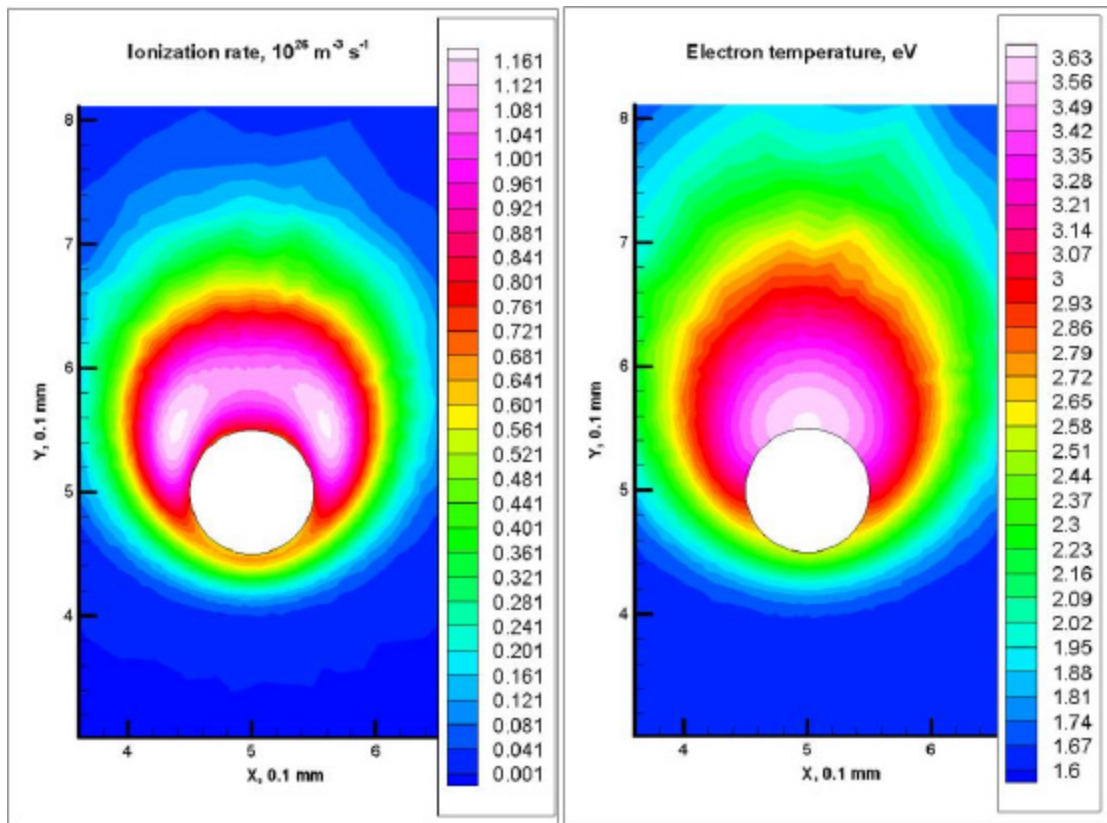
Fig. 3.6. Distributions of plasma ionization rate and electron temperature at M = 1.5 and the probe potential of 42 V
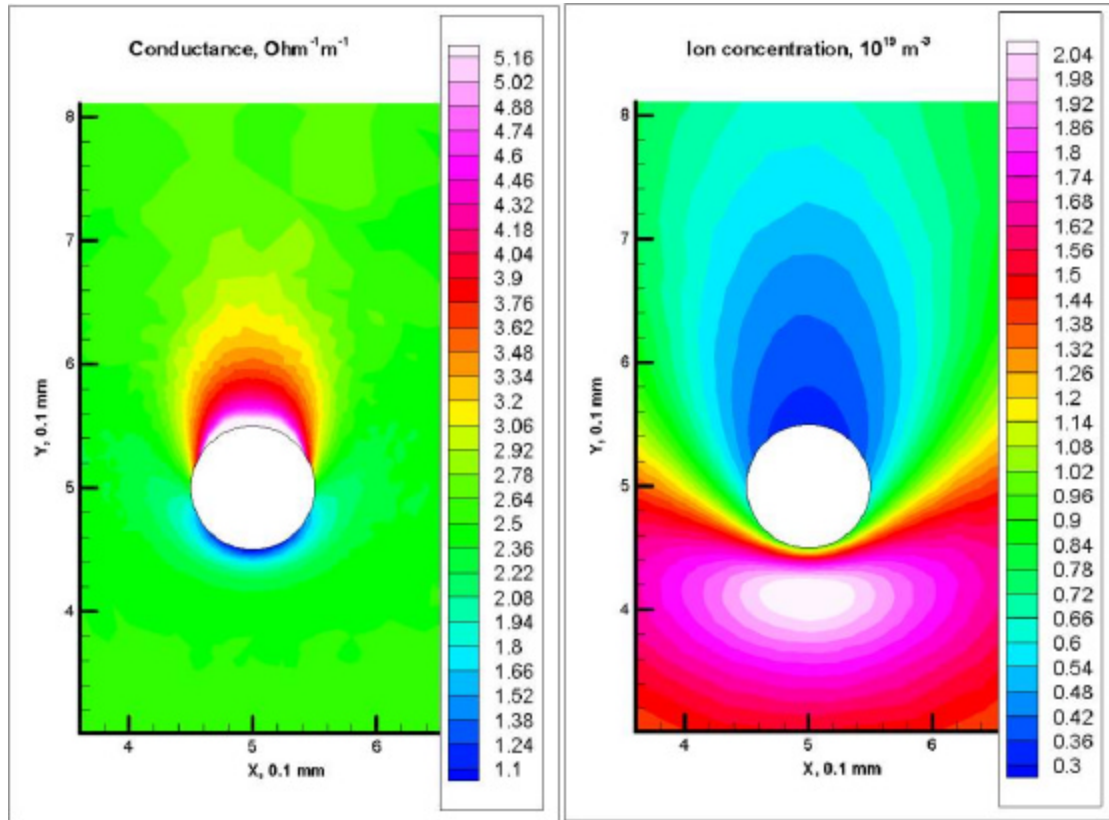
Fig. 3.7. Distributions of plasma conductance and ion density at M = 1.5 and the probe potential of 0 V
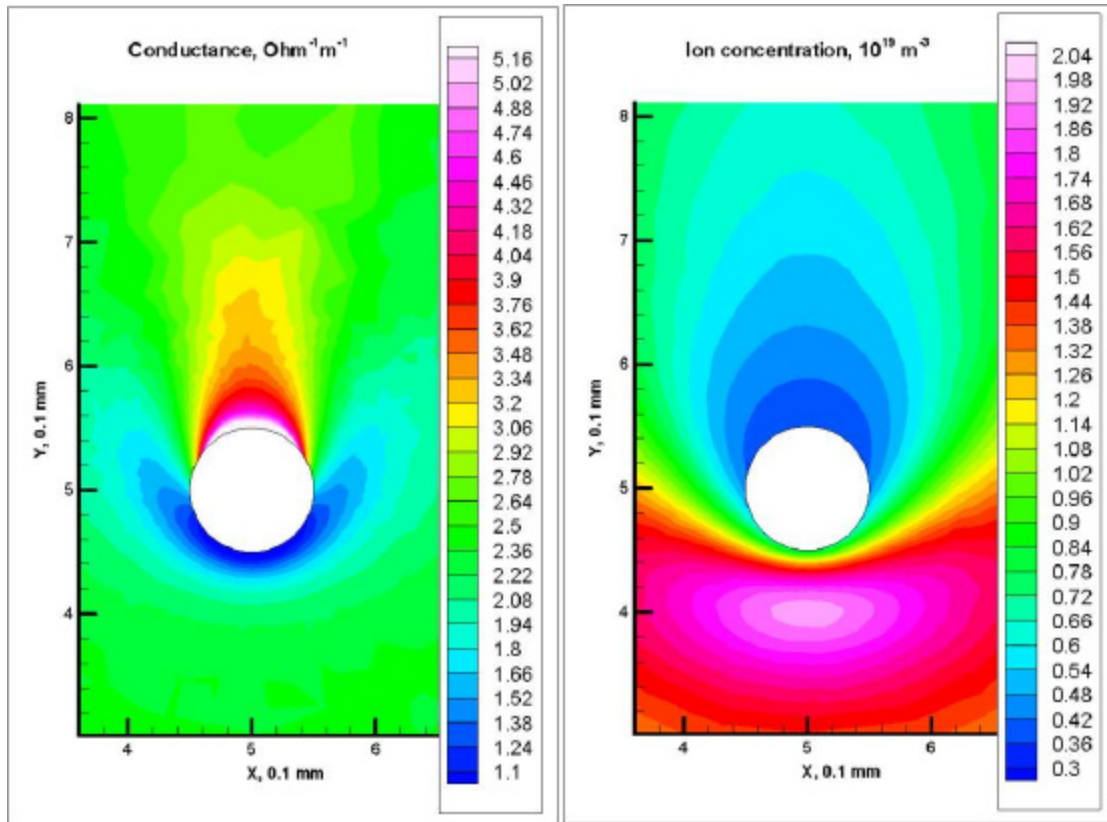
Fig. 3.8. Distributions of plasma conductance and ion density at M = 1.5 and the probe potential of 16 V
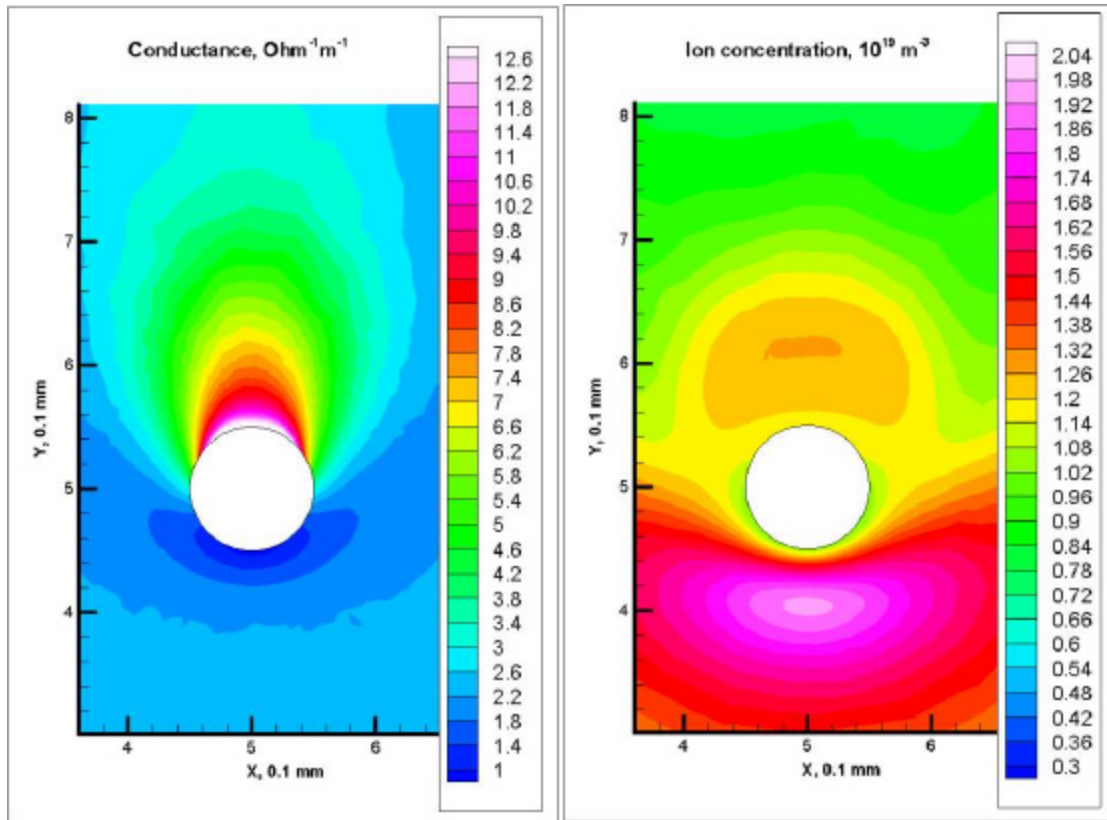
Fig. 3.9. Distributions of plasma conductance and ion density at M = 1.5 and the probe potential of 42 V
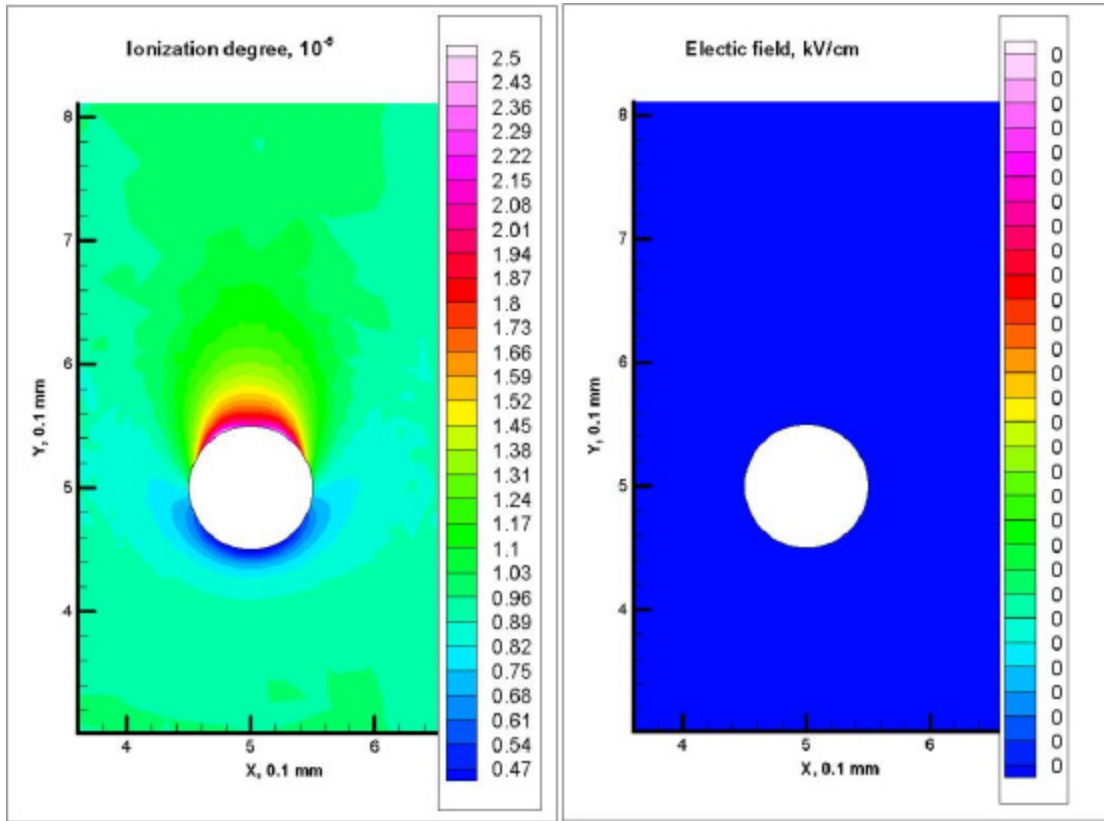
Fig. 3.10. Distributions of n_i / n_g and electric field at M = 1.5 and the probe potential of 0 V
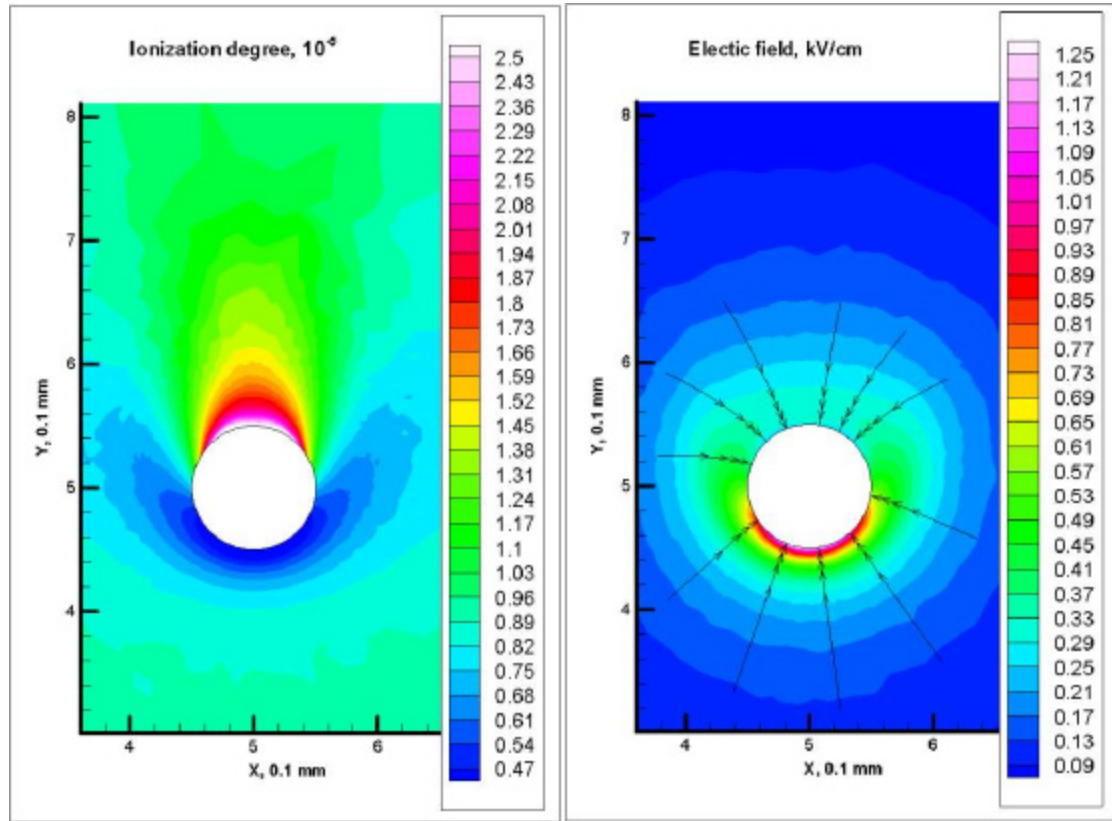
Fig. 3.11. Distributions of n_i/n_g and electric field at M = 1.5 and the probe potential of 16 V
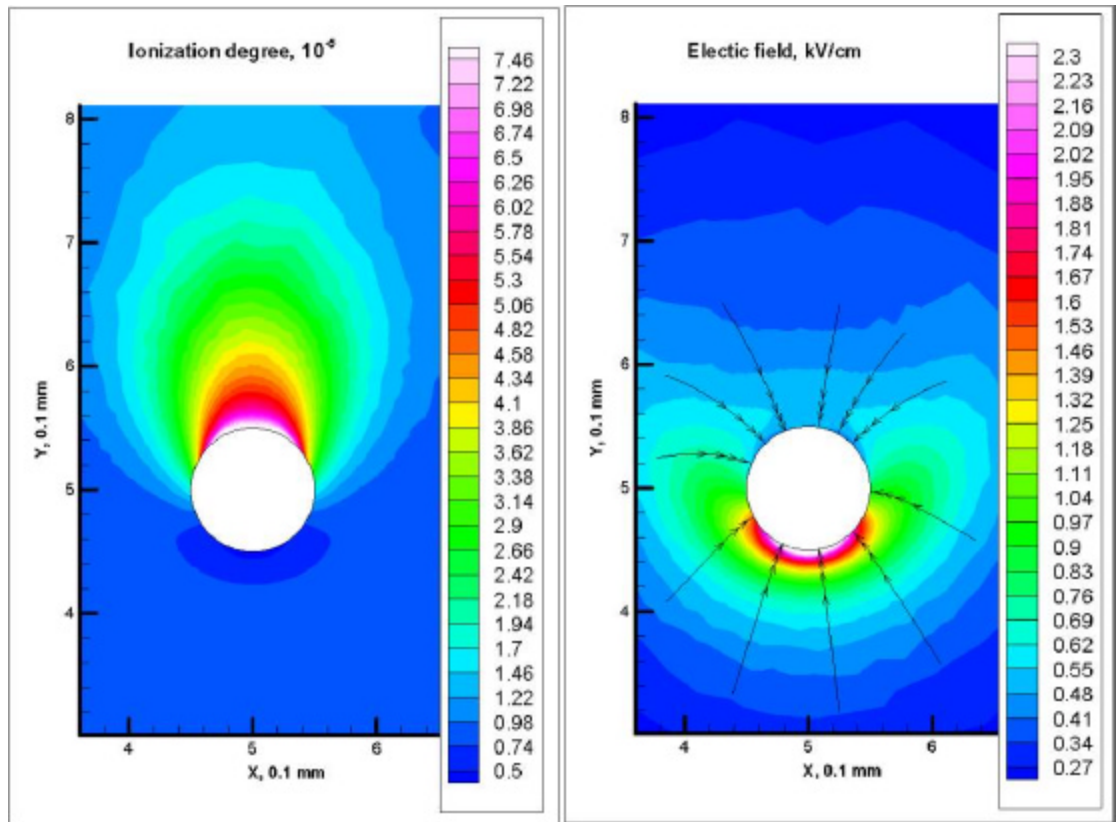
Fig. 3.12. Distributions of n_i/n_g and electric field at M = 1.5 and the probe potential of 42 V
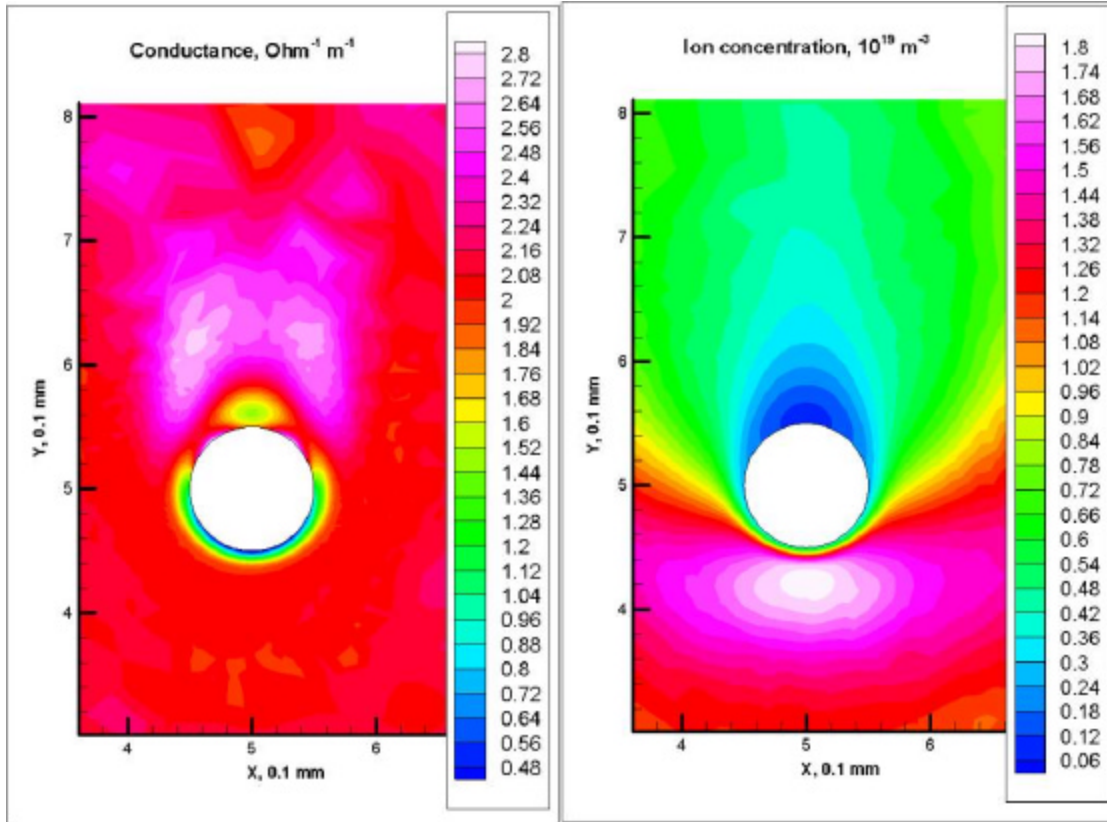
Fig. 3.13. Distributions of plasma conductance and ion density at M = 1.5 and the probe potential of 28 V, computation with $T_e = 1.5$ eV = const
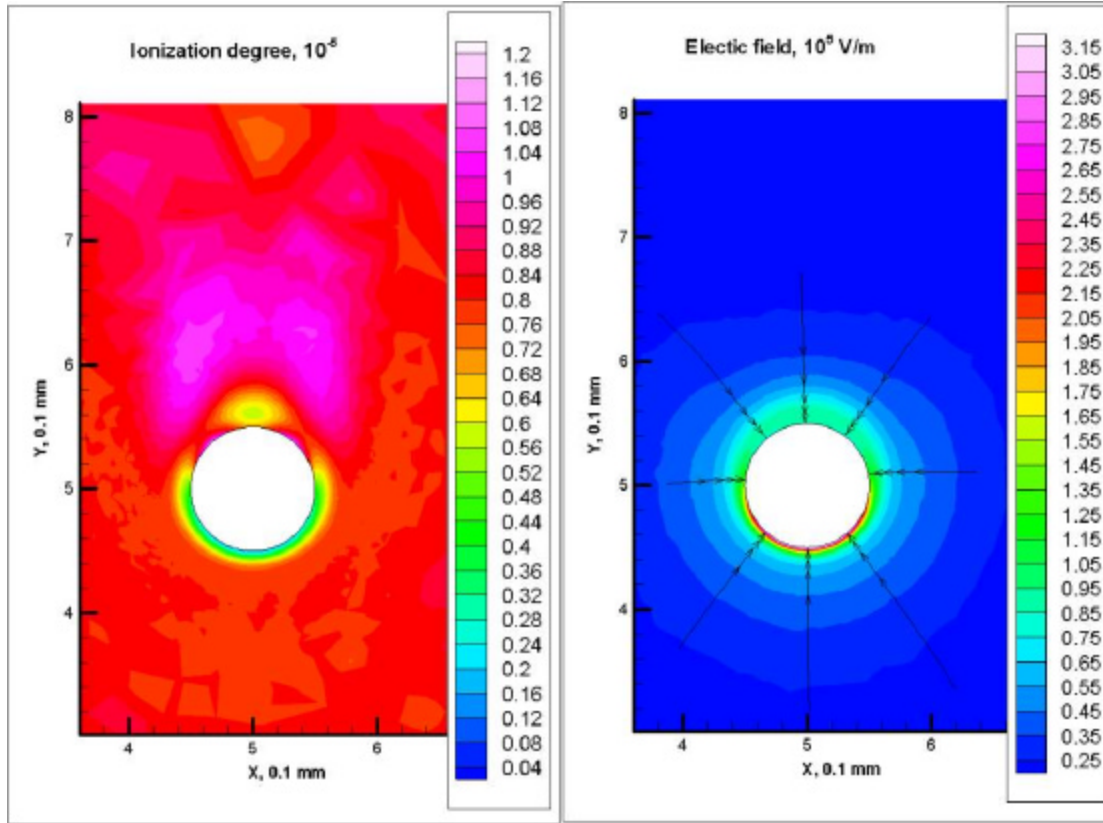
Fig. 3.14. Distributions of n_i/n_g and electric field at M = 1.5 and the probe potential of 28 V, computation with $T_e = 1.5$ eV = const
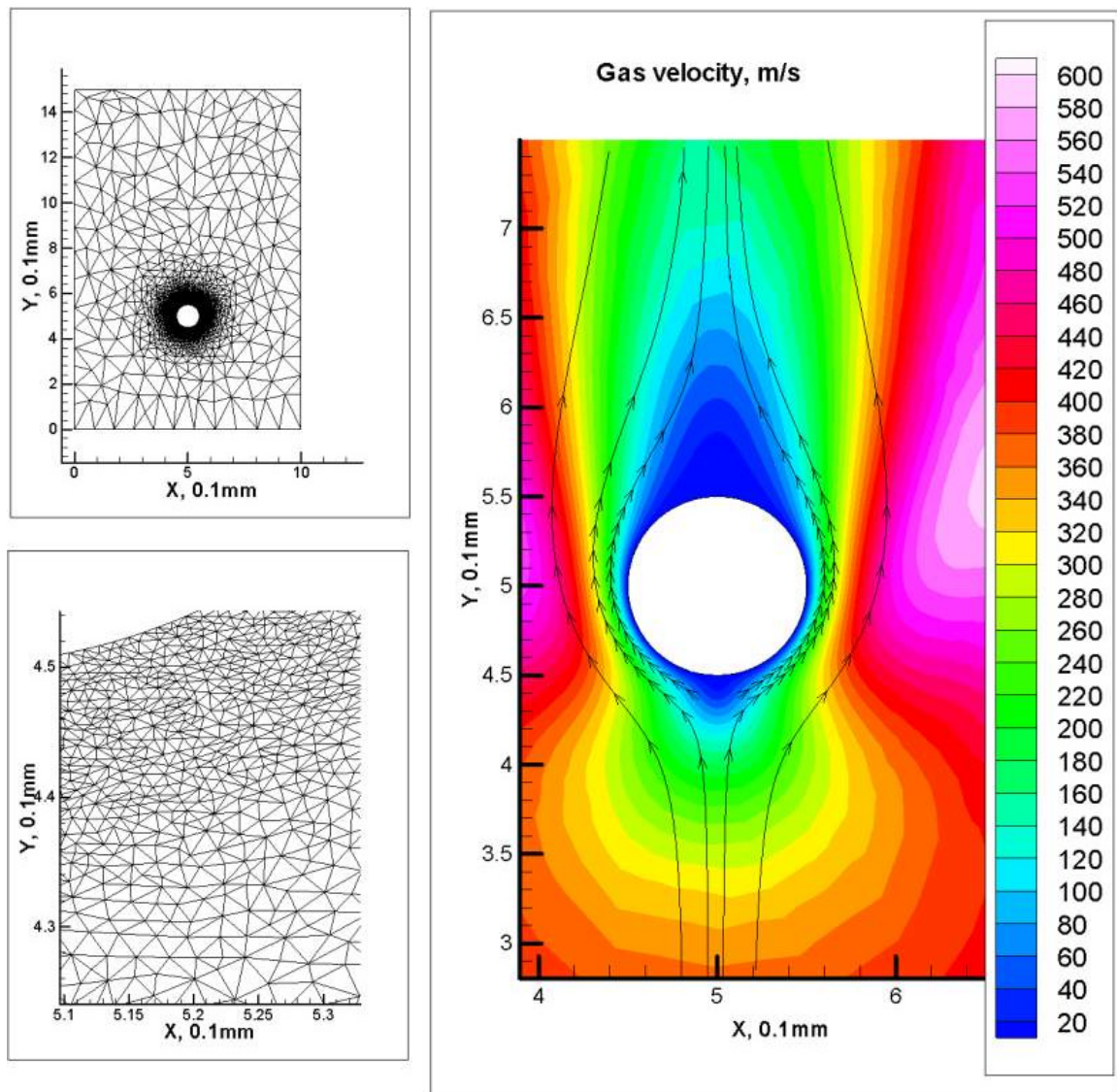
Fig. 3.15. The computational mesh and the plasma velocity distribution at M = 0.85
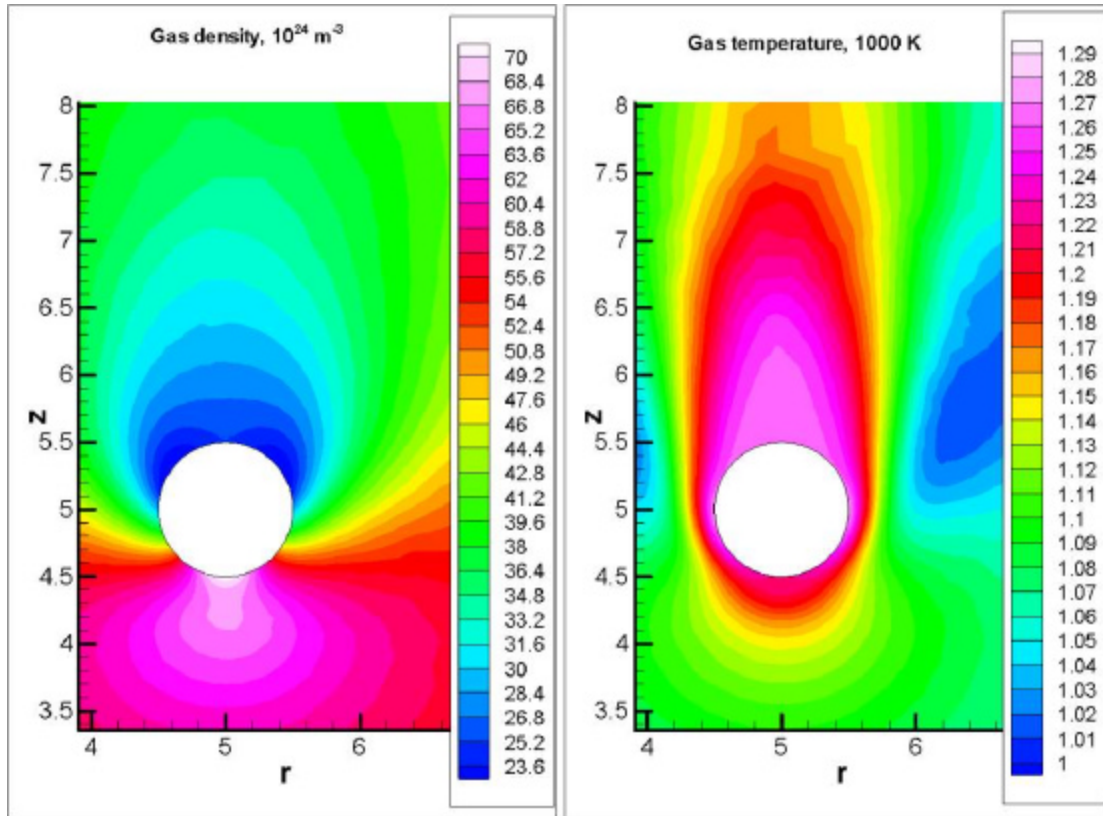
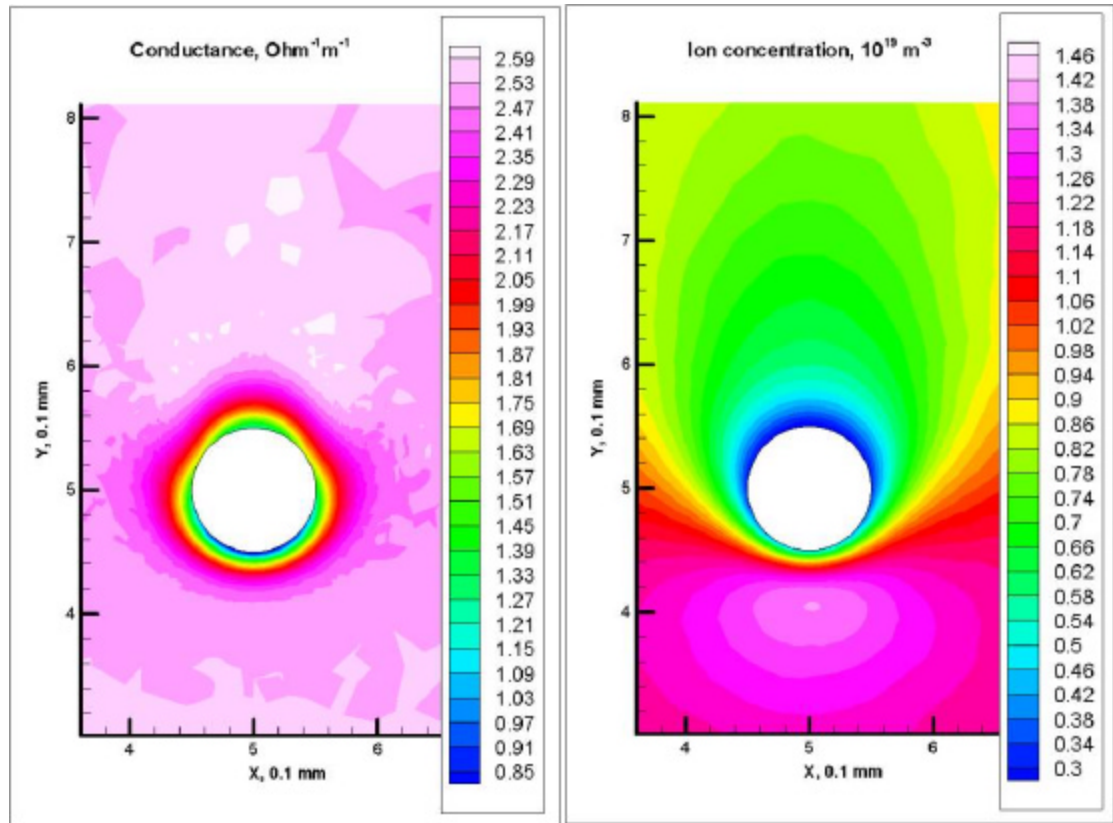**Fig. 3.16. Distributions of gas density and temperature at M = 0.85**
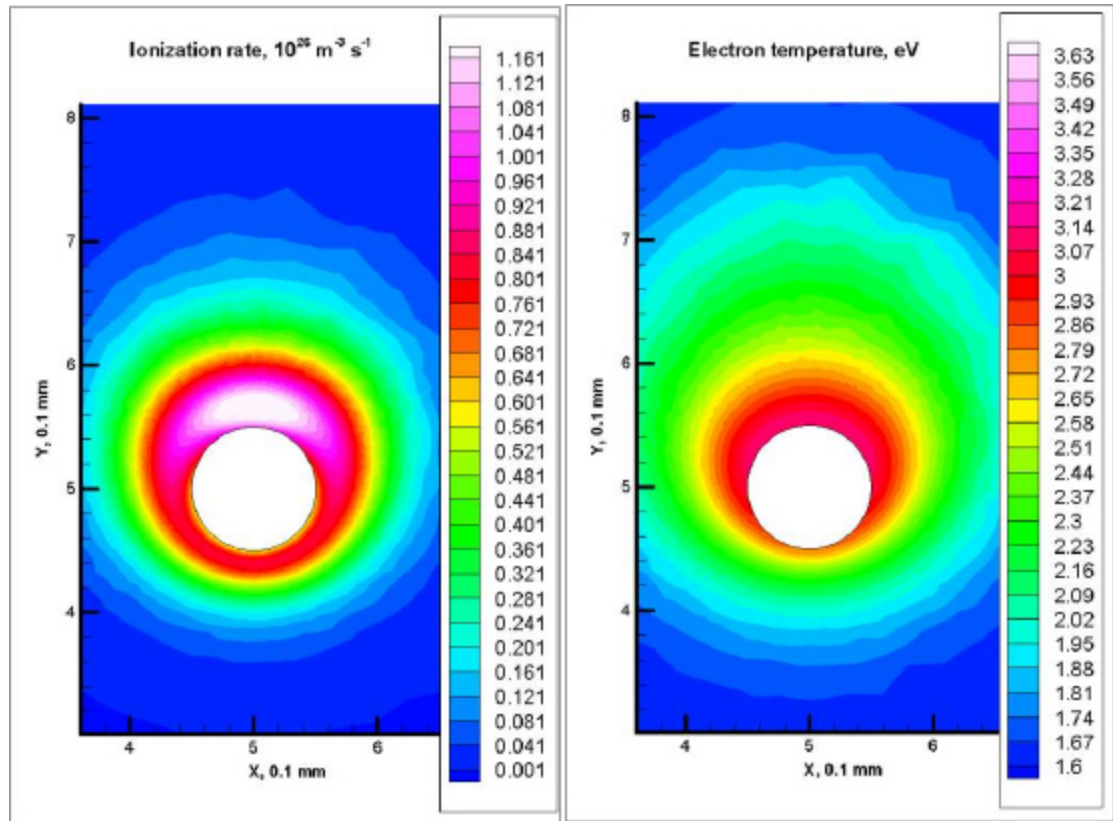
Fig. 3.17. Distributions of plasma ionization rate and electron temperature at M = 0.85 and the probe potential of 42 V
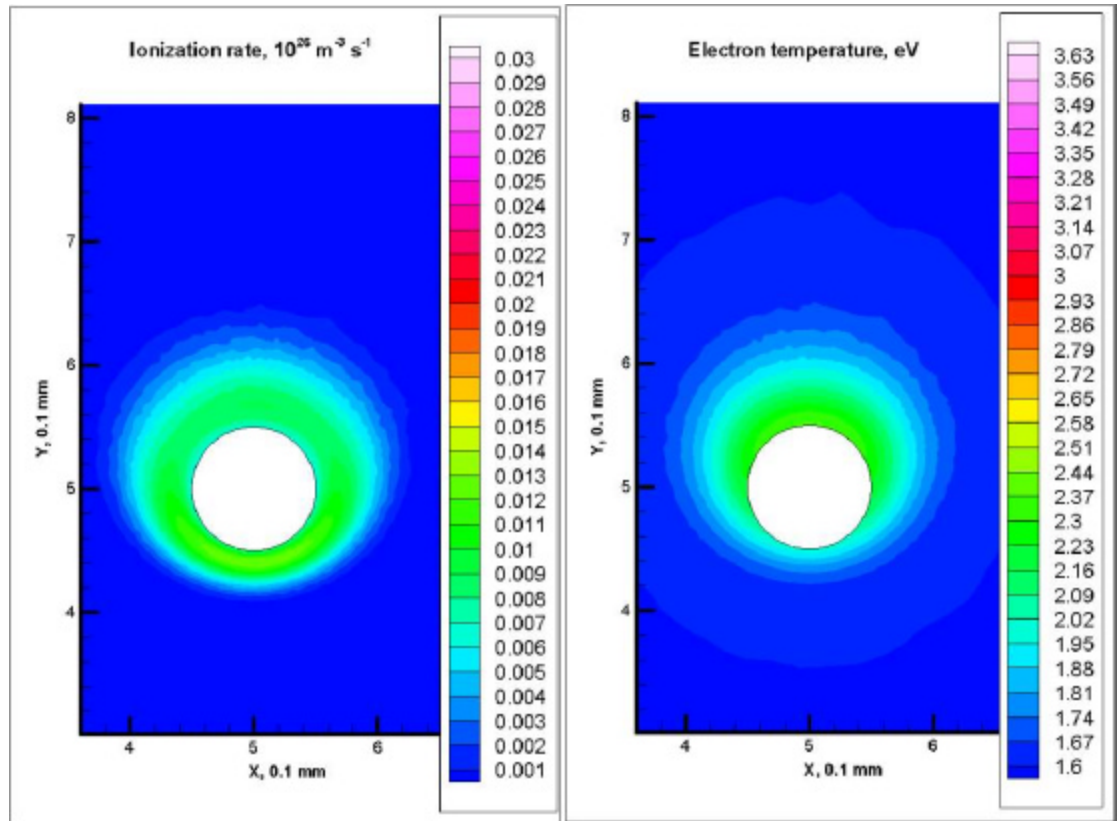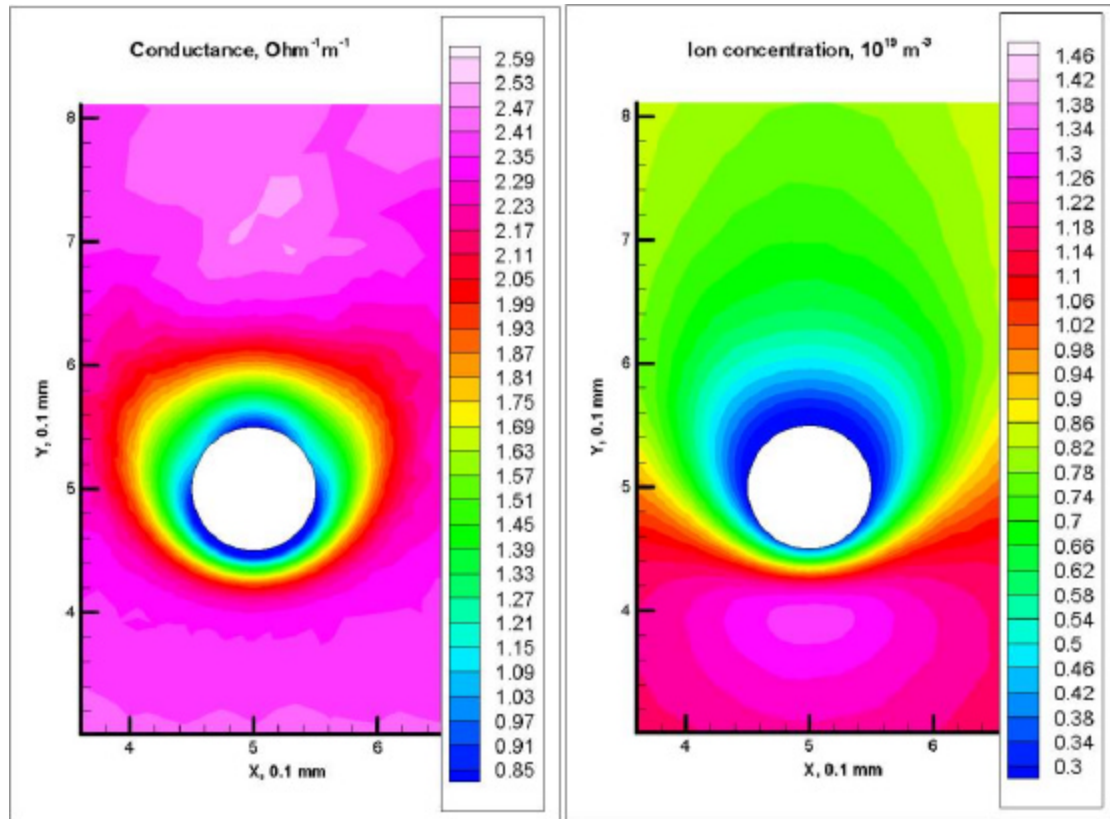
Fig. 3.18. Distributions of plasma ionization rate and electron temperature at M = 0.85 and the probe potential of 16 V

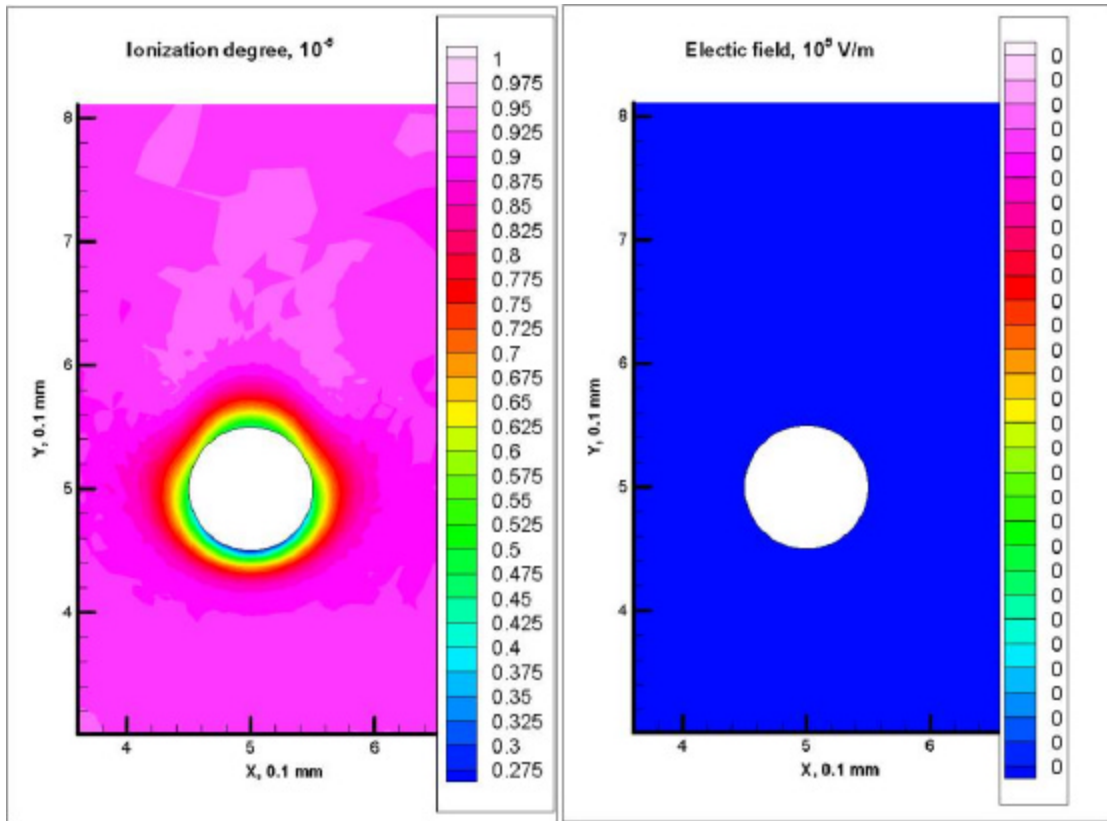**Fig. 3.19. Distributions of plasma conductance and ion density at M = 0.85 and the probe potential of 0 V**
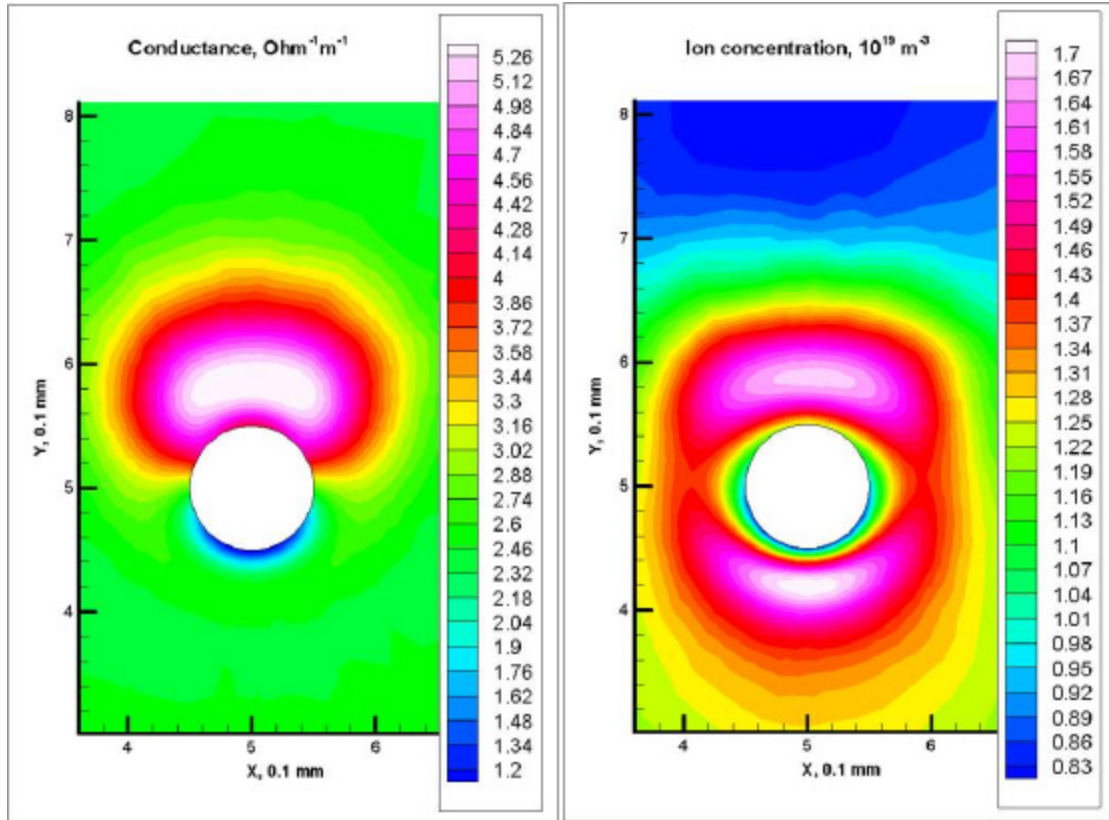
Fig. 3.20. Distributions of plasma conductance and ion density at M = 0.85 and the probe potential of 42 V
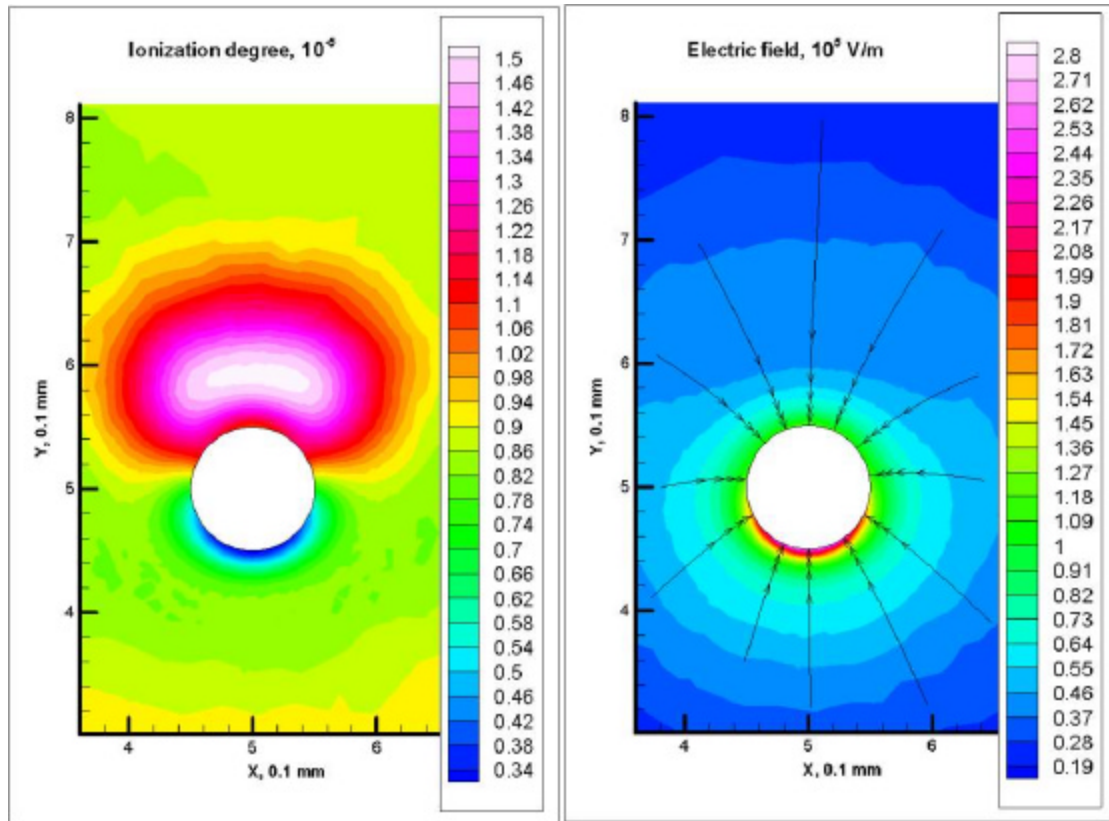
Fig. 3.21. Distributions of plasma conductance and ion density at M = 0.85 and the probe potential of 16 V
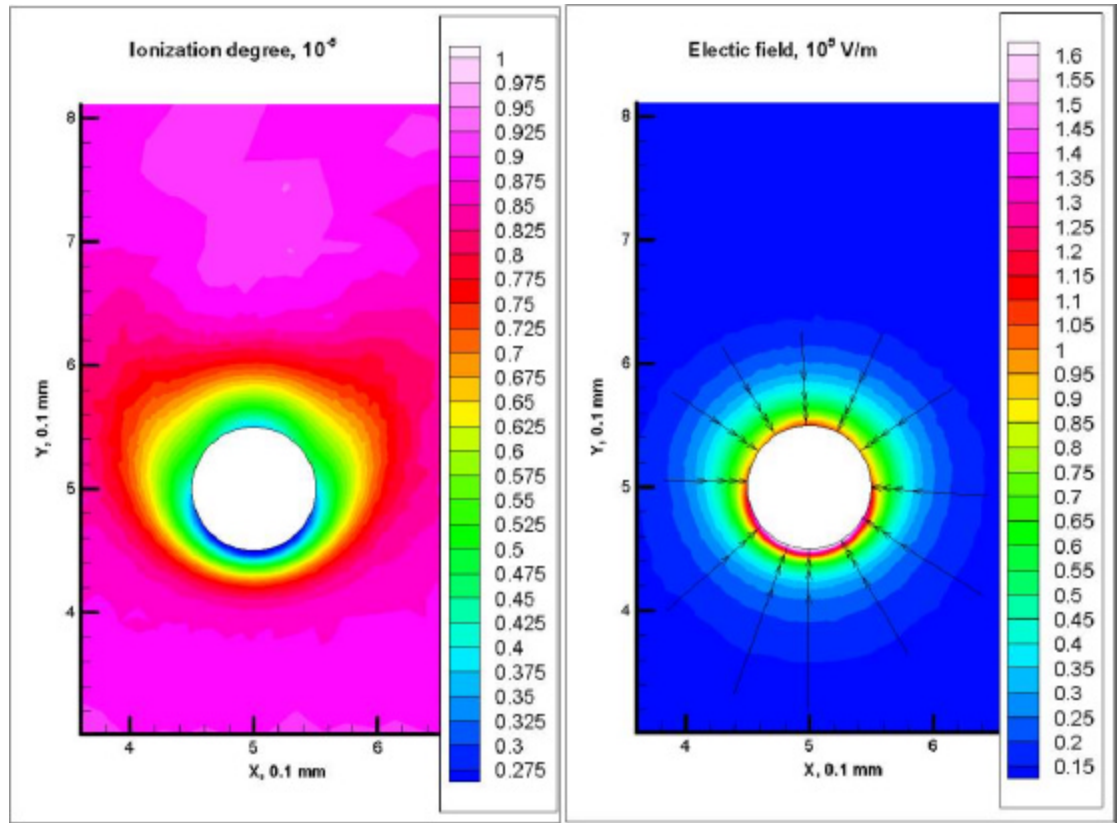
Fig. 3.22. Distributions of n_i/n_g **and electric field at M = 0.85 and the probe potential of 0 V**
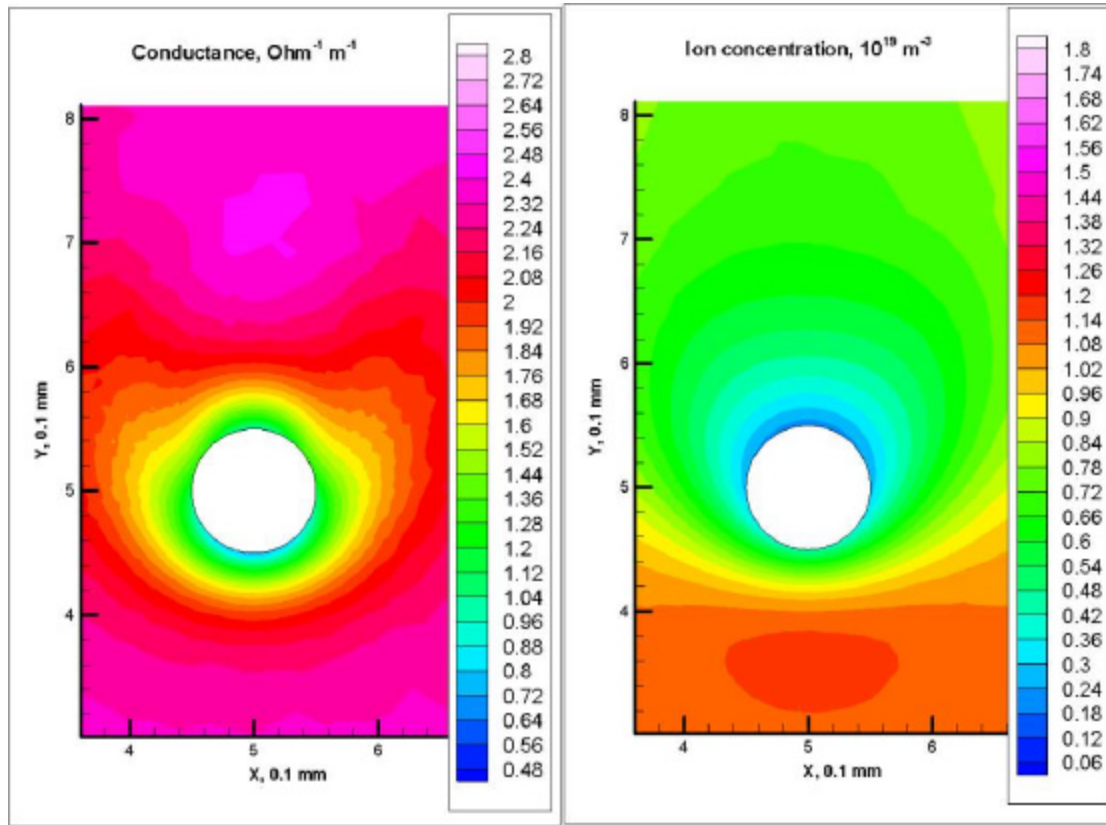
Fig. 3.23. Distributions of n_i/n_g and electric field at M = 0.85 and the probe potential of 42 V

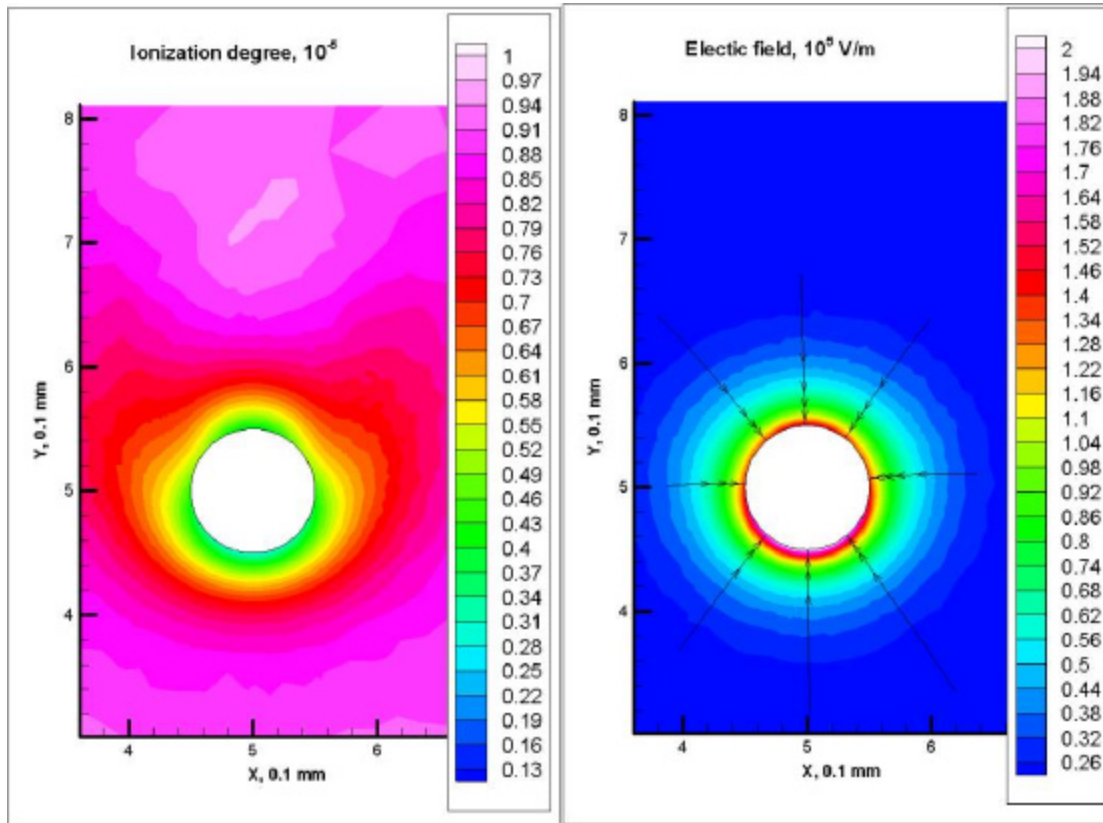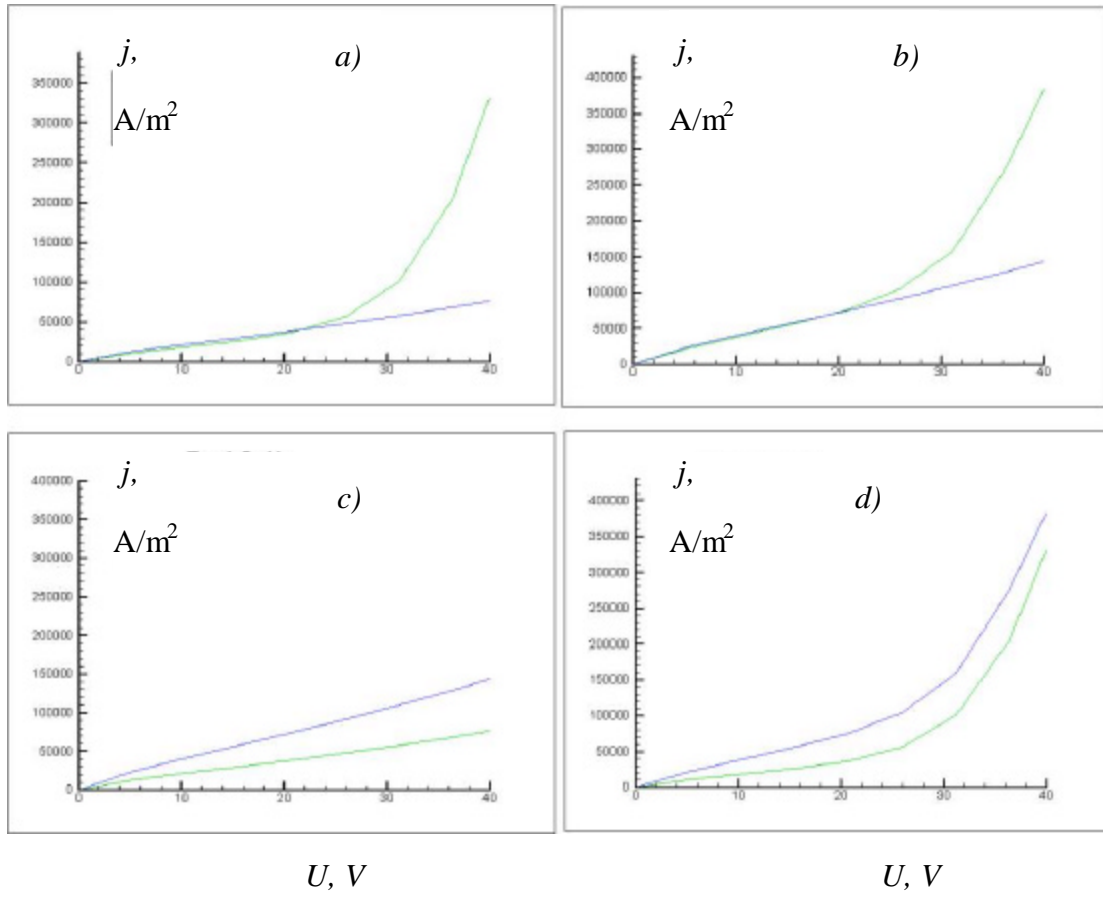**Fig. 3.24. Distributions of n_i/n_g and electric field at M = 0.85 and the probe potential of 16 V**

Fig. 3.25. Distributions of plasma conductance and ion density at M = 0.85 and the probe potential of 28 V, computation with $T_e = 1.5$ eV = const

Fig. 3.26. Distributions of n_i/n_g and electric field at M = 0.85 and the probe potential of 28 V, computation with T_e = 1.5 eV = const

Fig. 3.27. Computed probe voltage-current characteristics:

a - for M = 0.85, *b*- for M = 1.5, upper curves − the complete problem, lower curves − with no account to the chemical reactions (T_e = 1.5 eV);

c - for T_e = 1.5 eV, M = 1.5 (the upper curve), T_e = 1.5 eV, M = 0.85 (the lower curve);

d - the complete model, M = 1.5 (the upper curve), M = 0.85 (the lower curve)

Three values of the probe voltage are taken for every case of the basic computations: 0 V, 16 V (weak effect of the plasma chemical reactions, see below) and 42 V (strong effect of the plasma chemical reactions). As there is no effect of plasma processes on the dynamics of the neutral gas, the distributions of gas density, temperature and velocity are the same for all the plasma distributions with the corresponding initial Mach number.

The distributions of gas dynamical parameters in the subsonic and supersonic cases differ from the classical ones because of a strong influence of viscosity: the characteristic size of the probe (0.1 mm) is small enough, and the gas density is sufficiently low for the flow to be laminar.

In the supersonic case the neutral gas density is considerably higher before the probe and considerably lower behind it in comparison with the ambient gas flow. One can see that the viscous friction heats the gas as it passes by near the probe surface. The heated parts of gas masses gather behind the probe to form a hot region with low speed and low density. The electric field is however closer to be axially symmetrical. Thus, the plasma parameter E/n_g in the supersonic case is greatly enhanced behind the probe. Note that the value of this parameter defines the electron distribution function and thus the electron temperature and the rates of plasma reactions. That is why the electron temperature is maximal behind the probe near its surface (where E/n_g is the highest).

The same takes place in the subsonic case too, but the density profile in the subsonic case is smoother. The growth of the parameter E/n_g is much less there.

In the supersonic case the diffusion layer is strongly asymmetric due to the effect of plasma flow. One can see that the plasma density n_i falls near the probe surface. It is a result of plasma diffusion with recombination on the surface. However, the degree of ionization $x = n_i /n_g$ can even grow behind the probe. The ambipolar diffusion is effective in this rarefied region, the distribution of plasma density is smoothed by the diffusion, while the distribution of gas density n_g is not. This can result in a dramatic growth of $x = n_i /n_g$ even at no probe electric field. This effect of synergetic interaction of the supersonic flow and the ambipolar diffusion on the value of x is especially high in comparison with the fall of x as a result of the diffusion only. (This fall has proved to appear before the probe). This growth of x results in a proportional

growth of plasma conductance near the probe, and thus it affects the voltage current characteristic. The effect is evidently higher at higher Mach numbers (see Fig. 3.27).

We have never seen in the literature any description of this effect of synergetic interaction of the supersonic flow and the ambipolar diffusion on the probe voltage current characteristic.

The electric field is enhanced before the probe and lowered behind it, for the plasma conductance distribution is not even. The highest difference of electric field takes place at higher voltage in the supersonic case.

At higher values of the probe voltage the electric field appears to be high enough to enhance the plasma density in the regions where the parameter E/n_g is maximal. At the probe voltage of 42 V in the supersonic case the value of x behind the probe is 7 times as high as in the ambient flow. It results in a considerable growth of probe electric current, which in this case corresponds to the perturbed, enhanced value of plasma density. In this case one cannot derive the ambient value of $x_¥$ on base of the probe electric current.

This dramatic effect of plasma reactions is vividly seen on the probe voltage current characteristic. The curve is close to be linear in the case with no account for the reactions, when the plasma temperature is taken to be a constant ($T_e = 1.5$ eV). The probe voltage current characteristic with an account of the plasma reactions coincides with the previous line at low probe voltage, and quickly grows at higher voltage values. This nonlinear part of the probe voltage current characteristic is in a direct proportion to the strongly perturbed plasma mean density, it cannot be applied for plasma diagnostics in the usual sense. The threshold of the effect of plasma reactions is about 20 V for the supersonic and about 25 V for the subsonic case. This difference is bound with higher maximal values of E/n_g in the supersonic case.

Note that the maximal value of voltage in the probe experiments was close to these threshold values. It means that this effect of plasma reactions can take place under characteristic experimental conditions. In such a case, the nonlinear part of the voltage current characteristic must be neglected, and the diagnostics must be carried out on base of the linear part of the voltage current characteristic.

Conclusion

New analytical formulae for ion drift regimes of probe operation in high, moderate and low external discharge electric fields are deduced. They can be used for diagnostics of dense non-thermal plasma flows characteristic for plasma aerodynamic systems.

There are two causes of dramatic deviations of the probe voltage-current characteristics for probes in high-speed flows with considerable ambipolar diffusion from the previously known results, which are valid for slow plasma flows. These causes are the effect of synergetic interaction of the supersonic flow and the ambipolar diffusion, and the effect of synergetic interaction of the supersonic flow and the plasma chemical reactions.

References to Chapter III.

1. Chernikov V., Chuvashev S., Ershov A., Shibkov V., Timofeev B., Timofeev I. Formation of Gas Discharges in Supersonic Flows of Air and Fuel-Air Mixtures. 3-rd Weakly Ionized Gases Symposium. AIAA-99-4904, Norfolk, VA, 1999.

2. Ershov A., Ardelyan N., Chuvashev S., Shibkov A., Timofeev I.. Probe Diagnostics of Gas Discharges in Supersonic Airflow. 3-rd Weakly Ionized Gases Symposium. AIAA-99-4951, Norfolk, VA, 1999.

3. Benilov M.S. Theory of Electric Probes in Weakly Ionized High Density Plasma Flows: Review //High Temperature. Vol.26. No. 5. Pp.993-1003, 1985.

4. Benilov M.S., Bochkarev G.G., Buznikov A.E., German V.O., Kovbasyuk V.I. Electrical Probe Characteristics in a Subsonic Plasma Flow// Academy of Science News. Liquid and Gas Mechanics. No.1. Pp.150-160, 1983.

5. Chen Xi. Ion Saturation Current Density and Specific Heat Flux on a Cylindrical Probe Immersed in a Dense Plasma Flow.// J.Phys.D: Applied Physics. Vol. !5. Pp. 1695-1708, 1982.

6. Akishev Yu.S., Napartovich A.N. On the Probe Diagnostics of a High Pressure Glow Discharge. Sov. Physics: Doklady. Vol.242. Pp. 812-815, 1978.

7. Mal'kov M.A., Devyatov A.M., Kuzovnikov A.A., Ershov A.P. Probe Diagnostics of the Plasma of Gas Discharge Light Sources. Moscow: MSU, 1991.

8. Protasov Yu.S., Chuvashev S.N. Physical Electronics of Gas Discharge Devices: Plasma Electronics. Moscow:Vysshaya Shkola. 1993.

9. Biberman L.M., Vorob'ev V.S., Yakubov I.T. Kinetic of low-temperature plasma. Moscow, Nauka,1970 (in Russian).

10. Alexandrov A.F., Konovalov V.P., Son E.E. The phenomena of charge particle transport into weakly ionized gas. Encyclopaedia of low temperature plasmas. Moscow, 2000. V.1. P. 550.

11. Zhdanov V.M., Son E.E. Phenomenological and Kinetic Description of Transport Phenomena in Low Temperature Plasmas. V.1. P.508.

12. Benilov M.S. Near-electrode layer in a weakly ionized plasma with a chemical equilibrium. Izvestija AN SSSR: Ser. Mechanics of Fluid and Gas. 1982. No. 1. Pp.147-153

13. Zeldovich Ya.B., Raizer Yu.P. Physics of SW and high temperature hydrodynamic phenomena. Moscow, Nauka, 1963.

14. Chung P., Talbot L., Touryan K. Electric probes in stationary and flowing plasmas: Theory and application. New York. Springer-Verlag. 1975.

15. Alekseev B.V., Kotelnikov V.A. Probe method for plasma diagnostics. Moscow. Energoatomizdat. 1988. 240 p. (in Russian)

16. N.V.Ardeljan, G.S.Bisnovatyi-Kogan, K.V.Kosmachevskii,S.G.Moiseenko An implicit Lagrangian code for the treatment of nonstationary problems in rotating astrophysical bodies. Astronomy and Astrophysics. Supplement Series v.115 pp. 1-22, 1996.

17. H.E.Trease, M.J.Fritts, W.P.Crowley (Eds). Adevance in Free-Lagrange Method. Proceedings of the Next Free-Lagrange Conference Held at Jackson Lake Lorge, Moran, WY, USA, 3-7 June 1990. Springer-Verlag Berlin Heidelberg 1991.

18. N.V. Ardelyan, K.V. Kosmatchevskii. Implicit Free-Lagrange method for Computing Two-Dimensional Magnetogas-Dynamic Flows. Computational Mathematics and Modeling. V 6, N 4, 1995, pp. 209-224, (translated from russian).

CHAPTER IV. PLASMA DIAGNOSTICS METHODS

§ 1 Electric Probe Method

1.1. Particularities of probe operation in plasma of an electric discharge in a supersonic flow

1.1 1. Requests to probe circuits

Electric discharges in supersonic high-pressure gas flows are characterized by inhomogeneous and unsteady parameters [1-3].

Under these conditions, the main advantage of the probe method (a possibility of local measurements with a high temporal resolution) becomes important. However, an application of the standard schemes and methods of processing of probe characteristics for such discharges is practically impossible due to the specific mode of operation of a probe in such discharges, which is characterized by a combination of several extreme conditions:

- high plasma potential ($V \geq 1$ kV)

- high discharge current ($I \geq 1$ A)

- large modulation of the discharge current and voltage

- high gas pressure ($p \geq 10$ Torr)

- a very high electric field ($E \geq 100$ V/cm) present in the discharge plasma

- supersonic flow mode ($M > 1$)

- chemical reactions (including ionization and recombination) in the air plasma.

The unsteady character of plasma parameters suggests a necessity of development of an automated scheme of probe measurements, which provides the necessary temporary resolution and allows one to measure the probe voltage-current characteristic with meeting a condition of sufficiently weak changes of plasma parameters. As a rule, the characteristic frequencies of oscillations of discharge current and voltage are about 3...30 kHz [2,4]. The available temporary resolution of a probe itself is sufficiently higher (better than 1 μs, see Chapter 1, p.1.1). Thus, the available temporary resolution of a probe method is defined by a probe measurement circuit. The resolution must be chosen from a condition that the time of measurement

of a probe voltage-current characteristic must be less than a threshold value, which should not exceed 10μs.

High discharge voltages define high probe potentials of a probe relatively the ground. As a result, the probe circuit must be isolated from a computer, which is a part of the measuring device. The situation is made still worse by secondary breakdowns characteristic for discharges in dense gas flows [4]. Values of voltage at secondary discharges at gas pressure of about hundreds of Torr are about 10 kV. That is why the galvanic separation must meet very high requirements. The optical separation based on transmitting a signal through an optical waveguide is a good solution of the problem.

High discharge current provides high values of plasma charge density and consequently high probe current values. Under the conditions of considerable local electric potential oscillations this excludes any possibility of application of single probes. Actually, during the process of potential variation a single probe can be subject to considerable electron current. The probe heating results at least in an uncontrolled growth of noise emission current, which masks the signal probe current, or even results in destruction of the probe. A double probe seems to be an optimal choice for the conditions described above. In such a case both probe surfaces always have a negative potential relatively the local plasma potential, and the probe current is always limited by the ion saturation current. If probes are both placed in the same equipotential surface of the plasma, the voltage between them is (in a certain approximation) independent of the local potential fluctuation. Besides that, double probe application has an advantage that it meets automatically a requirement that the probe circuit should not intercept a significant part of the discharge current.

Note also that our previous experiments in application of probes for diagnostics of supersonic plasma flows [5] have shown that transmitting of both measurement and control signals in a digit form makes it possible to apply a single optical waveguide. Thus, main requirements to a probe circuit are the following:

- double probe scheme application
- optical separation

- PC control

- voltage-current characteristic measurement time no more than 10 μs

- transfer of signals in a digital form

1.1.2. Requirements to Probe Design

Double probes collect the ion current, which is as a rule much lower than the electron current. On the one hand, under the conditions of considerable discharge noises the signal should not be very weak, and it is desirable to enhance the probe working surface area. On the other hand, it is important to minimize gas dynamical perturbations in a supersonic plasma flow, that is especially important for double probes. From this point it is desirable to minimize the probe size to the limit of mechanical stability in a supersonic flow.

Furthermore, according to the computer simulation of the situation around the probe (see Chapter III), a rarefaction of gas near the probe surface and external field concentration result in a multiple growth of the plasma characteristic parameter E/n_g, intensive ionization, multiple rise of plasma concentration and thus growth of the probe current. Determination of plasma concentration in such a case can be difficult (if possible). From this point of view it is desirable to decrease the probe radius too.

However the probe size can appear to be considerable in a case of necessity to chill its surface. Under the conditions of interest (high density of gas, high discharge current) probe surface heating is quite possible. In accord with Chapter 1, p. 1.4, this heating is negligible if thermal electron emission current is negligible. A rough estimate of the probe ion current is [6]

$$j_i = 0.25 \ e \ n_i v_i,$$

here n_i and n_i are the ion concentration and ion velocity on the boundary of the double charged layer. An estimate for the current of thermal emission is

$$j_T \sim 100 \ T_s^2 \ \exp(-ef/(k_B T_s)),$$

here T_s is the surface temperature, f is its work function. For refractory metals(W, Mo) at $T_s \sim 1500$ K the current $j_T < 10^{-3}$ A/cm^2, i.e. the yield of the possible thermal electron emission is negligible at $n_i > 10^{12}$ cm^{-3}.

Our experiments with DC discharges have shown that this condition is met even at high discharge current. In the pulsed periodical discharges the pulse duration has proved to be short enough to provide an absence of considerable heating of the probe surface. Thus, under the conditions of interest one can use probes without chilling, that makes it possible to choose minimal possible probe characteristic sizes.

A compromise between the factors considered above has resulted in a design of double cylindrical probe with a diameter of 0.2-0.5 mm and length of 3-5 mm, made of Mo or W wires and placed inside an Al_2O_3 capillary.

1.2. A PC-controlled probe measurement circuit
with an opto galvanic isolation

The principles of operation are based upon the transformation of measured analogue signal to a digital sequence, the transmission of the said sequence via optic fiber line for the required distance and the followed back transformation of the digit code to the analogue signal.

The block diagram of the device is presented in fig.4.1. Timing and controlling of the device are governed by the computer (13) via unit (11) and (12). At the time moment t_0 (start point of measurement of the probe voltage-current characteristic) the module (11) forms a start pulse, which is transmitted to the generator (12) of a current of injection and management of an emitter (14). The emitter (14) will transform an injection current pulse to a light pulse. A laser diode ????-301-1 with average power 300 mW and wavelength 790-820 nm is used as an emitter.

The 0.1 mcs long optical pulse is transmitted through a fibre-optical line (15) on a photosensitive site of the photoreceiver (16), which transforms the light beam to an electric current. The photodiode ? ? ? 1 with a wavelength 790-820 nm is used as the photoreceiver. The electric current signal is further transmitted to the block of amplification (17).
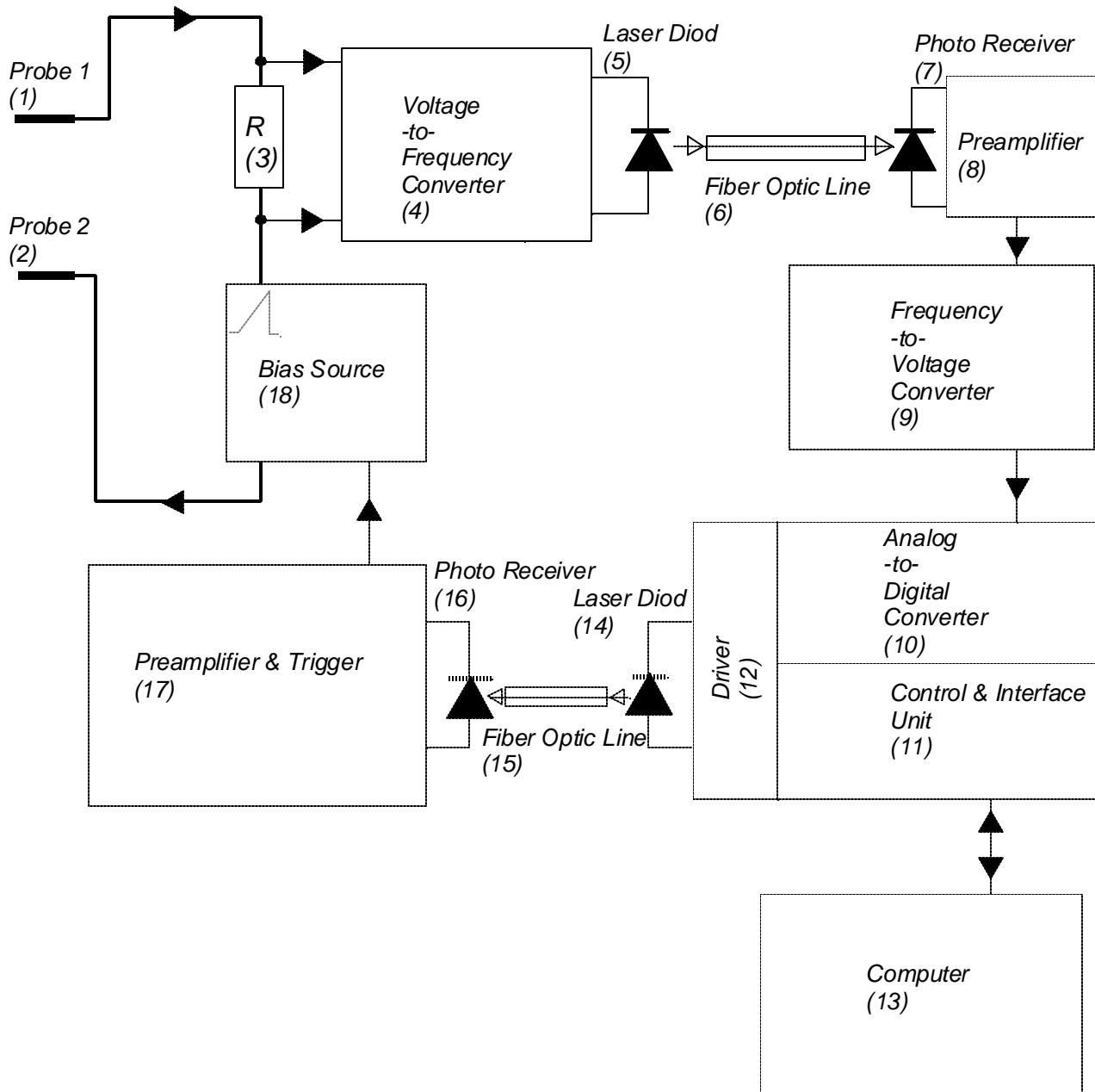
Fig.4.1. The Device for Probe Measurements in Plasma

The block of amplification (17) consists of a transimpedance amplifier, an amplifier - proofer and a threshold element. Transimpedance amplifier transforms a signal current of the photodiode to an integrated voltage. The amplifier - proofer is intended for amplification and restoring of the form of a signal. The threshold element forms a digital signal in levels of TTL (transistor-transistor logic) on an output of the block (17), and also allows to reduce modification of on-off time ratio of an output signal in a dynamic range. The threshold element is based on a comparator, which is connected in accord with the Schmitt trigger circuit design.

A 0.1-μs long electric switching pulse is formed in the unit (17) and is transmitted to the unit of formation of linearly growing bias voltage (18). This unit is designed as a voltage integrator on base of a powerful operational amplifier. The electric circuit of measuring of the double probe voltage current characteristic is comprised of the unit (18), the plasma under investigation, the probes (1) and (2), and a 15-Ohm resistor (3).

The voltage bias $U(t)$ in the probe circuit changes linearly from a minimal voltage of – 25 V to a maximal voltage of +25 V during 10 μs. The resulting probe current $i(t)$ in this circuit is continuously transformed by a unit (4) into a frequency of pulse repetition. This unit is a voltage-to-frequency transformer on base of the chip VFC110. The mean transformation frequency is 3.0 MHz.

The electric pulses, which are formed by (4), are transformed into a sequence of optical pulses by a laser diode ? ? ? 1 (5). The optical pulses are transferred through an optical guide (6) to an optical detector (7), then the signal is amplified in (8) and enters a unit (9), in which the inverse transformation of repetition rate into voltage is carried out. The unit (9) includes a transformer "frequency-to-voltage" based on the chip VFC110 and a low frequency adaptive filter based on the chip SHC615. The waveband of the unit (9) is 350 kHz (on the level of -3 dB). Thus, the output signal of the unit (9) is all the time in a direct proportion with the probe current $i(t)$. The electric circuit designs of the units (8) and (17) are absolutely identical.

In a moment of time t_0 a unit (11) also starts a sequence of 100 transformations, which

are carried out by a unit (10) in fixed intervals of 0.1 µs. The unit (10) is a 12-bit 3-ns analog-to-digit converter. As the temporary dependence of the bias voltage is also pre-determined, an array of 100 pairs of values $\{U(t_i), i(t_i)\}$ is formed in a memory of the computer (13), that is the measured voltage-current characteristic.

The parameters of the device are shown in the Table 1.

Table 1.

Duration of single probe VAC measurement	10 µs
Probe bias limits	±25 V
Probe current limits	±50 mA
Bandwidth (–3 dB level)	350 kHz
ADC	12 bit
Fiber optic line	< 300 m
High voltage isolation	not limited

A typical view of a probe current signal, which is formed by this electric scheme at a constant bias voltage, is presented in Fig. 4.2.

The double probe was positioned in the cathode (high-voltage) region of flow with a separation of 2 cm from the electrode. The measurement corresponds to the pulsed periodical discharge with a 300-µs pulse duration, initial electric current of 25 A (Fig.4.3) at the value of gas pressure in the chamber being 100 Torr, and the pressure in the receiver of the compressor being 1 atm.

One can see a bipolar noise signal, which corresponds to the discharge gap breakdown (Fig.4.3), and then a quick growth of the signal, which corresponds to an arrival of the plasma jet to the place of probe positioning.

Later, during the pulse, the absolute value of the probe electric current signal, which is proportional to the ion density, is oscillating chaotically, but its mean value is slowly decreasing in a correlation with the discharge current. The change of the signal polarity is a noise corresponding to switching off of the discharge pulse.
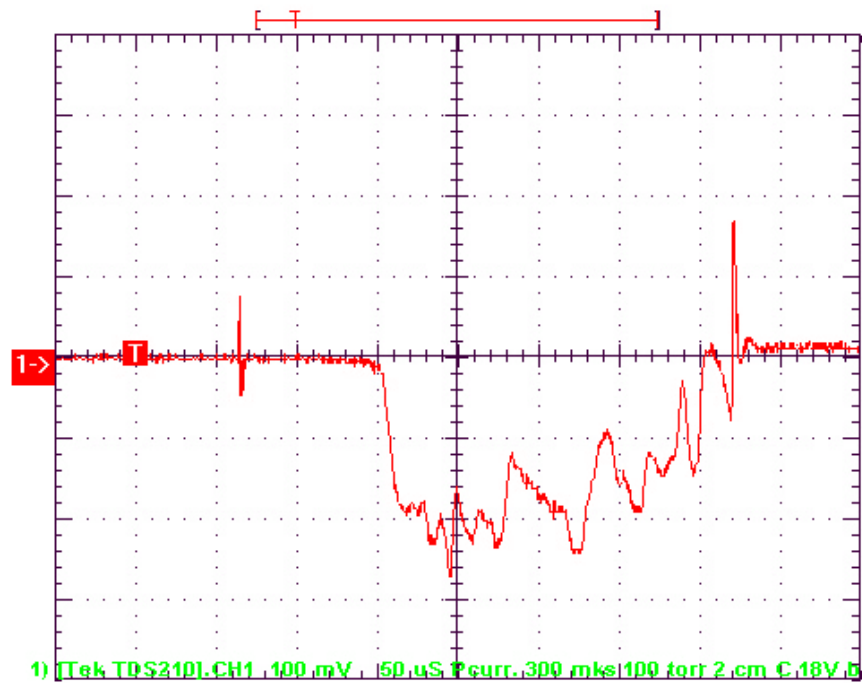
Fig.4.2 Temporary evolution of probe current in pulse-periodic discharge.

Probes $\varnothing$ 0.3 mm, l = 5 mm, bias voltage U_b = 18 V. Cathode flow, z = 2 cm.
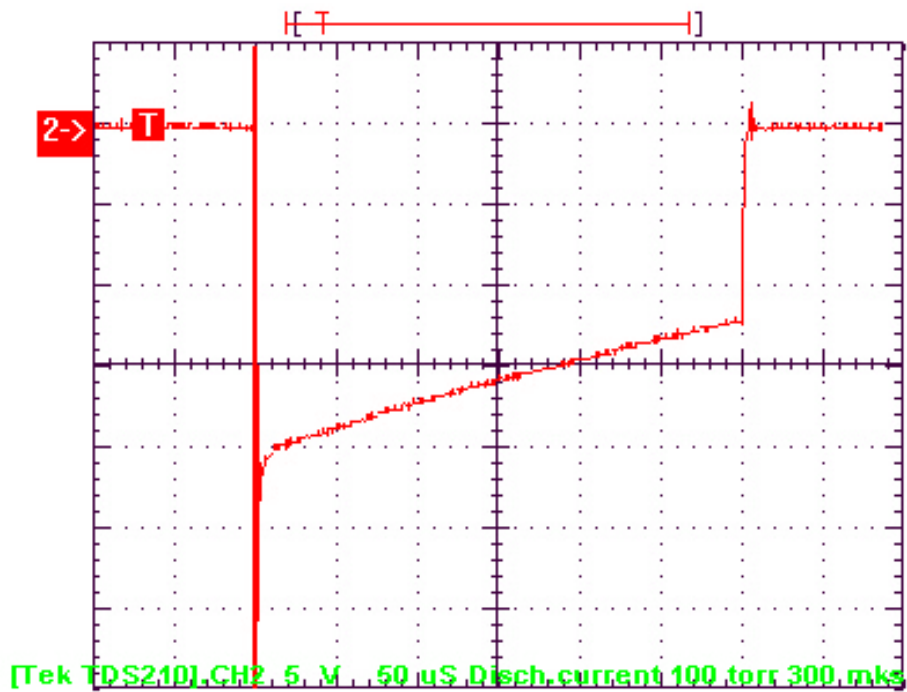
Fig. 4.3 Oscillogramm of discharge current in case of conditions of Fig.4.2.

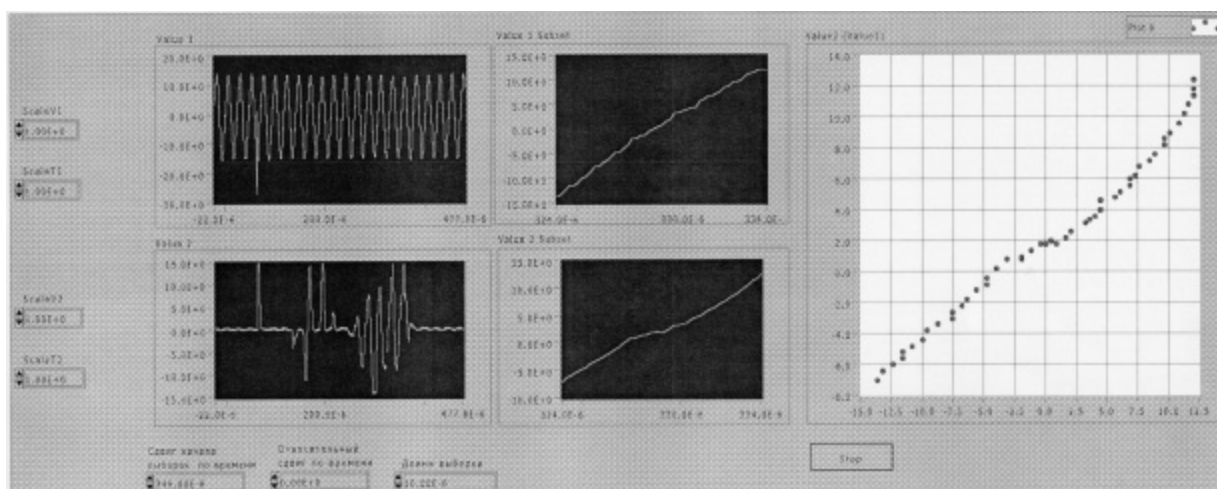Pulse-periodic discharge, τ= 300 μs, p =100 Torr, P = 2 atm.

At measuring the voltage-current characteristic of the double probe, the sawtooth voltage bias was applied. Typical oscillograms of the probe voltage and current are shown in Fig. 4.4 for a pulsed periodical discharge. One can see that within a 10-μs interval of voltage linear growth the oscillations of the probe current, which are bound with discharge instabilities, are not so high, and it is possible to derive a voltage-current characteristic of the double probe.

1) [Tek TDS210].REF1 5 V 5 uS Probe current
5) [Tek TDS210].REF2 10 V 5 uS Voltage bias
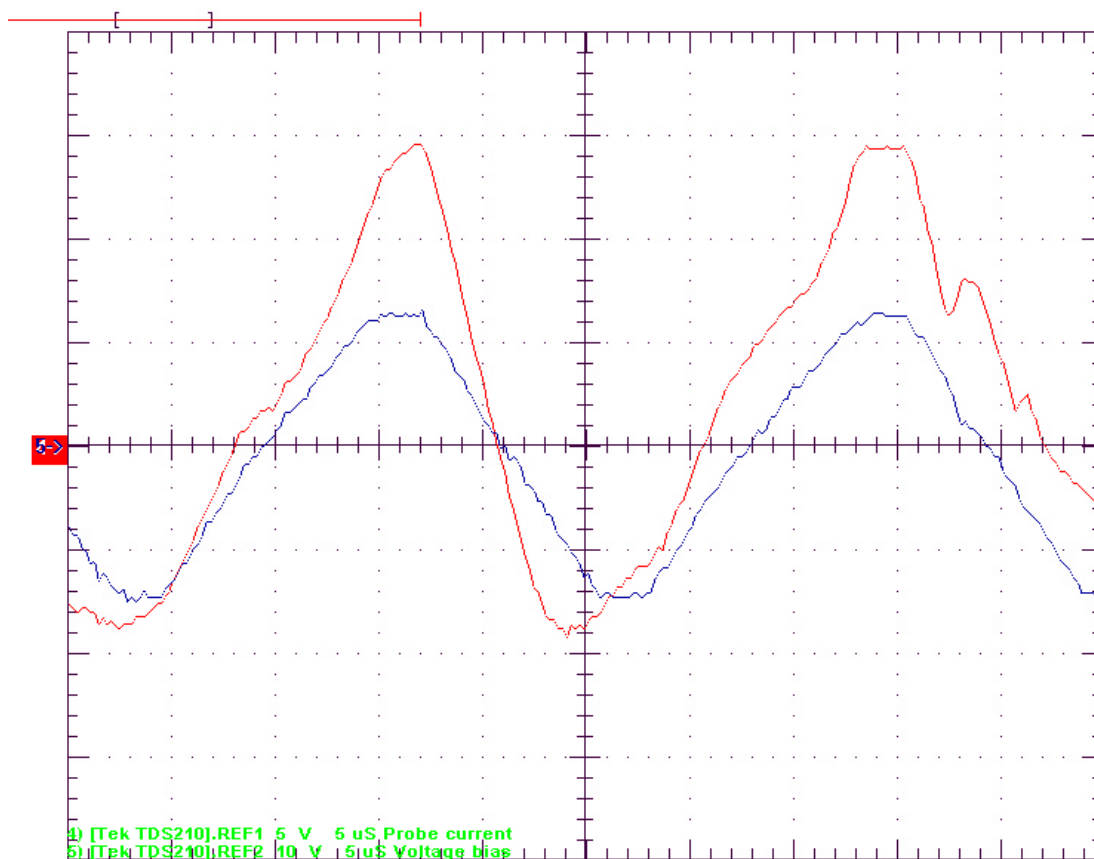
Fig.4.4 Oscillogram of probe current and bias voltage.

Probes ∅ 0.3 mm, l = 5 mm. U_b = ± 25 V, R = 5 Ohm. Anode flow, z = 5 cm.

Pulsed periodic discharge, τ= 300 μs, p =100 Torr, P = 2 atm.

Fig.4.5 Example of processing measured probe signal with the help of developed program.

Pulse-periodic discharge, $\tau = 300$ μs, p = 100 Torr.

I-V probe characteristic was determined with the help of special developed program (Fig.4.5). The program allows to look through the measured oscillograms of bias voltage and probe current (left pair of figures: upper figure- bias voltage, lower figure - probe current), to select a desirable recording area – middle pair of figures and to construct I-V probe characteristic - right figure. As it is visible, under these conditions it appears linear.

Another type of the scheme of a PC controlled probe with an opto galvanic isolation has been used also in plasmadynamic discharge. In this curcuit an opto galvanic isolation has been carried out with the help of opto-pairs.

The probe signal is formed on the resistor R and is transmitted on an input of the fitting amplifier for an amplification up to magnitude, sufficient for effective coding by an analog-to-digitial converter (ADC). ADC signals is transmitted on an input of the opto-pair. The allowable maximum voltage on isolation of a opto-pair is equal to 7 kV, the delay time does not exceed 5 μs. The exchange of signals with the computer is carried out through a 10 m long standard computer cable. The minimum interval between two sequential measurements is equal to 20 μs. The synchronization of discharge impulse with a cycle of measurements is stipulated in the circuit. The user sets magnitude of bias voltage between probes, number of measurements and delay

time between synchronization impulse and beginning measurement.

The temporary dependence probe current sample is shown on fig.4.7 in the case of plasmadynamic discharge. One can see a noise signal, which corresponds to the discharge gap breakdown and 650 µs later a quick growth of the signal, which corresponds to an arrival of the plasma jet to the plase of probe positioning z.
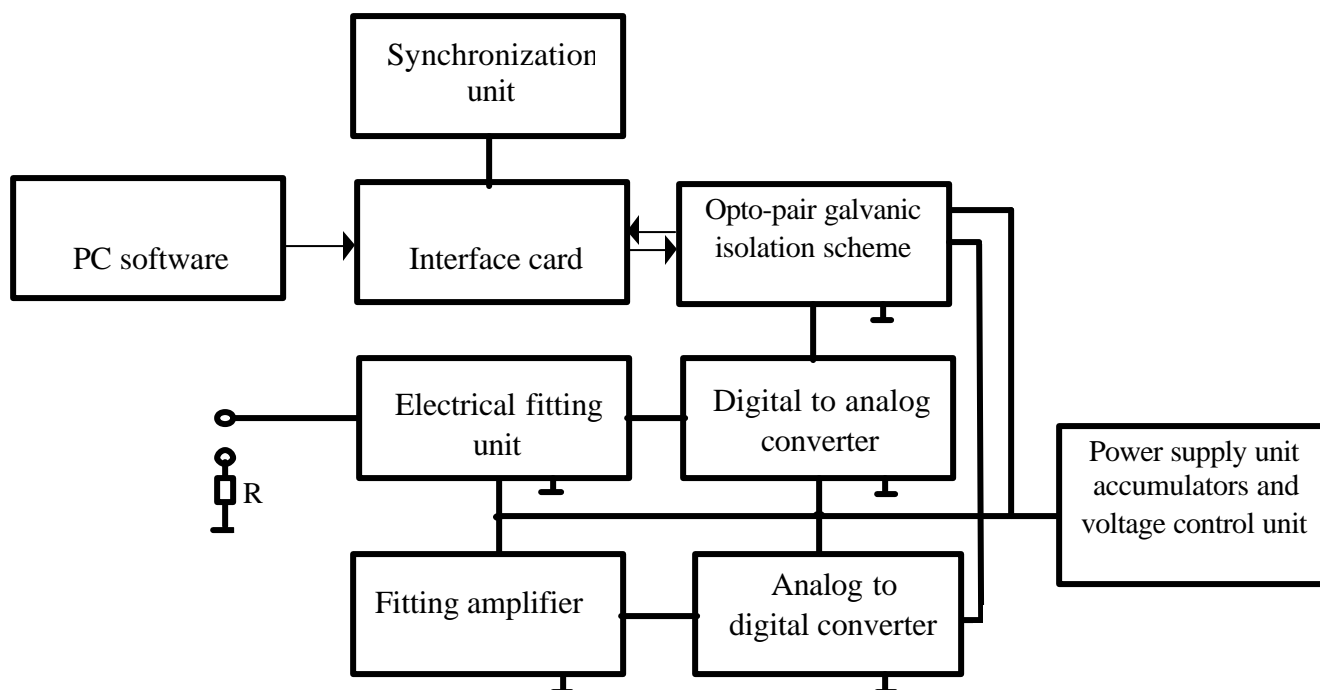
Fig.4.6. Draft design of a circuit for measurement of voltage- current characteristic of the double probes
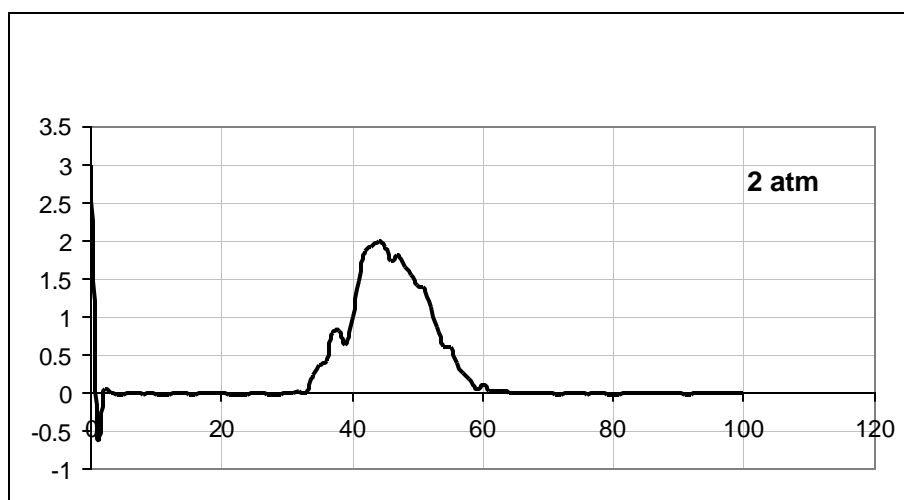
Fig.4.7. Temporary dependence probe current signal, which is formed opto-pair isolation circuit, in plasmadynamic discharge.P=300 Torr, z = 22 cm.

1.3. Electric Field and Floating Potential Measurements

The discharge electric field E is defined as a gradient of plasma potential f

$$E = - \text{grad } f .$$

At probe measurement of the electric field, voltage-current characteristics of two identical single probes situated in points with coordinates z_1 and z_2 are often obtained, then potentials are derived, and the mean electric field is calculated as

$$E_z = (f_1 - f_2)/(z_1 - z_2).$$

Such a scheme is applicable for steady or very stable pulsed-periodical discharges. If temporary resolution of measurement is necessary, then a difference of floating potentials is applied. As a floating potential is defined from a condition $I(V_f) = 0$, each of the probes is grounded through a divider with a high input resistance. The difference is measured with use of, e.g., a differential amplifier. Such a scheme of field measurement (Fig.4.8) has been applied in the current experiments.
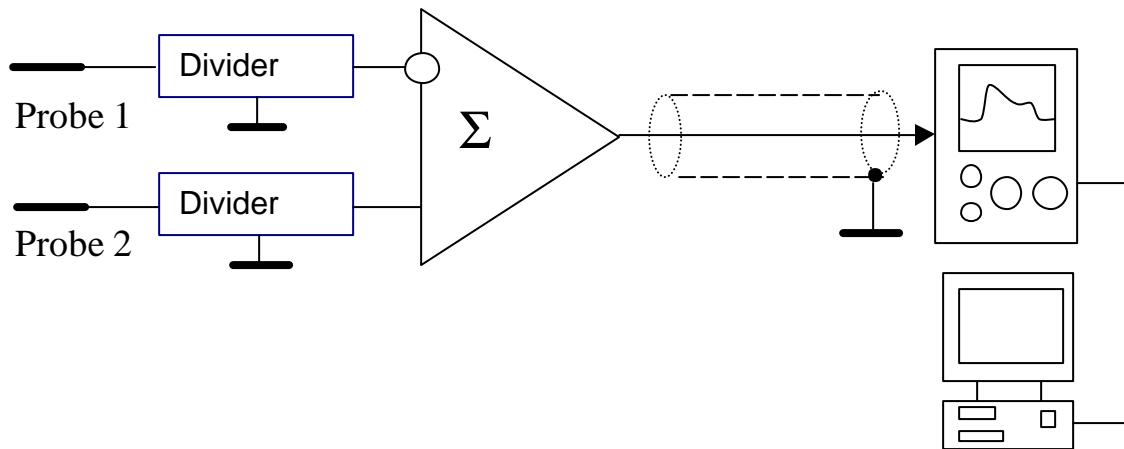
Fig.4.8. Scheme of Measurement of Electric Field in a supersonic plasma flow

A basic circuit diagram of field measurement in a supersonic plasma flow is shown in Fig. 4.9.
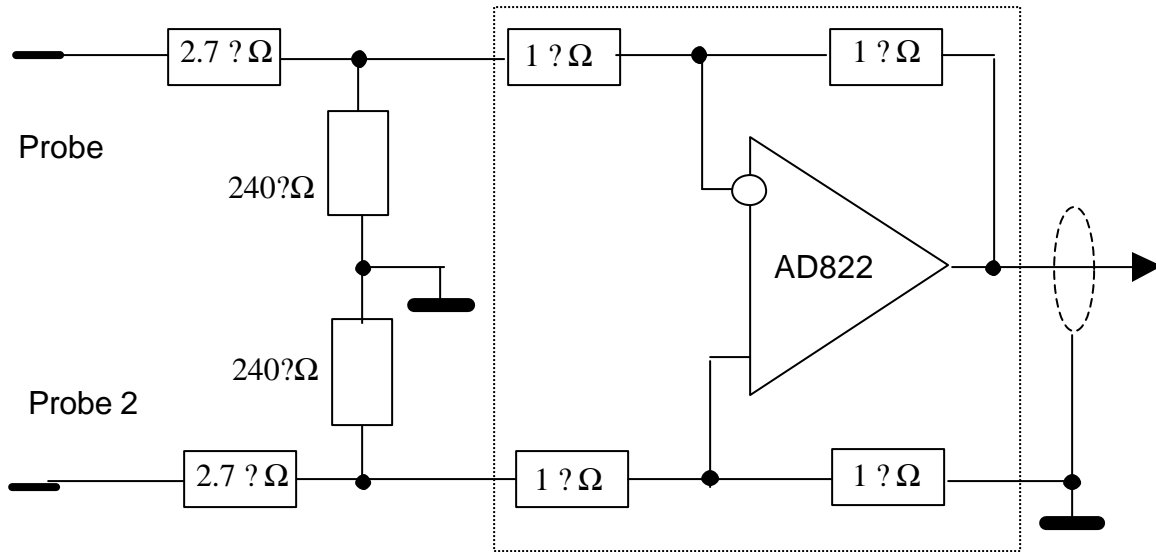
Fig.4.9.Basic circuit diagram of field measurement

Each of the probes was grounded through a divider 1:11 with 3-MOhm input resistance. For discharges in supersonic flows, only an input resistance of about 1 MOhm can provide that the point on the voltage-current characteristic corresponds to the floating potential. Actually, assuming that the value of potential relatively the ground is about 1 kV, one can estimate the probe leakage current to be about fractions of mA. The probe ion current is about 10 mA under such conditions. Thus, the leakage current is already few percent of the probe current. If this percentage grows, the working point on the voltage-current characteristic shifts from the floating potential to its ion part, and the signal corresponds to the temporary dependence of the charge density instead of that of the potential.

The signal from the calibrated resistors enters the input of a chip AD 822AN-based differential amplifier with a coefficient of transmittance 1 (parameters of the amplifier for the applied power supply regime Vs= $\pm$ 15volts are presented in Table 2).

The differential amplifier is necessary to select the signal (the difference of potentials between the probes) and to suppress powerful synchronous phase noise that is generated by the discharge. The output of the differential amplifier is connected with

a digital memory oscilloscope, which transfers the digitized data into a computer.

Table 2
AD 822AN SPECIFICATIONS   Vs=$\pm$15volts

Parameter	Min.	Typ.	Max.	Units
INPUT CHARACTERISTICS				
Common-mode voltage range	-15.2		14	V
Input impedance				
Differential		10^{13} / 0.5		Ω / pF
Common mode		10^{13} / 2.8		Ω / pF
DINAMIC PERFORMANCE				
Unity gain frequency		1.9		MHz
Settling time to 0.1%		4.1		mks

Bot longitudinal (along the flow) and transversal components of the electric field have been measured in the scope of current experiments. For so doing, a couple of cylindrical tungsten probes was positioned in a plane, which was parallel or normal to the flow. The axes of the probes were always normal relatively the flow. As a rule, $\varnothing$0.4×5 mm probes with 2.5 mm separation were applied.

The mechanical system has been used for a precise positioning of the probes in the discharge region. Fig.4.10 shows its appearance. The probe can be slowly moved both in the vertical and in the horizontal planes by a couple of electric motors. The mechanical system is installed inside the work chamber. The control of its operation is carried out with use of a control desk that is placed outside the chamber, it is joined with the mechanical system through a hermetic connection.

The probe coordinates relatively the electrodes were determined with use of a He-Ne laser beam.

At the measurements of the floating potential, the signal was taken from the resitance of the 240 kOhm divider.
A typical view of the signals, which are proportional to the floating potential (the lower beam) and to the transversal electric field (the lower beam) is shown in

Fig.4.11. for the case of the pulsed periodical discharge with pulse duration of 300 μs and the initial gas pressure of 100 Torr.
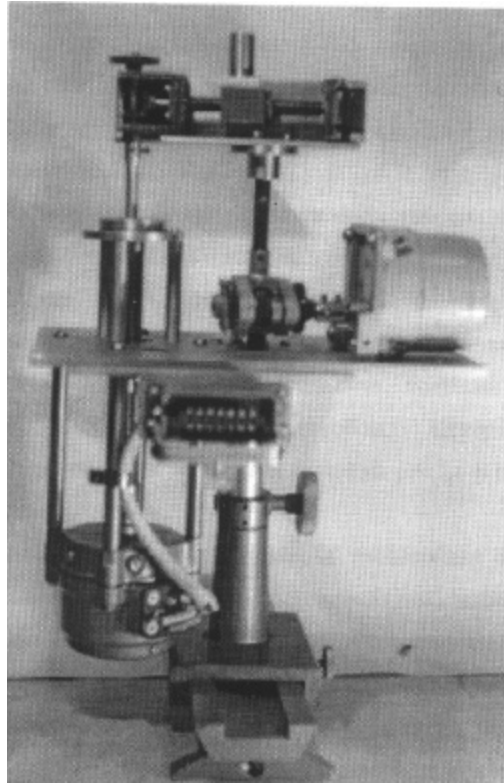

Fig.4.10. Appearance of installation for a precise positioning of probes

The probe that measures the floating potential was positioned in the cathode (high voltage) plasma jet 6 cm below the electrodes. Some 5 mm below a pair of probes was positioned normally to the flow.

The first signal on both of the rays is a noise corresponding to the discharge gap breakdown (starting off of the pulse). Some ≈ 90 μs later, the plasma jet reaches the first probe. One can see a potential jump, which corresponds to the cathode jet potential in the point z =6 cm in this moment of time. Then the potential continues to grow till its fall to zero at the end of the pulse (see Chapter 5, p.5.2).

The electric field signal appears later, for the measuring probes are positioned downstream. One can see that the electric field does not change significantly during the pulse. When the discharge voltage is switched off, the scheme shows a high peak of the signal, and then the signal disappears.
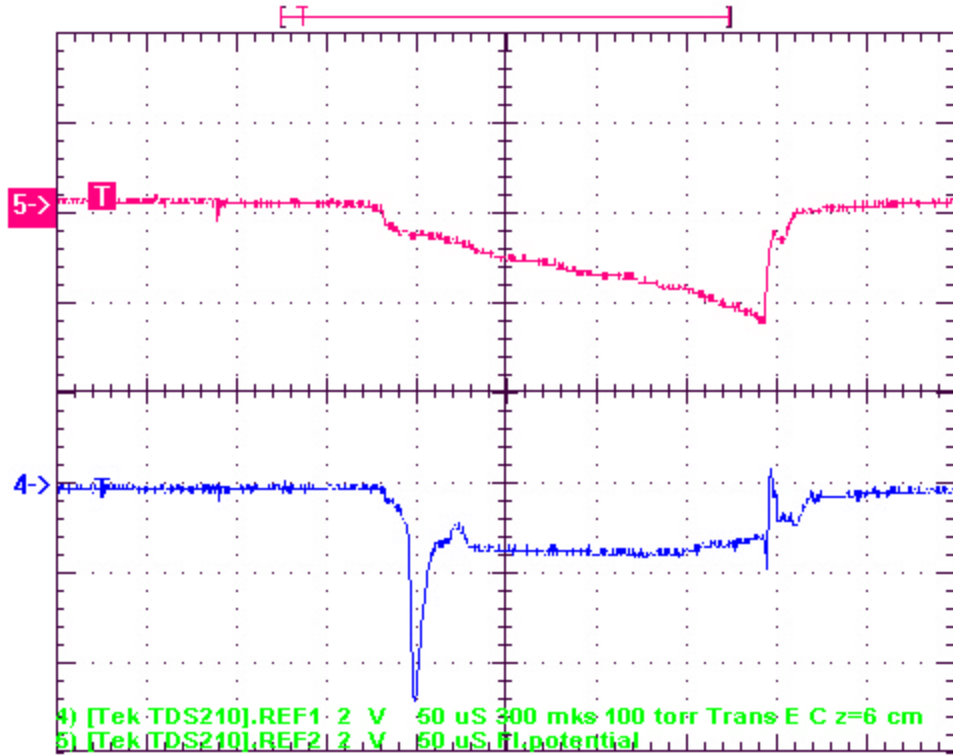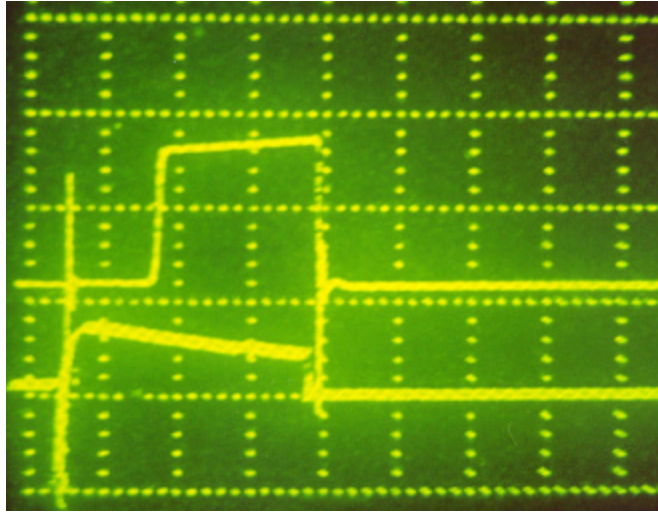
Fig.4.11. Signal of floating potential (upper beam) and signal of transversal electric field (lower beam) in plasma of pulse periodic discharge.

Pulse duration $\tau = 300\ \mu s$, pressure in the chamber $p = 100$ Torr, discharge current I ~ 20 A. Cathode part of flow, z =6 cm, 50 μs/div.

In some cases an analog memory oscilloscope C8-17 was applied instead of the digital memory oscilloscope. Typical oscillograms are shown in Fig.4.12, 4.13 for the anode jet. The electric current pulse was registered by the lower beam. Fig.4.12 shows an oscillogram of the transversal field, and Fig.4.13 shows the longitudinal field in the anode part of the pulsed periodical discharge at separations of probes from the electrodes z = 5 cm and z =2 cm, correspondingly. Analogously to the Fig.4.11, at the moment of breakdown a noise is generated, and a fast signal growth corresponds to the moment when the plasma jet reaches the probes. One can see that both the longitudinal and transversal fields are weakly varying with time.
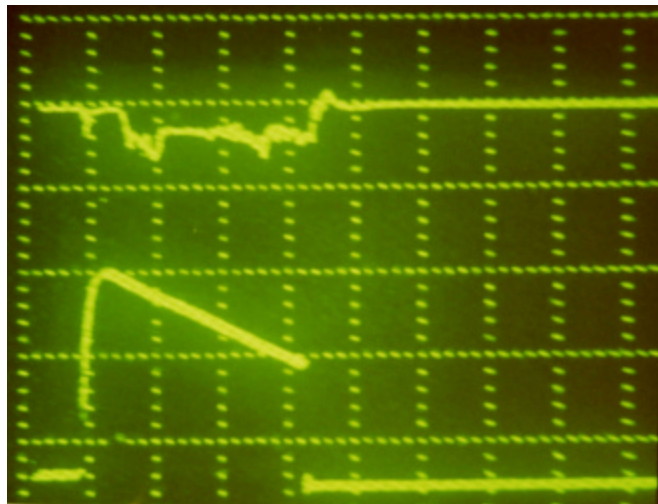
Fig.4.12. Signal of transversal electric field (upper beam) and signal of discharge current (lower beam) in plasma of pulse periodic discharge

Pulse duration $\tau = 340$ μs, pressure in the chamber p = 190 Torr, pressure in the receiver P = 1 atm, discharge current I ~ 8 A.
Anode part of flow, z = 5 cm, 100 μs/div.

Fig.4.13. Signal of longitudinal electric field (upper beam) and signal of

discharge current (lower beam) in plasma of pulse periodic discharge.

Pulse duration $\tau = 340$ μs, pressure in the chamber p = 100 Torr, discharge current I ~ 24 A. Cathode part of flow, z = 2.5 cm, 100 μs/div.

§ 2. Spectroscopic methods

2.1 A Set up for Spectral Diagnostics

For gas and vibration temperatures measurement at the discharge in supersonic airflow, a diagnostic set up has been assembled. Radiation of the discharge that is formed in supersonic airflow, is projected on input slots of two spectral devices through the windows of chamber, the mirrors, and the focusing quartz lenses (with focal length f = 20 cm). The lens diameter and f were chosen so that to provide projection of the discharge's image with reduction k = 10, and use of all the light-gathering power of the devices. A spectrograph ???-1 and monochromator ? ? ? - 3 were used, their inverse linear dispersions being 0.35 and 1.3 nm/mm accordingly for the spectral region of 300…400 nm. In order to measure the discharge gas and vibration temperatures spatial distribution, a prism was used that could provide orientation of the discharge image either parallel or normal to the slot. Either axial or radial discharge spectral brightness distribution was registered, which yielded either longitudinal or radial temperature distribution (for fixed radial or axial coordinate).

2.2. Electronic Analyzer of Optical Spectra

The electronic analyzer of optical spectra on base of a personal computer registers plasma radiation in visible, ultraviolet and infrared spectral ranges. The system is designed on base of an IBM-compatible personal computer. The sensor of plasma radiation on base of a CCD image sensor forms a video signal directly proportional to the radiation intensity in the spectral band 300 – 900 nm. The video signal is coded by an analog-to-digital converter situated on an Interface card and is sent to the PC memory as an array of data. The discharge spectra can be visualized on the monitor or printed out with use of program codes. The system can operate in two regimes: synchronous and asynchronous. At synchronous operation the pulses of discharge ignition are synchronized with the CCD cycles of exposition and pickup. This regime makes it possible to research pulsed discharges or to integrate the information on pulsed-periodical discharges. The asynchronous operation yields spectra that are averaged during all the time of exposition, it is useful for research of DC or AC discharges.

A schematic design of the device is shown on fig.4.14 A CCD image sensor Toshiba

TCD 1300D is used, its basic characteristics are listed in the Table 3 below.
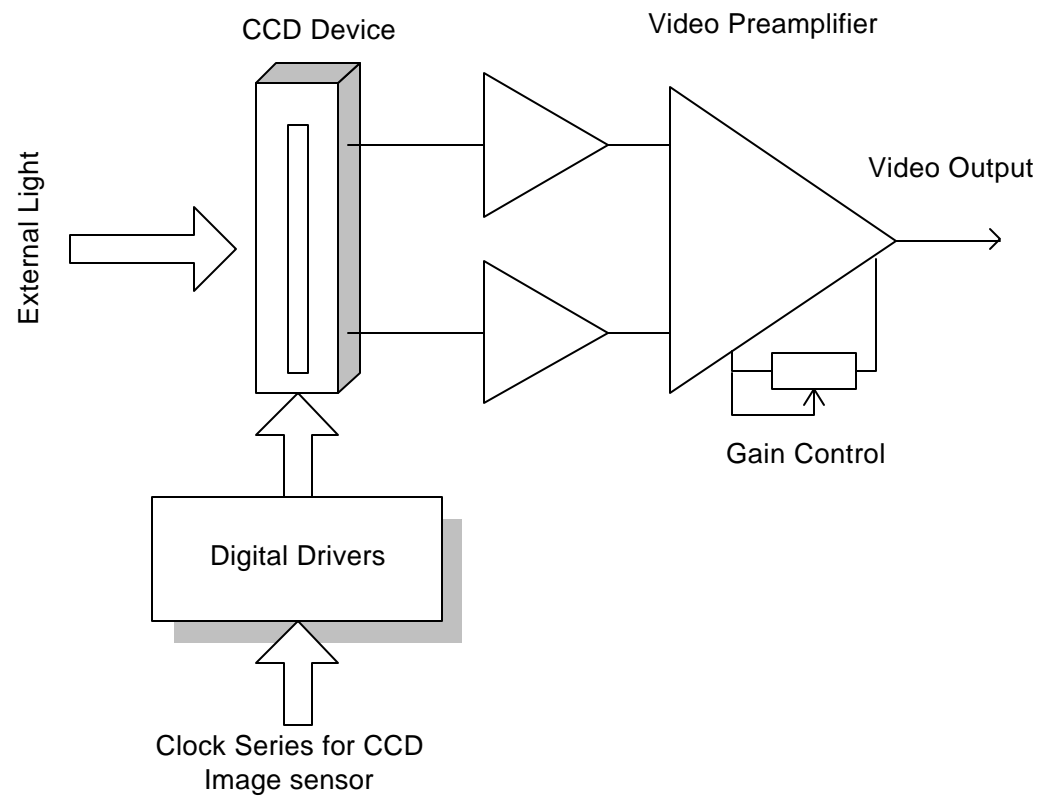
Table 3

Number of Image Sensing Elements	3648
Image Sensing Elements Size	8 μm by 8 μm on 8 μm
Photo sensing Region	Hi sensitive pn photodiode
Sensitivity	6 V/lx s
Saturation Exposure	0.3 lx s
Total Transfer Efficiency	92%

The video signal formed by the CCD is passed to a broad-band differential amplifier for compensation of a constant component and amplification to the level sufficient for further coding by the analog-to-digital converter. Drivers of digital signals are necessary for formation of CCD controlling pulses.

The interface card (fig.4.15) contains a 12-bit analog-to-digital converter, a quartz generator and a scheme of generation of synchronizing pulses for controlling of CCD, a universal parallel interface of control of executive devices (valves, pumps etc.) and an interface logic for fitting the card with the ISA bus.
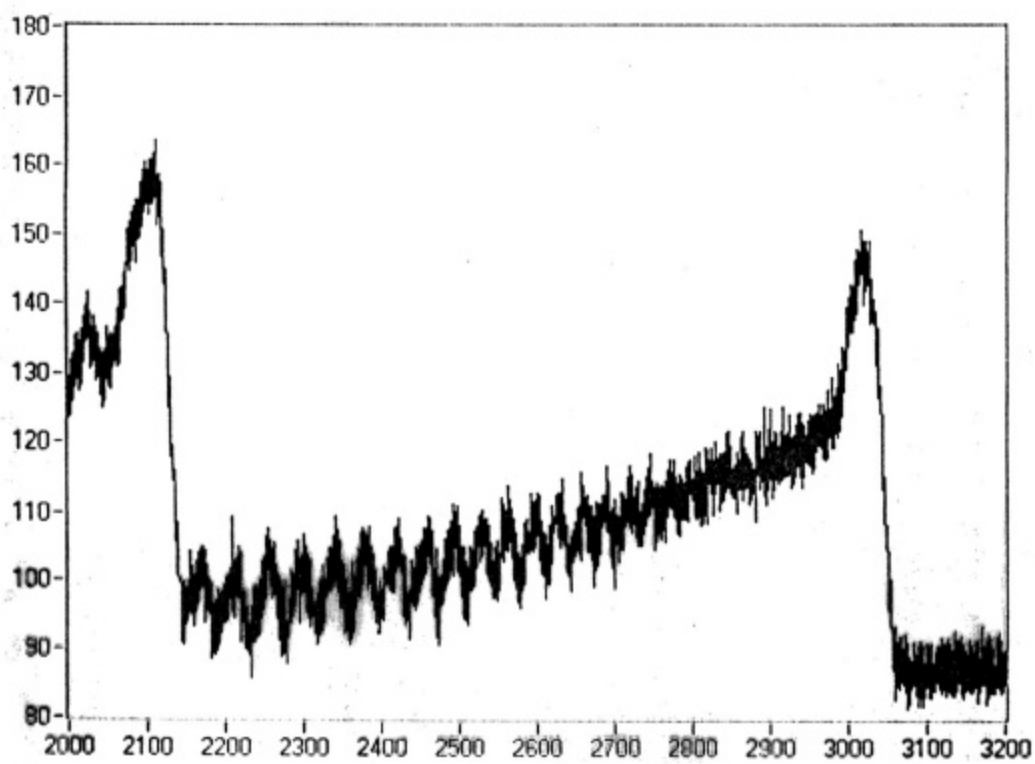
An experimental spectrum of band (0;2) λ=3805 A$^{\circ}$ of a second positive system of nitrogen (measured signal, arbitrary units, over the numbers of sensor cells of the CCD image sensor), registered by the developed system, shows on fig.4.16. Registration time for one frame is 20 ms. Integration of signals over several periods of CCD scanning and a digital low frequency filtration was applied for suppression of noises of the amplifier and of the thermal noise. During one experiment (duration of the discharge being about 1.5 s) several spectra were registered, that made it possible to measure the gas and vibration temperatures with temporary resolution about 20ms.

CCD Device

Video Preamplifier

External Light

Video Output

Gain Control

Digital Drivers

Clock Series for CCD
Image sensor

Fig.4.14

Fig.4.15

Fig.4.16

2.3. Kinetic model of non-equilibrium molecular plasma

The methods of mathematical simulation, along with conventional experimental methods of investigation of plasma objects, start playing an ever more important role. These methods enable one both to interpret the observed phenomena and to predict the performance and optimum operating conditions of apparatuses being developed. We have performed a mathematical simulation of the kinetics of a gas heating and creation of active particles in the nonstationary nonequilibrium plasma of a discharge in dry air. For it a nonstationary kinetic model was used.

It is known that vibration-excited molecules in discharges in air, N_2, CO, CO_2, and other molecular gases form an energy storage. The discharge parameters depend considerably on the method by which this energy is redistributed between various degrees of freedom of molecular gas. In so doing, strong correlation exists between vibration-excited nitrogen molecules in the ground electron state $X^1\Sigma_g^+$ and the energy distribution function of electrons, as was first demonstrated by Nighan [1]. This correlation is mainly due to collisions of the second kind between electrons and vibration excited nitrogen molecules, this leading to an increase of the fraction of fast electrons in the discharge plasma and, accordingly, to an increase in the average energy of electrons. This, in turn, brings about a sharp increase of the rates of electron excitation and ionization and an increase of the concentration of electron-excited and active particles in the plasma. The reactions occurring in a nonequilibrium plasma and involving such particles lead to a rise in the gas temperature greatly affecting the rate constants of reactions involving heavy particles.

In these report, the main attention is given to revealing the creation of active particles in nonequilibrium molecular plasma and the basic mechanisms and concrete channels of energy transfer to the translational degrees of freedom of molecular gas, which lead to its heating. Intensive theoretical and experimental investigations of the kinetics of gas heating at high values of reduced electric field E/n>100 Td have been under way recently [2].

Studies into the heating of molecular gas under conditions of free-localized microwave discharge have revealed that, upon pulsed switching on of the field, the gas is rapidly heated at the rate of tens of degrees per microsecond, and this heating rate decreases sharply after a period of 10-20 μs because of the discharge motion

toward the source of radiation and because of the electric field decrease due to the skin effect. For quite some time, the evolution of the gas temperature in time could not be explained using the then known mechanisms, and, accordingly, the gas heating observed at the beginning of the effect of powerful microwave radiation on the plasma was referred to as anomalously fast.

Various mechanisms are known which might lead to the heating of molecular gas [2]. In the case of elastic interaction, part of the electron energy is transferred to the translational degrees of freedom of molecules. However, because of the great difference between the mass of interacting particles and the small degree of plasma ionization (under our experimental conditions $n_e/n_o = 10^{-6} - 10^{-5}$) the rate of gas heating due to elastic interactions does not exceed one hundredth of a degree per microsecond, which is several orders less than the measured value (tens of degrees per microsecond).

For moderate values of reduced field $E/n \approx 50$ Td, the main part (up to ~80%) of electron energy is spent for vibrational excitation of molecules (Fig.4.17). In so doing, owing to vibrational-translational relaxation, part of the energy may be transferred to heat the gas. In the case of nitrogen, however, because of the magnitude of vibrational quantum, the probability of VT-relaxation at low temperatures is low, and, as demonstrated by the experimental results of [2], the time of VT-relaxation at the low-lying vibrational levels of the ground state of nitrogen amounts to hundreds of milliseconds, while the time of gas heating is approximately 10-20 μs.

The mechanism of relaxation of excited molecules on a surface involving the transfer of a part of vibrational energy of molecules to the translational degrees of freedom was suggested once to explain the heating of gas at low pressures in a dc glow discharge confined by walls. However, the results of experiments under conditions of free-localized discharge have demonstrated [2] that, in the absence of a surface, the gas is heated as effectively as in the case of a discharge confined by walls: that is, the mechanism under consideration is not a determining one.

Under the experimental conditions, the gas could be heated owing to the process associated with the quenching of vibration-excited NO molecules formed in a microwave discharge in the air, because the probability of VT-relaxation of NO molecules is much greater than that of vibration-excited nitrogen molecules.

However, the results of experiments in the pulse-periodic mode of microwave discharge in air have demonstrated [2] that the gas starts being heated even in the first pulse after the switching-on of the microwave energy, while a significant concentration of NO molecules is produced in the plasma only after several tens of pulses. Moreover, the gas is heated effectively in the absence of NO (free-localized microwave discharge in nitrogen [2]) as well.

An important part in forming the vibrational level distribution of molecules is played by vibrational quantum exchange. This process, with due regard for the anharmonicity of vibrations, is accompanied by conversion of only a small part of vibrational energy to translational. Therefore, its rate is high even at low temperatures, and, in principle, it is capable of providing a fairly high rate of the gas heating. However, as demonstrated by the experimental results (Fig.4.19), the rapid heating of gas in a fixed region of space ceases after a time on the order of 10-20 μs, which is associated with the discharge motion and field screening, although, if VV-exchange was responsible for the heating of gas, rapid heating would have been observed even after the switching-off of the field. However, as demonstrated by the calculation results, the relatively slow heating of gas at the rate of ~0.1 K/μs, which is observed after the switching-off of the field in the stage of deionization, is supported by this process quite well.
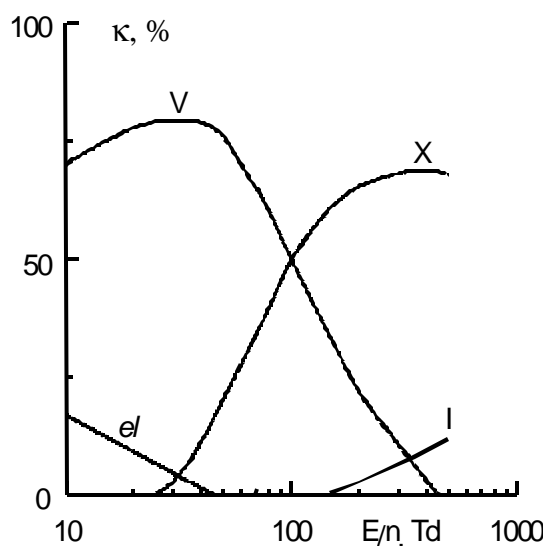
Fig. 4.17. The fraction of electron energy transferred to the various freedom degrees of nitrogen molecules as a function of reduced electric field.
V - vibrational excitation of molecules; *el* – elastic interactions;
X - excitation of the electron states of molecules; I – ionisation.

When the value of reduced electric field E/n increases, the fraction of energy transferred to vibrational excitation of molecules decreases, and the fraction of energy for excitation of the electron states of molecules increases (Fig.4.17). In so doing, it is known that, if vibrational-transiational relaxation in the air is slow, the processes of quenching of electron-excited molecules, which occur in various channels and involve the transfer of a part of energy to translational degrees of freedom, are rather fast and may, in principle, support the observed rapid heating of gas.

2.3.1 Non-stationary kinetical model of discharge in dry air

In order to understand the physics of nonequilibrium plasma systems, one needs to know the full kinetics of the processes occurring in plasma. For this purpose, we treat the nonstationary kinetic model that includes the nonstationary Boltzmann equation (1) for the energy distribution function of electrons $f(\varepsilon,t)$; the system of nonstationary balance equations (2) for the populations n_v of vibrational levels of the ground state $X^1\Sigma_g^+$ of the nitrogen molecule; equations (3) for the populations n_X of electron-excited states $A^3\Sigma_u^+$, $B^3\pi_g$, $C^3\pi_u$, $a'^1\Sigma_u^-$, $a^1\pi_g$, $a^1\Delta_g$, $b^1\Sigma_g^+$ of nitrogen and oxygen molecules; equations (4) for active particles n_y (N, O, O_3, NO, NO_2, N_2O); equations (5) for charged particles n_i (n_e, O^-, O_2^-, O_3^-, O_4^-, NO^-, NO_2^-, N_2O^-, n^+); and the nonstationary heat equation (6) for the gas temperature,

$$\frac{\partial f(e,t)}{\partial t} = -\frac{\partial J_f}{\partial t} - \frac{\partial J_l}{\partial t} + In + Sup + Rot \tag{1}$$

$$\frac{\partial n_v}{\partial t} = \left(\frac{\partial n_v}{\partial t}\right)_{eV} + \left(\frac{\partial n_v}{\partial t}\right)_{VV} + \left(\frac{\partial n_v}{\partial t}\right)_{VT} + \left(\frac{\partial n_v}{\partial t}\right)_{eD} + \left(\frac{\partial n_v}{\partial t}\right)_{VD} + \left(\frac{\partial n_v}{\partial t}\right)_{XV}, \tag{2}$$

$$\frac{\partial n_x}{\partial t} = \left(\frac{\partial n_x}{\partial t}\right)_{eX} + \left(\frac{\partial n_x}{\partial t}\right)_{XX} + \left(\frac{\partial n_x}{\partial t}\right)_{XY} + \left(\frac{\partial n_x}{\partial t}\right)_{XV} + \left(\frac{\partial n_x}{\partial t}\right)_{XR}, \tag{3}$$

$$\frac{\partial n_y}{\partial t} = \left(\frac{\partial n_y}{\partial t}\right)_{Yi} + \left(\frac{\partial n_y}{\partial t}\right)_{YX} + \left(\frac{\partial n_y}{\partial t}\right)_{YY}, \tag{4}$$

$$\frac{\partial n_i}{\partial t} = \left(\frac{\partial n_i}{\partial t}\right)_{ii} + \left(\frac{\partial n_i}{\partial t}\right)_{iX} + \left(\frac{\partial n_i}{\partial t}\right)_{iY} + \left(\frac{\partial n_i}{\partial t}\right)_{iV} \tag{5}$$

$$cn_0\frac{\partial T_g}{\partial t} = \left(\frac{\partial T_g}{\partial t}\right)_{el} + \left(\frac{\partial T_g}{\partial t}\right)_{VT} + \left(\frac{\partial T_g}{\partial t}\right)_{VV} + \left(\frac{\partial T_g}{\partial t}\right)_{XT} - Q_q. \tag{6}$$

This model, allowing for various processes of energy transfer between different

degrees of freedom of molecular gas, enables one to calculate the evolution in time of the electronic, vibrational, and translational energy both in the active phase in the presence of the large electric field and in the stage of deionization of discharge plasma in dry air.

The kinetic model at hand for the calculation of the energy distribution function of electrons includes the nonstationary homogeneous Boltzmann equation derived from a two-term approximation and written as

$$
\begin{aligned}
\frac{1}{n}\frac{\partial f(\varepsilon,t)}{\partial t} = &\frac{1}{3}\left(\frac{eE_{ef}}{n}\right)^2\frac{2}{m}\frac{1}{\varepsilon^{1/2}}\frac{\partial}{\partial\varepsilon}\left(\frac{\varepsilon^{3/2}}{\tilde{n}_c}\frac{\partial f(\varepsilon,t)}{\partial\varepsilon}\right)+ \\
&+2\frac{m}{M}\frac{1}{\varepsilon^{1/2}}\frac{\partial}{\partial\varepsilon}\left(\tilde{\nu}_c\varepsilon^{3/2}f(\varepsilon,t)+\frac{kT_g}{e}\frac{\partial f(\varepsilon,t)}{\partial\varepsilon}\right)+ \\
&+4\,B_0\frac{1}{\varepsilon^{1/2}}\frac{\partial}{\partial\varepsilon}\left(\tilde{\nu}_{re}\varepsilon^{1/2}f(\varepsilon,t)\right)- \\
&-\sum_v\frac{n_v}{n}\sum_l\left[\tilde{\nu}_{vl}f(\varepsilon,t)-\left(\frac{\varepsilon+\varepsilon_{vl}}{\varepsilon}\right)^{1/2}\tilde{\nu}_{vl}(\varepsilon+\varepsilon_{vl})f(\varepsilon+\varepsilon_{vl},t)\right]- \\
&-\sum_v\frac{n_v}{n}\sum_w\left[\tilde{\nu}_{vw}f(\varepsilon,t)-\left(\frac{\varepsilon+\varepsilon_{vw}}{\varepsilon}\right)^{1/2}\tilde{\nu}_{vw}(\varepsilon+\varepsilon_{vw})f(\varepsilon+\varepsilon_{vw},t)\right]- \\
&-\sum_v\frac{n_v}{n}\sum_w\left[\tilde{\nu}_{wv}f(\varepsilon,t)-\left(\frac{\varepsilon-\varepsilon_{vw}}{\varepsilon}\right)^{1/2}\tilde{\nu}_{wv}(\varepsilon-\varepsilon_{vw})f(\varepsilon-\varepsilon_{vw},t)\right],
\end{aligned}
\tag{7}
$$

here, $f(\varepsilon,t)$ is the electron energy distribution function, normalized such that, for any moment of time, $\int_0^\infty f(e,t)e^{1/2}\,de=1$; ε is the energy of incident electrons;

$\tilde{\nu}_c=(2/m)^{1/2}\varepsilon^{1/2}\sigma_c(\varepsilon)$, $\tilde{\nu}_{re}=(2/m)^{1/2}\varepsilon^{1/2}\sigma_{re}(\varepsilon)$, $\tilde{\nu}_{vl}=(2/m)^{1/2}\varepsilon^{1/2}\sigma_{vl}(\varepsilon)$,

$\tilde{\nu}_{vw}=(2/m)^{1/2}\varepsilon^{1/2}\sigma_{vw}(\varepsilon)$ denote the normalized collision frequency for different processes under consideration; e and m denote the electron charge and mass, respectively; T_g is the gas temperature; σ_c is the transport cross section of electron-molecule scattering; σ_{re} is the cross section of electron impact excitation of rotational levels; σ_{vl} is the cross section of electron-molecule inelastic collisions upon their excitation from the v-th to l-th state; σ_{vw} is the excitation cross section of vibrational level w upon collision of an electron with a molecule at level v of the ground state; ε_{vl} and ε_{vw} denote the threshold energy for the transitions being treated; n is the total concentration of molecules; n_v is the concentration of molecules at the v-th vibrational

level of the ground state $X^1\Sigma_g^+$ of the nitrogen molecule; and $x_v = n_v/n$ is the relative number of molecules in the v-th state, which satisfies the condition $\sum\limits_v x_v = 1$.

Equation (7) implies that the variation in the total electron flux along the energy axis (the first three terms in the right-hand part, associated with the electric field effect, elastic collisions, and excitation of rotational degrees of freedom) is due to the arrival and departure of electrons owing to inelastic collisions of the first and second kind. Equation (7) was replaced by a difference equation which was solved by the sweep method [2].

In the explicit form, the set of balance equations (2) for the populations of vibrational levels n_v of the state of $N_2(X^1\Sigma_g^+)$ may be written as

$$
\begin{aligned}
\frac{dn_v}{dt} &= n_e \sum_{\substack{w=0 \\ w \neq v}} n_w k_{wv}^e - n_e n_v \sum_{\substack{w=0 \\ w \neq v}} k_{vw}^e + n_{v-1} n P_{v-1,v} + n_{v+1} n P_{v+1,v} - \\
&- n_v n \left(P_{v,v-1} + P_{v,v+1} \right) + n_{v-1} \sum_{w=0}^{n-1} n_{w+1} Q_{v-1,v}^{w+1,w} + n_{v+1} \sum_{w=0}^{n} n_w Q_{v+1,v}^{w,w+!} - \\
&- n_v \left(\sum_{w=0}^{n-1} n_{w+1} Q_{v,v+1}^{w+1,w} + \sum_{w=0}^{n} n_w Q_{v,v-1}^{w,w+1} \right) + R(v)
\end{aligned}
\tag{8}
$$

where $P_{v,v-1}$ and $Q_{v,v-1}^{w,w+1}$ are the rate constants of VT-relaxation and VV-exchange, and $k_{wv}^e = \int\limits_{e_{wv}}^{\infty} s_{wv}(e) \sqrt{\dfrac{2e}{m}} f(e)\, de$ is the rate constant of population of vibrational level v by electron impact as a result of the process

$$
N_2\left(X^1\Sigma_g^+, w\right) + e \underset{k_{vw}}{\overset{k_{wv}}{\rightleftarrows}} N_2\left(X^1\Sigma_g^+, v\right) + e
\tag{9}
$$
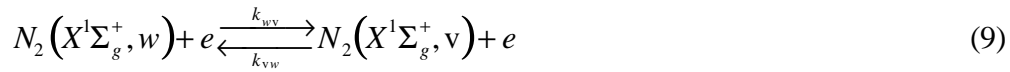
The calculations included the excitation and de-excitation of the first ten vibrational levels of the ground state $X^1\Sigma_g^+$ of the nitrogen molecule by electron impact as a result of reaction (9), where $0 \leq v \leq 10$ and $0 \leq w \leq 10$. The cross sections of direct processes were determined using the data of [3, 4], and the cross sections of inverse processes were calculated using the principle of detailed equilibrium [5]. The coefficients of the rates of VT- and VV-processes of energy exchange were calculated from the SSH theory [6, 7] modified for the VT- [8] and VV-processes [9]. The rate coefficients for inverse processes were found from the principle of detailed equilibrium [10]. The energy of vibrational levels was calculated using the

assumption of an anharmonic oscillator,

$$E_v = \hbar\omega(v+1/2) - x_e\hbar\omega(v+1/2)^2, \tag{10}$$

with $\hbar w = 2358,57 cm^{-1}$ and $x_e \hbar w = 14.32\, cm^{-1}$ [10]. Therefore, the level v=46 corresponds to the dissociation energy of nitrogen, and, accordingly, system (2) consists of 46 equations for 0<v<45.

The equations, defining the concentration of excited, active, and charged particles that form during the discharge existence, include the processes of excitation of electron states, ionization and dissociation of heavy particles by electron impact, associative ionization, electron attachment and detachment involving electrically positive components of air, electron-ion and ion-ion recombination, ion conversion, and chemical transformations of particles in the ground and excited states,

$$\frac{dn_k}{dt} = \sum_{m,q}(n_m w_{mk}^q - n_k w_{km}^q) + F_k - n_k G_k \tag{11}$$

where w_{mk}^q is the probability of transition from the state k to the state m under the effect of the q-th elementary process, and F_k is the source of formation of particles in the k-th state owing to the processes in which neither the particle in question nor its ion takes part; that is, F_k is independent of n_k (for example, dissociative recombination with the formation of an excited atom in the k-th state). Then, $F_k = n_2^+ n_e k_d^r$ (k_d^r is the rate constant of dissociative recombination with the formation of an excited atom in the k-th state, and n_2^+ is the number density of molecular ions). The group of processes G_k describe the loss of excited atoms as a result of processes in which no atoms of the element being treated are formed in either the ground or an excited state. Associative ionization may serve as an example of a process of the G_k type. In this case, $G_k = n_a k_a^i$ (k_a^i is the rate constant of associative ionization of an atom in the k-th state). In the case of diffusion, $G_k = (1/n_k)\mathrm{div}\, J_k$, where J_k is the diffusion flux of particles in the k-th state due to their motion in space. The reaction rate constants and their temperature dependences, essential for calculation of the particle number density, are given in [11-14] and in the references cited in these papers.

The following processes may lead to the heating of gas: energy transfer to the translational degrees of freedom during elastic electron-molecule collisions,

rotational-translational and vibrational-translational relaxation, vibration-vibration exchange, and quenching of electron-excited states. Then, equation (6) may be rewritten as

$$cn\frac{dT_g}{dt} = 2\frac{m}{M}n_e\frac{3}{2}k(T_e - T_g)\overline{v_e(\varepsilon)} + E_1\sum_{v=1}^{n}(1-2\chi_e v)\Big(n_v P_{v,v-1} - n_{v-1}P_{v-1,v}\Big) +$$

$$\backslash + 2E_1\chi_e\sum_{v=1}^{n}n_v\Bigg(\sum_{v=1}^{n}(w-v)n_{w-1}Q_{v,v-1}^{w-1,w}\Bigg) + \tag{12}$$

$$+ \eta_1\varepsilon_A k_{AA}^{XB}n_A^2 + \eta_2\varepsilon_A k_{AA}^{XC}n_A^2 + \eta_3\varepsilon_A k_{AX}^{XB}n_A n_X - Q_q$$

The first term in the right-hand part of equation (12) defines the energy transferred by electrons to heavy particles upon elastic collisions with gas molecules (M is the molecular mass; n_e and T_e denote the number density and temperature of electrons, respectively; and $\overline{v_e(\varepsilon)}$ is the elastic collision frequency averaged with respect to the energy distribution function of electrons). For E/n>10 Td the fraction of energy transferred by electrons to gas molecules upon elastic collisions is less than 10^{-3}.

As the reduced electric field increases to E/n≤100 Td, the main losses of electron energy are due to vibrational excitation of molecules. Because a significant amount of energy spent for vibrational excitation of molecules may be transferred back to electrons during superelastic collisions, it is necessary to solve the self-consistent problem of finding the energy distribution function of electrons and the function of distribution of molecules over vibrational levels of the ground state. In so doing, the fraction of fast electrons increases in the electron energy distribution function, this leading to a considerable increase of the rate constants of excitation of different levels of molecules. A part of the energy stored in the vibration storage may be spent to heat the gas either owing to VT-exchange between nitrogen molecules (the second term in the right-hand part of equation (12)), with a part of vibrational energy $\Delta E_{VT} = E_V - E_{V-1}$ transferred to the translational degrees of freedom of molecules, or owing to VV-exchange (the third term in the right-hand part of equation (12)), with $v + w = v' + w'$ and a minor part of energy $\Delta E_{VV} = E_V + E_W - E_{V'} - E_{W'}$ going to heat. Because the time of VV-exchange (for lower vibrational levels) is much less than that of VT-relaxation, the contribution by VV-exchange to the heating of gas may be much greater than that by VT-relaxation, in spite of the fact that it is only a minor part of energy that goes to heat. Apparently, the nitrogen atoms are capable of quenching vibrationally excited nitrogen molecules with the same, or even higher,

efficiency [15]. Therefore, if the concentration of nitrogen atoms in the discharge is high, one must take this process into account in studying the kinetics of heating of molecular gas.

However, as shown in [16, 17] for conditions close to those under discussion, the production of nitrogen atoms in the discharge occurs over times on the order of or more than several tens of microseconds, while, at the initial stage of discharge, when a rapid heating of gas is experimentally observed, the number density of gas atoms is negligibly small ($n_N \approx (10^{-2} \div 10^{-1}) n_N^{st}$) and the effect of this process may be ignored.

If E/n>100Td, a considerable part (~50% or more) of energy received by the electrons from the field goes to excitation of electron states of molecules and ionization (Fig.17). In this case, the concentration of electron-excited states of nitrogen may be high, and a part of their energy during quenching (the fourth-sixth terms of the right-hand part of equation (12)) goes to heat.

The coefficients of the rates of reactions involving metastable molecules $A^3\Sigma_u^+$, were borrowed from [18-20]. The values of $k_{AA}^{XC} = 1.1 \cdot 10^{-9}\ cm^3 s^{-1}$, $k_{AA}^{XB} = 2.6 \cdot 10^{-10}\ cm^3 s^{-1}$ [19], and $k_{AX} = 3 \cdot 10^{-10}\ cm^3 s^{-1}$ [20] were used in the calculations. In so doing, the energy of the particles involved in the reactions in question is divided between the translational and vibrational degrees of freedom of nitrogen molecule. Approximately one-half of the remaining energy goes to vibrational excitation, and the other half, to heating [21]. The fraction of energy that goes to heating as a result of the process $A + A \rightarrow X + B$, $h_1 \approx 0.5$, $h_2 \approx 0.13$ for the process $A + A \rightarrow X + C$, and $h_3 \approx 0.16$ for the process $A + X \rightarrow X + B, C$.

The energy losses to the environment, Q, for a free localized microwave discharge are defined by thermal conductivity due to translational-rotational degrees of freedom, by heat radiation in the volume radiator approximation, and by wind drift.

2.3.2 Results of numerical calculations of gas heating

As demonstrated by the numerical calculation results, the rate of gas heating depends considerably on the pumping intensity of the electron-excited states of molecules, that is, on the value of E/n, while the values of the constants $k_{AA}^{XC,B}$ and k_{AA} that considerably affect the concentration of excited nitrogen molecules have almost no effect on

the rate of gas heating (Fig.4.18). This conclusion is important in view of the fact that the values of constants given in literature by different authors differ from one another by orders of magnitude. One can see from the model calculation that, as the quenching constants increase, the rate of energy transfer to the translational degrees of freedom, which is proportional to the product of the constants and the concentration of electron-excited molecules, remains almost the same.
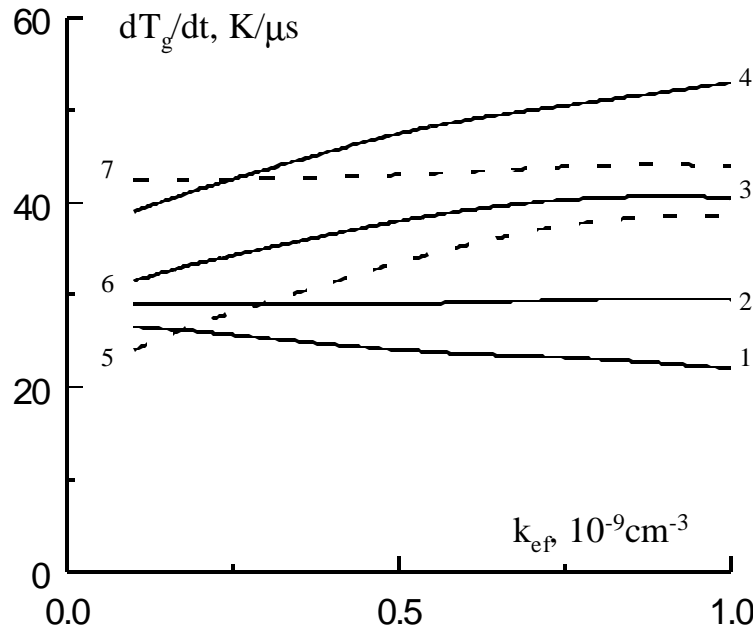

Fig.4.18. Dependencies of the gas heating rate on the values of the quenching constants of the metastable state of nitrogen at different values of the fraction of energy that goes to heating
Curve 1-4 $\eta_1 = 0.3$, $\eta_2 + \eta_3 = 0.1$ (1), 0.2 (2), 0.3 (3), 0.4 (4).
Curve 5-7 $\eta_2 + \eta_3 = 0.3$, $\eta_1 = 0.2$ (5), 0.3 (6), 0.4 (7).

It follows from the numerical calculation results (Fig. 4.19) that the model of heating due to VV- and VT-relaxation alone is characterized by the presence of time delay in the evolution of the gas temperature on the order of several tens of microseconds. The magnitude of this delay depends on the energy input to the discharge and on the pressure. In so doing, even some cooling of gas occurs during these periods of time due to the process of redistribution of molecules over the vibrational levels of the ground state, whereas the heating of gas due to quenching of electron-excited nitrogen molecules occurs almost without delay and provides for the experimentally observed heating rate (Fig.4.19 and 4.20).
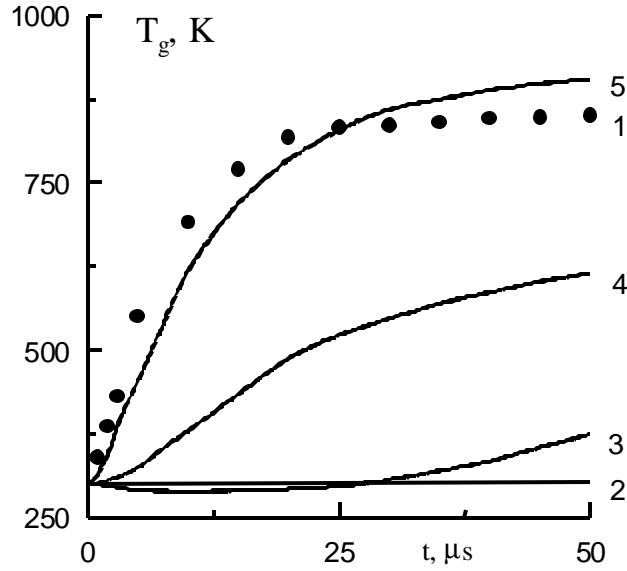
Fig.4.19. Comparison of measured time evolution of gas temperature at p=35 Torr, $n_e = 2\ 10^{12}$ cm^{-3}, E/n=200 Td (1) with calculated one at taking into account elastic *el* collisions (2), VT-relaxation and VV-exchange (3), quenching of metastable molecules by vibrationaly excited molecules (4) and at taking into account all processes *el*, VT, VV, XV and XX processes (5).
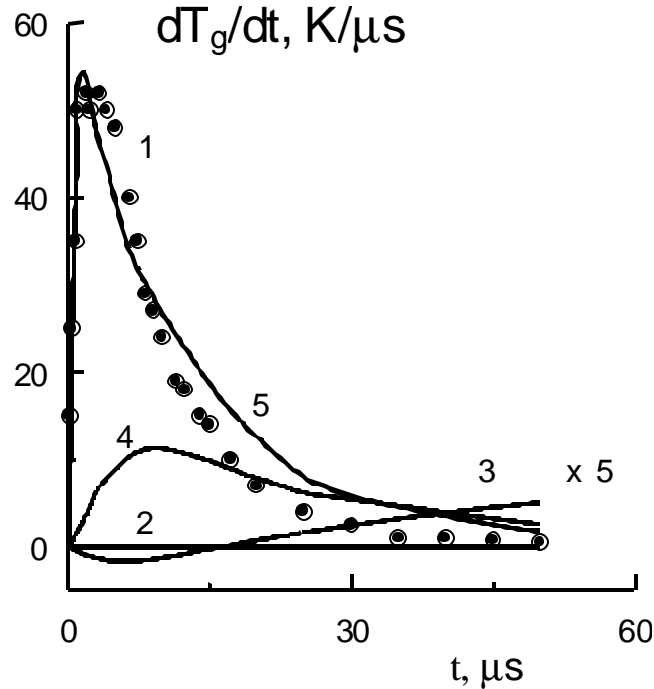

Fig.4.20. Comparison of measured time evolution of the gas heating rate at p=35 Torr, E/n=200 Td, n_e=2·10^{12} cm^{-3} (1) with calculated one at taking into account elastic *el* collisions (2), VT-relaxation and VV-exchange (3), quenching of metastable molecules by vibrationaly excited molecules (4) and at taking into account all processes *el*, VT, VV, XV and XX processes (5).

2.3.3. Gas heating under condition of aerodynamical experiment

For gas temperature measurement at the plasma aerodynamic the spectral diagnostics were used. A discharge radiation spectrum contains primarily molecular bands of second positive system of neutral nitrogen, and first negative system of molecular nitrogen positive ion; in some cases there are also molecular bands of CN. An analysis of such spectra shows that the gas temperature in a supersonic airflow is rather high (Fig.4.21). Gas temperature achieves ~2000 K at discharge current i=2.5 A and pressure of air p=40 Torr. The vibration temperature for these conditions is 3-5 times higher than the gas temperature. Plasma state is very far from equilibrium. A considerable part of plasma energy is accumulated in the vibration reservoir. It can affect on energy balance and all the conditions of supersonic flow over a body.
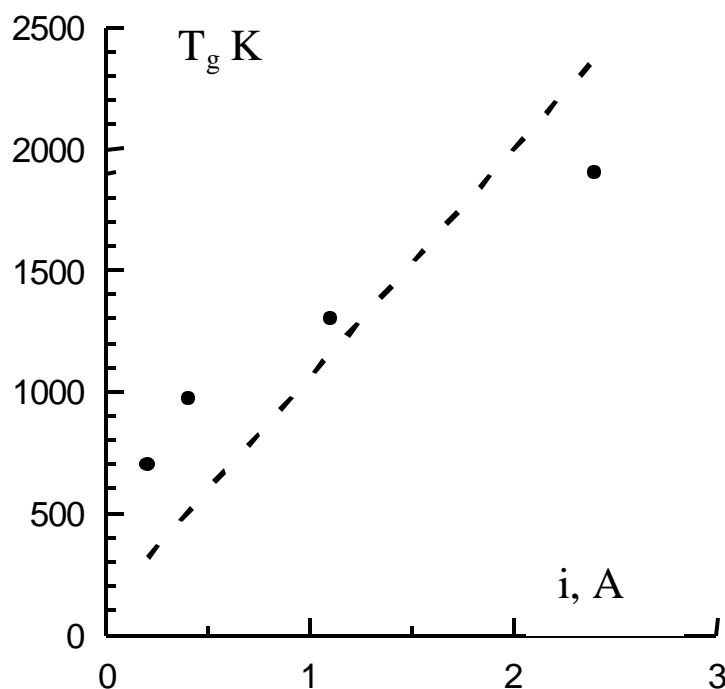
Fig.4.21. Comparison of the experimental (points) dependent temperature of gas in the plasma of the dc discharge in a supersonic airflow with the calculated value (dashed line): initial pressure in chamber p=40 Torr, Mach number M=2, initial gas temperature in airflow T_{go}=167 K, air density in flow n=5.6×10^{18} cm^{-3}.

For an explanation of the received results the computer modelling of the investigated phenomenon with the help of kinetical model, described in p.2.3.1, was carried out. The plot in Fig.4.5 compares the experimental results with the results of numerical calculation of dependence of gas temperature on discharge current. The calculations were made with using experimentally received data about electron density and electric

field in plasma [22]. One can see that there is a satisfactory agreement between calculation and experiment.

2.3.4. Plasma-chemical processes under conditions of a discharge in air

In special model experiments the measurements of a temporary evolution of concentration of nitrogen and oxygen atoms and exited molecules of nitrogen were carried out under condition of the pulsed-periodic discharge at high values of E/n. The temporary dependencies of concentration of atoms of oxygen and nitrogen are submitted on Fig.4.22. One can see that the time necessary for an creation of atomic oxygen and nitrogen decreases with increase of a discharge current and equals some tens microseconds in conditions of experiment. The dependences of relative concentration of oxygen atoms on time for pressure of a nitrogen-oxygen mixture p=0,4 Torr and discharge current i=0,65 A are submitted on Fig.4.23. The measured temporary dependencies of concentration of molecules $N_2(C^3\pi_u)$, $N_2(B^3\pi_g)$ and found on this data a temporary evolution of molecules $N_2(A^3\Sigma_u^+)$ are submitted on Fig.4.24. The received data well co-ordinate with density of active particles calculated from non-stationary kinetical model.

The model experiments on measurement of concentration of active particles in a pulsed microwave discharge in air were also carried out. The measurements have shown that at duration of a microwave pulse τ=10μs the degree of dissociation of oxygen α=O/2O$_2$ in the discharge equals 10-15%. With increase of a pulse duration up to 30μs the degree of dissociation reaches 40-60 %. Thus the rate of a creating of atomic oxygen linearly grows with increase E/n. The received results testify that there is a fast creating of atomic oxygen in a pulse microwave discharge in air. Dependencies of concentration $O_2(a^1\Delta_g)$ on a pulse duration, a pulse repetition frequency and specific energy deposition in the discharge for one pulse were obtained. The time decay of a metastable state $a^1\Delta_g$ was determined on change of an emission intensity of oxygen molecules at λ=1268nm in pauses between pulses. The time decay increases with pressure and equals 0,2-0,6s. The analysis of different processes taking place in plasma has shown that the time decay of a metastable state $a^1\Delta_g$ of oxygen molecules in the discharge is determined by a diffusion with subsequent deactivated on walls of a tube.
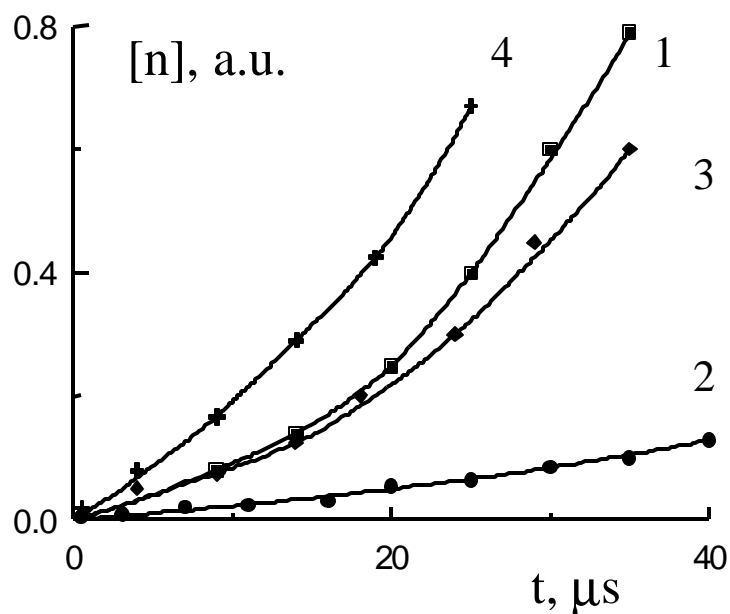
Fig. 4.22. The temporary dependencies of concentration of atoms of nitrogen (1) and oxygen for various values of a discharge current i, A: 2-1; 3-14; 4-20.
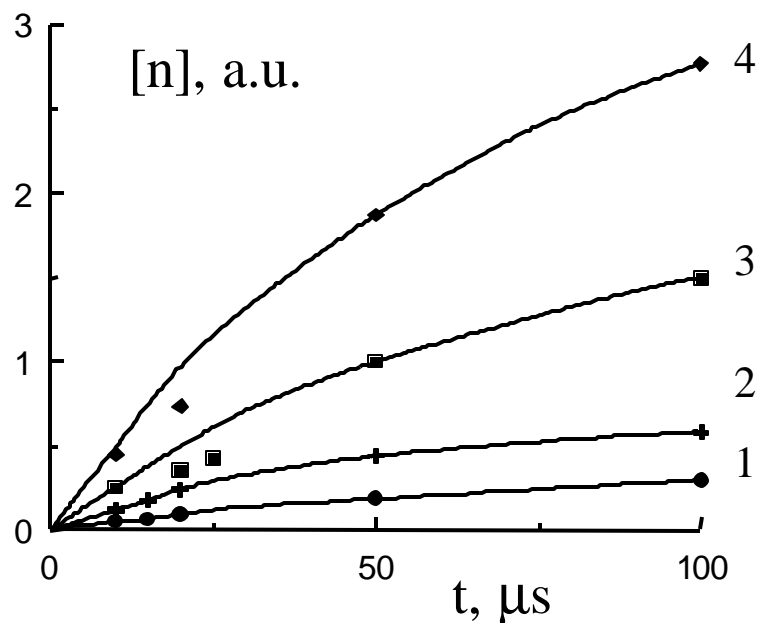

Fig. 4.23. **The time dependencies of relative concentration of oxygen atoms at p=0,4 torr, i=0,65 A and at various partial pressure of molecular oxygen ([O₂],%: 1-0,5; 2-4; 3-8,5; 4-20).**

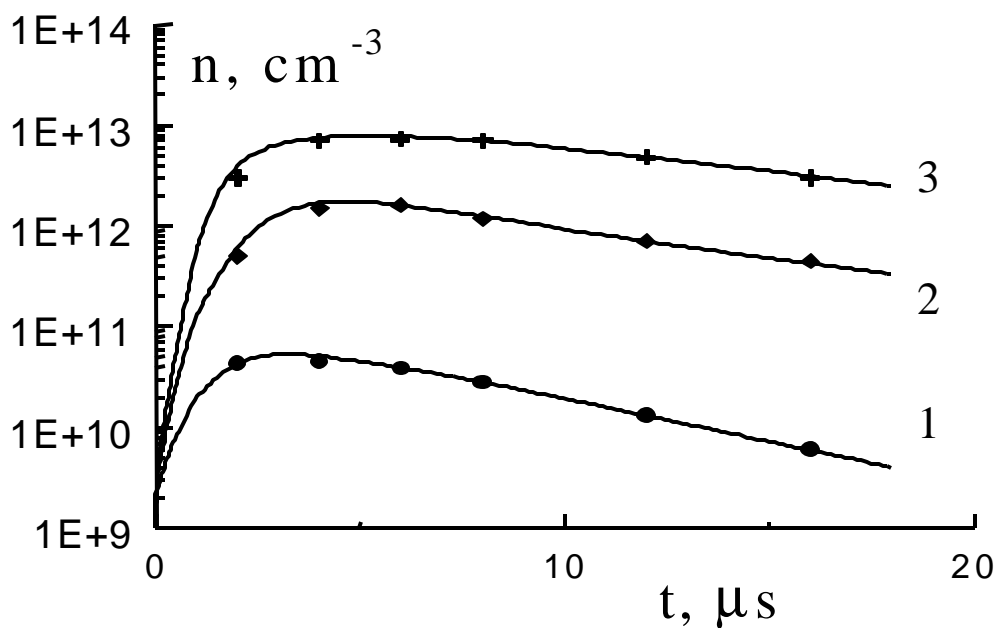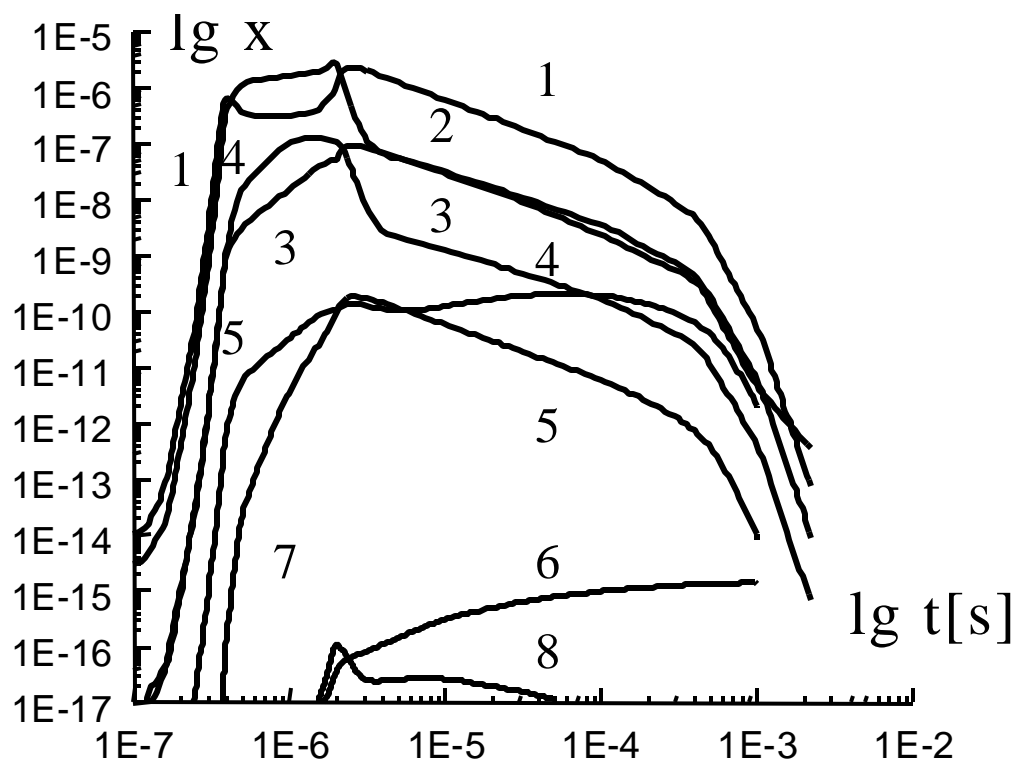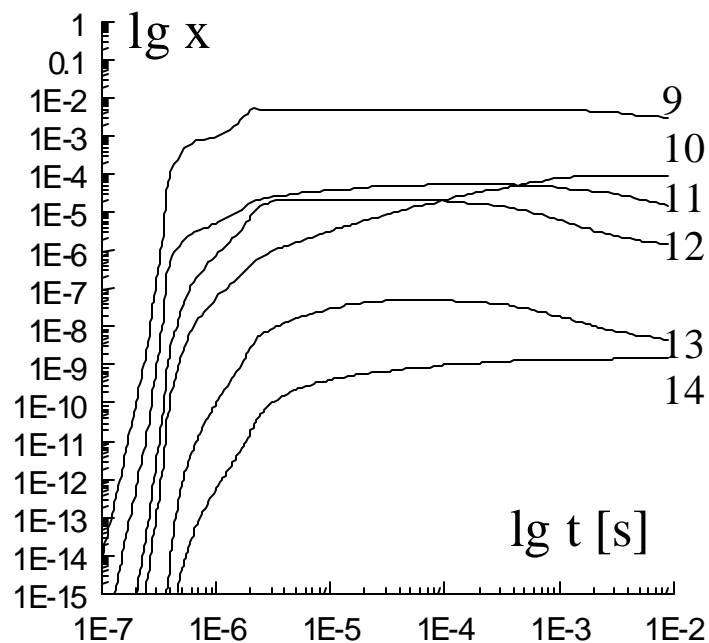**Fig. 4.24. The temporary dependencies of concentration of molecules $N_2(C^3p_u)$ - (1), $N_2(B^3p_g)$ - (2) and $N_2(A^3S_u^+)$ - (3).**

Fig. 4.25. The time evolution of concentrations of charged particles in non-equilibrium plasma of discharge in air

at p=35 torr, E/n=200 Td, τ=2 μs: n_e (1), O^- (2), O_2^- (3), O_3^- (4), O_4^- (5), NO^- (6), NO_2^- (7), N_2O^- (8).

151

Fig. 4.26. The time evolution of concentrations of active particles in non-equilibrium plasma of discharge in air

at p=35 torr, E/n=200 Td, τ=2 μs: O (9), O_3 (10), N (11), NO (12), NO_2 (13), N_2O (14).
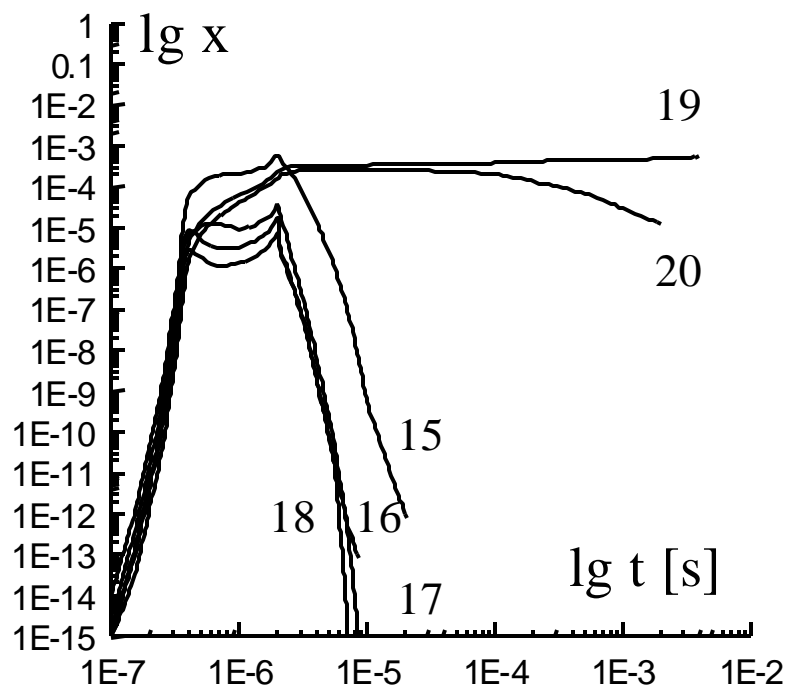
Fig. 4.27. The time evolution of concentrations of excited particles in non-equilibrium plasma of discharge in air

at p=35 torr, E/n=200 Td, τ=2 μs: $A^3\Sigma_u^+$ (15), $a'^1\Sigma_u^-$ (16), $B^3\pi_g$ (17), $C^3\pi_u$ (18), $a^1\Delta_g$ (19), $b^1\Sigma_g^+$ (20).

In order to understand the physics of non-equilibrium plasma systems, one needs to know the full kinetics of the processes occurring in plasma. For this purpose, we work out the non-stationary kinetic model. From results of mathematical modeling it is possible to see, that kinetics of the charged particles in a molecular plasma of electronegative gases strongly depends on presence of active particles created in plasma during existence of the discharge. So, in a regime of short pulses and high frequency of its repetition accumulation of active particles can occur from a pulse to a pulse. At this, character of plasma deionization changes from fast regime of attachment to slow regime of recombination. The ratio between values of concentration of active particles created during existence of the discharge, electron density and various kinds of negative ions depends on air pressure, pulse duration, and various stages of deionization plasma. For example, on Fig.4.25-4.27 the time evolution of main charged and active particle in non-equilibrium plasma of discharge in air at p=35torr, E/n=200Td, τ=2μs is submitted. At air pressure p=1torr the relative concentration of atomic oxygen is increased from $\sim 10^{-5}$ at τ=10μs up to $\sim 10^{-1}$ at τ=20 μs. Thus the relaxation time of the majority of active particles achieves several hundreds millisecond. The data of mathematical modeling well correspond to results of model experiments.

2.4. Spectral Methods of Measurement of Gas Temperature of a Air Plasma

2.4.1. Method of Measurement of Gas Temperature

Information about gas translation temperature T_g is important for study of plasma processes. The simplest possible case for molecular plasma corresponds to local thermodynamic equilibrium, then $T_g = T_V = T_R$, here T_V and T_R are vibration and rotation temperatures, respectively. T_V and T_R are parameters of fitting of population of vibration and rotation energy states of molecules to the Boltzmann function, they characterize distribution function of molecules. Both T_V and T_R can be extracted from plasma radiation spectra.

In non-equilibrium plasmas T_g can be also determined on base of measurement of T_R.. Spectra of plasma radiation provide information about rotation temperatures T_R^* of

molecules in excited electron states. The dependence of T_R^* on intensity of a rotation structure spectral line I_{lk}, that corresponds to a transition between l-th and k-th states is given by a formula

$$(k_B/B^*)\ln(I_{lk}/i\,\nu^4_{ik}) = C - j(j+1)/T^*_R,$$

here k_B is the Boltzmann constant, j is a total molecular moment of momentum, i is a quantum mechanical coefficient of intensity, ν_{lk} is the frequency of radiation quantum, C is a constant. One can extract T_R^* by plotting a function $(k_B/B^*)\ln(I_{lk}/i\nu^4_{ik})$ over j(j+1), and measuring its slope tgα:

$$T_R^* = 1/\text{tg }\alpha.$$

For a stable molecule a possibility of change its rotation energy at excitation is negligible, and rotation distribution functions for excited and basic molecular states are identical, $T_R = T_R^*$. Effective exchange of translation and rotation energies at collisions results in equality of T_g and T_R of molecules in basic electron state. But at realistic conditions there are some peculiarities that must be paid account to. If molecules take part in plasma chemical reactions, a part of their activation energy can transfer to rotation energy, that results in distortion of initial rotation distribution function, and $T_R \neq T_R^*$. It is especially characteristic to chemically active radicals. Another source of errors is bound with the fact that spectra yield not T_R but B^*/T_R, here B^* is the rotation constant for upper state at radiation transition. At electron impact excitation of this state, rotation energy distribution can be conserved, but it corresponds to a temperature

$$T_R = T_g\,B^*/B^o,$$

here B^o is the rotation constant for the basic state.

Thus, stable molecules with $B^* \approx B^o$ should be chosen for measurement of T_g.

The second positive band of nitrogen is widely used. Here one can take ν^4_{lk} to be a constant (the corresponding error $\approx 0.5\%$ is negligible), $\hat{A}^* = 1,826$; the formula for $\grave{O}_R$ looks like

$$0,89\ln(I_{lk}/i) = \text{Const} - j(j+1)/T_R.$$

In number of work it is suggested to determine the gas temperature of nitrogen at high

pressure on base of unresolved cyan bands with threshold wavelengths 3883 $\mathring{A}^o$ and 3871 $\mathring{A}^o$. Three ways of temperature measurement are available. These methods are based on: 1) – ratio of integrals of radiation of the two bands; 2) – ratio of threshold intensities of these bands; 3) – distribution of rotation transition intensities of (0;0) band with threshold wavelength 3883$\mathring{A}^o$.

2.4.2. Method of Measurement of Vibration Temperature

Vibration excitation in a molecular plasma as a rule affects ionization and gas heating. There is a method of determination of vibration levels population of nitrogen basic electron state $X^1\Sigma_g^+$. It is based on a measurement of radiation intensities in bands of the second positive nitrogen system. Conditions are pointed out, at which the electron state $C^3\pi_u$ is populated due to electron impact excitation of the basic $X^1\Sigma_g^+$ state. De-excitation of vibration levels of the state $C^3\pi_u$ is bound with radiation, because its characteristic time (10^{-7} s) is much less than that of vibration and rotation relaxation and of diffusion.

Let the vibration levels v''_X of the basic nitrogen electron state are distributed according to a function $f(v''_X)$, i.e.

$$n(v''_X) = n_0\, f(v''_X).$$

Then in case the conditions mentioned above are met, a stationary population of $C^3\pi_u$ vibration levels v'_C is given by

$$n(v'_C) = (n_e n_0/A(v'_C,v'_B))/\textstyle\sum_{v''_X} <\sigma(v'_C,v''_X)\, \upsilon>\, f(v''_X),$$

here n_0 is a number of molecules in $X^1\Sigma_g^+$ state and $v''_X = 0$; $<\sigma(v'_C,v''_X)\, \upsilon>$ is a mean cross section of excitation of $v'_C\, C^3\pi_u$ levels, n_e is electron concentration, $A(v'_C,v'_B)$ is a probability of radiation of the second positive nitrogen system, v''_X are vibration quantum numbers of $B^3\pi_g$ state.

As the process of excitation of the $C^3\pi_u$ vibration levels due to electron impact of the basic $X^1\Sigma_g^+$ state is fast in comparison with vibration period, these probabilities can be considered to be in a direct proportion to the Franc-Condon coefficients for the Tanaka system $C^3\pi_u \rightarrow X^1\Sigma_g^+$. Then the previous equation takes form

$$n(v'_C) = C \sum_{v'_C} q \ (v'_C, v''_X) \ f(v''_X),$$

here C is a constant independent on v''_X. At computation of the sum one can take only first 5 terms, because the population of the vibration levels is a steep falling function of v. Provided relative populations of the first 5 levels of the $C^3\pi_u$ state are known, one can calculate relative populations v''_X of the basic electron states as a solution of a set of equations

$$n(v'_C) = \alpha \sum_{v''_X = 0,1,2,3,4} q \ (v'_C, v''_X) \ n(v''_X),$$

here α is a normalizing coefficient. The relative populations of the $C^3\pi_u$ state levels can be determined experimentally with application of a usual method (on base of relative intensities of bands of the second positive nitrogen system $C^3\pi_u \to B^3\pi_g$).

Molecular spectroscopy gives the following formula for a radiation intensity of a electron-vibration band:

$$I(v'_C, v''_B) = C' \ S_e \ n(v'_C) \ v^4(v'_C, v''_B) \ q(v'_C, v''_B),$$

here S_e is a strength of electron transition, $q(v'_C, v''_B)$ are the Franc-Condon factors, $v(v'_C, v''_B)$ is a frequency of transition, C' is a constant independent on the quantum numbers v'_C and v''_B. After taking logarithm, one can get

$$\ln n(v'_C) = \ln C' + \ln[I(v'_C, v''_B)]/[v^4(v'_C, v''_B) \ q(v'_C, v''_B)],$$

Thus, one can get the relative populations v''_X and the vibration temperature of the nitrogen basic electron state on base of measurement of relative intensities of the electron-vibration bands v'_C.

In Fig.4.28 the radiation spectrum of CN in the range of wavelengths $\lambda = 380-390$ nm is submitted. The given spectrum is detected in plasma of discharge in C_3H_8-air mixture at static pressure P = 25 Torr. Mach number of the flow M=2, duration of the discharge current pulses $\tau = 200$ µs, frequency of their repetition is f = 20 Hz, the discharge current is I $\approx$ 10 A, the distance from electrodes downstream is z = 10 cm. Vibrational temperature measured by this spectrum is equal to $T_v = 3500$ K.
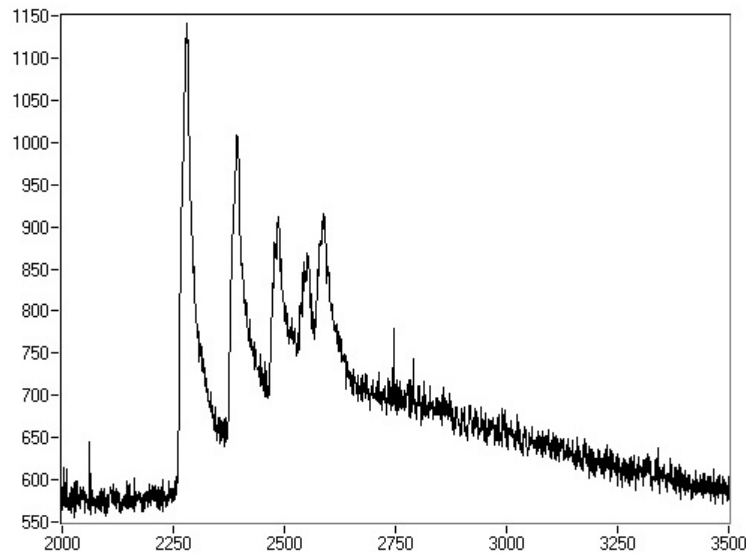
Fig.4.28. The radiation spectrum of CN (l=380-390 nm) detected in the plasma of the discharge in C_3H_8-air mixture at P_{st} = 25 Torr, M=2, t=200 ms, f=20 Hz, I » 10 A, at the distance z = 10 cm from electrodes downstream.

2.5. Spectral Method of Measurement of Electron Density

The Stark broadening effect in a stationary electrical field consists in splitting and displacement of spectral lines under action of an external electrical field. In the majority practically important cases an external field is not enough in comparison with an internal field of atom. In this case the influence of an internal field of atom can be considered as small indignation on atomic system. In plasma the radiating atom is under influence of high frequency fields of the next charged particles. In the first approximation the electrical field of ions is possible to consider quasistationary, resulting to usual splitting of a line. The influence of electrons on atom, on the contrary, is possible to consider as sharp impact which is breaking off packet of fluctuations of radiating waves or, if the impact was weaker, changing a phase of fluctuations. As a result of electron impacts a line is broadened.

The statistical and shock theory are extreme approximations of the common theory of the Stark broadening of lines, in which at first the splitting a line is calculated because of quasistatistical action of ions, then the broadening of each components at the expense of shock interaction with electrons is taken into account. Structure of a

spectral line receive by averaging on distribution of various ions fields. Thus, in the common theory the interaction both with ions, and with electrons are taken into account. The central part of a line is well described in shock approximation, on wings prevails statistical ions broadening.

In [11] structures of a lines of hydrogen are theoretically designed for various temperatures and density of electrons, that allows reliably to measure n_e on width of a line, using a ratio

$$n_e = C(n_e, T_e) \, (\Delta\lambda)^{3/2},$$

where $C(n_e, T_e)$ is a Stark constant, which is weak dependent on n_e and T_e. This ratio can be presented graphically as $\ln n_e = f(\ln \Delta\lambda)$. Most convenient for definition n_e is the H_β line. This is promoted by a number of the factors.

1. This line is located in spectral area, where the usual receivers of radiation have high sensitivity.

2. At concentration $n_e \geq 10^{13}$ cm^{-3} its broadening is great and its width it is possible to measure with the help of the usual spectral devices.

3. The accuracy of theoretical accounts of width of a line H_β is less than 5 %, while accuracy of accounts for other lines of hydrogen of the order 10 %.

4. The H_β line corresponds to transition between rather low laying levels. Therefore it is well radiated in plasma, even if the hydrogen is present as a small impurity, for example as pollution of plasma.

In this work the concentration of electrons in the plasma of discharge in supersonic airflow was determined by spectral method from Stark broadening of a spectral line H_β with $\lambda = 4861$ A^o. For it the hydrogen was added in small amounts in a supersonic flow of air. On fig.4.29 the profile of a hydrogen line H_β is submitted. The effect Doppler and apparatus function of the spectral device bring the appreciable contribution in profile of a registered line. In conditions of experiment the gas temperature is equal to 1000 K, that corresponds of a broadening line $\Delta\lambda=0.1$ A^o. Dependence of apparatus function of the spectral device on width of an entrance split was determined at registration of width of a line He-Ne laser ($\lambda = 6328$ A^o). Fig.4.30. At electron concentration $n_e \geq 10^{13}$ cm^{-3} the Stark broadening of hydrogen lines is the most effective mechanism of line broadening.
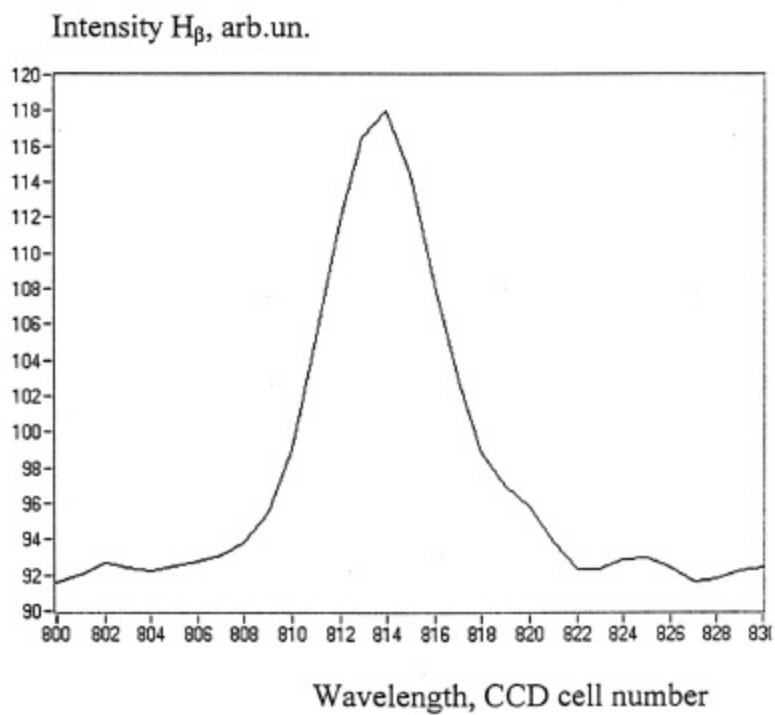
Fig. 4.29. The Stark shape of the H$_b$ hydrogen spectral line
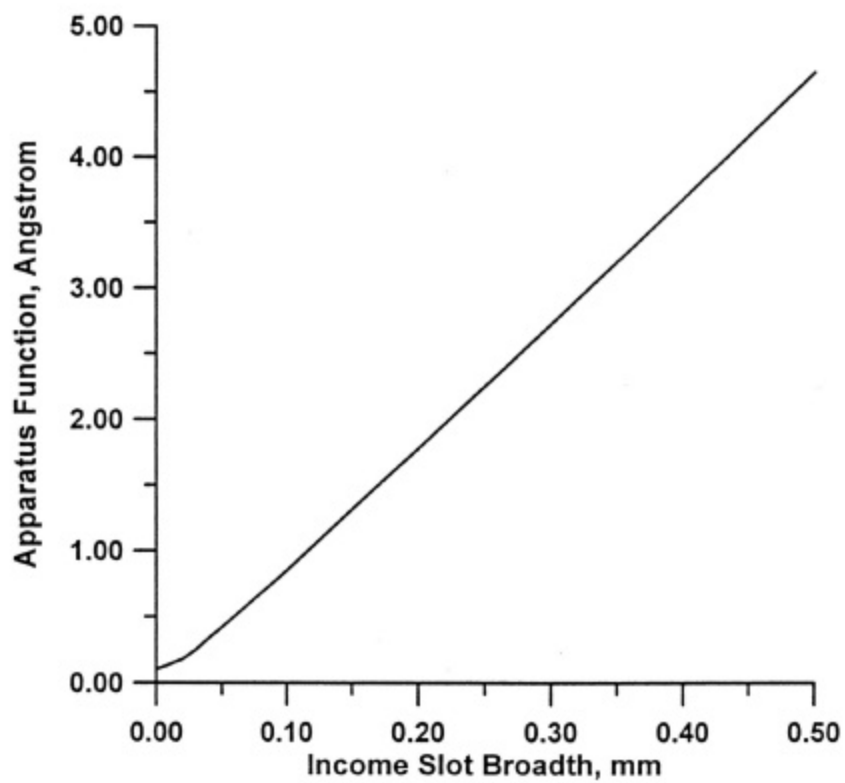p = 40 Torr, p$_0$ = 1 atm, I = 1 A.

Fig. 4.30. The apparatus function of the device over the slot broadth.

§3. Microwave Method of Plasma Diagnostics

3.1. Introduction

All the microwave methods of plasma diagnostics can be divided into three groups: passive diagnostics methods, interference based methods and plasma scattering based methods [29-30].

The interference based methods are the most widely used ones. They are based on an analysis of changes of an electromagnetic wave characteristics at its propagation through a plasma layer. In contrast with the passive methods, an arbitrary MW generator is necessary for the interference based methods. The changes of the electromagnetic wave characteristics in a plasma layer are studied with use of interference of this wave with a wave that is not passed through a plasma, and is independent of plasma properties. There are three interference based methods: the waveguide method, the resonator method and the free space method, the last one is applicable for diagnostics of supersonic plasma flows.

The sounding of a plasma volume by a MW is as a rule carried out with use of directed radiators, which provide the electromagnetic field localization in a region with transversal size about the wavelength l. The relations between the sounding wave characteristics and the plasma parameters are simple enough, if the plasma volume transversal size L is much longer than l :

$$L > l = 2pc/\omega \qquad (13)$$

Here c is the speed of light, ω is the circular frequency of radiation. Under such conditions, one can neglect the transversal dependencies of plasma parameters, and apply the geometrical optics approximation everywhere but in the reflecting plasma regions. In the opposite case interpretation of experiments is rather complicated. Thus, can be considered to be a condition of applicability of the method of diagnostics.

The simplest is an analysis of a planar MW radiation traveling through a planar infinite plasma layer with a thickness of d. One of its cases is the method based on the fact that at a high enough electron density n_e

$$n_e >> n_{cr} = mw^2 /(4pe^2) \qquad (14)$$

the MW signal does not pass through the plasma. If the inequality is not strong, $n_e \geq n_{cr}$, then the MW signal is present, but it is weakened.

Re-write the condition of applicability of the free space method (13) with the MW frequency being approximately equal to the plasma frequency $\boldsymbol{w}_p$:

$$L > 2\boldsymbol{p}c/\omega_p \approx 3.10^6/ n_e^{1/2} \ ?m. \tag{15}$$

Estimates of the plasma density for the pulsed periodical and the plasmadynamic discharges yield about 10^{13} ?m^{-3}. Then $2\boldsymbol{p}c/\boldsymbol{w}_p \approx 1$ cm, and for the supersonic flow discharges under investigation the condition (15) is met.

3.2. MW Interferometer Draft Design

A 8-mm MW interferometer with dielectric (polystyrene) antennae was applied for the MW diagnostics. Its draft design is presented in Fig. 4.31. A standard clystrone generator with an output power of 25 mW was applied as a MW source (1). The wave was passed a ferrite gate (2), and then it was divided into two by a directional coupler (3). The ferrite gate prevents a wave to pass back into the generator, that provides a normal work of the latter. The lets the MW power to pass forwards only.

The measurement branch contains a transmitting and receiving antennae (4) with an identical design.

The rectangular waveguide becomes a round one, having a rod type dielectric (polystyrene) antenna in its open side. This antenna's cross section is sharp from the waveguide side and is broadening till it achieves the value of the diameter of the waveguide (it is necessary to fit the antenna with the waveguide). Outside the waveguide the cross section is decreasing with the separation from the waveguide end (it is necessary to fit the antenna with the free space, and to achieve a desired directivity diagram). Rods made of a material with a low dielectric coefficient with a length of $L_a = (6...18)\lambda$ are known to provide very clean and narrow beams [31]. In our experiments $L_a \approx 18\lambda$, which provides a minimal beam divergence angle. The antennae were positioned normally to the axis of the plasma jet under study (11).
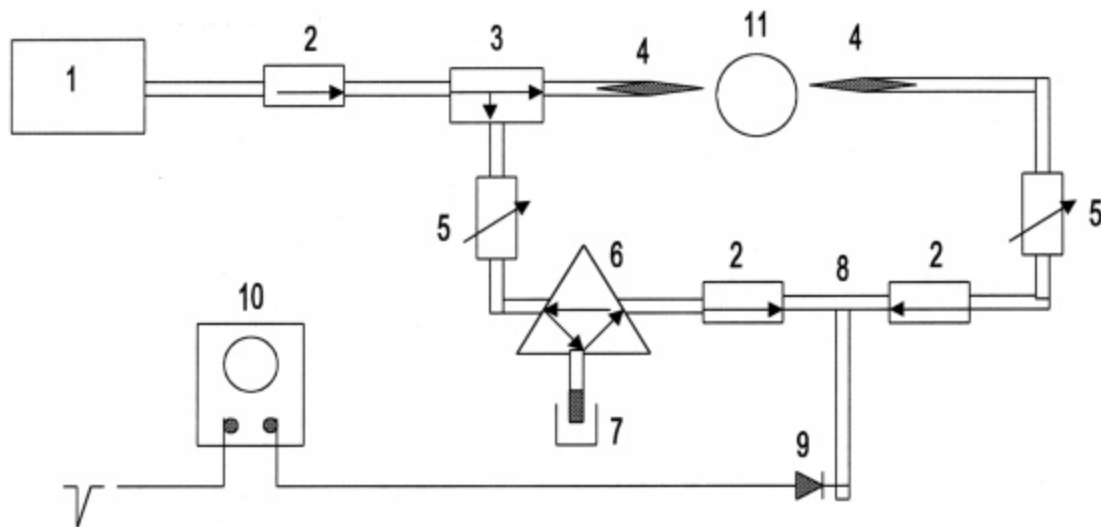
Fig.4.31.

1. MW generator.
2. Ferrite isolator.
3. Directional coupler.
4. Dielectric antenna.
5. Attenuator
6. Ferrite circulator.

7. Shortcut piston.
8. Waveguide T-connector.
9. MW detector.
10. Storage oscilloscope ? 8-17.
11. Discharge plasma.

A system comprising a ferrite circulator (6) and a shortcut piston (7) was applied as a calibrated phase shifter in the reference channel. It made it possible to replace a measuring line by a waveguide T-connector (8) and a detector probe (9). The ferrite circulator works as a valve device, it is a switch key of the waveguide channels.

Attenuators A (5) are used to equalize the amplitudes in the interferometer channels. The MW detector probe is a silicon diode. Up to 100 μW it has a quadratic characteristic (i.e. its voltage is in a direct proportion to the MW signal power).

Temporary dependencies of the MW detector were registered by a two-ray oscilloscope C8-17 (10) with a pass band of 10 MHz and with a high sensitivity (1mV/cm). The latter is essential because of weakness of the MW diode's signal.

3.3. Methods of MW Measurements in Supersonic Plasma Flows

In accord with p.3.1, at consideration of applicability of the MW diagnostic methods for the discharges in supersonic flows one has to account for:

- plasma density,

- plasma volume sizes

- frequency of electron-atom and electron-molecule collisions.

For the applied wavelength of $\lambda=8$ mm, the critical electron density $n_{e_{??}} = 1,65 \cdot 10^{13}$?m. Thus, at $n_e > n_{e_{??}}$ the radiation will no pass through the plasma, otherwise the electron density may be measured on base of the phase shift.

The latter case can be implemented for the AC discharge in a supersonic airflow at low enough electric current I $\leq$ 1 ? [32].

Then the mean electron density $<n_e>$ can be estimated with use of the model of infinitely long (in the transversal direction relatively the beam) planar plasma layer in the geometrical optics approximation [31].

This model is applicable if the antennae are positioned near the zone of joint between the anode and the cathode jets of the transversal discharge. Then the transversal size of the plasma volume is three times as long as λ, and one can neglect the refraction of the sounding wave. At smaller sizes the diagnostics is possible with account of the refraction until $L / \lambda \sim 1$ [33].

As the pressure of the free space is high enough, the phase shift $\Delta\varphi$ must be calculated with an account for the scattering frequency ν_{en}:

$$\Delta\varphi = -\pi F \frac{d < n_e >}{\lambda \; n_{e_{??}}} \frac{\omega^2}{\omega^2 + \nu_{en}^2}, \tag{16}$$

here F – is a form-factor, d is the plasma size along the beam, ω is the circular frequency of the MW radiation. As the maximal value of d was low, d $\leq$ 5 ??., i.e. d/$\lambda \leq$ ½, and the phase shift is rather small.

The accuracy of such diagnostics is restricted not only by errors in the phase shift measurements, but primarily by a strong inhomogeneity of the plasma both in the longitudinal and transversal directions relatively the sounding beam.

In the latter case, e.g., the integral phase shift at any density distribution will be less than that at the homogeneous plasma layer. Say, at a cosine distribution law the

integral phase shift will amount to 0.46 of that for the homogeneous plasma layer, and for the square of cosine law it will be 0.37 [31].

The application of the method based on the fact that at a high enough electron density $n_e \gg n_{cr}$ the MW signal does not pass through the plasma, seems to be more accurate. The condition can be met in the pulsed-periodical and in the plasmadynamic discharges. For the pulsed-periodical discharges the typical electric current is as a rule higher than 1 A. At the plasmadynamic discharges it is far much higher. As a result, the typical electron density must be high enough.

The plasmadynamic discharge plasma usually occupies all the mixing chamber volume, and the condition $L/\lambda \geq 3$ is usually met.

At the pulsed-periodical discharges the plasma size grows with the discharge current, however it is the transversal size normal to the plane of electrodes that is growing. The characteristic sizes of the cathode and the anode jets remain small enough, $d \leq \lambda$. Thus, the pulsed-periodical discharges can be sounded in one direction only.

If the collisional attenuation is present, the wave can propagate even at $n_e > n_{e_{??}}$; thus, one has to estimate the ratio of ν/ω.

For $\lambda = 8$ mm the corresponding frequency $\omega = 2.3 \ 10^{11} \ ?^{-1}$. Suppose that the jet pressure is close to that in the free space ($? \sim 40$ Torr) at some separation from the nozzle. Remember the spectroscopic data on the neutral gas temperature in the DC discharge [32]: 1000 - 2000 ? inside the visible part of the discharge. One can roughly estimate the neutral gas temperature in the pulsed-periodical discharge to be higher than 2000 K. As there are no data on the electron temperature, estimate it to be equal to that without the airflow. Then one can get an estimate for the electron collision frequency $\nu \sim 2 \ 10^{10} \ s^{-1}$, i.e. $\nu/\omega \sim 10^{-1}$. Thus, this method is applicable under the expected conditions.

A characteristic signals of the MW sensor for the different types of discharge are presented on Fig. 4.32-4.35. At low discharge current ($I < 1$ A) the installation worked as an interferometer, at high discharge current the basic leg was switched off, and the method based on the passing wave cutoff was used.

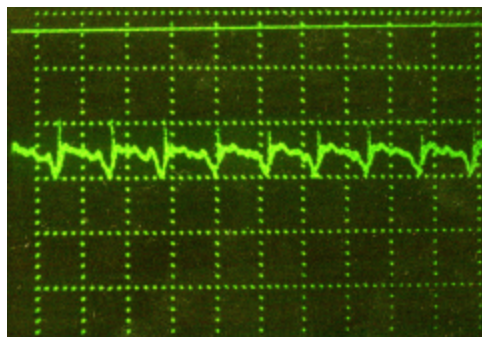A characteristic signal of the MW sensor (upper beam) for the case of DC discharge

is presented on Fig.4.32. The lower beam of the oscilloscope specifies the metal level. This is a panoramic frame with a very long sweep time 0.5 s/div., that shows the interferometer signal (with a negative polarity) at switching the discharge on and off. The period of the discharge existence is about 1.7 s. The signal is fluctuating in accord with the discharge current oscillation. The plasma cutoff concentration $1.6 \cdot 10^{13}$ cm^{-3} (averaged over all the cross section of the MW beam) is not achieved.
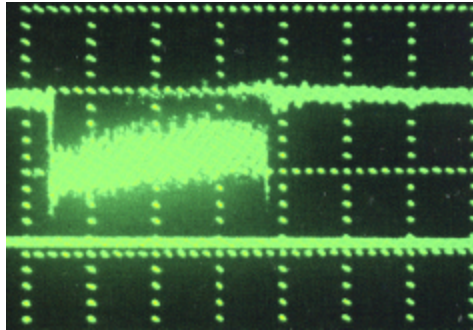
**Fig.4.32. Temporary dependencies of MW detector signal
in DC discharge in supersonic flow.**

P = 40 Torr, P = 1 atm, M = 2, I = 1.1 A, z = 5 cm, 0.5 s/div, 1 mV/div.

A signal of the MW sensor according a typical value of countdown time for the case of DC discharge is presented on Fig.4.33. The signal is fluctuating with period about 115 μs according with the discharge current oscillation (see Ch.5).

**Fig.4.33. Temporary dependencies of MW detector signal in DC discharge in
supersonic flow.**

P = 40 Torr, P = 1 atm, M = 2, I = 0.5 A, z = 5 cm, 100 μs/div, 1 mV/div.

A characteristic signal of the MW sensor (upper beam) for the case of pulse-periodic discharge is presented on Fig.4.34. The lower beam of the oscilloscope specifies the metal level. . The first sharp and narrow maximums of the both curves correspond to the discharge gap breakdown (discharge start), the second ones correspond to the discharge end. The cutoff is observed in this case, that corresponds to the fact that the plasma density in the beam cross section exceeds 10^{13} cm^{-3}.

Fig.4.34. Temporary dependencies of MW detector signal in pulse-periodic discharge in supersonic flow.

P = 40 Torr, P = 1 atm, M = 2, I = 2.8 A, pulse duration τ = 400 μs, z = 5 cm,

100 μs/div, 1 mV/div.

At last, Fig. 4.35 (upper beam) shows a signal in case of a single plasma jet, which has been injected into the channel. For a comparison, a signal of a double probe situated in the same cross section of the channel (separation from the electrode is z = 32 cm) is also presented here. One can see that the signal cutoff takes place in all the length of the jet.
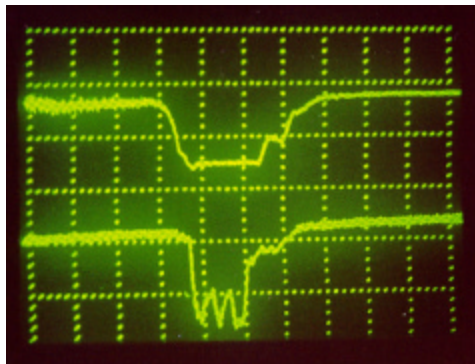
Fig.4.35. Temporary dependence of MW signal in a single plasma jet.

P = 300 Torr, p = 2 atm z = 32 cm, 200 μs/div. Lower beam – probe signal.

References to Chapter IV

1. Alferov V.I., Bushmin A.S., Kalachev B.V. Investigation of discharge glowprocess in high- velocity gas flow. ZhETF, 1966, vol.51, #5, pp.1281-1287.

2. V.V.Vitkovsky, L.P.Grachev, N.N.Gritsov, Z.M.Egorova, Yu.E.Kuznetsov, V.V.Lebedenko, V.V.Skvortsov, K.V.Khodataev, V.P.Jankov. Experimental investigation of DC electric discharge in supersonic and subsonic airflow. Trudy TsAGI, #2505, 1991.

3. S.N.Chuvashev, A.P.Ershov, A.I.Klimov, S.N.Leonov, I.B.Timofeev, V.M.Shibkov Flow around body and characteristics of AC/DC discharges in plasma aerodynamic experiment Proc. 2nd Weakly Ionized Gases Workshop, April 24-25,1998,Norfolk, Virginia,USA.p.57-65.

4. Dvinin S.A.,Ershov A.P., Timofeev I.B., Chernikov V.A.,Shibkov V.M.Features of the transversal gas discharge in a supersonic gas flow The 2nd Workshop on magneto-plasma-aerodynamics in aerospace applications. Moscow, 5 April-7 April 2000.pp.169-174.

5. Ershov A.P., Ardelyan N.V.,Chuvashev Shibkov Timofeev Probe diagnostics of gas discharges in supersonic airflow9 Int.Space Planes and Hypersonic Systems and Technologies Conf. Norfolk,VA,USA.1999

6. Chen Xi. Ion saturation current density and specific heat flux on a cylindrical probe immersed in a dense plasma flow. J.Phys. D.: Appl. Phys. 1982. V. 15. P. 1695- 1708.

7. A.S.Zarin, A.A.Kuzovnikov, V.M.Shibkov. Freely Localized Microwave Discharge in Air. Moscow: Oil & Gas. 1996. 204 p. (In Russian).

8. Samarskii A.A. Introduction to the theory of difference schemes. –M.: Nauka, 1971, 552p.

9. Schulz G.J. Vibrational excitation of N_2, CO and H_2 by electron impact. -Phys. Rev., 1964, v.135, N4A, p.A988-A994.

10. Eletskii A.V., Palkina L.A., Smirnov B.M. Transport Phenomena in Weakly Ionized Plasma. Moscow: Atomizdat, 1975, p. 248. (In Russian).

11. Vainshtein L.A., *Sobel'man I.I., Yukov E.A. Excitation of Atoms and Broadening of Spectral* Lines. -Moscow: Nauka, 1979. (In Russian).

12. Schwartz R.N., Slawsky Z.I., Herzfeld K.F. Calculation of vibrational relaxation times in gases. -J. Chem. Phys., 1952, v.20, N10, p.1591-1599.

13. Schwartz R.N., Herzfeld K.F. Vibrational relaxation times in gases (three-dimentional treatment). -J. Chem. Phys., 1954, v.22, N5, p.769-773.

14. Keck J., Carrier G.J. Diffusion theory of nonequilibrium dissociation and recombination. -J.Chem. Phys., 1965, v.43, N7, p.2284-2298.

15. Bray K.N.C. Vibrational relaxation of anharmonic oscillator molecules: relaxation under isothermal conditions. -J. Phys. B. (Proc. Phys. soc.), 1968, v.1, ser.2, p.705-717.

16. Loureiro J., Ferreira C.M. Coupled electron energy and vibrational distribution functions in stationary N_2 discharges. -J. Phys. D: Appl. Phys., 1986, v.19, p.17-35.

17. Kossyi I.A., Kostinsky A.Yu., Matveev A.A., Silakov V.P. Kinetic sheme of the non-equilibrium discharge in nitrogen-oxigen mixtures. -Plasma Sources Sci. Technol., 1992, v.1, N 3, p.207-220.

18. McEven M and Philips L. The Chemistry of the Atmosphere. London: Arnold, 1975.

19. Mnatsakanyan A.Kh., Naidis G.V., Solozobov Yu.M. Negative ions in oxygen plasma. -Khim.Fizika, 1987, v.6, N6, p.820-824. (In Russian).

20. Mnatsakanyan A.Kh., Naidis G.V. Processes of creation of charge particles in oxygen-nitrogen plasma. -In book: Khim.Plasmy. Moscow: Energoizdat, 1987, N.14, p.227-255. (In Russian).

21. Nonequilibrium Vibrational Kinetics. Capitelli M., Ed., Berlin: Springer, 1986.

22. Zarin A.S., Kulikov V.N., Mitsuk V.E. Measurement of density of atomic oxygen inmicrowave discharge. -Pis'ma Zh.Tekh.Fiz. 1986, v.12, N19, p.1186-1190. (In Russian).

23. Kalinin A.V., Shibkov V.M., Shibkova L.V. -Vestnik MSU, 1996, v.37, N1, p.38-42 (In Russian).

24. Bogatov N.A., Gitlin M.S., Golubev S.V. et al. Investigation of relaxation of metastable molecules $N_2(\grave{A}^3\Sigma_u^+)$ after pulsed discharge in nitrogen by the method of intraresonator laser spectroskopy. Preprint of Inst. of Applied Physics. USSR Acad. Sci. Gorki, 1988, N.219, 38p. (In Russian).

25. Hays G.N., Oskam H.J. Population of $N_2(B^3\pi_u)$ by $N_2(A^3\Sigma_u^+)$ during the nitrogen afterglow. -J. Chem. Phys., 1973, v.59, N 3, p.1507-1516.

26. Golubovskii Yu.B., Telezhko V.M., Stoyanov D.G. Excitation of $\tilde{N}^3\pi_u$ and $\tilde{N}'^3\pi_u$

states of nitrogen molecule at binary collisions of metastables $N_2(A^3\Sigma_u^+)$. - Opt.Spectrosk. 1990, v.69, N 2, p.322-327 (In Russian).

27. Boeuf J.R., Kunhardt E.E. Energy balance in a nonequilibrium weakly ionized nitrogen discharge. -J. Appl. Phys., v.D60, N 3, p.915-923.

28. Shibkov V.M. Kinetics of gas heating in plasma created in supersonic airflow. 9th International Space Planes and Hypersonic System and Technologies Conference. 1-4 November 1999, Norfolk, Virginia, USA. AIAA-99-4965, p.1-6.

29. Golant V.E. Microwave methods of plasma investigation. Moscow, Nauka, 1968.

30. Ershov A.P., Solntzev G.S. Plasma – microwave interaction and microwave discharges. Moscow, MSU, 1990. Pp. 49 –59.

31. Heald M.A. and Wharton C.B. Plasma diagnostics with microwaves. John Wiley & Sons. Inc., New York, London. 1965.

32. Dvinin, S.A., Ershov, A.P., Timofeev, I.B., Chernikov V.A., and Shibkov, V.M. "Features of the Transversal Gas Discharge in a Supersonic Gas Flow," The 2nd Workshop on Magneto-Plasma Aerodynamics in Aerospace Applications, 5 April – 7 April 2000, Moscow, Russian Academy of Sciences, Institute of High Temperatures of RAS (IVTAN), pp. 169-174.

33. Kuwahara Chiyo, Matsuura Kiyokata and Miyahara Akira. Density Measurement of Plasma with a Small Diameter by Microwave Interferometer. Japanese Journal of Applied Physics. 1974., v.13. No.2, p.327-333.

CHAPTER V. PLASMA PARAMETERS OF ELECTRIC DISCHARGES IN THE SUPERSONIC GAS FLOW

§ 1. Macroscopic parameters of the longitudinal and transversal discharges in supersonic airflows

The influence of the following external parameters of the discharge on its parameters has been studied.

- The pressure in the receiver of the compressor (full pressure); it was varied in the range $p_0 = 1$-10 atm.

- The pressure in the vacuum chamber; it was varied in the range $p = 10$ - 500 Torr.

- The discharge electric current; it was varied in the range $I = 50$ m? - 30 A.

- The inter-electrode distance; it was varied in the range $L = 5$ - 20 mm in case of transversal discharge, and $L = 100 – 200$ mm in case of longitudinal discharge.

- The pulse duration; it was varied in the range $t = 2$ - 1000 µs.

1.1. The longitudinal DC discharge in supersonic airflow

Fig.5.1. Longitudinal direct current discharge in supersonic airflow
$p = 40$ Torr, $P = 2$ atm, $I = 2$ A

As very high voltage about tens kilovolts is required for a breakdown of extended ($\sim 10^1$ cm) discharge gap in case of large pressure($\sim 10^2$ Torr), the circuit with an additional electrode was used for creation of the longitudinal discharge.

High-voltage electrode of the discharge and grounded additional electrode were placed in a plane, perpendicular supersonic flow, on a distance about 1 cm. Second grounded electrode of the discharge was placed along a flow on a distance about 10 – 15 cm.

The breakdown happened between a high-voltage electrode of the discharge and grounded additional electrode.

The plasma discharge channel of a transversal DC discharge was swept down by a flow with a speed equal to that of the flow; as a consequence its length grows continuously up to closure of discharge gap.

Appearance of longitudinal direct current discharge in free supersonic airflow is shown in Fig.5.1. The scale of Fig.5.1 is the external diameter of the nozzle, which is equal to 60 mm. Thus the length of the discharge on Fig.5.1 is equal to about 150 mm. A typical view of oscillograms of voltage and current of longitudinal direct current discharge in free supersonic airflow are shown in Fig.5.2-5.3.

It is visible, that in conditions of Fig.5.3 the noticeable oscillations of a discharge current and voltages are observed, whereas in conditions of Fig.5.2 they are small. The difference consists that in conditions Fig.5.3 the lower electrode is displaced rather upper on 5 mm in a direction, perpendicular flow.

Thus, even the small displacement of electrodes in a plane, perpendicular flow, creates a high level of oscillations of parameters of the longitudinal discharge characteristic for the transversal discharges.

Let's mark, that the longitudinal discharge, as it is visible from Fig.5.1, tends to move in area of a circumference of a jet.

Thus, the organization of really longitudinal discharge is possible mainly in conditions of a flow formed in wind tunnel.
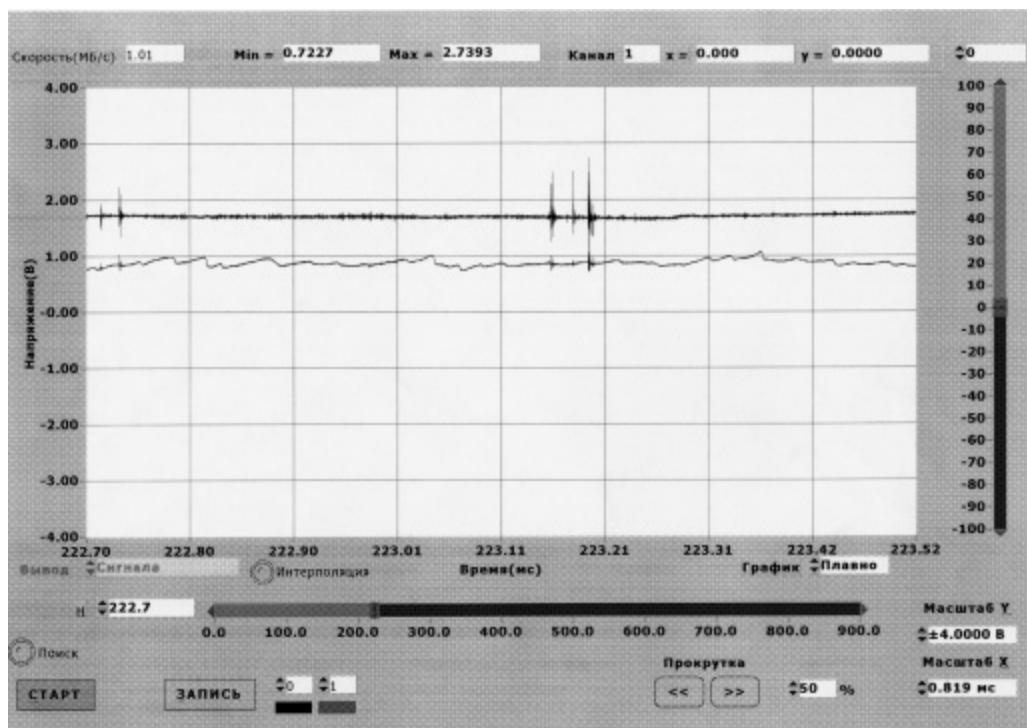
Fig.5.2. Oscillograms of current (upper beam) and voltage (lower beam) of longitudinal DC discharge in supersonic airflow (without displacement of electrodes)
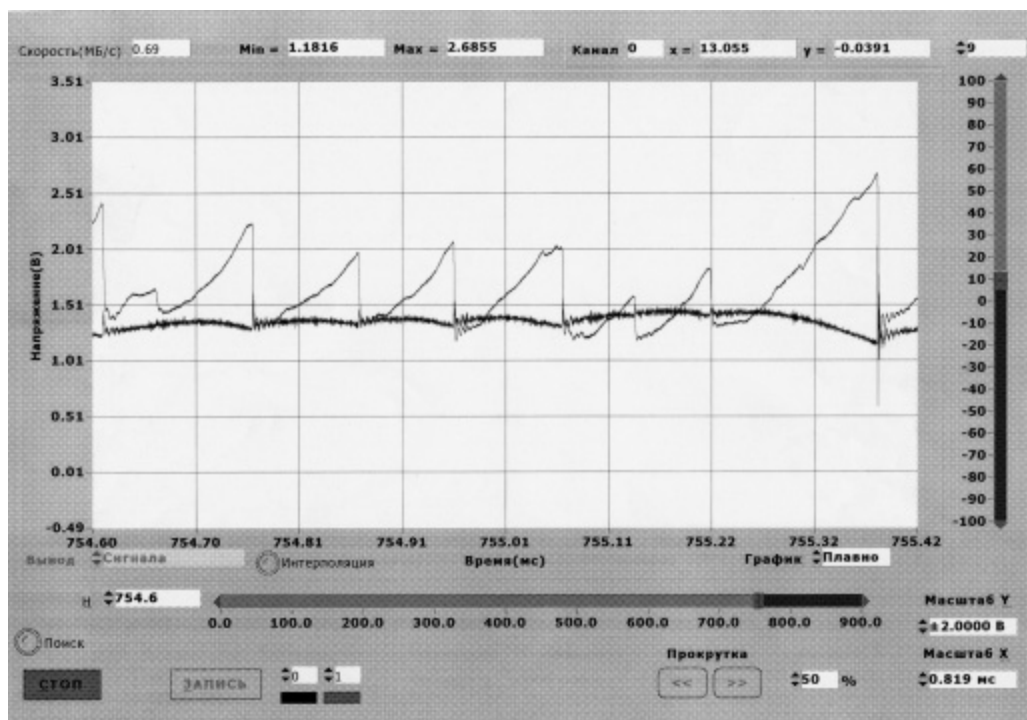
$P = 40$ Torr, $P_0 = 2$ atm.

Fig.5.3. Oscillograms of current (upper beam) and voltage (lower beam) of longitudinal DC discharge in supersonic airflow (with displacement of electrodes)
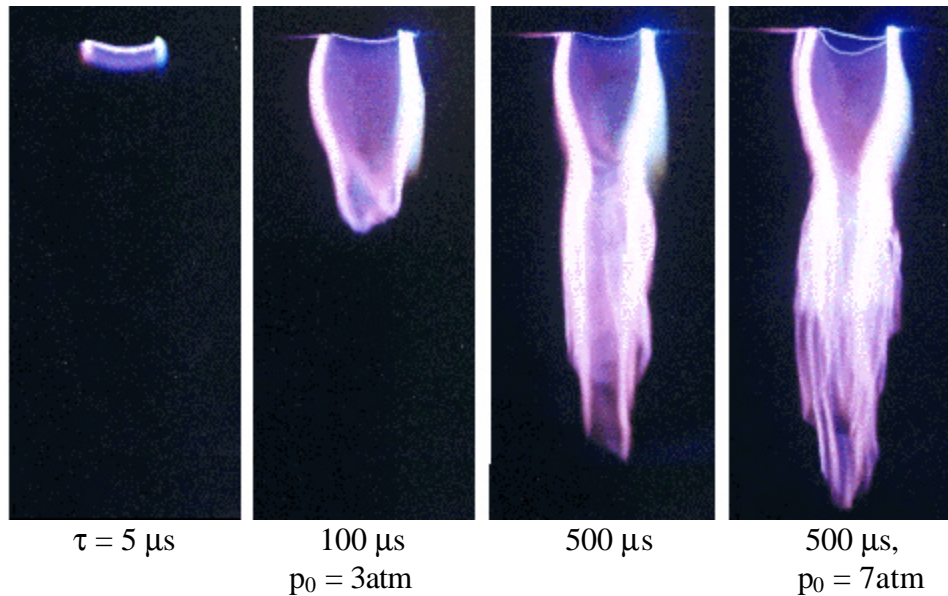
$P = 40$ Torr, $P_0 = 2$ atm.

1.2. The transversal discharges in the supersonic airflow

Typical appearance of the transversal discharge in the supersonic gas flow (Fig. 5.4-5.5) is characterized by the formation of the couple of extended brightly radiating plasma channels, and of less bright zone between them. The channels start on the electrodes, they are positioned in the direction parallel to the flow.

| $\tau = 25\ \mu s$ | 250 μs | 500 μs | DC |
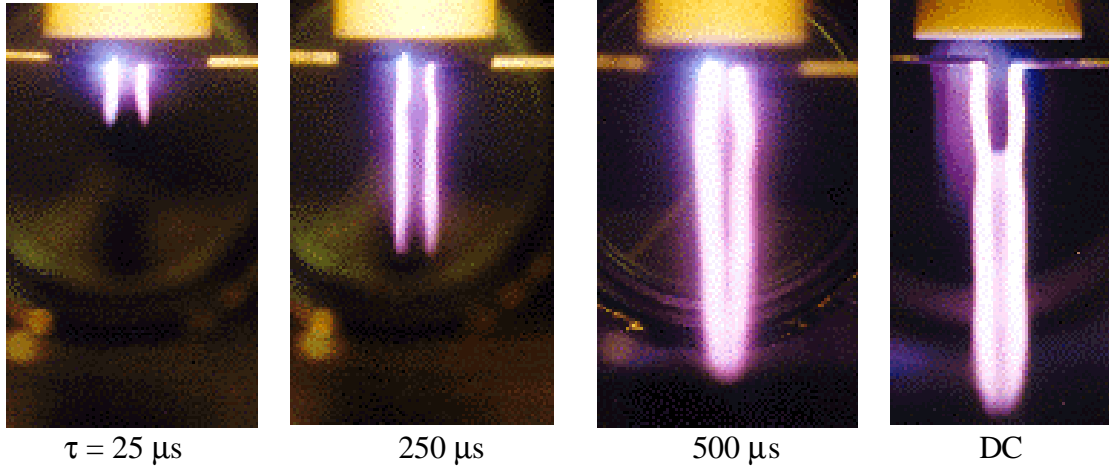
Fig.5.4. Transversal Pulse-Periodical Discharge in the Supersonic Airflow:

$M = 2$, $p_0 = 1$atm, $p = 40$ Torr, L=10 mm, I = 4,5 A, f = 70 Hz

| $\tau = 5\ \mu s$ | 100 μs $p_0 = 3$atm | 500 μs | 500 μs, $p_0 = 7$atm |

Fig.5.5. Transverse Pulse-Periodical Discharge in the Supersonic Airflow:

$p = 40$ Torr, $p_0 = 1$atm, $M = 2$, L=18 mm, I = 18 A, f = 30 Hz

The space structure of plasma channels is determined by the gasdynamics of the flow, i.e. the values of pressures p_0 and p. If the ratio of the pressure at the nozzle exit, p_1, to

a chamber pressure $n = p_1/p$ is close to 1, then smooth and homogeneous channels are observed (Fig.4). In Fig. 5.5 the plasma radiation "highlights" typical picture of the efflux of the under-expanded gas jet with $n \geqslant 2$ is represented. In the latter case at long duration of the pulse the discharge looks as a rule homogeneous only inside the first barrel, the area behind the first barrel looks as a structure with big number of fibers on a time-integrated photo. From the practical point of view it can play a positive role, since the highly developed surface of the discharge could facilitate the ignition of the supersonic stream of air-fuel mixture.

Another difference is connected with the bright thin ($\varnothing < 1$ mm) channel, observed between the electrodes in all the photos of the pulse-periodic discharge of Fig.5.5, whereas in photos of Fig.5.4 of the pulse-periodic discharge it is absent. For the explanation of this fact one should take into account, that the conditions of Fig.5.4 correspond to the magnitude of $p*L \approx 200$ Torr cm, and conditions of Fig.5.5 correspond to $p*L \approx 1000$ Torr cm ($p* \rho\ p\ 300/T$). In the first case the mechanism of the discharge gap breakdown is possibly connected with the formation of the diffuse conducting region. In the second case, the streamer mechanism of the breakdown is possible, as it is observed in the experiment.

The sage of the breakdown channel in the direction of the gas flow is, probably, connected with the existence of rarefaction waves at the electrode edges.

The length of the DC discharge is determined by the values of the flow velocity and the inter-electrode gap separation, which grows with their increase. The effects of a pressure alterations and the ratio n are not so significant. The length in case of pulse periodic discharges also depends on the pulse duration t: the length is in the direct proportion to t for short pulses, i.e. $t < t'$. At $t > t'$ it is equal to those of the DC discharge, the secondary breakdowns are observed between the anode and cathode channels mainly but not between the electrodes. At low values of $?_0$ and $n \gg 1$, the threshold pulse duration t' is about 500 μs (Fig. 5.4). At higher p_0 and n, $t' \approx 300$ μs.

The pulse periodic discharge voltage is practically constant in the absence of a flow (Fig.5.6), while the discharge current is falling slowly. The latter is connected with slow decrease of the modulator's voltage during the pulse. The discharge voltage values are about 100 V at the discharge current values being about few A and more.
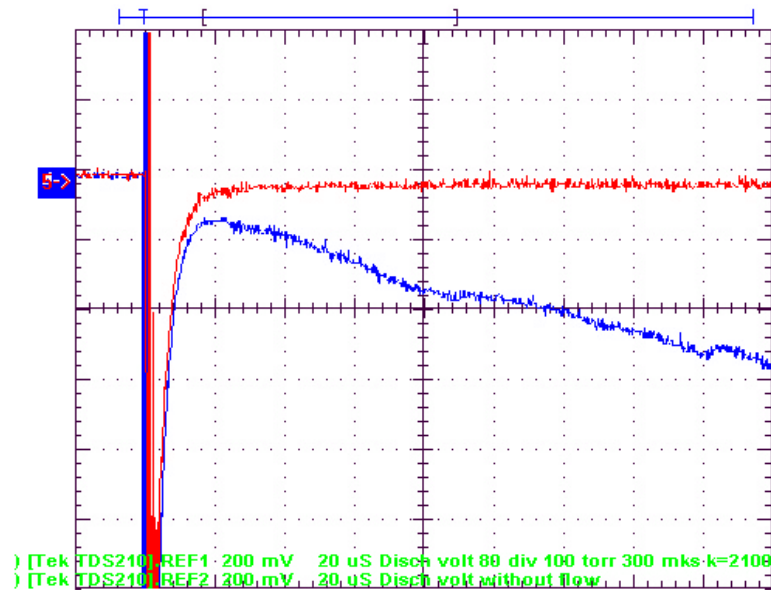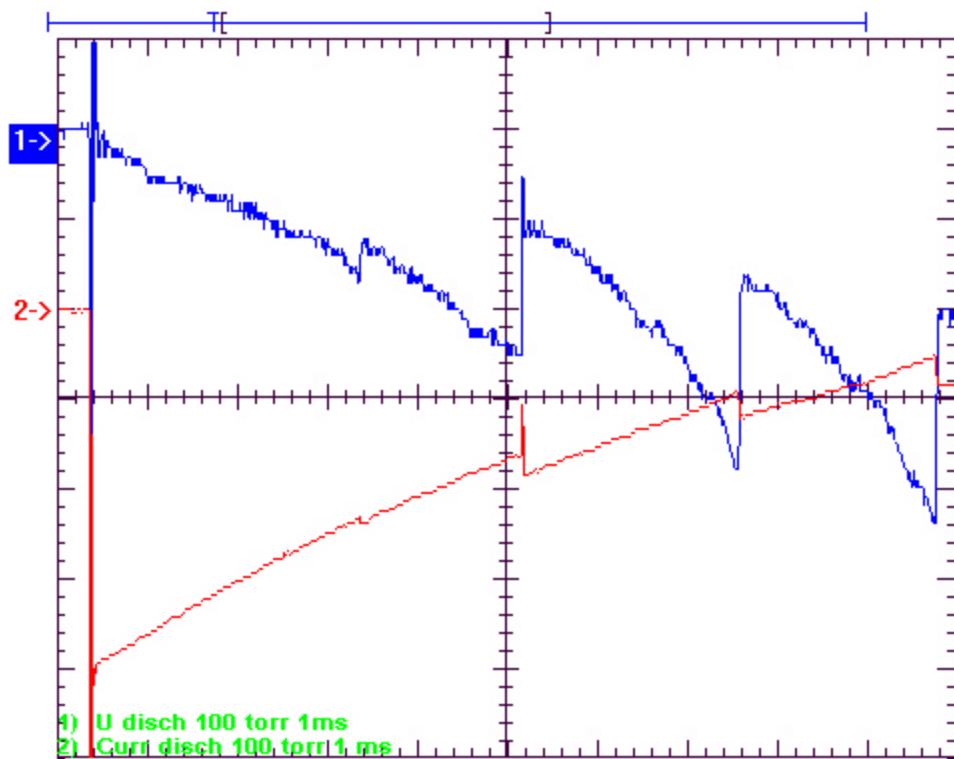

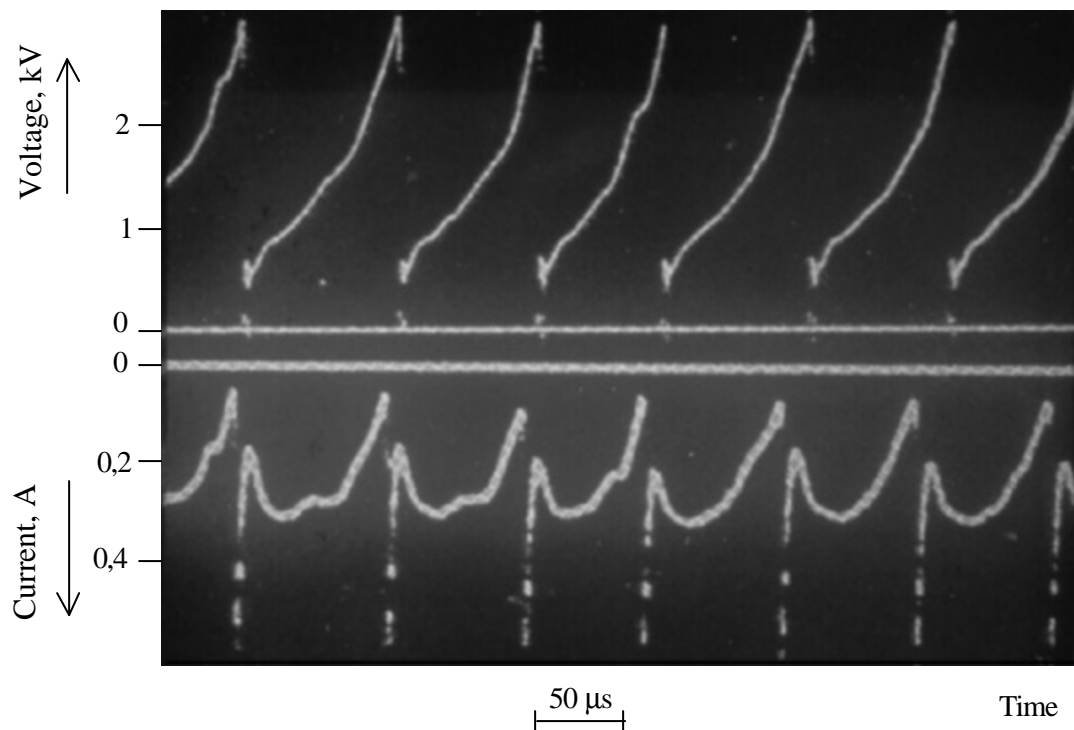**Fig.5.6 Oscillograms of discharge voltage in absence (red line) and with (blue line) supersonic airflow.**
P = 100 Torr, τ = 300 μs, 20 μs/div.

The supersonic airflow changes the situation radically. After the breakdown of inter-electrode gap the discharge voltage goes down to the voltage close to the voltage in the absence of a stream. Further the discharge voltage begins monotonically to grow, whereas the current slowly drops. If the pulse duration is longer than ~300 μs, then fluctuations of the discharge voltage and current appear, their relative amplitude is higher for the discharge voltage and lower for the discharge current (Fig.5.7).

The registrations of the discharge current and voltage wave-form in case of DC discharge (Fig.5.8) have shown, that these curves have a brightly expressed pulsing character with a frequency from 1 up to 50 kHz. The oscillation frequency similarly to case of pulse-periodic discharge depends on external parameters of the discharge.

Fig.5.7. Oscillograms of pulse-periodic discharge current and voltage :
p = 100 Torr, p$_0$ = 2 atm, *t*= 1ms. Scale factors for I - 10 A/div, U - 840 V/div.

**Fig.5.8. Oscillograms of voltage and current of a DC discharge in supersonic airflow.**
P=40 Torr, I=0.25 A, M=2, 50 μs/div.

Quantitative studies have shown that the period of these oscillations depends primarily on the inter-electrode gap size and the discharge current. As the discharge current grows, the relative amplitude of the voltage oscillations falls considerably and approaches the relative amplitude of the current oscillations.

The oscillation period grows with the discharge current. It may mean that two discharge types could be realized in the supersonic flow: at low currents $I < 1$ A the discharge is close to the glow discharge, and at higher currents it could be classified as an arc with the cold cathode.

If $L < 5$ mm, the oscillations degenerate.

The diagrams of oscillations period as functions of interelectrode distance L and value of discharge current I in Fig.5.9(a, b) are given. One can see that the period of oscillations with small currents ($I < 1$A) grows linearly with increase of interelectrode distance practically. The period of oscillations also grows linearly with increase of current at small discharge currents. The growth of oscillations period at the fixed interelectrode interval at currents of order 2 A is slowed down and at currents more than 4 A the curve ?(I) is equal constant. The discharge in supersonic flow at small discharge currents can be qualified as glow discharge and at large currents as arc with the cold cathode probably.
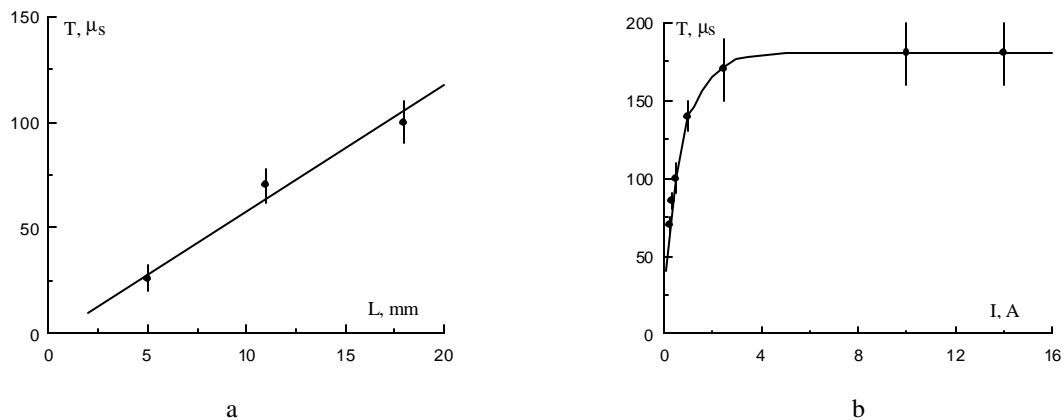

Fig.5.9. Period of oscillations as interelectrode distance L function (a - I = 0,5 A) and discharge current function I (b - L = 10 mm):
$P_{st} = 40$???, $P_r = 2$ atm., M=2

## §2. Microscopic parameters of the transverse discharges in a supersonic gas flow

High-speed photo of transversal gas discharge in supersonic airflow

The typical dynamic of transversal pulsed gas discharge is given in a fig 5.10-11. The exposition time of one photo frame is 32 μsec. In this case the Mach number of a flow is equal ? = 2, discharge current is 20 A, duration of current pulse is 700 μsec. It is visible that as anodi? and cathodic plasma jets have a complex appearance. Short circuit of discharge current takes place in the bottom part basically. Secondary and following breakdowns occur by in a random way in a place where favourably to be breakdown according to Pashen conditions. The secondary breakdown is observed on 352 μsec (Fig.5.10) and 448 μsec (Fig.5.11).
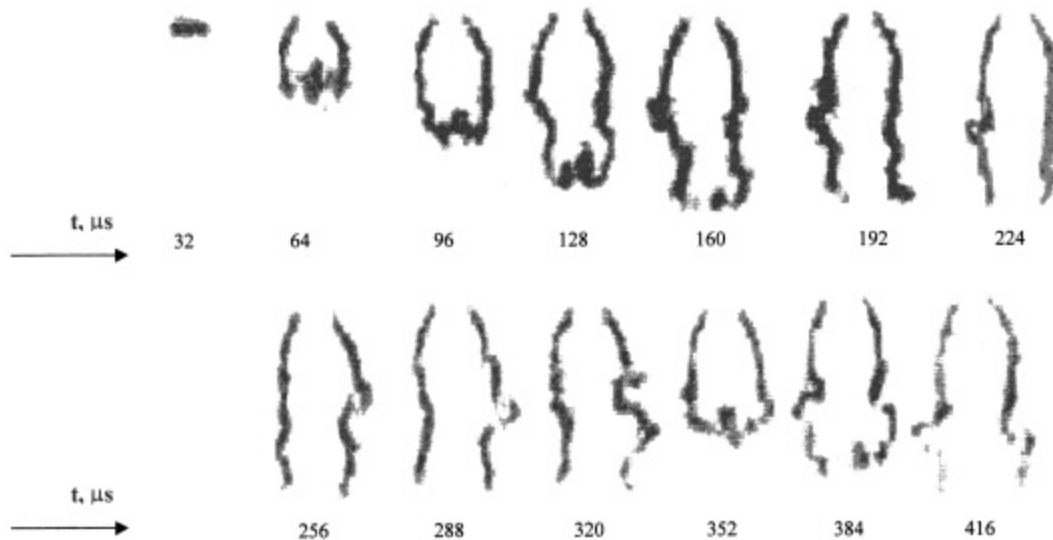
Fig.5.10. Dynamic of transversal gas discharge in supersonic airflow
$\tau = 700$ μs, I = 20 A, p = 200 Torr, $P_0 = 2$ atm, M = 2
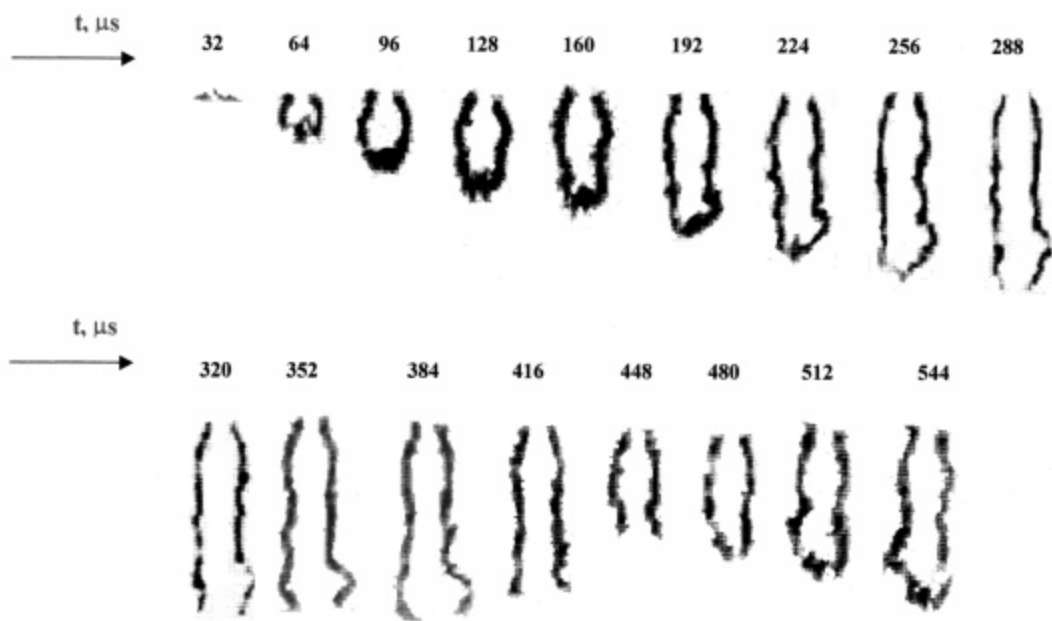
Fig.5.11. Dynamic of transversal gas discharge in supersonic airflow
$\tau = 800$ μs, I = 25 A, p = 100 Torr, P_0 = 2 atm, M = 2
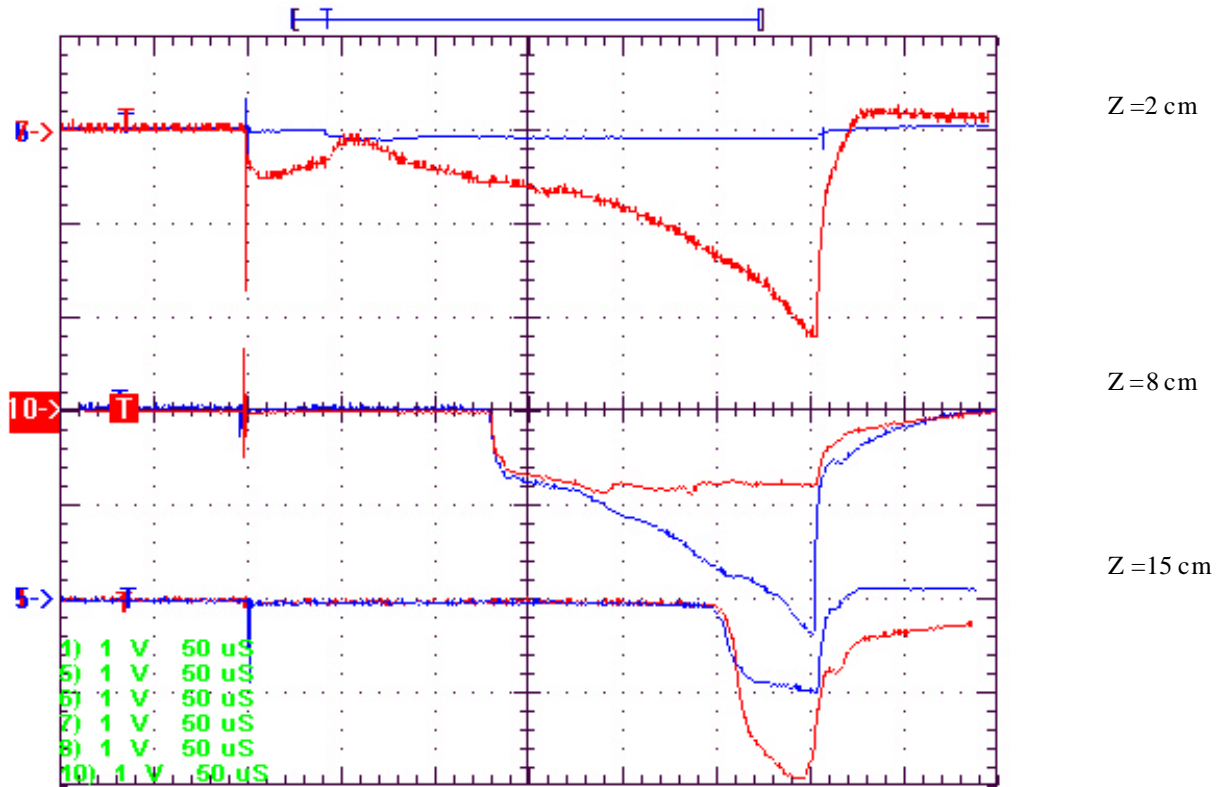
**Fig.5.12. Oscillograms of floating potential
in the anode and cathode parts of pulse - periodic discharge**

Red line - cathode jet, blue line – anode jet.
p = 100 Torr, P_0 = 2 atm, M ≈ 2, L = 12 mm

For the interpretation of obtained high-speed photos we have executed measurements of a temporary dependencies of plasma potential in anode and cathode parts of a pulse-periodic discharge.

The results of the oscilloscoping of the probe floating potential directed transverse the flow in each of the jets for a number of the fixed distances from electrodes along the flow are shown in Fig.5.12. The probe floating potentials are close to plasma space potentials. On the basis of these results we determined the space potential distribution in pulse-periodic discharge (Fig.5.13). So the curves reflect the instant potential distribution in the discharge along the flow in some points of time.

Note that the potential of the fixed area of the anode jet changes in time much weaker than the potential of the cathode jet, so in order not to increase the picture's complexity, we represented by the unique curve the spatially-temporal potential's dependence in the anode discharge part.
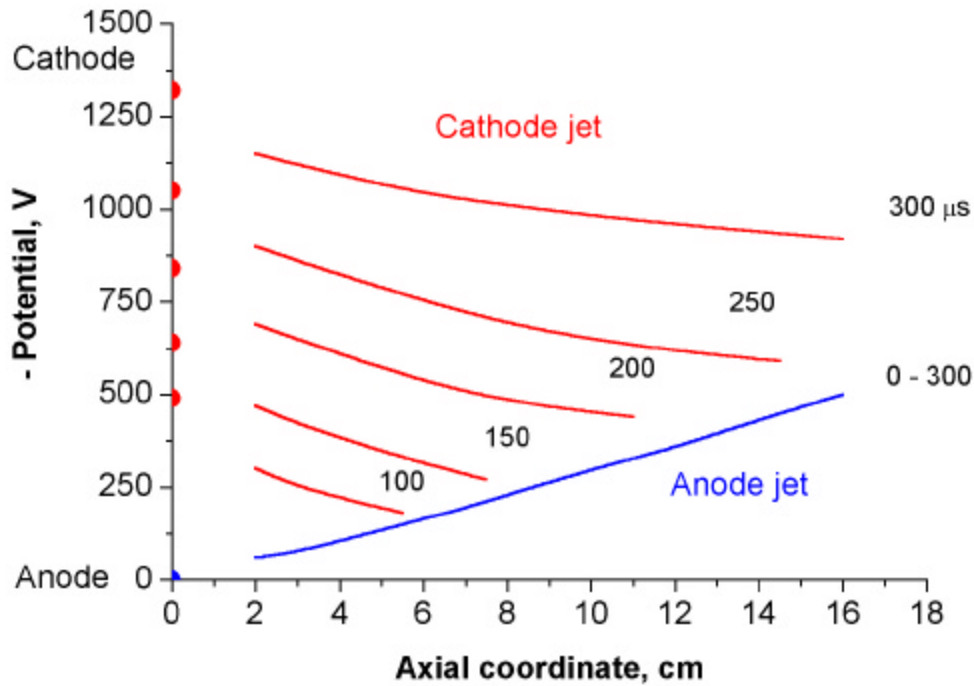
Fig.5.13. Space potential distribution in the anode and the cathode parts of the pulse-periodic discharge.
$p = 100$ Torr, $p_0 = 2$ atm, $I \approx 30$ A.

After the discharge gap breakdown the voltage at electrodes drops to values close to the voltage of the discharge burning in the flow absence. The electric field in the plasma transverse to the flow drops respectively. After the breakdown, in the result of the plasma drift by the supersonic flow, the plasma "traces" begin to form behind the cathode and anode. This leads to the appearance of the longitudinal, in respect to the flow, component of the plasma electric field. Along with the growth of the anode and cathode jet's extent in the whole the voltage on the discharge increases. However the change of the voltage on the discharge is connected not only with this increase.

Longitudinal components of the electric field in the anode and cathode jets are rather weakly differ from each other and do not change strongly in time. So the drops of the potential along each of jets are of the same order of the magnitude in the fixed time moment. At the same time the temporal dependencies of the potential in the anode and cathode parts are principally different. The potential in the anode jet in the fixed

cross section depends on time weakly, at the same time the potential in the cathode part rises quickly in correlation with the voltage at the discharge gap in general. It means that the transverse electric field decreased after the breakdown rises monotonously during the pulse along with the elongation of the discharge. In the result by some time moment appears the potential difference between the cathode and anode jets which leads to the breakdown between them. This process repeats later.

The plasma densities in case of the transversal discharges were measured by three methods. Some results of a comparison of the three diagnostic methods for the DC and the PP discharge plasmas in supersonic airflows are shown in Fig.5.14. The probe and spectral signals are received from an area of one of the discharge channels at a distance z = 30-40 mm from the electrodes, while the MW signal is obtained for z = 40-50 mm.

One can see that the three independent methods yield reasonably close values of the electron density n_e ~10^{13} cm^{-3}. Note that the MW method shows lower, and spectroscopic method - upper limits of n_e. This result confirms a validity of the newly developed probe method.

One can see that the plasma density is proportional to discharge current.
It is significant that the major parameters of plasma - charged particle density and neutral particle temperature - are slowly decreasing along a flow (Fig.5.15 -16).
Gas temperature in anode and cathode parts of the discharge slightly differs on an absolute value. It is interesting, that the dependence of temperature on pulse duration is observed. (Fig.5.17).

The absolute values of gas temperature fast grow with growth of a discharge current in the range of small currents. In case of values of a current about 10 A and more this growth is decelerated (Fig.5.18).
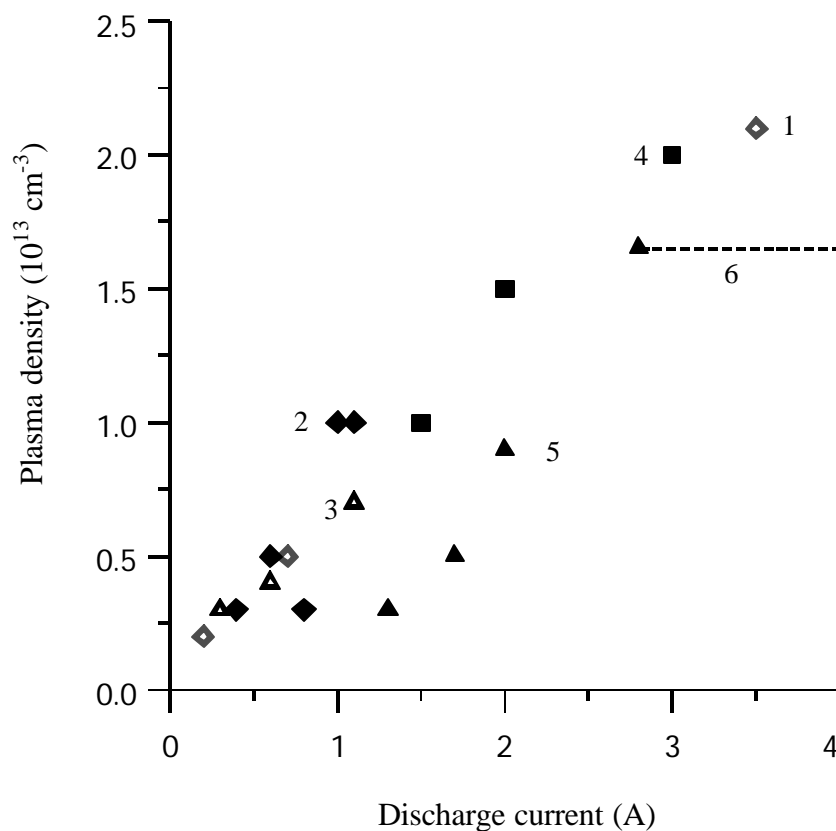
**Fig.5.14. Electron density measured by different methods over the discharge current at p=40 Torr.**

Macroscopic parameters: $p = 40$ Torr, $P = 1$ atm, $M \approx 2$, $L = 10$ mm.

1 - probe $R = 0.2$ mm; 2 - probe $R = 0.5$ mm; 3 - microwave interferometer; 4 - spectral method; 5 - microwave interferometer in the pulsed periodic discharge; 6 – the cutoff level.
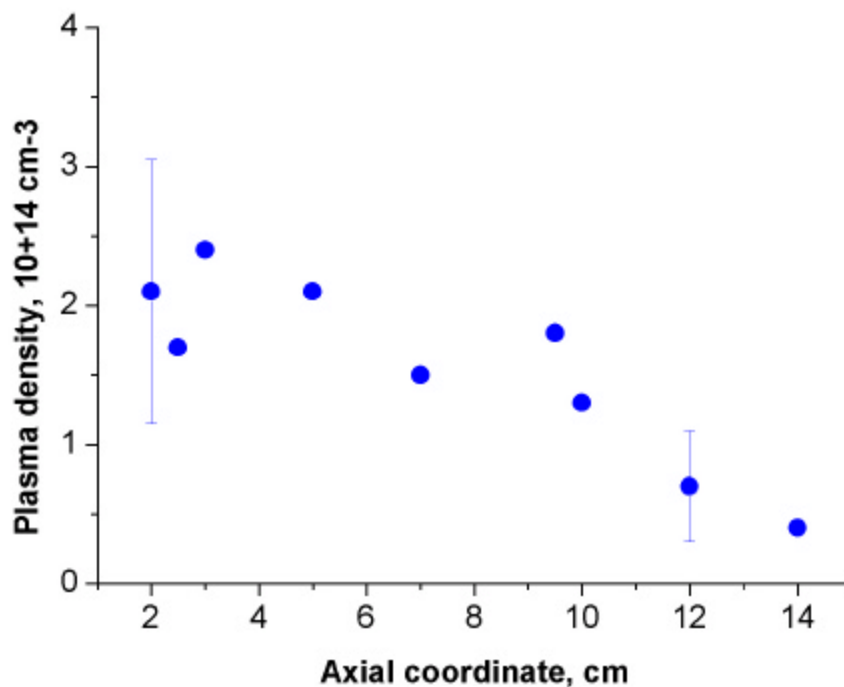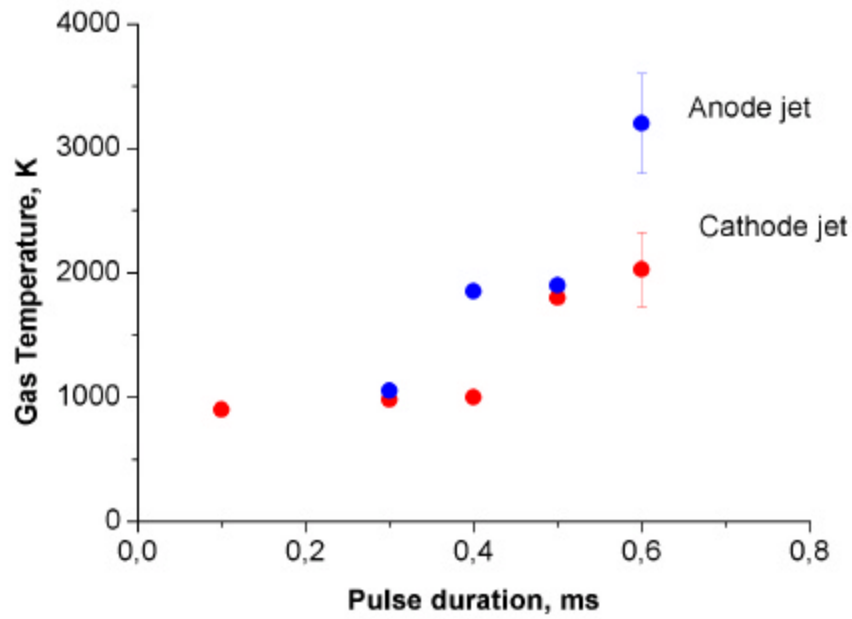
Fig.5.15. Ion density distribution along the axis of flow

Transversal pulse-periodic discharge in supersonic airflow. p = 100 Torr,
P = 2 atm, M ≈ 2, L =12 mm.
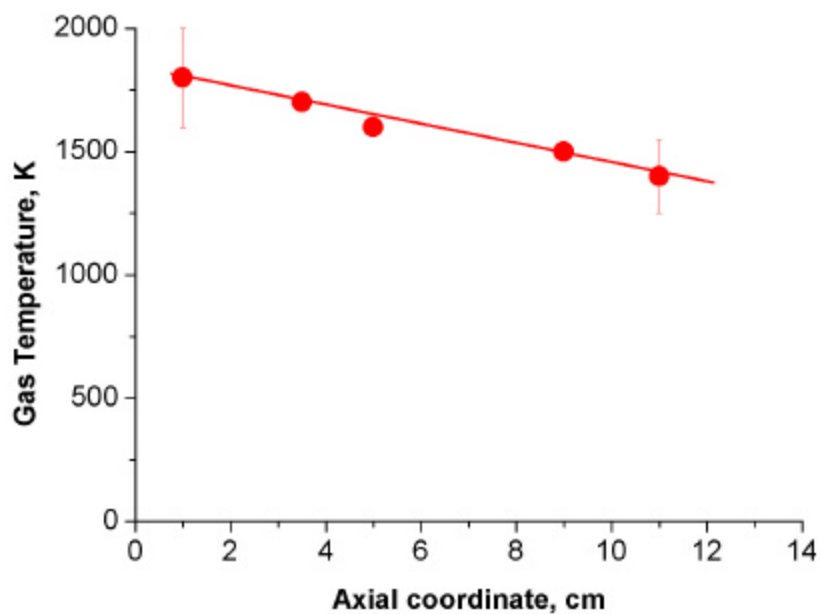
Fig.5.16. Gas temperature distribution along the axis of flow
DC discharge in supersonic airflow. p = 40 Torr, P = 1 atm, M ≈ 2, L =10 mm.

Fig. 5.17. Gas temperature as a function of pulse duration

Transversal Pulse-Periodic Discharge in Supersonic Airflow.

Distance from the electrodes z = 1 cm p = 100 Torr, P = 2 atm, M ≈ 2, L = 12 mm
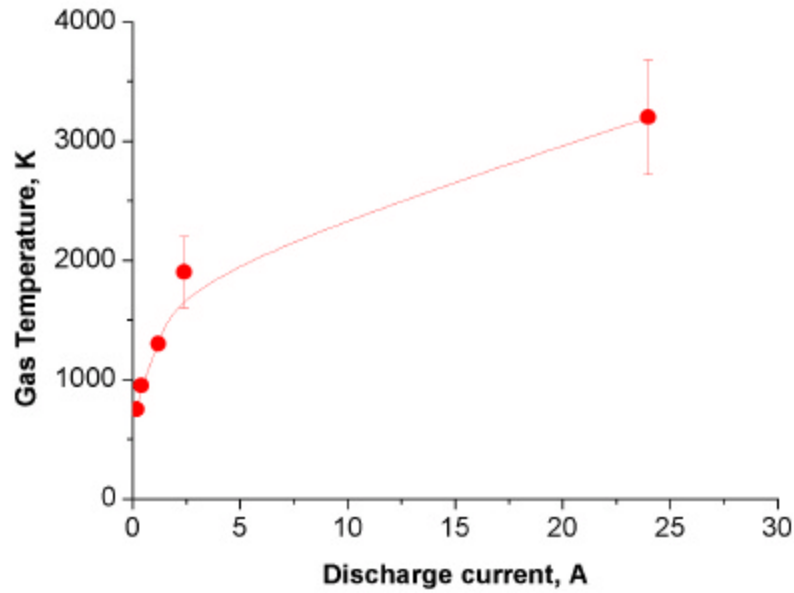
Fig.5.18. Gas temperature as a function of pulse duration

Transversal Pulse-Periodic Discharge in Supersonic Airflow.

Distance from the electrodes z = 1 cm. p = 100 Torr, P = 2 atm, M ≈ 2, L = 12 mm

Thus, transversal electric discharges in the supersonic airflow are characterized by the forming of areas near electrodes in which the fast heat and ionization of originally cold and dense gas occurs. The extended plasma behind these areas represents a medium with small variation of characteristic plasma parameters– *?/N*, n_e/N, *?*$_g$.

This approach allowed us to propose the physical model of the transverse DC discharge in the supersonic gas flow.

§3. The physical model of the electrode transversal gas discharge in supersonic flows

3.1. Introduction

The geometry used for discharge numerical modeling is given in a fig.5.19. The discharge forms between two electrodes (cathode C and anode A). The neutral gas stream moves along an axis OX.
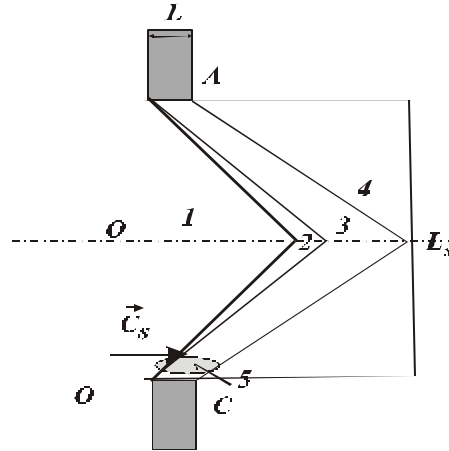
Fig.5.19. Structure of discharge in a crossed gas flow.

A – Anode, C – Cathode, 1 – Neutral gas area, (2 – 4) - area filled by plasma, 2 – cathode and anode ionization fronts, 3 – area supporting electric current (qualitatively), 4 – decaying plasma, 5 – cathode layer area, where the ions drift velocity exceeds gas flow rate.

The main problems of discharge model in a supersonic gas stream are connected with a diversity of ionization transfer types in space causing the motion of discharge towards to a flow. At low pressures (< 30 Torr) this transfer can be connected with

1. Drift of charged particles in an electrical field,
2. Ambipolar diffusion,
3. Free electron diffusion,
4. Transfer of radiation (photo ionization of gas before front, Penning ionization caused by a resonance emission, etc.).

At high pressures equilibrium discharge the transfer is connected with thermal conductivity, and the heat conduction can be caused by the neutrals, electrons, or radiation, depending on discharge degree of ionization.

At intermediate pressures, the rise of pressure leads to overheating instability, when the discharge development is connected with growth of frequency of ionization at

reduction density of the neutrals. The neutrals density falling is caused by heavy components heating and subsequent pressure equalization with ambient gas. Thus, the electrons temperature essentially exceeds temperature of heavy components. In this case, the gas warm-up can be connected with

1. Heat conduction of neutrals,

2. Diffusive or photoionizating electrons offset from heated high-ionized gas area with weakly ionized "preplasma" creation. Electric field heats the caused "preplasma" electrons with the subsequent thermal energy transmission from electrons to the neutrals. The neutrals warm-up leads to further falling of their density in new area of space.

3.2 Discharge mathematical model and equations

In the elementary discharge model considered below, we shall keep only one type of ionization transfer (ambipolar diffusion) and at the analysis current distribution in space, we shall consider plasma quasi-neutral. The deviations from quasi-neutrality are essential near to boundary of plasma and will be taken into account as appropriate boundary conditions. We shall neglect heating of the neutrals. The photo ionization does not play an essential role in maintenance anodic and cathode ionization fronts, because high energy photons, emitted by plasma, are absorbed by electrodes, or result in occur appearance of photoelectrons far from front, bearing to new non-steady third fronts of ionization.

The equations set for quasineutral discharge area can be obtained from double-fluid hydrodynamics for electrons and ions, and Maxwell equations. We consider, that the electrons n_e and ions n_+ densities are equal $n_e = n_+ = n$, that means a series development on small parameter $h = r_{De}/L$, where r_{De} – Debye length, L – the characteristic size of plasma inhomogeneity.

The set of equations, used in calculations, looks like.

$$\frac{\partial n}{\partial t} + div(n\vec{C}_S) - \vec{\nabla}D_a\vec{\nabla}n = F \tag{1}$$

$$\vec{E} = -\frac{D_e - D_+}{m_e + m_+}\vec{\nabla}\ln(n) + \frac{\vec{G}}{(m_e + m_+)n} \tag{2}$$

$$\vec{G}_e = n\vec{V}_e = n\vec{C}_S - D_a\vec{\nabla}n - \frac{m_e\vec{G}}{(m_e + m_+)} \tag{3}$$

$$\vec{G}_+ n\vec{V}_+ = n\vec{C}_S - D_a \vec{\nabla} n + \frac{m_+ \vec{G}}{(m_e + m_+)} \qquad (4)$$

In (1) – (4) and below we use denotations: V_e, V_+, C_S – speeds of electrons, ions and neutrals, m_e, m_+ – mobility of electrons and ions, D_e, D_i - coefficients of a free electron and ion diffusion, e - elementary electric charge, E - electric field strength in plasma, F - expression for sources of electron and ions, which are taking into account that they are born by pairs only, j - current density in plasma. The addends, containing C_S, take into account motion of a gas stream concerning electrodes resulting in to ions and electrons drift downstream. In the formulas (1) the denotation for an ambipolar diffusion coefficient

$$D_a = \frac{n_e D_+ + n_+ D_e}{m_e + m_+}$$

is entered. The standard expression for F is

$$F = n_i n_e - a n_e n_+ - b n_e^2 n_+ \qquad (5)$$

The expression (5) takes into consideration a straight-line ionization by electronic impact (n_i – frequency of ionization), and two and three - partial recombination (a and b – recombination coefficients). Frequency of ionization and the frequencies of a recombination are functions of temperature of electrons.[1] At pressure of the neutrals 30 Torr and above elastic energy losses of electrons predominate, and the character size of a non-uniformity is higher than character distance of heat transfer $l_{Te} = l_e (M/2m)^{1/2}$, where m and M – electronic and ion mass, l_e - the free length of an electron, therefore in the elementary models of discharge is possible to consider the temperature of electrons T_e to be a local function of an electrical field E in the given point of space. To determine this function we use electron density balance equation. This equation accounts energy transfer from electric current to electrons, energy transfer from electrons to neutral particles (elastic ant nonelastic collision) and loss of energy, expended to electric ambipolar field creation. At a record (3) and (4) we have limited by sluggish processes with reference frequencies less then collision frequency an ion the neutral. It is possible, because the character time of electrons density change is determined by ionization frequency and usually on some order below.

---

[1] On can use the model relation $n_i = n_{i0} (T_e / T_{e0})^{e_I/T_{e0}}$, [4].

Maxwell equation yields

$$\vec{G} = rot\vec{A} \tag{6}$$

$$rot\left(\frac{1}{(m_e + m_+)n} rot\vec{A}\right) = 0 \tag{7}$$

where A – vector potential of an electric current (it is proportional to a magnetic field, created by a current).

In the field of photo ionization (1 - in a fig.19) it was supposed, that the photoelectrons disappear due to attachment and consequently do not play any roles in discharge propagation. This requirement is possible so long as a field between the cathode and anode less breakdown one. At the solution of equation (1) in this area, we use a relation $F(\vec{r}) = -n_a n < 0$. Thus, numerical model could not describe processes of a secondary breakdown of a discharge gap.

Equations (1) and (7) should be supplemented by boundary conditions. The different views of boundary conditions can be obtained by integration a Poisson equation both dynamical equations and particles chemical kinetics equations on a surface. Hereinafter we shall consider boundary conditions at a plasma contact to a rigid body, which one can be dielectric or conductive.

1. Requirement of normal current density persistence on a cathode and anode surface.

$$\vec{j}_n = e\vec{G}_n = e\lfloor rot\vec{A}\rfloor_n = j_0 \tag{8}$$

2. Assumption of ions current absence on the anode

$$\vec{G}_{+n} = 0 \tag{9}$$

3. The part of electric current, transferred by electrons on the cathode is given [5]

$$\vec{G}_{en} = g\, j_0/e \tag{10}$$

The set of equations (1-10) was solved in rectangular area $O < x < L_x, O < y < L_y$. The cathode and anode placed on boundary of computation area. The requirements of a current absence through boundary and requirement of plasma density symmetry concerning boundary were set on a remaining part of boundary
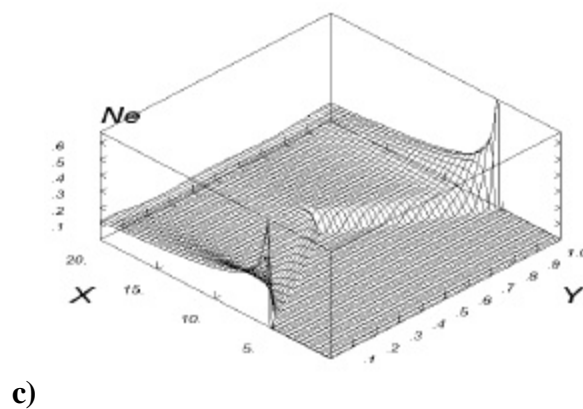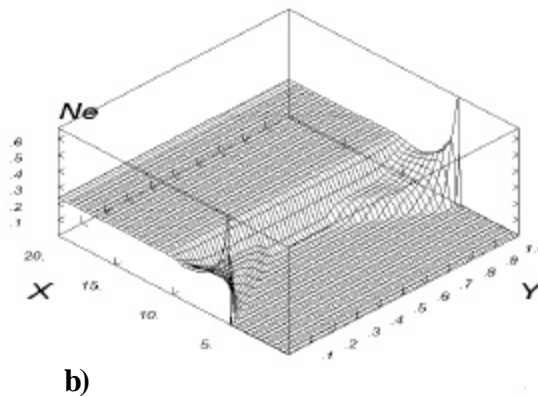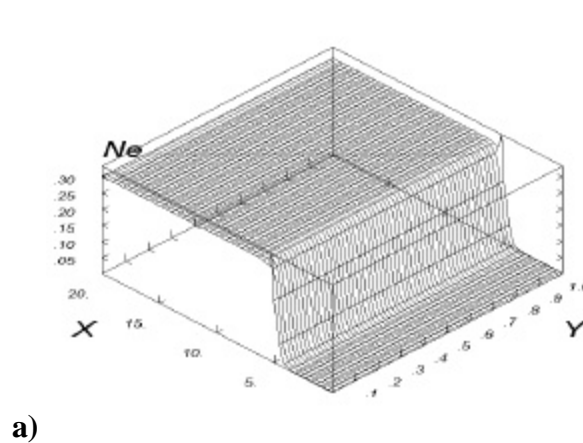
$$\vec{j}_n = e\vec{G}_n = e\lfloor rot\vec{A}\rfloor_n = 0 \tag{11}$$

$$\lfloor \vec{\nabla}n\rfloor_n = 0 \tag{12}$$

3.3 Computational results.

The numerical calculation has shown:

1. At the identical geometry and neutral gas environmental conditions, the same discharge state will be realized, despite arbitrary initial plasma density (Fig. 20).


a)

b)

c)

Fig. 5.20. Temporary discharge, maintained by the current $J = 1$ A/cm, evolution. Cathode length – 1 cm. X and Y - actual discharge sizes in cm, neutral gas flow rate 50000 cm/s, Ne - charged particles density in 10^{14} cm^{-3}.

The calculation corresponds to neutrals pressure 200 $Torr$.

The figures $a), b), c)$ correspond to time value $t = 6, 225, 500$ нs

2. The cathode and anodic ionization fronts represent not separate areas near to the cathode and anode, but also all boundaries between plasma and no ionized area lying upwards on neutral gas fluxion.

3. The current in plasma flows past on a narrow bandwidth by the size about electrode separation adjoining to front ionization. (Fig. 5.21).
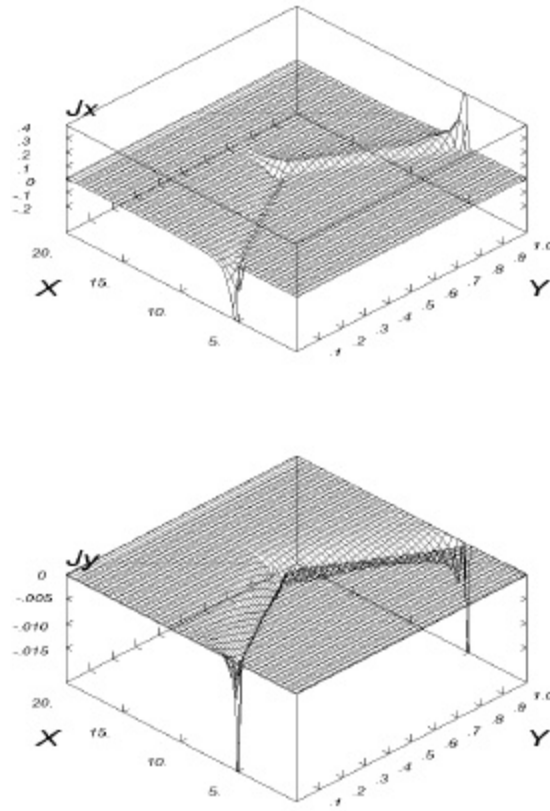
Fig. 5.21. Direct current density J distribution (relative units).

The figures correspond to fig. 5.20d)

4. The maximum ionization happens near to electrodes, where the current density has maximum too. As the current weep path between the cathode and anode has the least value near to ionization front, in any plasma cross-sections, parallel to axis 0X, an electrical field, tangential to ionization front surface, has maximum value near front. An electrical field, normal to front is generated by plasma non-uniformity and has maximum at plasma boundary. Thus, in any plasma cross-section lengthwise axis 0X the ionization frequency has maximum value at plasma boundary. This current stipulates a heating of electrons and ionization as at the front and near to plasma boundary.

5. Sharp boundary (by the size of the order $\sqrt{D_a/\mathbf{n}_i}$) between space area held by plasma and free from it (so-called front of ionization) is formed. The conducted analysis yields, that boundary between plasma and not ionized gas behavior is subject to an equation similar to Kolmogorov–Petrovsky–Piskunov equation [6].

6. As the diffusive ionization front speed is perpendicular to its surfaces and is peer $V = 2\sqrt{D_a/\mathbf{n}_i}$ and the front simultaneously communicates downstream with flow rate of the neutrals C_s, that the angle α_0 between front and a flow rate direction can be used for an of ionization frequency estimation on plasma boundary

$$\sin(\mathbf{a}_0) = V/C_s = 2\sqrt{D_a\mathbf{n}_i}/C_s \qquad (13)$$

Equation (14) yields

$$\mathbf{n}_i = C_s^2 \sin^2 \mathbf{a}_0 / 4D_a \qquad (14)$$

Thus, the ionization tracks both cathode, and anode represents a wedge (in flat geometry), and the angle between tangent to ionization front boundary and neutral hydrodynamic flow rate is determined by the formula (13). Behind ionization front, plasma density is great enough and the recombination processes can be essential. Thus, it is possible to expect, that in this area the balance of particles can be local, and the diffusion processes are incidental. It means that the set of equations behind front can be abbreviated for neglecting transfer processes in plasma.

In area behind plasma forward boundary the role of diffusion is small and we can use Raizer and Paschenko [6] analysis for discharge description, supplementing it by relation between plasma cross-sectional area on which one the current flows past and longitudinal coordinate (See equation (13)). Ionization frequency and longitudinal electric field in (13)–(14) (far from electrodes, in flowing plasma) is determined by local particle balance equation.

$$n_e(\mathbf{n}_i(E_C) - \mathbf{a}(E_C)n_+) = 0, \qquad (15)$$

However, since the gas flow is perpendicular to a straight line connecting the cathode and anode (transversal discharge in a gas stream, fig. 19), a positive column has a point, where its boundary is perpendicular to flow velocity, and charged particles drift is also perpendicular to a flow, therefore both electrons, and ions will move downstream at any speed of neutral gas. That completely corresponds) to outcomes of the numerical score (see fig. 5.20 and 5.21).

Thus, in absence of the transfer processes, the transversal d.c. discharge is always «supercritical». Therefore, we have the transitions from «up to stream» to «over stream» charged particles drift velocities towards to a flow near each electrode.

To obtain real space form of transversal discharge one have to take into account transfer properties (ambipolar diffusion coefficient in our case).

Experiments described earlier shows that discharge in transversal gas flow is periodic (not stationary), as it predicted by numerical results. Apparently, it is connected with electric field growth between cathode and anode when plasma moves downstream, before the steady state is achieved. After the sufficient Voltage between cathode and anode is achieved, the breakdown is watched. The model of this breakdown must take into consideration gas photo ionization and capability of current closing between the cathode and anode by displacement current. As the angle between a plasma surface and flow rate after a breakdown exceeds α_0, that the part of plasma removed from electrodes starts to communicate downstream and steady front begin to forms according to numerical results. Then the fixed front formation process is again interrupted by a new breakdown, and thus discharge passes in the periodic form.

For building-up alternating discharge theory it is necessary to view not only strongly ionized area, but also the weakly ionized plasma area.

In the whole requirement of embodying of the different shapes of discharge in a cross flow of gas can be formulated as the Table I.

Presence of the different kinds of an alternating discharge (arc and diffuse) at different rates of flow marked in [1], can be explained by change of the discharge propagation mechanism towards to a stream. At low speeds (strong heating of gas, feeble fields in a positive column) - it may be the mechanism connected with heat conductivity, at major - (feeble heating of gas, diffusive discharge) it may be mechanism circumscribed in the present work.

Table I

<table>
<tr><td colspan="4" align="center">**The direct current discharge in transversal gas flow**
Classifications</td></tr>
<tr>
<td rowspan="5" align="center">**Subcritical discharge similar to discharge without transversal flow**
$C_S < V_f \approx 2\sqrt{D_a n_i}$</td>
<td colspan="3">Supercritical discharge as two sphenoid ionization tracks behind the cathode and anode

$C_S > V_f \approx 2\sqrt{D_a n_i}$ $\sin a \approx V_f / C_S$</td>
</tr>
<tr>
<td colspan="2">Stationary discharge</td>
<td>Alternating discharge</td>
</tr>
<tr>
<td colspan="2">$\dfrac{U_{steady}}{U_{break}} < \sin a \approx \dfrac{V_f}{C_S}$</td>
<td>$\dfrac{U_{steady}}{U_{break}} > \sin a \approx \dfrac{V_f}{C_S}$</td>
</tr>
<tr>
<td colspan="2">The anodic positive column</td>
<td>The cathode positive column</td>
</tr>
<tr>
<td colspan="2">Always subcritical (in Raizer and Paschenko sense [6])</td>
<td>Subcritical if $C_S \cos a < u_+$</td>
<td>Supercritical, if $C_S \cos a > u_+$</td>
</tr>
</table>

§4. Numerical simulation of inviscid supersonic flow over an electric discharge region

Numerical simulation of a supersonic flow over an electric discharge region is carrying out for inviscid formulation. The energy supply is interpreted as an energy source of predetermined intensity. Previously such approach was used for the computation of an action of local energy sources on the flow over different bodies [11, 12]. In present paper the possibility of organization of appropriate conditions for the supersonic air-fuel mixture ignition is investigated. Correspondingly the obtaining of high temperature in the wake and new principles of deceleration of the supersonic flow are a subject of particular interest.

The non-steady motion with a distributed energy supply is described in cylindrical coordinates r, z by Euler equations:

$$\frac{\partial}{\partial t}\begin{pmatrix} r \\ ru \\ rv \\ e \end{pmatrix} + \frac{\partial}{\partial r}\begin{pmatrix} ru \\ p+ru^2 \\ ruv \\ (e+p)u \end{pmatrix} + \frac{\partial}{\partial z}\begin{pmatrix} rv \\ ruv \\ p+rv^2 \\ (e+p)v \end{pmatrix} = = \frac{1}{r}\begin{pmatrix} -ru \\ -ru^2 \\ -ruv \\ -(e+p)u \end{pmatrix} + \begin{pmatrix} 0 \\ 0 \\ 0 \\ r\dot{Q} \end{pmatrix}$$

The total energy of a volume unit is determined for an ideal perfect gas by an equation of state:

$$e = \frac{p}{g-1} + \frac{r}{2}\left(u^2 + v^2\right)$$

The energy supply density (to a mass unit per time unit) is assumed to be the predetermined function of coordinates and time:

$$\dot{Q}(r,z,t) = Q_0 f(t)\exp\left(-\left(\frac{r}{\Delta r}\right)^2 - \left(\frac{z-z_0}{\Delta z}\right)^2\right)$$

The supersonic stream in actual experiment is formed as a result of an outflow throw the nozzle from an open space into the low-pressure chamber. For numerical computations the flow is assumed to be "unbounded", that is effects of a real stream are neglected. Undisturbed flow parameters p_1, T_1 (initial data for numerical approach) are determined by a given Mach number M_1 on a nozzle outlet and critical stagnation parameters p_0, T_0 in the open space.

$$\frac{p_0}{p_1} = \left(1 + \frac{g-1}{2}M_1^2\right)^{\frac{g}{g-1}}, \quad \frac{T_0}{T_1} = 1 + \frac{g-1}{2}M_1^2$$

For all computations: $g = 1.4$, $M_1 = 2$, $p_0 = 101320 \text{N/m}^2$, $T_0 = 300$ K. Density is determined by an equation of state: $r = p/RT$, where $R = R_0/m$, $R_0 = 8314.32$ J/(Kkmol) – universal gas constant, $m = 28.964420$ kg/kmol – molecular mass of an air. Thus: $r_0 = 1.176 \text{kg/m}^3$, $p_1 = 12950 \text{N/m}^2$, $T_1 = 166.7$K, $r_1 = 0.270 \text{kg/m}^3$. The procedure of reduction of formulation to the dimensionless form using p_0, r_0 and typical length $l_0 = 10^{-2}$ m was applied. Pressure is measured by p_0, density – by r_0, velocity – by $\sqrt{p_0/r_0}$, distances – by l_0, time – by $l_0/\sqrt{p_0/r_0}$. Parameter Q_0 is measured by $(p_0/r_0)^{3/2}/l_0$ and characterized the energy source intensity. The total power input $W(t)$ depends on the complete task solution and can be calculated during the computation process.

$$W(t) = \left(\int_V r \dot{Q} dV \right) p_0 l_0^2 \sqrt{\frac{p_0}{r_0}} \quad \text{(Watt)}$$

When similarity conditions (by g, M_1, Q_0) are fulfilled the same numerical decision can be applied. Formula for $W(t)$ shows, that under the decreasing of energy source size (that is equivalent to l_0 decreasing) the same parameters, in particular temperature, can be obtained for a narrow wake with indefinitely small energy input.

An action of a steady energy supply on the supersonic flow structure can be estimated by comparison of different energy sources of the same cross size $\Delta r = 0.15$:

$(1) - \Delta z = 0.15$, $Q_0 = 40$, power $W = 475$ Watt

$(2) - \Delta z = 0.15$, $Q_0 = 100$, power $W = 913$ Watt

$(3) - \Delta z = 0.15$, $Q_0 = 200$, power $W = 1340$ Watt
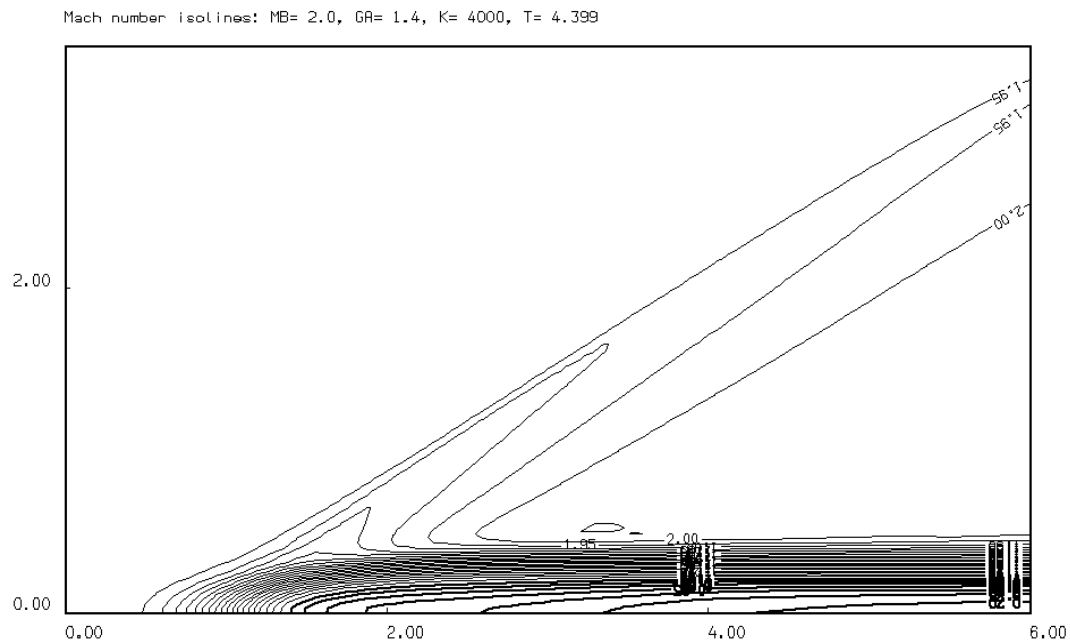
$(4) - \Delta z = 0.75$, $Q_0 = 40$, power $W = 828$ Watt

Intensities Q_0 for spherical (3) and ellipsoidal (4) energy sources were selected so that $Q_0 \Delta z = \text{const}$. The computed steady power input W for ellipsoidal (4) energy source is even smaller than for spherical one (2).

For the steady flow over energy sources the infinite high temperature wake with a cross size determined by the energy source cross size is formed. Parameter $\Delta r = 0.15$ was selected in such a way that the wake cross size had to be equal to the experimentally observed value 0.25. The remote wake cross profiles are conservative

in z direction since the absence of the dissipation for inviscid flows. The wake is characterized by decreased values of density, total pressure, Mach numbers and increased velocity. The static pressure increase locally in the source center vicinity and for the remote wake is practically equal to the ambient flow pressure.

Mach number isolines: MB= 2.0, GA= 1.4, K= 8000, T= 6.513
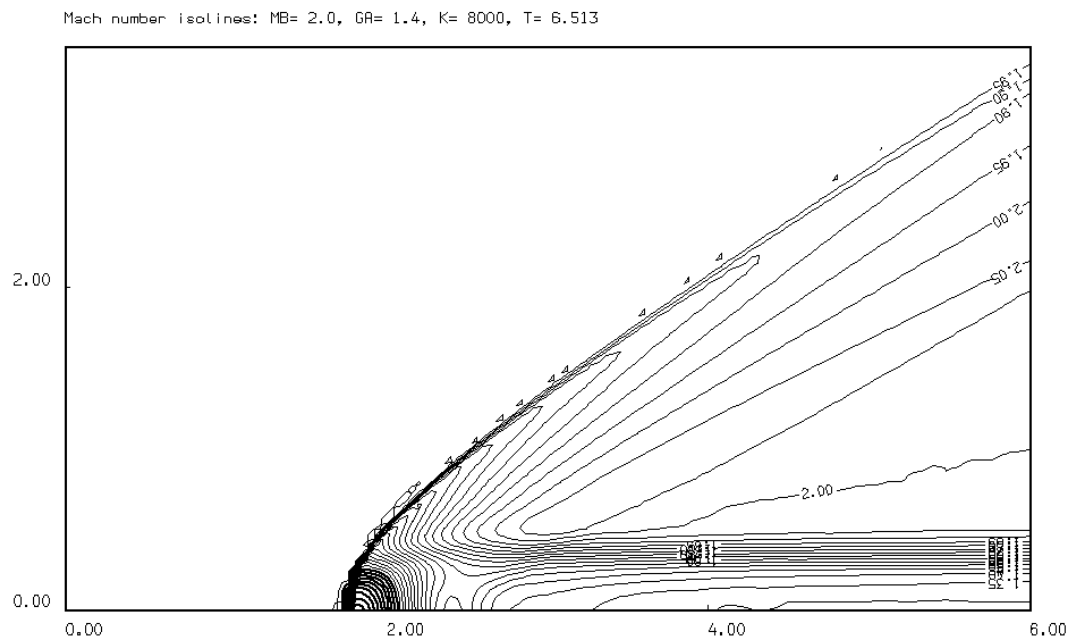
a) regime with a local subsonic region (3)

Mach number isolines: MB= 2.0, GA= 1.4, K= 4000, T= 4.399

b) regime with infinite subsonic trace (4)

Fig.5.22 Steady regimes of flows over energy sources (Mach number isolines).

Flow pictures and distributions of different parameters in longitudinal and cross directions for computations (1)–(4) are presented in Figures 5.22-5.26. For spherical energy sources of high power (1)–(3) existence of a local subsonic region (remote wake is supersonic) and a bow shock wake are typical (Fig.5.22a). For "equivalent" (by $Q_0\Delta z$) ellipsoidal energy source (4) the continuous deceleration of the flow down to a subsonic speed is taking place (Fig.5.22b). The infinite subsonic wake and hanging shock wave are formed in this case.

Mach number distribution (Fig.5.23) demonstrates the effect of "saturation of the flow with energy", previously observed in [12]. At conservation of the spherical shape of the energy source (curves 1–3) it is impossible to decrease the Mach number in the remote wake by increasing the energy source intensity Q_0. For ellipsoidal energy sources the restrictions of this effect can be negotiated – the subsonic remote wake is formed. It is necessary to underline qualitative differences for longitudinal velocity component v (Fig.5.24) and static pressure p (Fig.5.25) behavior for examined flows. For ellipsoidal energy source (4) static pressure is changed slightly and smoothly, while for spherical ones (1–3) the occurrence of a distinctive peak, corresponded to the bow shock wave, is typical. The remote wake velocities are determined by the energy source intensity Q_0 (curves 1,4). The greater is Q_0, the higher wake velocity observed. Thus, the energy input is consumed for kinetic energy increasing, which is unfavorable for high temperature obtaining.

As a result of numerical computations it is shown that such critical quantity (for the air-fuel mixture ignition) as temperature is determined by synthetic parameter $Q_0\Delta z$. Temperature profiles for "equivalent" computations are closed to each other (curves 3,4 on Fig.5.26). For ellipsoidal energy source (4) the temperature in the remote wake is two times greater than for spherical ones (2), in spite of smaller steady power input. Thus, the increasing of the longitudinal energy source size is the preferable method of an optimization of the energy supply. Ellipsoidal energy source provides continuous deceleration of the flow down to a sub wake.
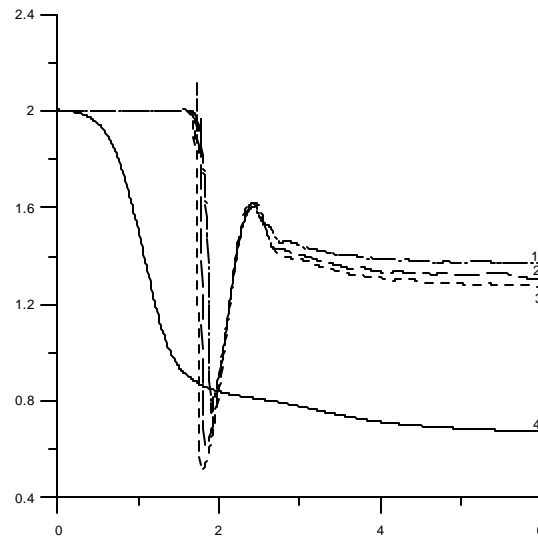
Fig.5.23. Mach number distribution along the symmetry axes for different energy sources.
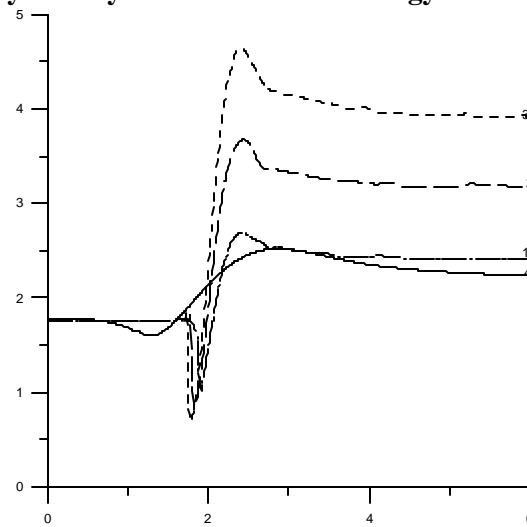
Fig.5.24 Velocity $v/\sqrt{p_0/r_0}$ distribution along the symmetry axes for different energy sources.
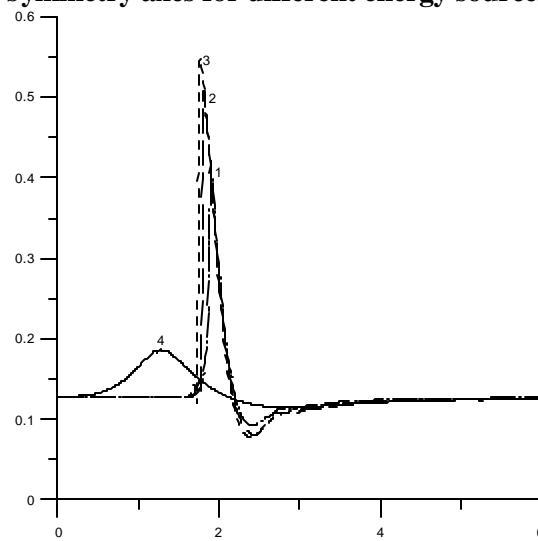

Fig.5.25 Pressure p/p_0 distribution along the symmetry axes for different energy sources.

The supersonic flow over pulse-periodic energy sources was investigated. For determinacy the spherical energy source $\Delta r = 0.15$, $\Delta z = 0.15$, $Q_0 = 200$ with steady power input $W = 1340$ Watt was selected. It was assumed that pulses are rectangular: energy supply is powered on during the time t_0 in the beginning of every period of duration T_q. Correspondingly function $f(t)$ that modulate energy supply density $\dot{Q}(r,z,t)$ with time looks as follow:

$$f(t) = \begin{cases} 1, & \mathrm{mod}(t, T_q) \le t_0 \\ 0, & \mathrm{mod}(t, T_q) > t_0 \end{cases}$$

Computation results will be presented as distributions by space for typical time moments and time oscillograms in selected point $z = 6$ on the symmetry axes.
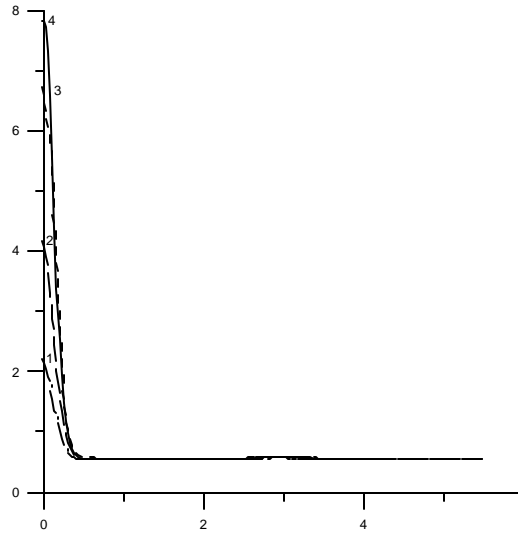

Fig.5.26. The cross distribution of temperature T/T_0 in the remote wake.

In the first stage the conditions of the real experiment were approximated $T_q = 1\,\mathrm{ms}$ ($T_q = 29,3$ for dimensionless form accepted), $t_0 = 0.1\,T_q$. The regime of "long single pulses" is realized (Fig.27). The formation of ellipsoidal high temperature region with size depended on the ambient flow velocity and pulse duration is typical for this case. The elongation of the region due to the ejection of hot particles outside the source by the flow is taking place when energy supply is powered on. After the energy source is down the high temperature region is drifted downstream with the velocity of ambient flow and the bow shock wave transforms to a characteristics. The pulse duration t_0 is long enough so that flow picture (Fig.5.27a) in observed region $0 \le z \le 6$ is in agreement with the steady regime. Time oscillograms (Fig.5.27b) have typical
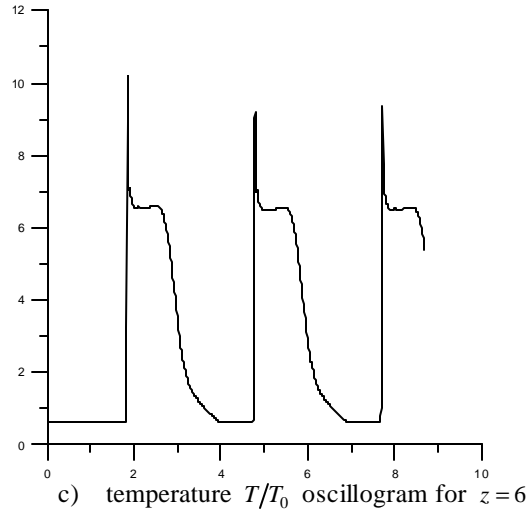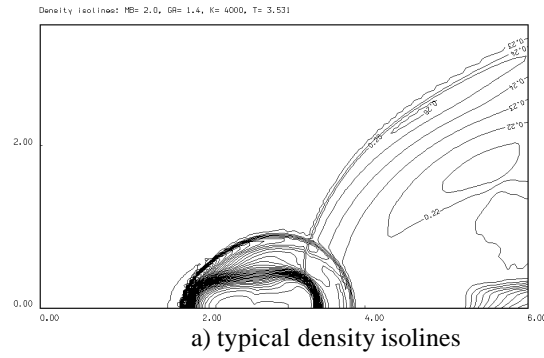
horizontal segments with steady values of parameters. The main conclusion: time characteristics of the energy source, chosen for experiments, allow to simulate the results of an action of the steady energy source on a supersonic flow during the shot time.

For investigation of the action of a pulse repetition frequency on processes dynamic the computation series with $t_0 = 0.5\,T_q$ was carrying out.

For period $T_q = 0.1$ ms the regime of "short single pulses" is observed (Fig.5.28). In this case every new pulse is still realized in undisturbed region.

a) typical density isolines

b) temperature T/T_0 oscillogram for $z = 6$
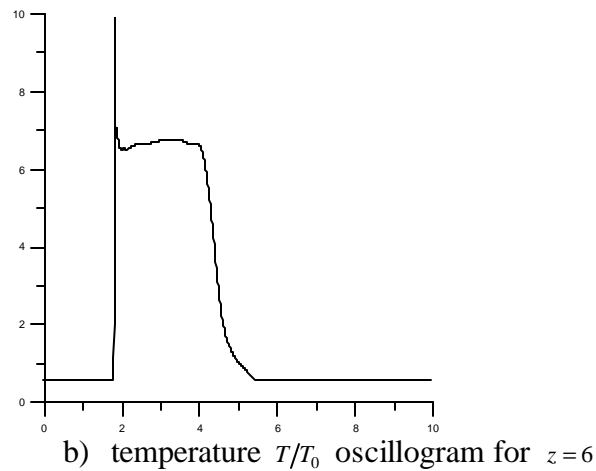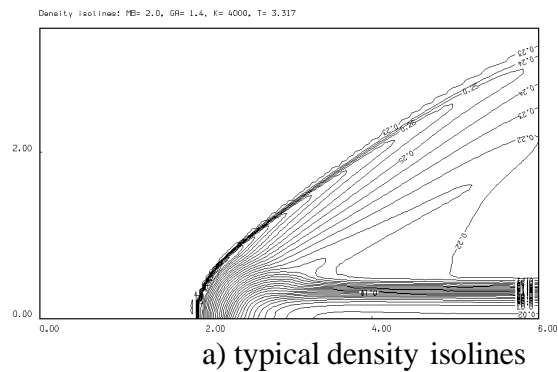
Fig.5.27. The regime of "long single pulses".

a) typical density isolines

c)   temperature T/T_0 oscillogram for $z = 6$

Fig.5.28 The regime of "short single pulses".

The bow shock wave is drifted by the ambient flow downstream the source center before the end of every period. The short ellipsoidal high temperature region is formed (Fig.5.28a). Horizontal segments with steady values of parameters are still presented on oscillograms (Fig.5.28b). The flow dynamics in the observed region $0 \le z \le 6$ is essentially unsteady.

The criteria of quasi-stationary flow is determined from the condition that the upstream front of the shock wave, induced by the energy impulse, isn't drifted downstream the energy source center [13]. This regime is corresponding to the period $T_q = 0.04\,\text{ms}$ (Fig.5.29). The complicated pulsing shock wave structure is formed in this case. The pulse duration is short and ellipsoidal high temperature region is not identified in Fig.5.29a. The temperature is composed by typical sharpen peaks with sudden fore front and gently sloping back front (Fig.5.29b). Thus the action of such a source on the flow is unsteady. The appropriate title for this case – "regime with quasi-stationary bow shock wave".

a) typical density isolines

b) temperature T/T_0 oscillogram for $z = 6$
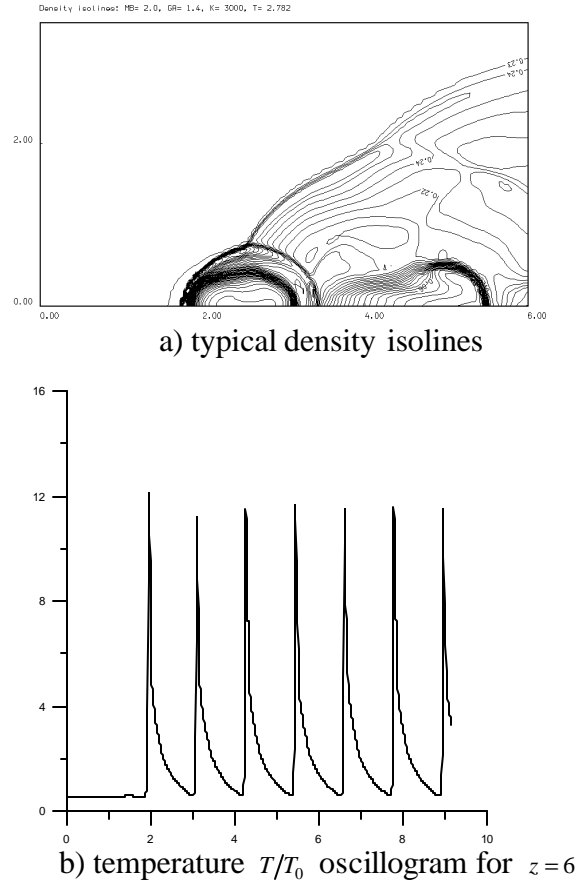
Fig.5.29. The regime "with quasi-stationary bow shock wave".

"Quasi-stationary regime" is realized for period $T_q = 0.01\,\text{ms}$ (Fig.5.30). In this case the practically steady shock wave and the pulsing high temperature wake are formed (Fig.5.30a). The flow field is close to steady one (Fig.5.22a). However, as distinct from the steady case, the energy source is powered on for half of a period ($t_0 = 0.5\,T_q$). So the correct comparison by absolute values will be for $Q_0 = 100$ (computation (3)). The oscillogram temperature (Fig.5.30b) illustrates quasi-steady action of the energy source on the flow structure. The temperature oscillates near new value, determined by the steady regime $Q_0 = 100$. For intervals between pulses when the power is off the temperature not drop down to undisturbed values, as it was for all previous cases. For further increasing of pulse repetition frequency the temperature oscillation amplitude will decrease.

a) typical density isolines

b) temperature T/T_0 oscillogram for $z = 6$
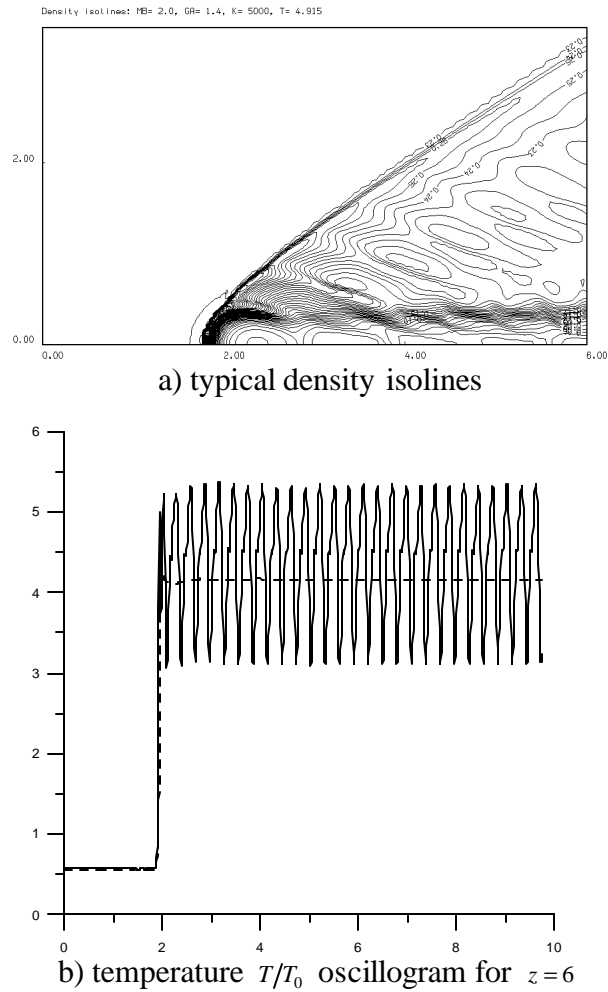
Fig.5.30 The "quasi-stationary" regime.

Thus, pulse-periodic energy input in quasi-stationary mode not only simulate the steady source for a short time interval, but is completely equivalent to the steady source by an action on the supersonic flow.

The comparison of experimental and theoretical researches of transversal gas discharges interaction (direct current, pulse and pulse-periodic) with a supersonic gas flow is showed that the basic regularity of the gas discharge formation in a supersonic flow have not bad agree with results of computational modeling of airflow a non-stationary thermal source.

Spatial distribution of gas temperature and its value are in good consent with results of account.

§5. Plasmadynamic discharge in a supersonic flow

The posing of experiments of studying properties of the plasmadynamic discharge in a supersonic flow was the following.

The plasma jet was generated by a pulsed plasmatron and was injected into an aerodynamic channel normally to the flow. In the current experiments the channel was a $\varnothing 32$(internal)$\times 430$ mm tube made of a molybdenum glass. Three pairs of $\varnothing 0.3$ mm molybdenum probes were sealed into the tube, the first of them was 12 cm from the electrodes, the rest were positioned with a 10-cm separation from each other. The fourth $\varnothing 1$ mm probe was positioned in the channel end.

Temporary dependencies of distributions of charged particles density along the channel can be determined with use of probes with a fixed bias voltage. Two schemes of measurement were applied: with the galvanic separation based on optical waveguides and on optrons.

In the same time a MW signal cutoff was detected. For so doing, the dielectric antennae of the interferometer were positioned in an arbitrary cross section of the channel.

The measurements were carried out in a regime of single pulse with a voltage of the generator being equal to 4 kV. The values of the pressure in the chamber, the pressure in the receiver of the compressor, and the contents of propane were varied.

The influence of variation of the pressure in the receiver of the compressor on the temporary dependence of plasma density in the $z = 12$ cm cross section of the channel is shown in Fig. 5.31, a, b, c.

The upper beam shows the signal of the double probe, the lower beam is the signal from the Rogowskii coil, which is in a direct proportion to the discharge current. With an account of the voltage in the generator, the period of energy input was about 100 μs.

One can see that the first sharp jump of the upper beam is a noise, which corresponds to the breakdown of the discharge gap.

Some 120 μs later, the plasma achieves the cross section of the first double probe. The derived speed of movement of the plasma jet is about 1 km/s, that is much higher than the speed of the supersonic flow. One can be quite sure that it is the speed of

propagation of the plasma jet itself, which is being injected into the channel and is interacting with the opposite wall.

The density of plasma as a rule remains rather high for rather a long time (hundreds of µs) after the energy input end. Not only the head, but also the back end of this distribution is rather steep.

As the pressure in the receiver is enhanced, the length of the plasma slug becomes less: at P = 1 atm it is 700 µs, and at P = 4 atm. it is 400 µs (Fig.5.31 a,b,c).

This effect is present along all the channel − in the channel's end the length falls from the same 700 µs at P = 1 atm. to 500 µs at P = 4 atm. (Fig.5.32 a,b,c).

The effect of growth of the pressure in the chamber on both value and temporary dependence of the plasma density is practically absent up to 500 Torr. A comparison of currents of the probes positioned along the channel shows that in all the cases the fall of plasma density along the channel is insignificant.

In order to determine absolute values of density of charged particles, voltage current characteristics of the double probes have been registered. For so doing, the sawtooth bias voltage (10 µs, ±26 V) was applied between the probes.

A typical registration of oscillograms of the probe voltage and current with a long scanning time is presented in Fig.5.31. For the given conditions an interval with minimal density variation was chosen with use of a delay generator. Then oscillograms of the probe voltage and current with a short scanning time were registered – see Fig.5.32.

One can see that the probe voltage current characteristics here tend to saturation, contrary to the case of pulsed periodical discharges.

The analysis of the probe characteristics can be based on the asymptotic analysis for a probe in a slow flow [14,15]: which is valid if $Re_D \gg 1$, $c \ll 1$, $e \ll 1$, $j_m \gg 1$, and if $(cRe)^{-1}$, $j_m/(Re^{1/s})$, $s>1$ are limited. Here $Re_D = v_g R/D_i$, $c = n_e D_i/(WR^2)$, $e = k_B T_g e_0/(n_e e^2 R^2)$, $j_m = e j_p/(k_B T_g)$, e_0 is the dielectric constant, j_p is the probe potential, W is the characteristic rate of plasma chemical reactions.
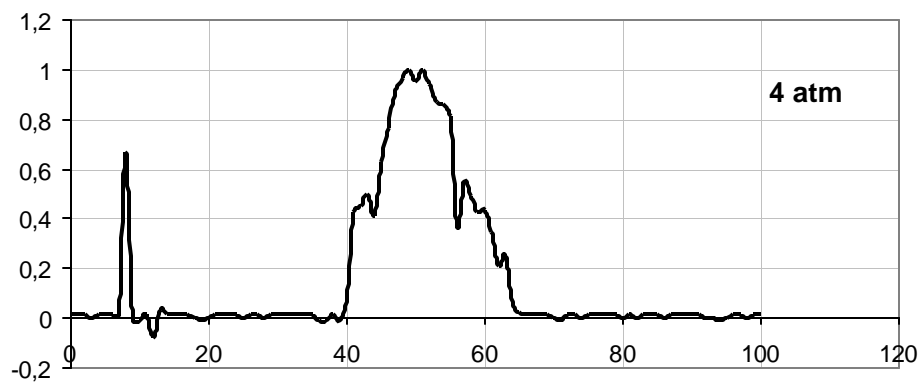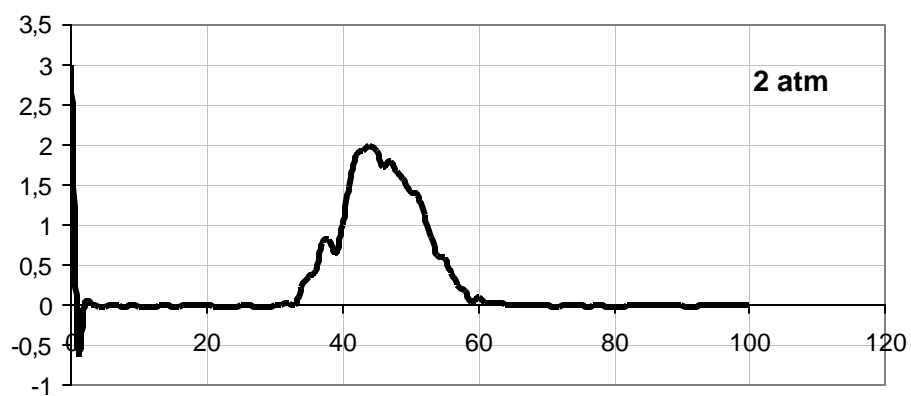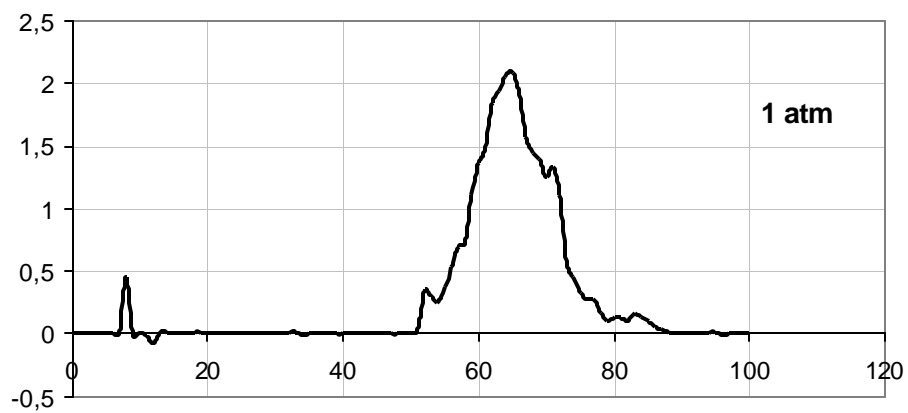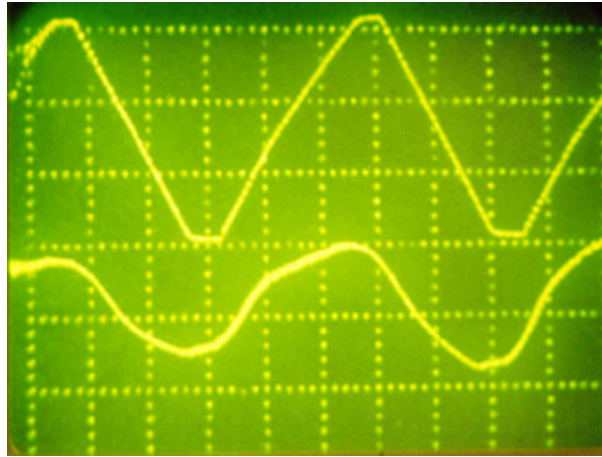
a
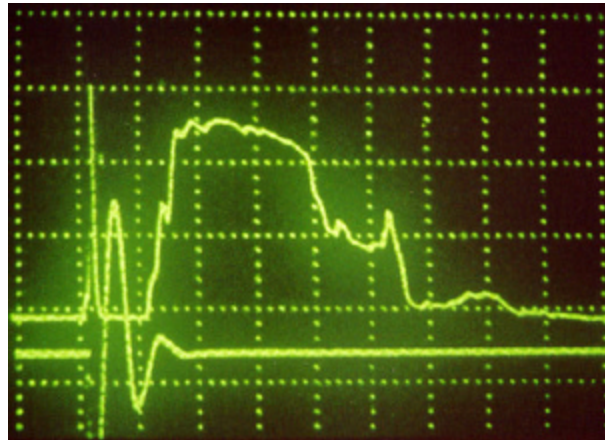
b

c

Fig.5.31. Oscillograms of probe current, proportional to plasma concentration, at different pressure in receiver
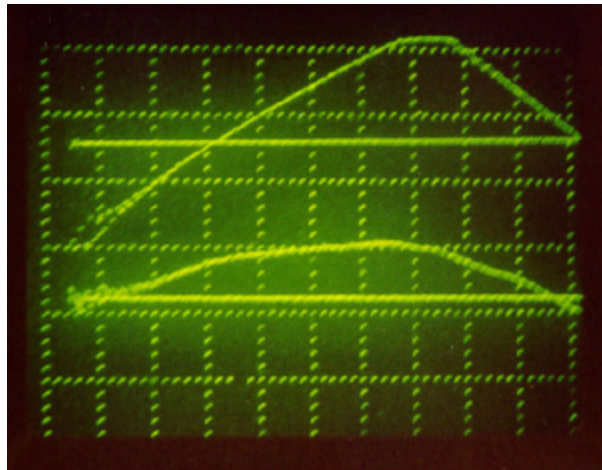
a – $P_0 = 1$ atm, b – 2 atm, c – 4 atm

p = 300 Torr

Fig.5.32.Oscillogram of probe current at z =32 cm

p = 300 Torr

**Fig.5.33. Oscillograms of probe voltage bias (upper beam)
and current (lower beam)**

P=300 Torr, P_0=2 atm, 5 µs/div

**Fig.5.34. Oscillograms of probe voltage bias (upper beam)
and current (lower beam)**

P=300 Torr, P_0=2 atm, 2 µs/div

Estimates for the current experiments with the decaying plasma of the plasmadynamic discharge ($E = 0$, $T_g \gg T_e \sim 2000...5000$ K, $n_e = 10^{18}...10^{21}$ m^{-3}) have shown that these condition are met: $Re \approx (0.6-1)*10^3$; $j_m \approx 3-300$; at $n_e = 10^{18}$ m^{-3} — $e \approx (1-3)*10^{-4}$; at $n_e = 10^{21}$ m^{-3} — $e \approx (1-3)*10^{-7}$; $c \ll 1$.

The analysis [15] says that at $e\,Re^2 \ll 1$ the probe voltage is defined by the Debye layer, and the voltage-current characteristic is saturated. At $e\,Re^2 \gg 1$ the probe voltage is defined by the region outside the boundary layers, and the voltage-current characteristic is linear. For the air plasma $eRe^2 \approx 0.13*10^{-33}*v^2*n_g^2/n_e$, and at $n_g = 10^{24}$ m^{-3}, the threshold value $eRe^2 = 1$ corresponds to $0.5.10^{20}$ m^{-3}. In our case, the forms of voltage-current characteristics are intermediate, that says that $eRe^2 \approx 1$, i.e. n_e is about 10^{20} m^{-3}.

The results of probe measurements were compared with results of microwave sounding of the plasma. A typical view is shown in Fig. 5.35. One can see that the MW radiation does not pass through a major part of the plasma volume, i.e. any measurable probe current corresponds to a plasma density, which is higher than the critical density $1.6\ 10^{13}$ cm^{-3}.
This is true even for the end of the supersonic channel.
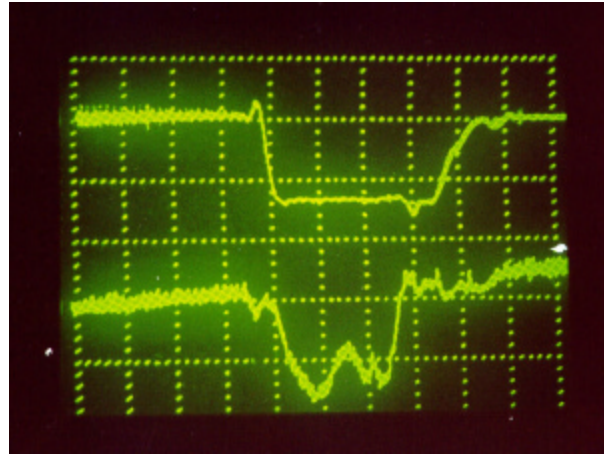
Fig.5.35. Oscillograms of MW signal (upper beam) and probe current at fixed bias (lower beam)

P = 300 Torr, z = 32 cm, P$_0$=2 atm.

Thus, it is shown that the density of the charged particles can achieve values of about 10^{14} cm^{-3} and higher, and slowly drops along the length of the channel. It is confirmed by the data of microwave measurements. The cut-off of MW sounding radiation can take place even in the end of the supersonic channel, i.e. there the electron density is higher than $1.6 \cdot 10^{13}$ cm^{-3}.

In a number of cases the signal with two sharply expressed maximums was registered in outflow face of the supersonic channel, where the third probe was located. (The third probe was located on a distance of 32 cm from the pulsed plasmatron, and the plasmatron was located on a distance of 12 cm from the outflow face of the Laval nozzle).

Such a behavior of the probe current is in good conformity with results of the work [16].

At first two series of experiments on studies of interaction of the pulsed plasma with the supersonic airflow was carried out. These experiments have shown that the character of plasma interaction with the supersonic airflow in the supersonic channel essentially differs from the case of plasma outflow in the supersonic flow in free space. In case of the supersonic flow limited by walls of the combustor the plasma jet is heated up to significant temperatures during some tens of microseconds. The pressure in the area of the plasma jet sharply grows and the plasma begins to extend along an axis of the channel in both directions (upwards and downwards). Thus there is a formation of two plasma fronts. One of such fronts is propagating along the airflow, another one goes upstream. Probably the plasma piston propagating upstream blocks the flow for some time. The speed of movement of the piston gradually decreases. When the pressure in the piston and in the airflow become close to each other, the plasma begins to move along the flow. Thus the speed of plasma is equal to the speed of the airflow. The study of dynamics of plasma front driven along the flow shows the following. First, the initial speed of the motion of plasma border considerably exceeds the speed of the airflow. Secondly, the speed of the plasma piston depends on the entry conditions. In our experiments it changed from 650 m/s (fore front of plasma piston) up to values of the order 700 m/s (hinder front of plasma piston).

§6 Propane addition influence on plasma parameters of discharges in supersonic airflow

6.1. Pulse-periodical discharge

The transversal gas discharge was used to study of the opportunity of the ignition in air - propane mixture. The discharge was formed in a zone of the braking of the gas flow (zone of the sudden expansion). The researches were carried out at the flow Mach number M=2 in a wide range of the entry conditions. The static pressure in the channel changed from 40 up to 600 Torr. The duration of the input energy pulse varied from 20 up to 1000 μs. The discharge current varied from 1 up to 20 ?. The single and periodical pulse modes of the ignition of the combustible mixture were studied. The maximal repetition rate of the ignition pulses was 500 Hz.

The ignition process of the air-propane mixture with the help of pulsed-periodic discharge in the supersonic channel at the gas static pressure p=450 Torr are illustrated in Fig.5.36.

Fig. 5.36(a) corresponds to the pulse duration τ_p=50 μs and the pulse repetition rate f=500 Hz, and Fig. 5.36(b) - to τ_p=200 μs and f=10 Hz. The pulse power is 40 kW. The average power consumption in the first case is 400 W, in the second – 80 W.

a   b
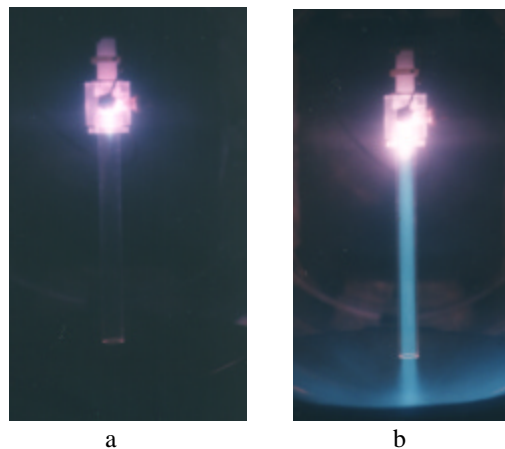
Fig.5.36. Transversal gas discharge in the supersonic combustor in air-propan mixture

Mach number M = 2, current discharge I = 20 A, p = 450 Torr

The propane mass fraction was about the stoichiometric one. The ignition of the combustible mixture is observed at the pulse duration exceeding 200 µs and gas static pressure exceeding 200 Torr.

The earlier experiments on a breakdown of an air – propane mixture under these pressures have shown, that the propane addition changes breakdown voltage in the limits of (10 – 20) %.

As breakdown voltage is the most sensing parameters of the discharge, it is necessary to expect that the propane addition influence on plasma parameters of pulse-periodic discharge will be minimal.

So, the systematic propane addition influence on period of oscillations of a discharge current and voltages did not detected.

Let's take into account now, that the measurements of spatially - temporary evolutions of plasma parameters were investigated in case of pulse-periodic discharge in free jet, and ignition experiments were carried out in the supersonic channel.

The direct comparison of parameters in this case is impossible. Therefore we have limited investigation of propane addition influence on a spectrum of a plasma radiation of pulse-periodic discharge in the same conditions..

At the use of the propane-air (C_3H_8-air) mixture, a lot of the carbon should be formed at burning of such mixture. That is the harmful phenomenon for the real engine. However at the same time, the intensive formation of the carbon should be the certificate of C_3H_8-air mixture burning.

The radiation spectrum of the discharge plasma in the supersonic airflow without the propane in the range of wavelengths λ=500-600 nm is submitted in Fig.5.37(a) and the spectrum of the discharge in the supersonic flow of C_3H_8-air mixture is given in Fig.5.37(b). Static pressure in the chamber is 300 Torr, Mach number of a flow is 2, duration of pulses of the discharge current is 500 µs, frequency of their repetition is 5 Hz, discharge current is 10 A and the distance from electrodes downwards on the flow is 10 cm.

From the Fig.5.37 one can see, that the intensive formation of the carbon takes places with the addition of C_3H_8 in air. It undoubtedly testifies the ignition of a propane-air mixture in our conditions.

a   b
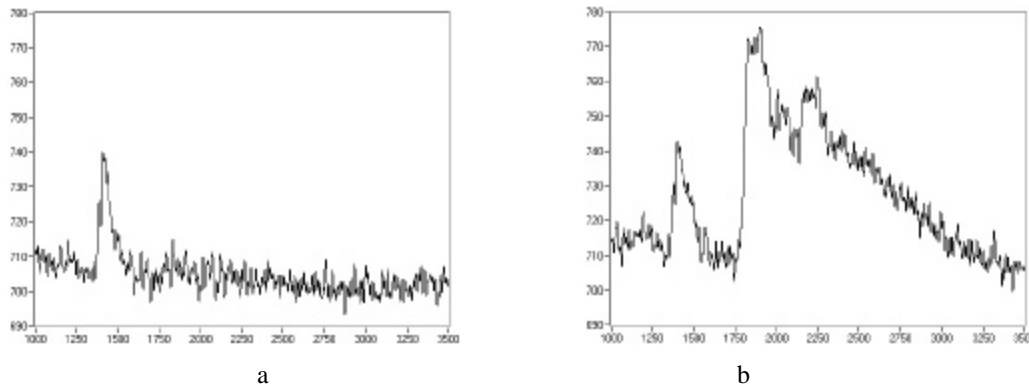
Fig.5.37. The radiation spectrum of the plasma of the discharge in a supersonic flow of air without a propane in the range of wavelengths l=500-600 nm.

P_{st} = 300 Torr, M = 2, τ = 500 µs, f = 5 Hz, I=10 A, and z=10 cm.

a – without propane, b - with propane

6.2. Plasma jet

On Fig.5.38 the photos of the supersonic air - propane flow ignition are given at Mach number ? = 2. One can see that the ignition occurs over the whole length of the combustor.
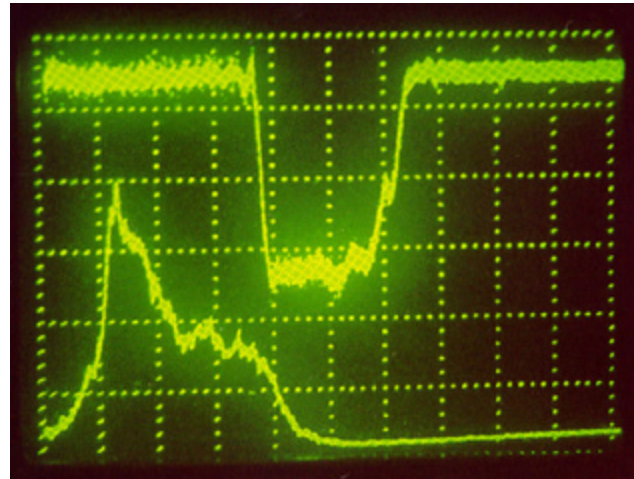
Ignition of propane-air supersonic flow by plasma jet was investigated in the same conditions that the measurements of plasma parameters of plasmadynamic discharge.

As result, more detailed investigation propane addition influence on plasma parameters was performed.
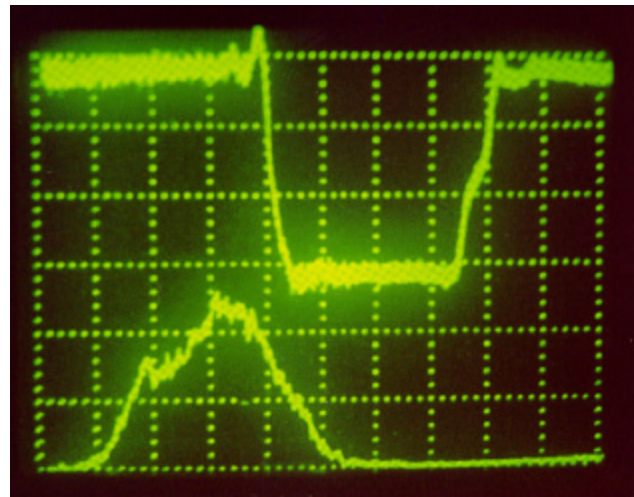
Some results of measurements by microwave and probe methods are shown in Fig.5.39 –40. The experiments have shown lack of essential difference both in parameters of plasma and in dynamics of the plasma jet.
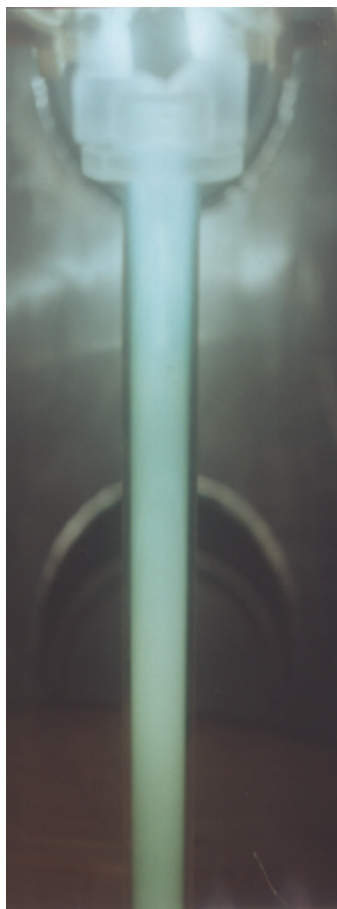
Fig.5.38. Photo of air-propane mixture ignition.

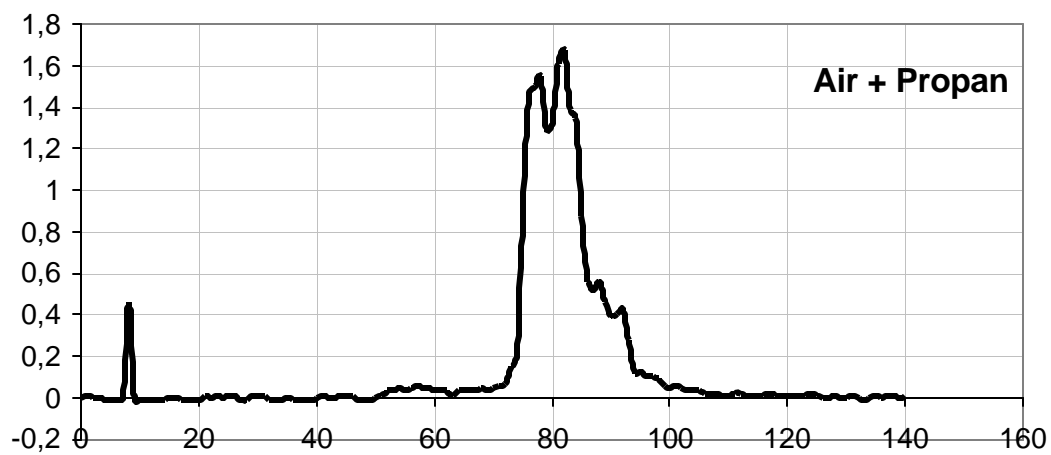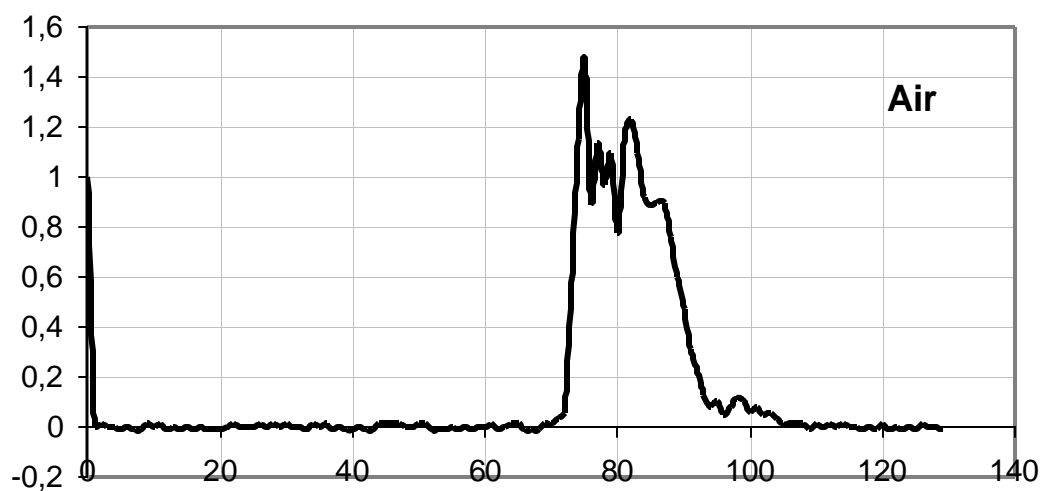Single pulse regime. M = 2, P = 300 Torr, P_0 = 2 atm.

air-propane

air

Fig.5.39. Oscillograms of MW-signal (upper beam) and H$_a$ line intensity (lower beam) at injection of plasmadynamic jet into supersonic flow.

P = 300 Torr, P$_0$ = 2 atm, z = 22 cm. 200 μs/div.

Fig.5.40. The propane addition influence on probe signal of plasma jet.

P = 300 Torr, P_0 = 2 atm, z = 43 cm.

References to Chapter V.

1. Alferov V.I., Bushmin A.S., Kalachev B.V. Investigation of discharge glowprocess in high-velosity gas flow. ZhETF, 1966, vol.51, #5, pp.1281-1287.

2. V.V.Vitkovsky, L.P.Grachev, N.N.Gritsov, Z.M.Egorova, Yu.E.Kuznetsov, V.V.Lebedenko, V.V.Skvortsov, K.V.Khodataev, V.P.Jankov. Experimental investigation of DC electric discharge in supersonic and subsonic airflow. Trudy TsAGI, #2505, 1991.

3. Georgievsky P.Yu., Gromov V.G., Ershov A.P., Levin V.A., Timofeev I.B., Chernikov A.V., Chernikov V.A., Shibkov V.M. Gas discharge in a supersonic gas flow. The 2nd workshop on Magneto- Plasma- Aerodynamics in Aerospace Applications. Moscow, 5 April - 7 April 2000. P. 169-174.

4. Smirnov B. M. Ions and excited atoms in plasma. ? .: ???????????, 1978.

5. Raizer Yu.P. Gas discharge physics. Moscow, Nauka, 1982.

6. Pashenko N. T., Raizer Yu. P. A glow discharge in a longitudinal gas stream. Plasma Physics. V.8, 1982. P. 1086–1092 (in Russian).

7. [7]. Kolmogorov A.N., Petrovsky I.G., Piskunov N.S. MSU Bulletin. Mathematics and Mechanics. 1937, v.1, p.1.

8. Dvinin S.A., Chernikov A.P., Ershov A.P., Shibkov V.M., Timofeev I.B, Features of transversal gas discharge in a supersonic gas flow. The 2nd workshop on Magneto- Plasma- Aerodynamics in Aerospace Applications. Moscow, 5 April - 7 April 2000. P. 169-174.

9. V.Chernikov, S.Chuvashev, A.Ershov, V.Shibkov, I.Timofeev, B.Timofeev. Formation of gas discharges in supersonic flows of air and fuel-air mixture. 3 Weakly Ionized Gases Workshop, 9 International Space Planes and Hypersonic Systems and Technologies Conference, November, 1999, Norfolk, USA, AIAA-99-4904.

10. A.Ershov, N.Ardelyan, S.Chuvashev, V.Shibkov, I.Timofeev. Gas Discharge in Supersonic Airflow. 3 Weakly Ionized Gases Workshop, 9 International Space Planes and Hypersonic Systems and Technologies Conference, November, 1999, Norfolk, USA, AIAA –99-4851

11. Georgievsky P.Yu., Levin V.A. Supersonic flow over space-distributed energy sources // Mechanics, modern problems. Moscow. MSU Pub. 1987. Pp.93–99

12. Georgievsky P.Yu., Levin V.A. Supersonic flow over bodies in presence of external heat supply sources // Pisma v GTF. – 1988. – Vol.14, No.8. – P.684–687

13. Tretyakov P.K., Grachev G.N., Ivanchenko A.I., etc. Stabilization of an optical discharge in a supersonic flow of argon // DAN. 1994. Vol.336, No.4. P.466–467

14. Benilov M.S. Theory of Electrical Probes in Flows of High Pressure Weakly Ionized Plasma (a review). High Temperature. Vol. 26, No. 5, 1988, pp. 780-793 / Teplofizika vysokih temperatur. 1988, V.26, ? 5, PP. 993-1004 (in Russian).

15. Benilov M.S., Kosov V.F., Rogov B.V., Sinelshikov V.A. Saturation currents on electrical probes in flows of chemical reacting plasma with different kinds of ions. High Temperature/ Teplofizika vysokih temperatur. 1987. V.25. ? 3. P.573 (in Russian).

16. V. Chernikov, A.Ershov, V. Shibkov, I. Timofeev, B. Timofeev, V. Vinogradov, D. Van Wie. Gas Discharges in Supersonic Flows of Air-Propan Mixture. 4^h Weakly Ionized Gases Workshop, 11-14 June 2001/ Anaheim, CA, AIAA-2001-2948

CONCLUSIONS

The complex of diagnostic methods – probe, spectral and microwave - applicable under the plasma aerodynamics conditions have been developed in the current project.

For these purposes an experimental installation has been created, which provided a supersonic (M = 2) airflow at the static pressure range 10 - 500 Torr with a direct current discharge, pulse-periodic discharge and pulsed plasma jets.

The main efforts were required for application of the probe method for diagnostics of discharges in supersonic flows. It is connected with the fact that application of the standard schemes and methods of processing of probe characteristics for such discharges is practically impossible due to the specific mode of operation of a probe in such discharges.

A PC-controlled double probe measurement circuit with an opto galvanic isolation has been developed, produced and tested. It makes it possible to measure the probe voltage-current characteristic at extremely high plasma potentials and high level of fluctuations. The total period of time of measurement of the probe voltage-current characteristic amounts to about 10 μs.

A class of regimes is analyzed, in which the voltage-current characteristic is determined by the "inviscid flow region". New analytical formulae for these regimes in high, moderate and low discharge electric fields are deduced. They correspond with numerical simulation data and experiments, and can be recommended for diagnostics for most cases of the plasma aerodynamic experiments.

A detailed two-dimensional non-stationary mathematical model of probe - supersonic plasma flow interaction has been developed. The model includes the Navier-Stokes equations for gas, a quasi-steady equation for the electric field and equations for the quasi-neutral plasma with account for the ambipolar diffusion and heat conductance, the ion drift, plasma chemical reactions of ionization and recombination, inelastic collisions of electrons with molecules with excitation of vibrational and electronic states, etc. These equations demanded a development of a new set of boundary conditions. A detailed numerical simulation has been carried out for conditions

characteristic for a part of regimes of electric discharges in supersonic gas flows. Two new effects on the voltage-current characteristics have been found out: the synergetic interaction of the gas density profile formation in the viscid high-speed flow with 1) the ambipolar diffusion, and 2) the plasma chemical reactions. They can both lead to considerable gains in the electron density, the plasma conductance and the probe current. It means that the probe diagnostic formulae to have been previously described in the literature are not applicable for such high-speed flows. These effects want further studies with goals of deduction of new practicable formulae for diagnostic applications, and determination of limits of applicability of probe diagnostics.

The spectral methods have been analyzed and adapted to experimental conditions. The non-stationary kinetic model for substantiation of spectroscopic methods of diagnostics of chemically active non-equilibrium non-stationary plasma of the discharge in a supersonic gas flow was developed. This model includes the non-stationary Boltzmann equation for the electrons energy distribution function $f(\varepsilon, t)$; the system of non-stationary balance equations for the populations n_V of vibrational levels of the ground state $X^1\Sigma_g^+$ of the nitrogen molecule; equations for the populations n_X of electron-excited states $A^3\Sigma_u^+$, $B^3\pi_g$, $C^3\pi_u$, $a'^1\Sigma_u^-$, $a^1\pi_g$, $a^1\Delta_g$, $b^1\Sigma_g^+$ of nitrogen and oxygen molecules; equations for active particles n_y (N, O, O_3, NO, NO_2, N_2O); equations for charged particles n_i (n_e, O^-, O_2^-, O_3^-, O_4^-, NO^-, NO_2^-, N_2O^-, n^+); and the non-stationary heat equation for the gas temperature.

Electron density has been measured from Stark broadening of the hydrogen line H_b line with $l = 4861$ A^o. The application range in the discharge plasma is at $I > 1$ A. Rotation temperature has been measured over relative intensities of lines of the rotational structure of the band (0;2) with the quantum wave length $l = 380.5$ nm of the second positive system of nitrogen molecule and the band (0;0) with quantum wave length $l = 388.3$ nm of the CN molecule. Vibrational temperature has been evaluated by the relative intensity of the molecular bands of the second positive system of nitrogen molecule.

The application of MW cutoff method for independent measurements of plasma density has been shown in conditions of experiment.

The experimental investigation of spatial and temporary evolution of plasma parameters of the transversal direct and pulse-periodic discharges in supersonic airflow was carried out with Mach number M=2 in a pressure range 40 –200 Torr. Under these conditions a change in discharge currents from 0.1 up to 25 A results in a change in the values of an electron density from 10^{12} cm^{-3} up to 10^{14} cm^{-3}, the gas temperature from 1000 K up to 4000 K, the vibrational temperature from 8000 K to 3500 K, an electrical field from 300 V/cm to 20 V/cm.

A numerical simulation of a supersonic flow over pulse-periodic discharge has been carried out. An analysis of temperature, flow velocity, pressure and other parameters distribution dynamics in this case has been performed. A comparison of the computations with the experiments has shown their good coinciding.

On the basis of these results the conclusion is done about an opportunity of ignition of supersonic flows of air-fuel mixtures by the pulse-periodic electric discharge.

Project Manager   A.Ershov